THE FEASIBILITY OF USING A CARBON FIBRE FIELD EMITTER AS AN ELECTRON SOURCE IN CATHODE RAY TUBES.

David Archie WILSON

A thesis submitted for the degree of Doctor of Philosophy at The University of Aston in Birmingham.

February 1981

The University of Aston in Birmingham

Summary of a thesis submitted by David Archie Wilson for the degree of Doctor of Philosophy in 1981.

"The Feasibility of using a Carbon Fibre Field Emitter as an Electron source in Cathode Ray Tubes."

An ultra high vacuum electron optical bench has been designed to develop a demountable prototype tube using a computer designed two-anode electrostatic lens to focus the beam. This system has demonstrated that a carbon fibre field emitter has a satisfactory electron optical performance in a CRT and an adequate lifetime. However, there is a residual problem of emitter instabilities which lead to the visual display flickering.

The energy spectra of the emitted electrons have been measured using an UHV high resolution spectrometer. The half-width and spectral shift were both found to increase with increasing field. Electroluminescence has also been found to accompany the electron emission. Since fluctuations in the final image are almost certainly related to instabilities in the emission current, various stabilisation techniques have been investigated. The noise characteristics of the emission current have been analysed and related to the instability of the emission image as recorded cinematographically, which showed the pattern to consist of individual spots which "switch-on" and "switch-off". Scanning electron microscopy has revealed that the onset of emission is accompanied by an explosion of the emitter endform.

To explain the experimental observations a model has been proposed for the emission mechanism based on a composite emission regime involving an insulating amorphous pocket overlaying a metallic-like substrate.

KEY WORDS: FIELD EMISSION, CATHODE RAY TUBES, CARBON FIBRE

ACKNOWLEDGEMENTS

This work was supported by the Science Research Council and the M-O Valve Company.

I wish to acknowledge the help given to me by the following people. Firstly, Dr R V Latham for supervising this work by providing advice, encouragement and many productive discussions over several years. Mr L S Allard for the interest shown in this work and for helping to make my visits to the M-O Valve Company enjoyable. Mr F Lane and his workshop staff for making several of the intricate components for the vacuum systems. Mrs S Onions for her care and efficiency in typing this manuscript.

CONTENTS

	Page
PRELIMINARIES	
Title page	i
Summary	ii
Acknowledgements	iii
List of Contents	iv
List of Figures	vii
1. INTRODUCTION	1
2. THE THEORY OF FIELD EMISSION FROM METALS AND SEMICONDUCTORS	7
2.1 Introduction	7
2.2 Derivation of the Fowler-Nordheim Equation for Field Emission from Metals	11
2.3 Background to Field Emission from Semiconductors	20
2.4 Current Density and Energy Distribution of Electrons Field Emitted from Semiconductors	32
3. CARBON FIBRES	40
3.1 Physical Properties of High Modulus Carbon Fibres	40
3.1.1 History	40
3.1.2 Atomic Structure of a Graphite Crystal	40
3.1.3 Chemistry and Production Process	43
3.1.4 The Structure of Carbon Fibres	44
3.1.5 Surface Studies	50
3.2 Previous Work on Field Emission from Carbon Fibres	50
4. ELECTRON OPTICAL CONSIDERATIONS FOR THE APPLICATION OF A FIELD EMITTER TO A CATHODE RAY TUBE	57
4.1 Fundamental Limitations on Cathode Current Density	57
4.2 Conventional Design of a Cathode Ray Tube	59
4.3 Electron Optical Tube Distortions	62
4.4 Review of Electron Guns Suitable for a Field Emission Cathode	63

5. DESIGN AND OPERATION OF AN ULTRA HIGH VACUUM SYSTEM AND SPECIMEN MANIPULATOR FOR THE DEVELOPMENT OF A PROTOTYPE CATHODE RAY TUBE 71

5.1 Introduction 71
5.2 Vacuum Chamber 71
5.3 Viewport and Phosphor Screen 77
5.4 Specimen Manipulator 78
5.5 Specimen Holder 83
5.6 Electrode Module 88
5.7 Pumping System 90
5.8 Performance of Vacuum System 95

6. DEVELOPMENT AND PERFORMANCE OF A PROTOTYPE CATHODE RAY TUBE USING A CARBON FIBRE FIELD EMITTING CATHODE 97

6.1 Introduction 97
6.2 Mounting Techniques 97
6.3 Etching Procedure 99
6.4 Background to the Design of a Prototype Tube 104
6.5 Angular Confinement of Electrons Emitted from a Carbon Fibre 107
6.6 Initial Diode Regime of the Prototype Electron Gun 110
6.7 Electron Optical Properties of the Electrostatic Lens 121
6.8 Testing of the Electrostatic Lens 129
6.9 Performance of the Prototype Cathode Ray Tube 148
6.10 Fluctuations of the Visual Display 159

7. STUDY OF THE PHYSICAL CHARACTERISTICS OF FIELD EMISSION FROM CARBON FIBRE 173

7.1 The Energy Distribution of Electrons Field Emitted from Carbon Fibre 173
7.2 The Observation of Electroluminescence from Carbon Fibre 194
7.3 Changes in Emitter Profile Observed by Scanning Electron Microscopy 201
7.4 Noise Characteristics of Carbon Fibre Field Emitters 223
7.4.1 Analysis of the Frequency Dependence of Emission Current Noise 223
7.4.2 Influence of the Vacuum Environment on Emission Current Stability 226
7.4.3 Investigation of the Spatial and Temporal Variations of the Field Emission Pattern 234

8. DISCUSSION 243

9. CONCLUSION 258

APPENDIX 265

REFERENCES 282

LIST OF FIGURES

		Page
2.1	Free electron model of a metal and the effect of a high electric field.	8
2.2	Potential energy and wavefunction of an electron near the surface of a metal with strong applied field.	10
2.3	Potential energy V(x) of an electron as a function of its distance x to the metal surface.	12
2.4	Typical Fowler-Nordheim plot for a metallic emitter.	19
2.5	Schematic diagram of the two highest bands for an insulator, a metal and an intrinsic semiconductor	21
2.6	Donor and acceptor levels are within the band gap close to the conduction and valence band edges respectively.	24
2.7	The Fermi function for an intrinsic and an extrinsic semiconductor.	25
2.8	Bending of the conduction band due to field penetration	27-28
2.9	Energy diagram for a semiconductor having an internal potential drop due to field penetration and the bulk resistivity.	29
2.10	The effect of surface states on the band structure of a semiconductor.	31
2.11	Theoretical energy spectra reproduced from work by Arthur.	35
2.12	Theoretical energy spectra according to Modinos.	37
3.1	Graphite lattice	42
3.2	Schematic representation of the ribbon type structure of high modulus carbon fibres.	46

3.3	The layers for high modulus carbon fibres are relatively straight in the longitudinal direction.	47
3.4	Structural model for high modulus carbon fibre.	49
4.1	Conventional cathode ray tube.	60
4.2	Crewe lens.	65
4.3	Munro lens.	66
4.4	Cleaver probe forming system.	68
4.5	Cleaver tetrode gun.	70
5.1	General view of the experimental lay-out.	72
5.2	Vacuum chamber and specimen manipulator.	73
5.3	Configuration of vacuum components.	75
5.4	Four way manifold.	76
5.5	Phosphor screen and holder.	79
5.6	Specimen manipulator.	81
5.7	Bellows assembly.	82
5.8	Tripod clamp to enable bake-out.	84
5.9	Specimen holder.	85
5.10	Copper block.	87
5.11	Electrode assembly holder.	89
5.12	Photograph illustrating the specimen holder and electrode assembly holder in use.	91
5.13	Pumping system.	92-93
5.14	Additional pumping system allowing gas analysis	96

6.1 (i)	Etching procedure.	101
6.1(ii)	Electron micrograph of a carbon fibre field emitter tip.	102
6.2	Field emission pattern from a carbon fibre	109
6.3	Experimental arrangement for investigating different apertures in the extraction electrode.	113
6.4	Tabulated results for an extraction electrode with a 10.5mm diameter aperture.	116
6.5	Tabulated results for an extraction electrode with a 6.0mm diameter aperture.	117
6.6	Tabulated results for an extraction electrode with a 1.0mm diameter aperture.	118
6.7	Diagram explaining nomenclature used in the analysis of the initial diode region.	119
6.8	General form of electrostatic lens investigated.	123
6.9	Graph of magnification as a function of the voltage ratio V_I/V_O. Electrostatic lenses, 10mm electrode separation and apertures of 2, 4, 6, 8 and 10mm.	125
6.10	Graph of object position So as a function of the voltage ratio V_I/V_O.	126
6.11	Graph of spherical aberration as a function of the voltage ratio V_I/V_O.	127
6.12	Graph of chromatic aberration as a function of the ratio V_I/V_O.	128
6.13	Scale drawing of lenses chosen for electron gun.	130
6.14	Graph of object position as a function of the voltage ratio V_I/V_O. 3mm electrode separation and apertures of 2 and 4mm.	131
6.15	Graph of magnification as a function of the voltage ratio V_I/V_O. 3mm electrode separation and apertures of 2 and 4mm.	132
6.16	Graph of chromatic aberration as a function of the voltage ratio V_I/V_O. 3mm electrode separation and apertures of 2 and 4mm.	133

6.17 Graph of spherical aberration as a function of the voltage ratio V_1/V_0. 3mm electrode separation and apertures of 2 and 4mm. 134

6.18 Properties of lens with 2mm apertures, a separation between anodes of 3mm and an image distance of 300mm. 135

6.19 Properties of lens with 4mm apertures, a separation between anodes of 3mm and an image distance of 300mm. 136

6.20 First electron gun. 137

6.21 Second electron gun. 139

6.22 Images formed on the phosphor screen as the first electron gun was focussed. 141

6.23 Modified second electron gun: includes an aperture stop. 144

6.24 Images formed on the phosphor screen as the second electron gun, with a 2mm aperture stop, was focussed. 145

6.25 Images formed on the phosphor screen as the second electron gun, with a 1mm aperture stop, was focussed. 146

6.26 Formation of a halo 147

6.27 Final design of electron gun. 149

6.28 Satisfactory images obtained on the phosphor screen as the electron gun was focussed. 150

6.29 Drawing of the prototype cathode ray tube. 151

6.30 Photograph of the experimental electrode module forming the basis of the prototype cathode ray tube. 153

6.31 Lissajous' figures displayed on the prototype CRT. 155

6.32 Sinusoidal waveforms displayed on the prototype cathode ray tube. 156

6.33 Single shot traces of varying duration as displayed on the prototype CRT. 158

6.34	Photometer circuit using a FET op. amp.	160
6.35	Light variations from the prototype CRT.	162
6.36	Comparison of light variations from: (a) a conventional CRT, and (b) a field emission CRT.	163
6.37	Comparative traces for the electron current from the emitter and the light intensity at the screen.	165
6.38	Typical emission current fluctuations obtained (a) with no stabilisation; (b) with 100MΩ in series; and (c) with 350MΩ in series.	166
6.39	Typical emission current fluctuations obtained (a) unstabilised; (b) with the 'constant-current' power supply; and (c) with 100MΩ in series.	168
6.40	Traces recorded simultaneously showing - (a) the beam monitor signal, and (b) the photodiode screen current.	171
7.1	Field electron emission energy analyser.	176
7.2	Lay out of analyser in vacuum chamber.	177
7.3	Essential features of the electron optical system.	179
7.4	Typical electron energy distributions from a carbon fibre emitter.	182
7.5	Electron energy spectra obtained from a carbon fibre emitter and a reference tungsten emitter. (69)	184
7.6	Set of energy spectra obtained for different emission currents and fields	186-189
7.7	Fowler-Nordheim characteristics of the carbon fibre field emitter whose energy spectra are shown in Fig 7.6.	192
7.8	Typical energy distributions showing the sensitivity of the emission to optical radiation.	193

7.9	Schematic representation of the experimental arrangement used to study electroluminescence from carbon fibre.	196
7.10	Fibre mount.	197
7.11	Photograph of the vacuum chamber and image intensifier.	198
7.12	Photograph showing the pin-point of light associated with field electron emission from a carbon fibre.	200
7.13	Alfrey-Taylor plot for electroluminescence from a carbon fibre.	202
7.14	Spectrum of radiation emitted from a carbon fibre during field electron emission.	203
7.15	Photograph of the scanning electron microscope used to examine the profile of the emitter.	206
7.16	Photograph of the system used for obtaining emission under vacuum conditions of $\sim 10^{-7}$ torr.	207
7.17	Scanning electron micrographs of an emitter before and after in-situ emission of 10μA in a vacuum of 2×10^{-5} torr.	209-210
7.18	Scanning electron micrographs of an emitter before and after in-situ emission of 1μA in a vacuum of 3×10^{-5} torr.	212-214
7.19	Scanning electron micrographs of an emitter which suddenly 'exploded'.	216-217
7.20	Scanning electron micrograph of an emitter before and after emission of 10μA in a vacuum of 1×10^{-7} torr.	218-219
7.21	Scanning electron micrographs showing the long term effects of emission of 10μA in a vacuum pressure of 10^{-7} torr.	221-222
7.22	Typical noise spectrum obtained from a carbon fibre.	225
7.23	Influence of the vacuum on the stability of the emitter.	227

7.24 Variation of current with time for different levels of emission current, obtained under an identical vacuum pressure of 2 x 10^{-8} torr. 229

7.25 Comparison of the stability of the emitter in air and in nitrogen. 231

7.26 Comparison of the stability of the emitter in air and in oxygen. 232

7.27 Comparison of the stability of the emitter in air and in helium. 233

7.28 Table showing the sequence in which two emission spots were either on or off over a time period of 85 consecutive frames of 1/24th second duration. 236

7.29 A selection of frames showing the emission spots referred to in the previous figure. 237-241

8.1 Energy band and surface barrier configuration of the composite emission site in the absence of an applied field. 247

8.2 Energy band and surface barrier configuration after the application of a high field. 248

8.3 Energy band and surface barrier configuration of the metal-insulator micro-emission site after switching. 252

LIST OF SYMBOLS

A	Emitting surface area
β	Geometrical factor
C_c	Chromatic aberration coefficient
C_s	Spherical aberration coefficient
$D(W)$	Transmission coefficient
ΔS	Change in Fermi energy due to field penetration
ΔV_R	Potential energy drop due to the resistivity of the emitter
e	Charge on the electron
ϵ	Fermi energy
F	Electric field strength
FL	Fermi level
h	Planck's constant
I	Electric current
J	Current density
k	Boltzmann's constant
m	Mass of the electron
$N(W)dW$	Supply function
p	Momentum
$P(W)dW$	Normal energy distribution
ϕ	Work function
T	Absolute temperature
V	Potential difference
$V(x)$	Potential energy

$1\,\text{Å} = 1 \times 10^{-10}\,\text{m}$

CHAPTER 1

INTRODUCTION

Field electron emission is the mechanism whereby electrons may be emitted from a solid into vacuum due to the presence of a high electric field at the solid-vacuum interface. In the case of metals at room temperature, this field has to exceed a value of $\sim 3 \times 10^9$ volts per metre for the mechanism to occur. Such high electric fields cannot be realised over extended area plane-parallel electrodes without breakdown occurring: they can however be achieved over a localised area by using a point-plane cathode-anode geometry where all the field lines concentrate on the point. Thus, they are usually obtained in the laboratory by using a filamentary cathode that is etched to a micropoint having a radius of curvature of ~100nm. With such a geometry, the required fields can be obtained by applying a few kilovolts between the cathode and anode.

The use of a field emission cathode as a practical electron source has been considered by numerous workers over the past 2-3 decades for a variety of technological applications. These include microwave amplifiers, switch tubes, transducers, flash x-ray

devices and electron microscopes.[1,2] The work presented here considers the feasibility of using a field emitter electron source in a cathode ray tube as an alternative to the conventional thermionic cathode. Such a source would offer the potential advantage of high resolution applications resulting from its small optical source size (about 3nm) and large current density (about $10^{10} Am^{-2}$ is obtainable under continuous operation).[3] In addition, a field emission cathode is a "cold" source of electrons which enables instantaneous operation and eliminates heater power consumption. Since these features make such a device of great industrial interest, financial support was given jointly by G.E.C.'s M-O Valve Company and S.R.C. to develop a source for an instrument tube. In order for a field emitter to be viable for commercial use in cathode ray tubes, it would have to satisfy certain basic performance criteria such as a reasonable current stability in a well focussed beam of a few microamps, and have a long life compatible with use in sealed-off tubes. A further important practical requirement is that such a source should be readily incorporated into current manufacturing techniques, which demands that the emitter functions according to the above specifications in relatively poor vacuum conditions of about 10^{-7} torr.

There are various properties desirable in an ideal field emitter in order to achieve both current stability and a reasonable lifetime. The material should be a good electrical conductor and microscopically strong enough to withstand the mechanical stresses imposed by the high electric field acting at its tip. In order to reduce the influence of residual gases, the emitter material should firstly have a work function which does not change significantly as a result of gas adsorption. Secondly, a material with a low work function is generally to be preferred since, for a fixed geometry of cathode and anode, and for a given emission current, the lower the work function the lower the applied voltage: in addition, at these relatively high pressures, sputtering processes become important and the lower the ion energy, the smaller the damage to the cathode.

The majority of field emission work has used tungsten as the cathode, since it is a material that is readily available and satisfies some of the previous requirements. Although the high work function (4.5 eV) and the sensitivity to gas adsorption are drawbacks, it is still widely used as a field emitter. However, the satisfactory operation of such a source in an electron optical device requires an ultra high vacuum of the order

of 10^{-10} torr,[4] in addition to the provision of complicated cleaning techniques for the in situ processing of the tip (see, for example, the work of Swanson and Crouser.[5]) In this respect, the tungsten field emitter is at a great disadvantage to the thermionic cathode which may be stably operated in the vacuum region 10^{-5} to 10^{-7} torr. The tungsten emitter also suffers from the disadvantage of being readily destroyed by a discharge, such as would follow from excessive localised emission. Even under high vacuum conditions a tungsten cathode is locally melted and evaporated by a vacuum arc discharge, resulting in a globular tip. For the present application, an alternative to tungsten as the emitter material is therefore required that will operate under poorer vacuum conditions. The work of Baker, et al.[6] and other groups (see Ch. 3.2) has shown that carbon fibre offers considerable promise of being such a material. However, although it is known that carbon fibre will operate in the desired pressure region, i.e. 10^{-7} torr, and have a long emission lifetime, there remains the major problem of both short and long term beam current stability. The main objective of this work has, therefore, been to investigate whether these undesirable features can be accommodated in order to provide a satisfactory electron source for use in cathode ray tubes.

It was decided that the investigation would have two main lines of approach. The first involved studying the performance of a carbon fibre field emitter in a standard production cathode ray tube. However, since such tubes are designed specifically for use with a thermionic cathode it was necessary to develop a field emission electron gun with optimised beam current efficiency and focussing that was also compatible for interfacing with the deflecting and accelerating stages of a conventional tube. To develop such an electron gun in systematic stages a demountable vacuum system, complete with a specimen manipulator, was designed and constructed specially for this purpose. A prototype cathode ray tube could then be developed enabling its performance, in terms of focussing, stability and the influence of residual gases, to be systematically evaluated.

The second approach was concerned with a fundamental study of the physical parameters that determine the emission process. This was necessary because the reasons for both the carbon fibre emitter operating in the pressure region of 10^{-7} torr with a long emission lifetime, and the instabilities of the short and long term beam current are directly attributable to the emission mechanism operating at the field emitting tip. Such

analytical techniques as field emission microscopy, electron energy spectrometry and scanning electron microscopy were employed to provide further information on this mechanism. The experimental details and results obtained using these analytical techniques are presented in Chapter 7. From these findings it was deduced that the emission process was more complex than had previously been assumed and the data obtained could not be interpreted using the theory for field emission from metallic surfaces. In order to provide a satisfactory explanation of these experimental observations, a theoretical model is proposed which considers emission from a composite surface consisting of a semiconducting pocket and a metallic substrate.

CHAPTER 2

THE THEORY OF FIELD EMISSION FROM METALS AND SEMICONDUCTORS

2.1 Introduction

Although a "classical" approach leads to a satisfactory theory of thermionic electron emission (Richardson-Dushman eqn.) and field-assisted thermionic emission (Richardson-Schottky eqn.), it is unable to explain the phenomenon of field or "cold" electron emission that is associated with the presence of very high electric fields at an electrode surface. Figure 2.1(a) shows the Sommerfeld free electron model of a metal at O K and with zero surface field. The upper limit to the energy of the electrons in the metal corresponds to the Fermi level, so that the electrons are confined within the metal by a potential barrier of height ϕ , the work function, above the Fermi level. When a high electric field is applied to the surface, the potential barrier might be thought to assume the triangular shape of Fig. 2.1(b) but, because of the image force potential of the electron, it is rounded off as shown in Fig. 2.1(c). The classical potential barrier is thus lowered in the presence of an electric field with a consequent small reduction in the work function. This phenomenon, known as the Schottky effect, has been experimentally verified for thermionic emission at re-

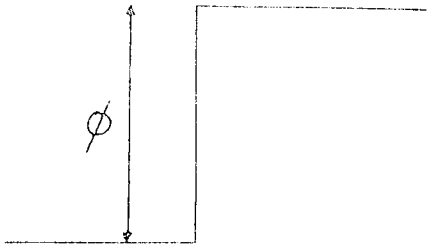

(a) Basic potential barrier

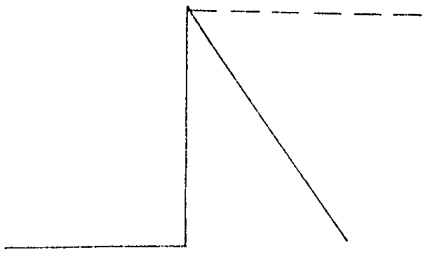

(b) Application of field

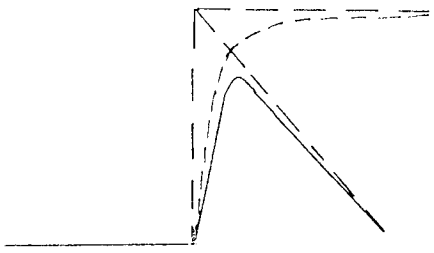

(c) With image force correction

Fig. 2.1 Free electron model of a metal and the effect of a high electric field.

latively low fields ($\lesssim 10^5$ V m^{-1} [1]), but failed in the case of field emission to predict the observed relationship between applied fields and emitted current density.

Fortunately, it is possible to theoretically explain the experimental evidence of field emission by using quantum mechanics. If the electric field applied to the surface is very high, the potential barrier then drops so sharply that the energy of an electron at a short distance Δx from the surface is equal to the energy of an electron within the metal at the Fermi level (figure 2.2). If Δx, the barrier width, is sufficiently small ($\lesssim 10^{-9}$ m) the electrons can then 'tunnel' through the potential barrier to a position outside which has the same energy; i.e. provided the barrier width is comparable to the de Broglie wavelength of the electrons near the Fermi level, the electron wave function will not have decayed before entering the vacuum where the potential drops below the Fermi level, which results in a finite probability of an electron being either side of the barrier. It also follows from this reasoning that no energy is exchanged when an electron is emitted by this tunnelling mechanism so that electrons do not require the provision of external energy to surmount the potential barrier.

To date, workers have interpreted field emission

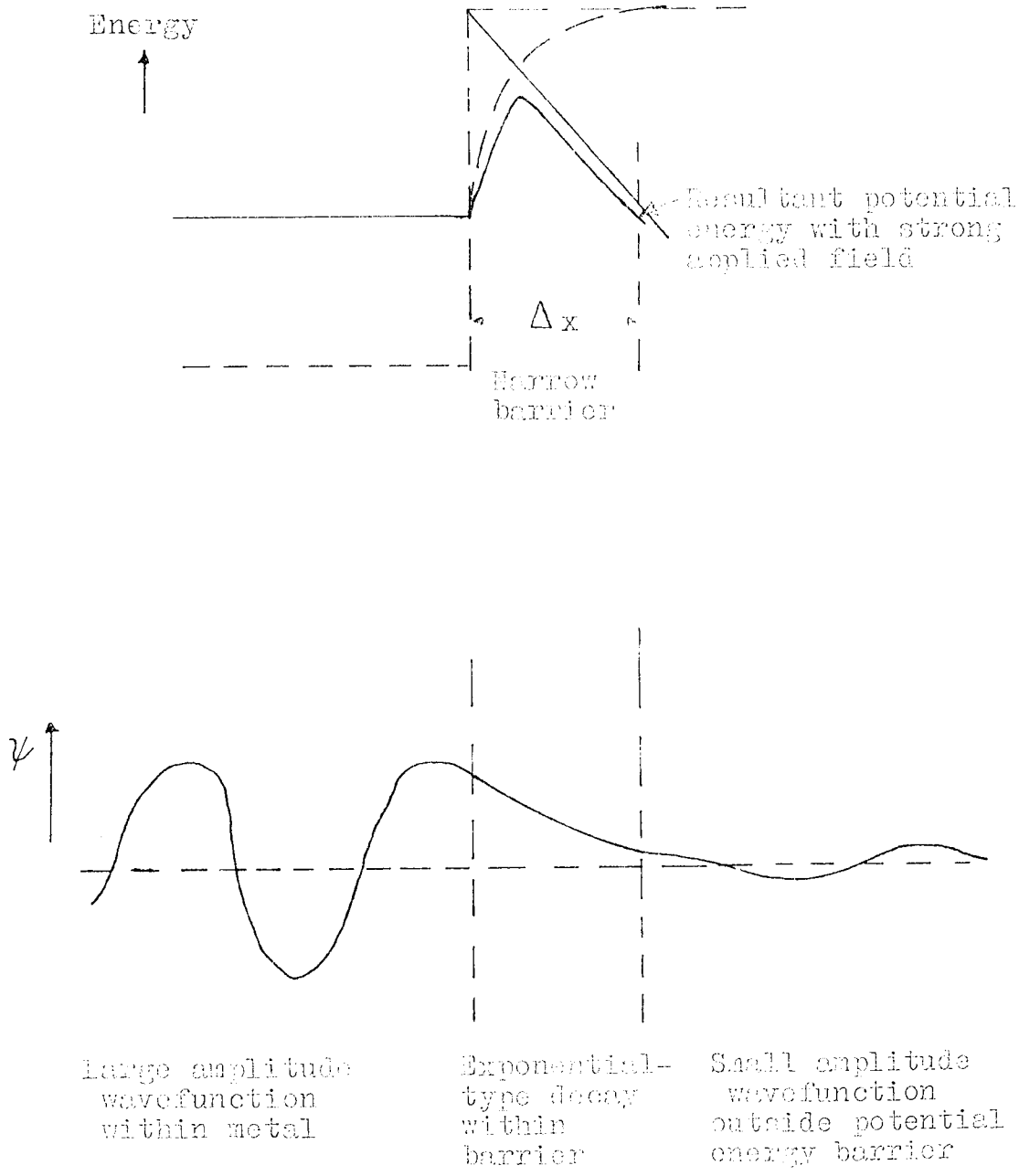

Fig. 2.2 Potential energy and wavefunction of an electron near the surface of a metal with strong applied field.

data from a carbon fibre emitter by assuming the theory for metallic surfaces to be valid. This is understandable given the limited amount of research previously undertaken and the added complexities of the semiconductor field emission theory. During the course of the present work on carbon fibre, however, it has become increasingly evident that the emission process involved has similarities with that from semiconducting surfaces and consequently emission from both types of surface will now be reviewed.

2.2 Derivation of the Fowler-Nordheim Equation for Field Emission from Metals

In 1928, Fowler and Nordheim[7] proposed a quantum mechanical explanation for the phenomenon and derived an equation for the total field emitted current density from cold metals. The model considered one-dimensional tunnelling from a Sommerfeld free-electron metal at O K. The theory assumes the surface of the metal to be smooth and plane, and the potential barrier close to the surface in the vacuum region to consist of the classical image-force potential and a potential due to the applied electric field. Figure 2.3 shows the resulting one-dimensional potential energy, $V(x)$, of an electron as a function of the distance, x, from the surface.

With no applied electric field the potential energy of an electron far from the metal surface is chosen to

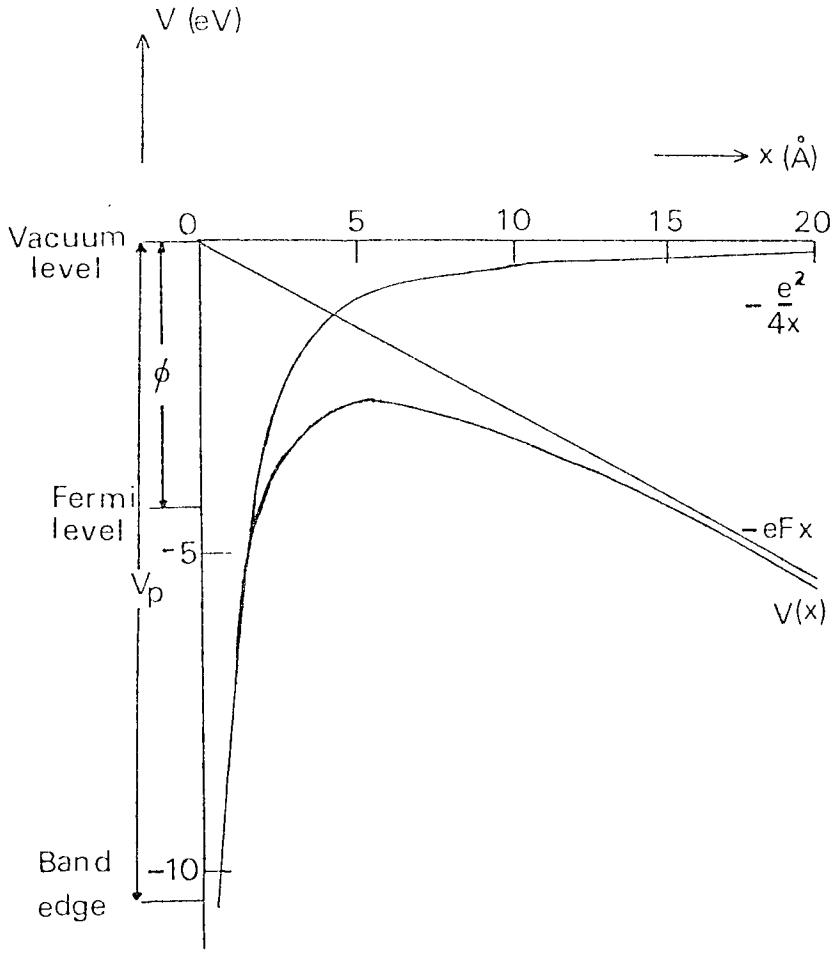

Fig.2.3 Potential energy V(x) of an electron as a function of its distance x to the metal surface.

be zero. The potential energy of an electron inside the metal Vp is assumed to be constant, so that the potential energy will be given by

† $$V(x) = -Vp \qquad \text{for } x < 0 \qquad (2.1)$$

and $$V(x) = -\frac{e^2}{4x} - eFx \qquad \text{for } x > 0 \qquad (2.2)$$

where e is the charge on the electron and F is the electric field strength. The Fowler-Nordheim model assumes that only the x-part of the energy of an electron determines its probability of penetrating the potential barrier shown in figure 2.3. Thus, if the total energy of an electron is denoted by U, the x-part of this energy W is defined by

$$W = \frac{p_x^2}{2m} + V(x), \qquad (2.3)$$

where p_x is the momentum in the x-direction and m is the mass of the electron.

The usual derivation of the Fowler-Nordheim equation uses the following definitions:

† N.B. The derivation involving equations 2.1 - 2.21 follows the traditional treatment[9,18,48] employing mixed units.

The supply function = N(W)dW = the number of electrons with the x-component of their energy within the range W to W + dW incident on the surface per unit area and time.

The transmission coefficient = D(W) = probability that an electron of energy W will penetrate the potential barrier and appear outside the metal.

The number of electrons in the range W to W + dW tunnelling from the metal into the vacuum region, usually known as the normal energy distribution, is the product of the supply function and the transmission coefficient, i.e.

$$P(W)dW = N(W)D(W)dW , \qquad (2.4)$$

The Fowler-Nordheim equation, relating the current density J, the electric field strength F and the work function ϕ, is then found by integrating (2.4) over all values of W and multiplying by the electron charge, i.e.

$$J = e \int_{V_p}^{\infty} P(W)dW . \qquad (2.5)$$

Using Fermi-Dirac statistics, the supply function is given by

$$N(W)dW = \frac{4\pi mkT}{h^3} \ln \left\{ 1 + \exp\left(\frac{-W - \phi}{kT} \right) \right\} dW, \quad (2.6)$$

where k is Boltzmann's constant, T the absolute temperature and h Planck's constant.

The transmission coefficient D(W) is found by solving the Schrodinger equation,

$$\frac{\partial^2 \psi}{\partial x^2} + \frac{2m}{\hbar^2} \left(W - V(x) \right) \psi = 0 \quad (2.7)$$

by inserting the assumed potential energy as given in (2.2). This equation has been solved rigorously by Nordheim[8.] and approximately by Good and Muller[9.] who used the WKB approximation[10.]: this technique is, however, valid only when the energies of the electrons are appreciably less than the energy corresponding to the maximum height of the barrier, which is the case for field emitted electrons. Following this approach, the transmission coefficient is,

$$D(W) = \exp\left(\frac{-4\sqrt{2m|W|^3}}{3\hbar eF} f(y) \right) \quad (2.8)$$

where $f(y)$ is a slowly varying function tabulated by Good and Muller.[9] Since field emitted electrons have energies in the neighbourhood of the Fermi level, the exponent of (2.8) can be approximated by the first two terms in a power series expansion at $W = \phi$, which results in

$$D(W) = \exp\left\{ -C + \frac{W - \phi}{d} \right\} \tag{2.9}$$

where $$C = \frac{4\,(2\,m\,\phi^3)^{\frac{1}{2}}}{3\,\hbar\,e\,F}\, f(y) \tag{2.10}$$

$$d = \frac{\hbar\,e\,F}{2\,(2\,m\,\phi)^{\frac{1}{2}}\,t(y)} \tag{2.11}$$

$$t(y) = f(y) - \frac{2}{3}\,y\left[\frac{d\,f(y)}{dy}\right] \tag{2.12}$$

and $$y = \frac{(e^3\,F)^{\frac{1}{2}}}{\phi} \tag{2.13}$$

Substituting (2.6) and (2.9) in (2.4) gives

$$P(W)\,dW = \frac{4\pi m\,(\phi - W)}{h^3} \exp\left[-C + \frac{W - \phi}{d}\right] dW \qquad (2.14)$$

Integrating over all values of W and multiplying by the charge on the electron yields

$$J = \frac{e^3 F^2}{8\pi h\,\phi\, t^2(y)} \exp\left[-\frac{4\,(2m)^{\frac{1}{2}}}{3\hbar e}\,\frac{\phi^{\frac{3}{2}}}{F}\, f(y)\right] \qquad (2.15)$$

which is the Fowler-Nordheim equation.

Finally, substituting the numerical values for the constants and expressing the current density in A/m^2, the electric field strength F in V/m and the work function in eV leads to

$$J = 1.54 \times 10^{-6} \frac{F^2}{\phi\, t^2(y)} \exp\left[-6.83 \times 10^9\,\frac{\phi^{\frac{3}{2}}}{F}\, f(y)\right] \qquad (2.16)$$

For experimental work on field emission, it is more useful to have an equation relating the total emitted current I in amperes to the potential difference V in volts between

the cathode and anode.

These quantities are related to the current density J and the electric field strength F by the following relationships:

$$I = \int_{0}^{A} J \, dA \qquad (2.17)$$

and $$F = \beta V \qquad (2.18)$$

where A is the emitting surface area in square metres and β is a geometrical factor in m^{-1}. Substituting (2.17) and (2.18) in (2.16) results in,

$$I = 1.54 \times 10^{-6} \frac{\beta^2 V^2 A}{\varphi t^2(y)} \exp\left[-6.83 \times 10^9 \frac{\varphi^{\frac{3}{2}}}{\beta V} f(y) \right] \qquad (2.19)$$

The curve obtained by plotting log (I/V^2) vs $10^4/V$, as shown in Fig. 2.4, is referred to as the Fowler-Nordheim plot and is the generally accepted method of comparing experimental observations of field emission from metals. The slope m at any point of this curve is given by

$$m = -2.97 \times 10^3 \frac{\varphi^{\frac{3}{2}}}{\beta} s(y) \qquad (2.20)$$

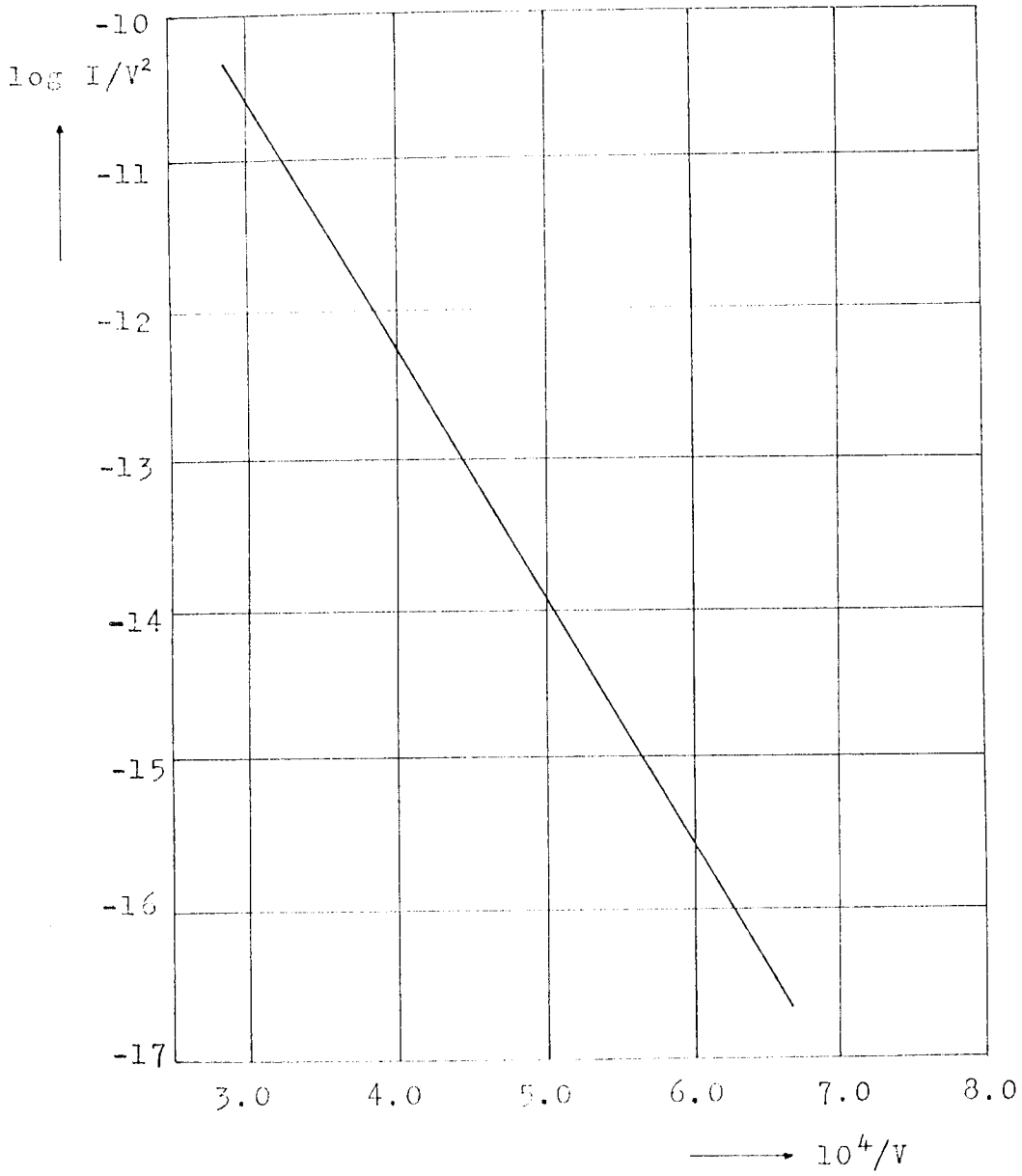

Fig. 2.4 Typical Fowler-Nordheim plot for a metallic emitter.

where $$s(y) = v(y) - \frac{y}{2}\frac{dv(y)}{dy} \qquad (2.21)$$

is an elliptic function, tabled in reference (11); it changes slowly and lies practically always between 0.90 and 0.95. Therefore the slope is nearly constant and the Fowler-Nordheim plot is a straight line suitable to determine the work function of the emitting area.

2.3 Background to Field Emission from Semiconductors

As was previously mentioned, during the course of the present work on carbon fibre the emission mechanism was found to have similarities to that from a semiconducting surface. In fact in a later chapter (Ch. 8) a model is proposed and discussed which is based on emission arising from composite emission sites comprising a semiconducting pocket and a metallic-like substrate. It is therefore necessary to review the theory of field emission from semiconductors in addition to that from metals.

The distribution of the electronic states of metals, semiconductors and insulators have been determined by using the band theory of solids. Represented in Fig. 2.5, are the band schemes of an insulator, a metal and a semiconductor. In order to transmit a current through a solid, electrons must be accelerated in a particular direction, which means that they must be raised to a higher

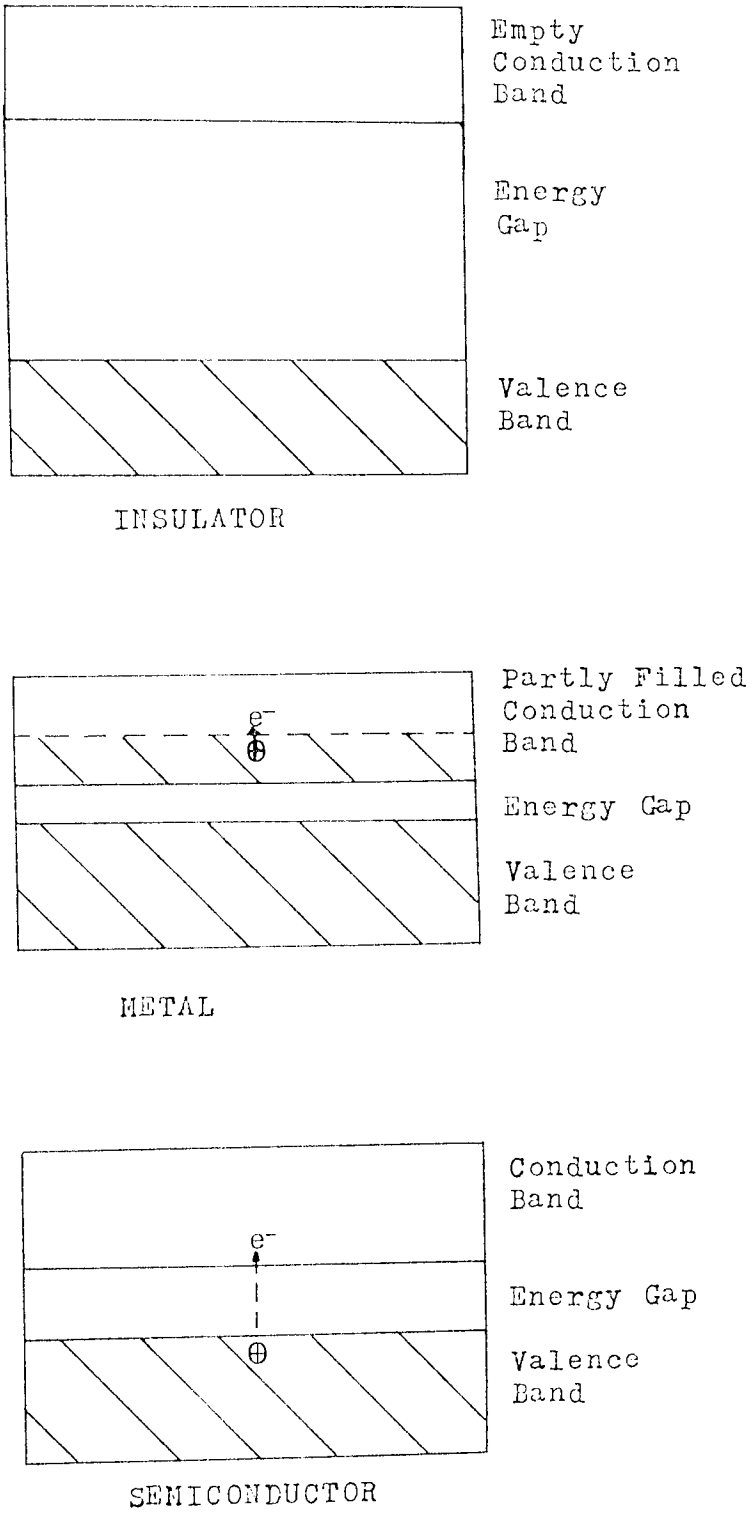

Fig. 2.5 Schematic diagram of the two highest bands for an insulator, a metal and an intrinsic semiconductor.

energy state. This is easily possible in the case of a monovalent metal where the conduction band is only partially filled. This is not the situation for an insulator which has a wide energy gap separating an empty conduction band and a filled valence band. Under these circumstances electrons cannot be raised to a permitted level in the conduction band because they cannot obtain sufficient energy (e.g. from thermal excitation) to jump the forbidden energy gap. However, materials such as pure silicon and germanium, which are intrinsic semiconductors, have a small energy gap of $\sim$0.75 eV and $\sim$1.1 eV respectively. For intrinsic semiconductors at room temperature a few electrons can be excited from the top of the valence band to the bottom of the conduction band. This enables electrical conduction to take place arising from both electrons in the conduction band and holes in the valence band. It follows that the number of electrons excited into the conduction band, and hence the electrical conductivity, increases with temperature.

The electrical properties of semiconductors are modified by the presence of small amounts of certain impurities and are then known as extrinsic semiconductors. The addition of impurities, referred to as doping, result in impurity levels within the energy gap. Depending on the electronic properties of the dopant, these impurity levels consist of donor levels close to the conduction band and

acceptor levels close to the valence band which promote electron (n-type) and hole (p-type) conduction respectively, as shown schematically in Fig. 2.6. The position of the Fermi energy for extrinsic semiconductors is quite different from that for the intrinsic material, as is illustrated in Fig. 2.7. The Fermi energy $\mathcal{E}$ is defined as the energy of a state for which the probability of occupation is $\frac{1}{2}$. At room temperature the Fermi energy for an extrinsic material is close to the impurity level.

The study of field emission from semiconductors is a natural development from the work on metals; however, until the mid fifties there was very little work reported. This was almost certainly due to difficulties in obtaining suitable materials and then producing clean micropoint cathodes with clean emitting surfaces. Theoretically, the emission process for semiconductors is more complex than for metals. This is due to important effects caused by the penetration of an external field into the semiconductor surface layer, electronic surface states, and the field emission current through the emitter. The effects caused by these factors will now be considered.

When an electric field is applied to the surface of a metal or semiconductor a surface charge is induced. The effect of this charge is negligible in the case of a metal because the number of additional charges is small compared

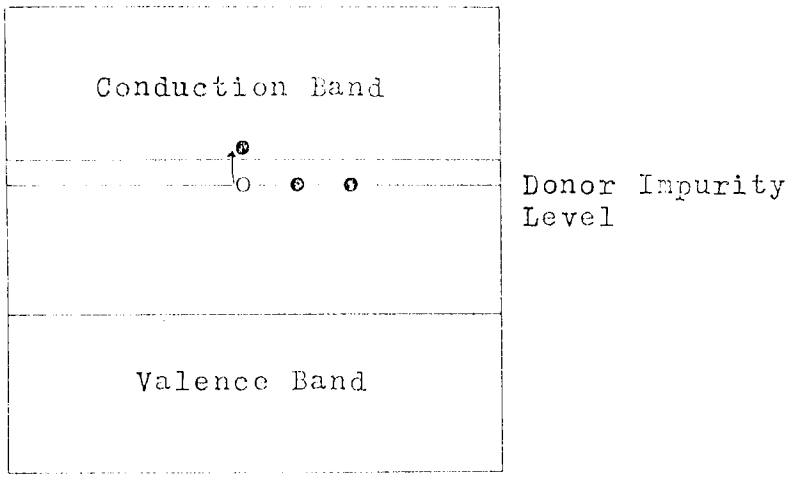

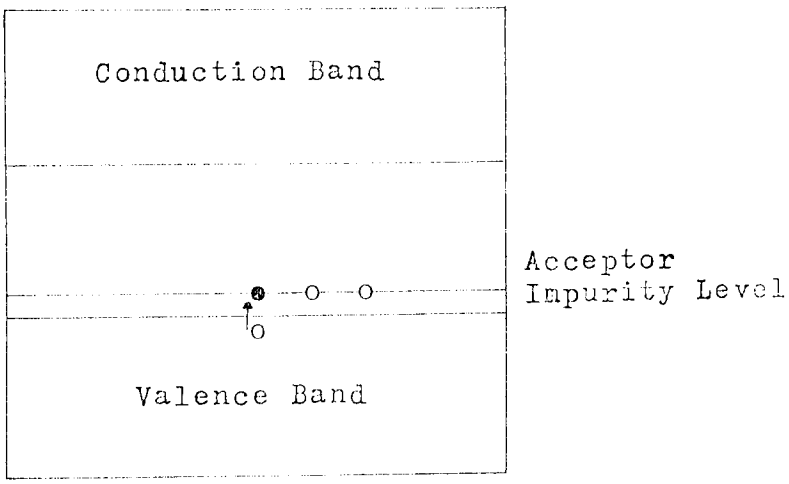

Fig. 2.6 Donor and acceptor levels are within the band gap close to the conduction and valence band edges respectively.

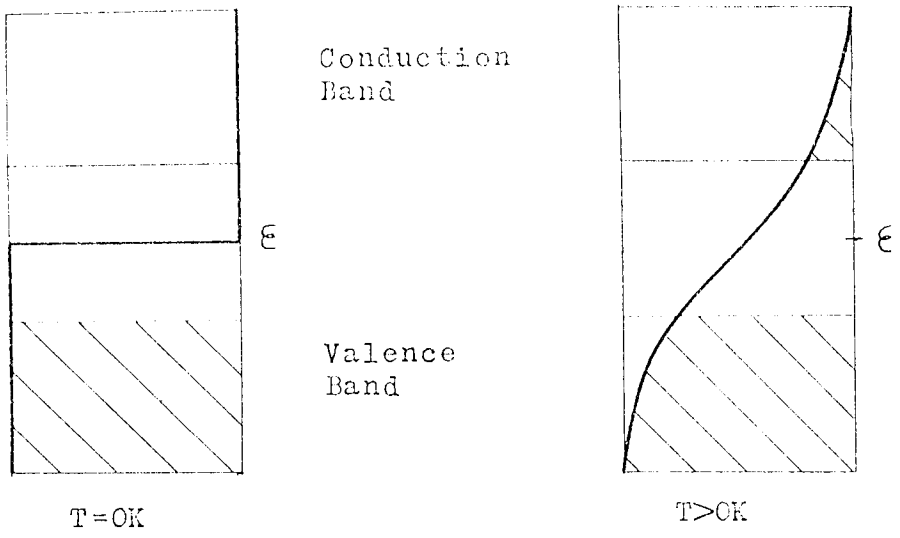

INTRINSIC SEMICONDUCTOR

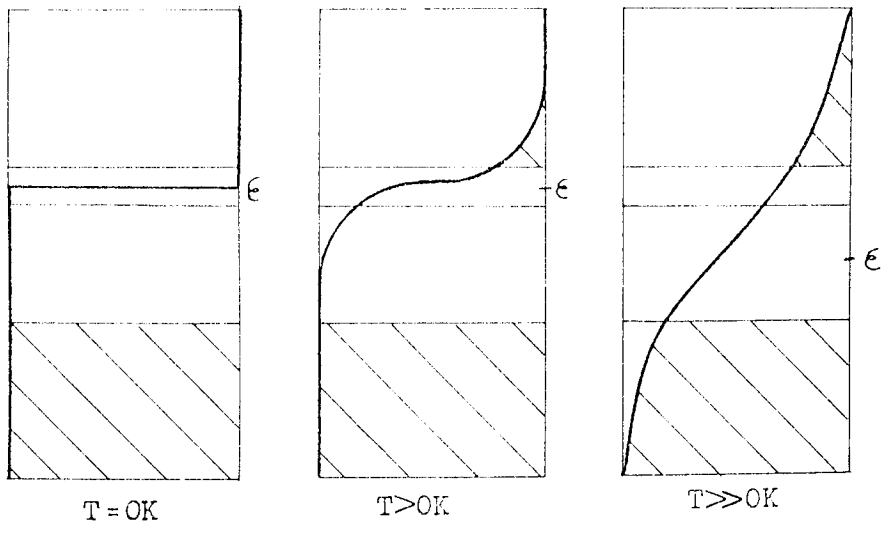

EXTRINSIC SEMICONDUCTOR

Fig. 2.7 The Fermi function for an intrinsic and an extrinsic semiconductor.

to the number of available conduction electrons. For a semiconductor, however, the position is different because the number of electrons in the conduction band is relatively small under most conditions. Due to the polarity of the applied field used in field emission experiments, the induced surface charge results in a decrease in electric potential as the surface is approached from the interior. This decrease in potential is represented in Fig. 2.8(a) in which the bands bend down at the semiconductor surface. In the case of very high electric fields the band bending can be sufficient for the bottom of the conduction band to fall below the Fermi level, at which point the Fermi energy is positive and the surface electrons are degenerate. This case is shown in Fig. 2.8(b), where $-\mathcal{E}$ is the Fermi energy of the bulk material and ΔS is the maximum change in the Fermi energy.

The flow of large field emission currents through a semiconductor emitter can result in a voltage drop ΔV_R down the shank of the emitter with a consequent variation in the Fermi level. This effect is particularly pertinent to semiconductors which have a high value of resistivity. The voltage drop is mainly concentrated at the apex of an emitter, and the temperature of this localised region may be raised by Joule heating. The electron potential energy diagram for a semiconductor having an internal potential drop due to field penetration and the resistivity of the emitter is shown in Fig. 2.9.

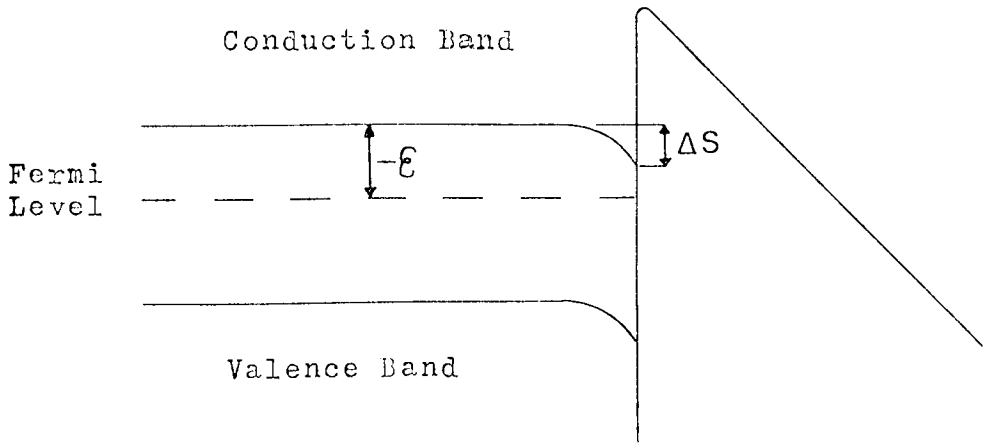

(a) NON-DEGENERATE

Fig. 2.8 Bending of the conduction band due to field penetration.

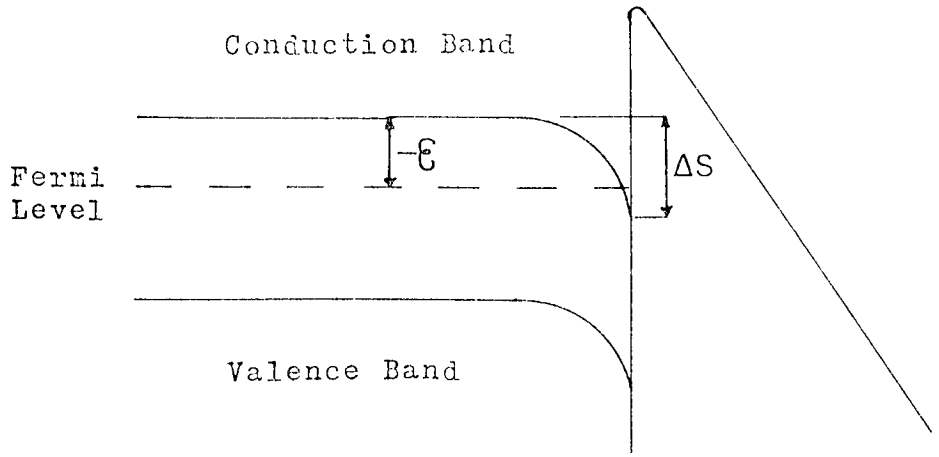

(b) DEGENERATE - HIGHER FIELD

Fig.2.8 Bending of the conduction band due to field penetration.

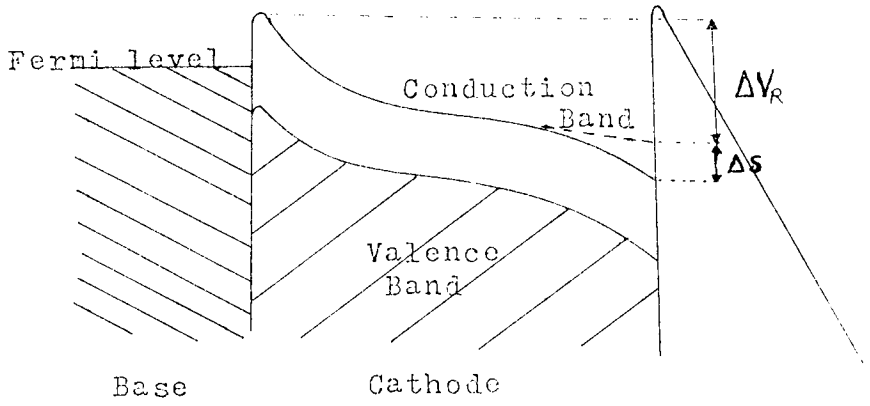

Fig. 2.9 Energy diagram for a semiconductor having an internal potential drop due to field penetration and the bulk resistivity.(14.)

In addition to the impurity levels in semiconductors, there may be localised electronic states associated with the surface with energies distributed in the band gap between the conduction and valence bands. Such states may arise partly in consequence of the discontinuity in periodic potential at the surface, as suggested by Tamm[12.] and Shockley,[13.] or in part from impurity atoms, oxide layers and structural imperfections at the surface. If charge (either electrons or holes) is situated in these surface states it will result in electrostatic fields penetrating into the solid, and thus a varying electrostatic potential on passing from the surface to the interior. This varying potential distorts the band structure of the bulk solid and an example of band bending due to the presence of surface states is illustrated in Fig. 2.10. The particular case illustrated in this figure is for an n-type semiconductor having a substantial number of acceptor-type surface states (which are charged when occupied and neutral when empty). At absolute zero electrons from the conduction band or from the donor level will fill up the surface states to the Fermi level creating a layer of negative charge at the surface which repels electrons within the conduction band of the semiconductor from the surface and which, therefore, leaves a positive surface space charge layer arising from uncompensated donor ions. The result will be a strong electric field

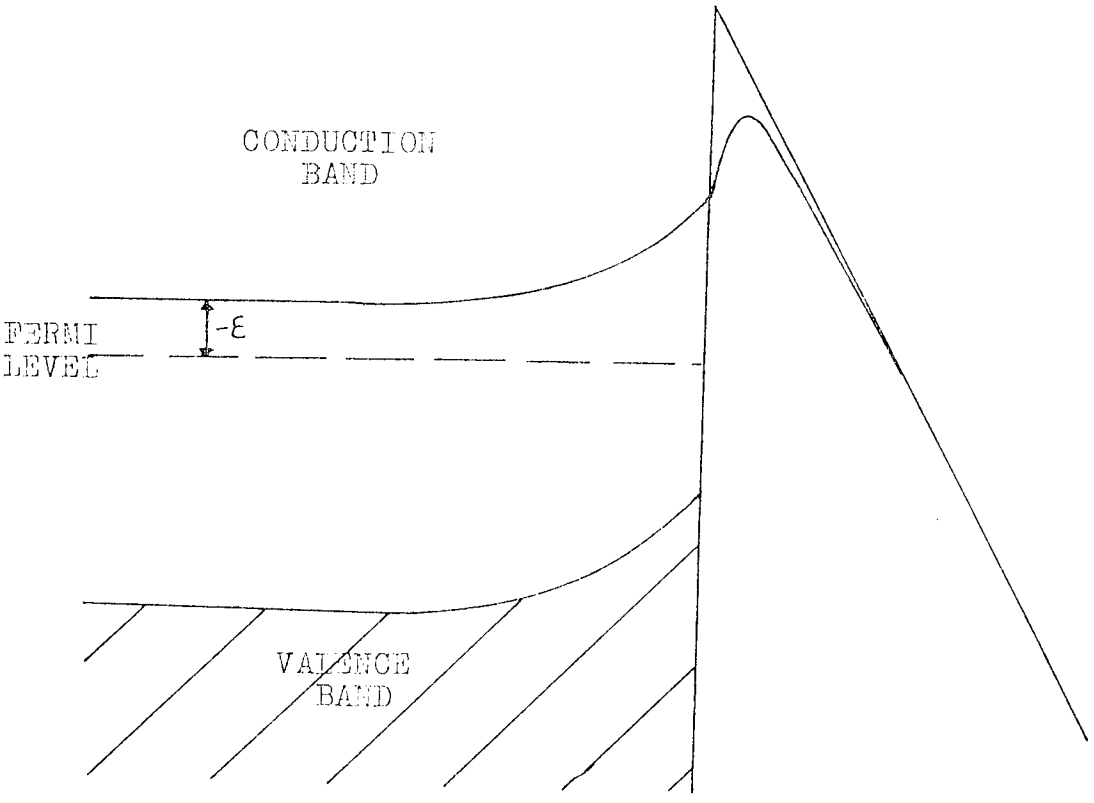

Fig. 2.10 The effect of surface states on the band structure of a semiconductor.

directed towards the surface so as to oppose the flow of more electrons into the surface states so that the energy of the surface is raised with respect to the bulk material as shown in Fig. 2.10.

2.4 Current Density and Energy Distribution of Electrons Field Emitted from Semiconductors

In 1955 Stratton[14] published the first extensive paper on the theory of field emission from semiconductors. He assumed a Fowler-Nordheim type of barrier at the surface and modified the transmission probability to include the dielectric constant of the material. The barrier was then applied to different models of a semiconductor surface: with and without field penetration, and with and without surface states. Stratton showed that the presence of an appreciable number of surface states should give very low current densities until fields high enough to overcome the screening by charge in these states are applied. When this occurs, or if there are no surface states, the field will penetrate into the semiconductor and lead to a lowering of the conduction band edge. As the field increases, the increased electron population in the conduction band gives rise to a greatly enhanced emission not unlike that of a metal. This would result in curvature in a plot of the logarithm of current density versus the reciprocal of the external electric field (Fowler-Nordheim plot).

In 1962 Stratton[15.] published another paper on the theory of field emission from semiconductors which extended his previous work. He again used a Fowler-Nordheim barrier and produced expressions for the emitted current density from both the valence band and the conduction band which included effective electron mass corrections allowing for variation in band shapes. He also considered the effect of surface states in more detail but did not allow for the possibility of emission from such states. In general, the theory predicts that at low fields the emission will occur predominantly from the valence band and at high fields from the conduction band, both situations producing essentially linear Fowler-Nordheim plots. In the transition region between these extremes, the current will increase more rapidly with field as the conduction band population increases.

Theoretical total energy distributions of electrons emitted from a semiconductor conduction or valence band were plotted by Arthur,[16.] using expressions previously derived by Stratton,[17.] in an attempt to explain the experimental distributions he had obtained from germanium. Two separate cases were considered corresponding to a semiconductor with and without surface states. In the absence of surface states, penetration of the external field may cause the conduction band to bend until the edge is below the Fermi level, when it is known as being degenerate.

Arthur calculated that a field of 4.5×10^9 V/m at a germanium surface will bend the conduction band edge below the Fermi level by an amount $\int \simeq 0.3$V. He therefore plotted the energy distribution for emission from the conduction band for the degenerate cases of the conduction band edge lying at various values below the Fermi level. These distributions are reproduced in Fig. 2.11(a) where the normalised electron current per unit energy is plotted against electron energy. As can be seen from this figure, in the case of extreme band bending the distribution approaches the result found for metals.[18.] Distributions were also plotted by Arthur for the case where the external field is screened by charge residing in surface states so that the conduction band is nondegenerate. The energy distribution for emission from the conduction band and the valence band is reproduced in Fig 2.11(b) for the specific case of the conduction band edge lying 0.05V above the Fermi level, when the current densities from both bands are of comparable magnitude. In general, when the conduction band edge is at another position, only one peak in the distribution is expected to be observable since the emission from one band will completely dominate.

More recently, Modinos[19.] has proposed a theory which includes emission from surface states. Modinos was primarily concerned with low current density emission

(a)

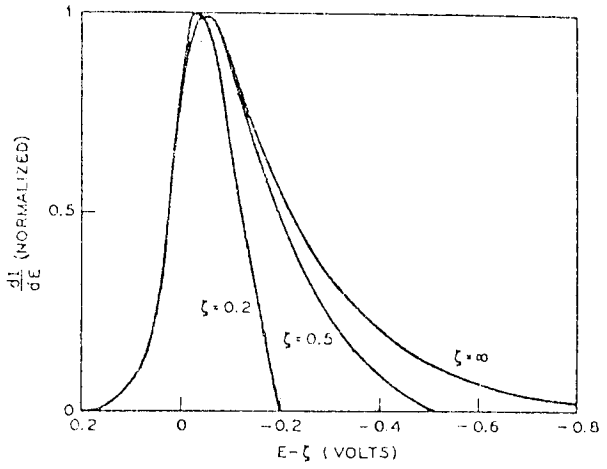

Theoretical energy distribution for emission from degenerate conduction band. $F = 4.5 \times 10^7$ V/cm.

(b)

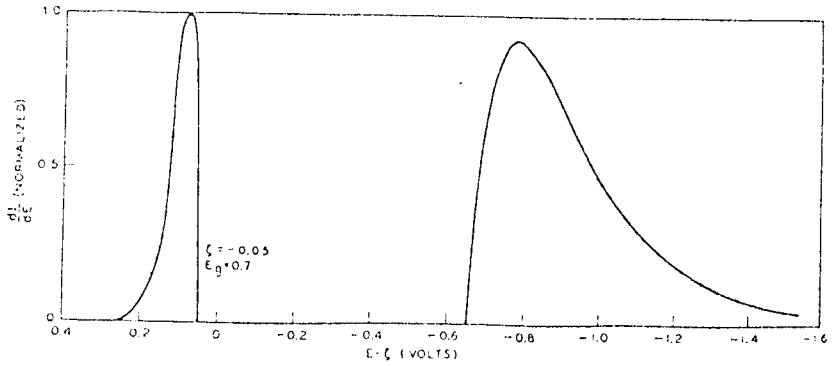

Theoretical energy distribution for emission from non-degenerate conduction band and valence band. $F = 4.5 \times 10^7$ V/cm.

Fig. 2.11 Theoretical energy spectra reproduced from work by Arthur (16).

from germanium and adopted a model for the surface states of a semiconductor originally proposed by Handler.[20.] The model assumes that a band of surface states exists in the region of the energy gap and overlaps with the valence and conduction bands. Stratton's expressions[15.] for nondegenerate conduction and valence band emission are modified by including the effect of surface state emission. Modinos calculated the total energy distributions corresponding to a p-type, intrinsic and an n-type semiconductor and these are shown in Fig. 2.12 for three different values of the applied external field. The calculations were based on parameters for germanium at 300K. The x-axis of the distributions correspond to the electron energy measured from the top of the valence band in the bulk of the specimen. From Fig. 2.12 it can be seen that the energy spectra for the p-type, the intrinsic and the n-type specimen are practically identical except for a displacement in the energy axis corresponding to the different position of the Fermi level. The theoretical prediction of Modinos's theory is that at low current densities ($< 10^2$ A cm^{-2}) most of the emitted electrons come from surface states and to a lesser degree from the valence band. At higher current densities ($\sim 10^3$ A cm^{-2}) emission from the conduction band is significant but still a small proportion of the total emission

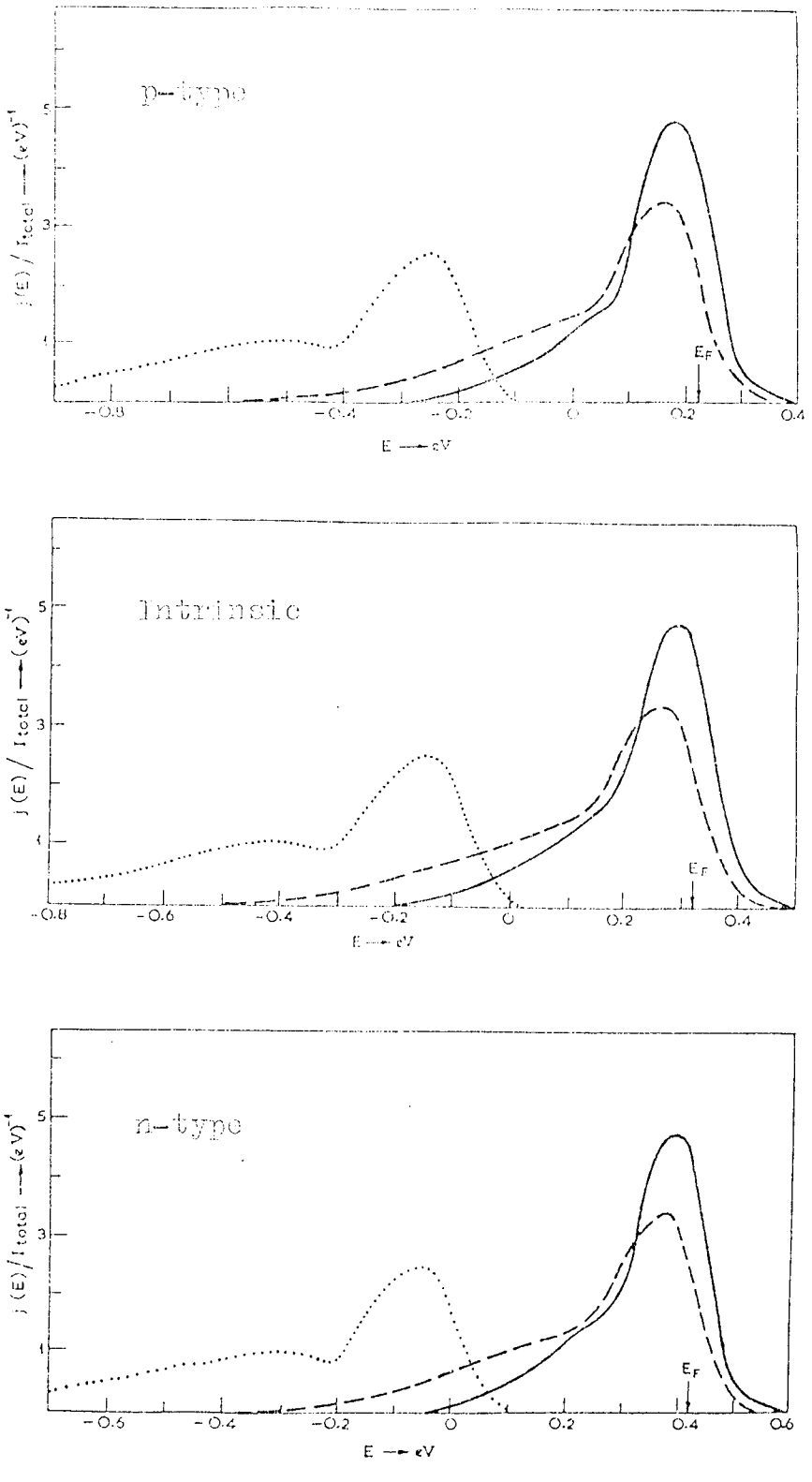

Fig. 2.12 Theoretical energy spectra according to Kodinos (19).

Values of applied field: solid line F=0.2 V/Å, broken line F=0.3 V/Å, dotted line F=0.4 V/Å.

current. At even higher current densities ($> 10^4$ A cm^{-2}) the conduction band becomes degenerate and the theory in its present state is no longer applicable. Referring to the shape of the total energy distributions in Fig. 2.12, the high energy peak corresponds to emission from surface states whilst a low energy peak (or a shoulder) arises from valence band emission. As the applied electric field increases the valence band contribution widens, to a lesser degree the high energy peak broadens, and the ratio of the high peak amplitude to the low peak amplitude decreases. One further feature that is of considerable interest is the shift of the total energy distribution towards lower energies for larger current densities (corresponding to higher applied fields). This displacement of the spectrum has been observed experimentally[21] but attributed to an internal resistive potential drop.

It will be appreciated that due to the added complexities of semiconductor band structures the theoretical explanations of the experimental observations of the emission process are not complete. There are, however, certain features characteristic of a semiconducting emission process which are significant to the present experimental observations and these will be resumed. As the magnitude of the applied external field is increased there are expected to be observable variations in the

energy spectra. There is a shift in the spectrum towards lower energies, a broadening of the distribution, the emergence of an additional peak, and a change in the relative predominance of the peaks.

CHAPTER 3

CARBON FIBRES

3.1 Physical Properties of High Modulus Carbon Fibres

3.1.1 History

Interest in carbon fibres and filaments extends back to before 1880 when Edison[22.] made carbon for an incandescent lamp. However, after the introduction of tungsten filament lamps in the early 1900s, research in filamentary carbons declined. In the 1950s the search for new materials for structural composites created a renewed interest in carbon fibres. Commercial carbon fibres were made first from rayon precursors in the late 1950s and later from polyacrylonitrile, lignin, and pitch fibres. A significant breakthrough in carbon fibres technology occurred in the 1960s when it was discovered that highly oriented, high modulus carbon fibres could be obtained by subjecting the precursor fibre to a continuous tensile stress during the high temperature treatment.[23-25]

3.1.2 Atomic Structure of a Graphite Crystal

There are two naturally occurring forms of crystalline carbon; diamond and graphite. Diamond is a very hard, transparent, electrical insulator, which has a characteristic cubic structure. Graphite in single crystal form has a metallic appearance and can be easily cleaved; it is an electrical conductor and is very much more anisotropic than diamond. The structure of graphite was orig-

inally determined by Bernal[26.] to be a closely packed hexagonal layer structure having a separation of 141.5pm. The atoms in the layers are covalently bonded, but the bonds between the layers are of the weak van der Waals type. The interlayer spacing is, therefore, very large having a minimum separation of 335.4pm. The layers are stacked in a hexagonal ABA sequence, as shown in Fig. 3.1. The hexagonal unit cell has a height of 670.8pm and an edge dimension of 246pm. The layer structure of graphite explains many of the peculiar features of the material, and in particular why orientation in polycrystalline graphite is so important. The crystal is extremely anisotropic: Young's modulus measured parallel to the layer planes is 1020GN/m^2, while measured perpendicularly, it is 36.3GN/m^2 [27.] An ideal carbon fibre would, therefore, have the individual crystallites oriented within their layer planes parallel to the fibre axis.

Many carbons have an imperfect form of graphite structure which is essentially two dimensional, lacking a regular stacking sequence of the layer planes. This type of graphite is known as turbostratic graphite.[28.] It has a fixed interlayer spacing and the atomic packing within the layers is identical to the single crystal. The lack of three dimensional order is due to the layers

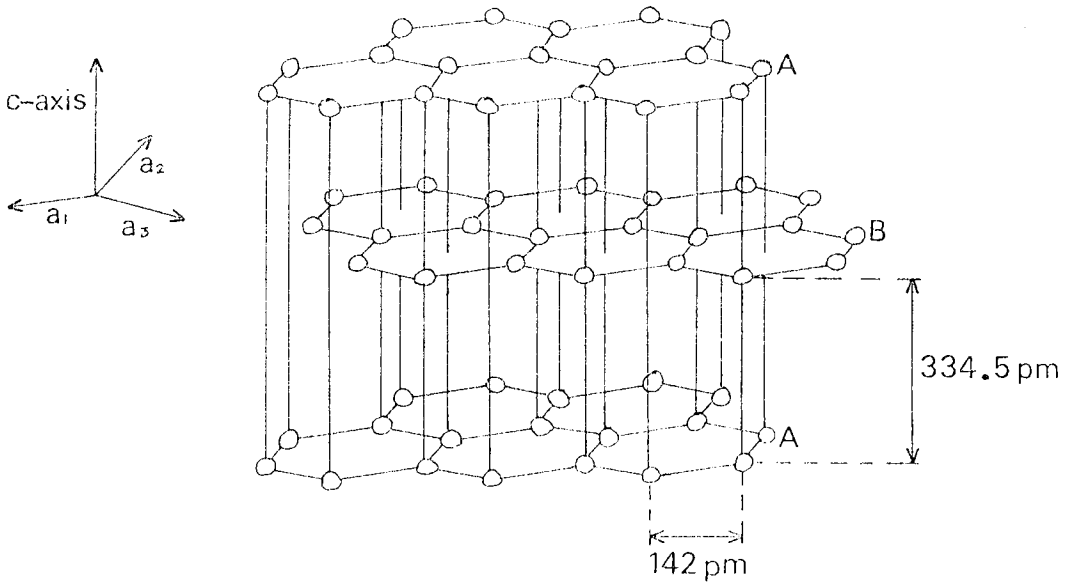

Fig. 3.1 Graphite Lattice.

having a random stacking sequence, with neighbouring layers rotated out of register with each other about the crystal c-axis. This rotational disorder increases the spacing of the layers from 335.4pm (for a perfect crystal) to a minimum value of 344pm.

Carbons are generally classified according to their ability to form a three dimensional graphite lattice with an interlayer spacing of 335.4pm. If they do this, they are termed graphitising, or alternatively, soft carbons. Carbons which do not form three dimensional order for normal graphitising heat treatments are termed non-graphitising, or alternatively, hard carbons.

3.1.3 Chemistry and Production Process

Carbon fibres are manufactured from a precursor of organic fibre, such as rayon, polyacrylonitrile or pitch. The most commonly used precursor today is polyacrylonitrile. Polyacrylonitrile fibres for conversion to carbon fibres are produced as tows containing approximately ten thousand individual fibres. Conversion of the precursor to carbon fibre is completed in two main stages, oxidation and carbonisation. The oxidation stage provides cross-linking of the polymer chains in order to prevent the fibres melting during carbonisation.

Tows of polyacrylonitrile fibres are wound onto frames

to restrain shrinkage and are heated to 220°C in an air oven, when they turn black. The molecular structure is changed from a linear polymer to an oxidised ladder polymer. This latter structure is approximately parallel to the fibre axis and may be regarded as the template for the formation of the oriented carbon fibre. After removing the fibres from the frames they are carbonised to 1000°C in an inert atmosphere and heated to temperatures between 1500 and 3000°C. During the carbonisation process intermolecular reactions occur resulting in crosslinking and elimination of hydrogen, oxygen and nitrogen. The final heat-treatment temperature depends on the required Young's modulus of the fibres.

3.1.4 The Structure of Carbon Fibres

A great deal of work has centred on determining the microstructure and texture of carbon fibres by using the analytical techniques of x-ray diffraction, electron diffraction, electron microscopy and optical microscopy. Various models for the structure of carbon fibre have been proposed, the most notable being due to Johnson and Tyson,[29] and Ruland.[30] Analysis of x-ray diffraction data is most easily achieved using the model of Johnson and Tyson, which is based upon discrete crystalline building blocks. Very high resolution transmission electron microscopy, however, has shown that high modulus carbon fibre has a continuous

ribbon-like structure. The following description of the structural features of carbon fibre is, therefore, based on the model which was originally proposed by Ruland[30] and is depicted in Fig. 3.2.

The carbon atoms form two-dimensional hexagonal layers in the form of long winding ribbons having a width of about 6nm and a length greater than 200nm.[31] The ribbons are stacked above each other forming structural units, which are termed microfibrils. The microfibrils are preferentially oriented parallel to the fibre axis so that the parallel stacking of the layers is preferentially perpendicular to the fibre axis. The orientation of the carbon layers improves with increasing heat treatment temperature and stretching, so that for high modulus fibres (as used in the present work) the layers are relatively straight in the longitudinal direction (as shown schematically in Fig 3.3.) The orientation of the two-dimensional hexagonal structure of the layers with respect to the layer normals is random, and the separation of layers is 344pm, i.e. the layers are turbostratic. The bending and twisting of the microfibrils results in voids which are determined by the shape and orientation of the microfibrils. The voids constitute a system of micropores which are long (greater than 300nm)

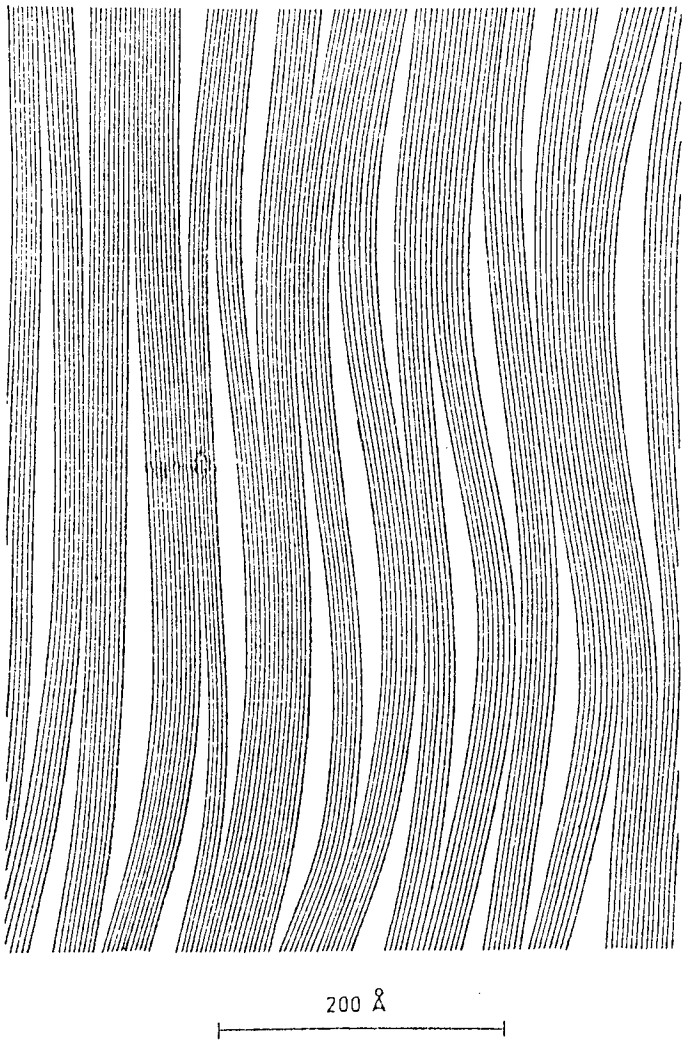

Fig. 3.2 Schematic representation of the ribbon type structure of high modulus carbon fibres.

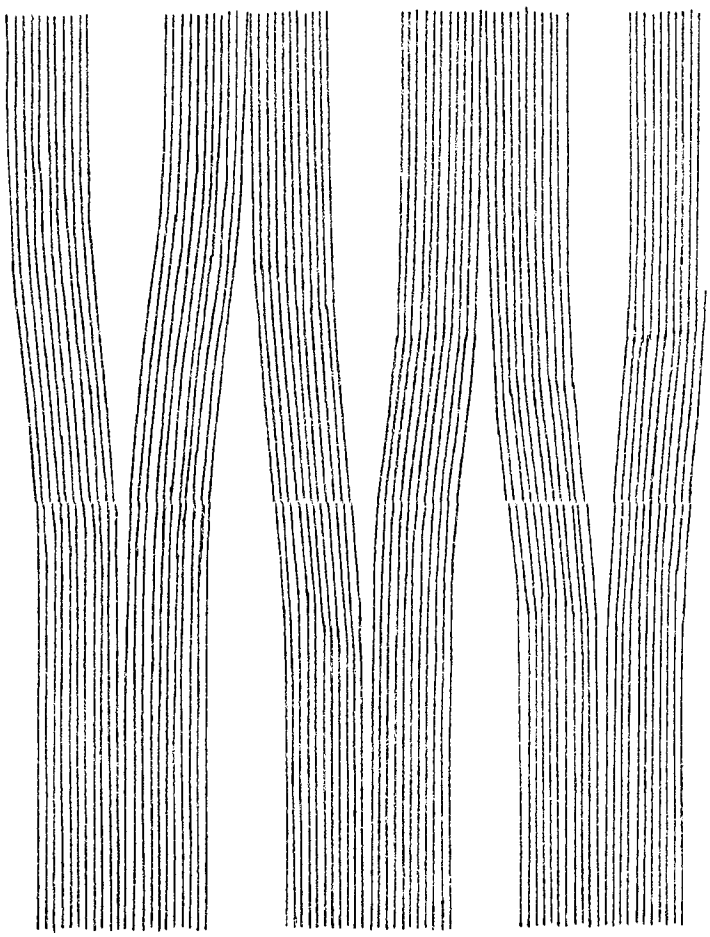

Fig. 3.3 The layers for high modulus carbon fibres are relatively straight in the longitudinal direction.

and narrow (average cross-section about 1.5nm).[32.] The pores possess the same preferred orientation as the microfibrils because they are bounded by the larger planes of the microfibrils.

The cross-sectional structure of carbon fibre, as shown in Fig 3.4, consists of a concentric three-zone, skin-sheath-core structure[33.] originating in the oxidation of the precursor fibre before high temperature treatment.[34.] In high modulus fibres, the sheath has a thickness of approximately 1 μm and separates a core approximately 3 μm in diameter from an outer skin approximately 1.5 μm in thickness.[33.] The microfibrils in the skin are more highly aligned than in the remainder of the fibre. The proposed orientation of the graphitic layers about the fibre axis is concentric in the skin, radial in the sheath and random in the core.[35.] The skin has a continuously undulating crystalline structure, with the graphitic layers running parallel to both the fibre axis and the circumference. There is an interweaving of the microfibrils in the skin with pores and surface flaws also present. The sheath consists of radial crystalline webs, with the graphitic layers generally running parallel to both the fibre axis and the fibre radii. This radially oriented structure extends down the length

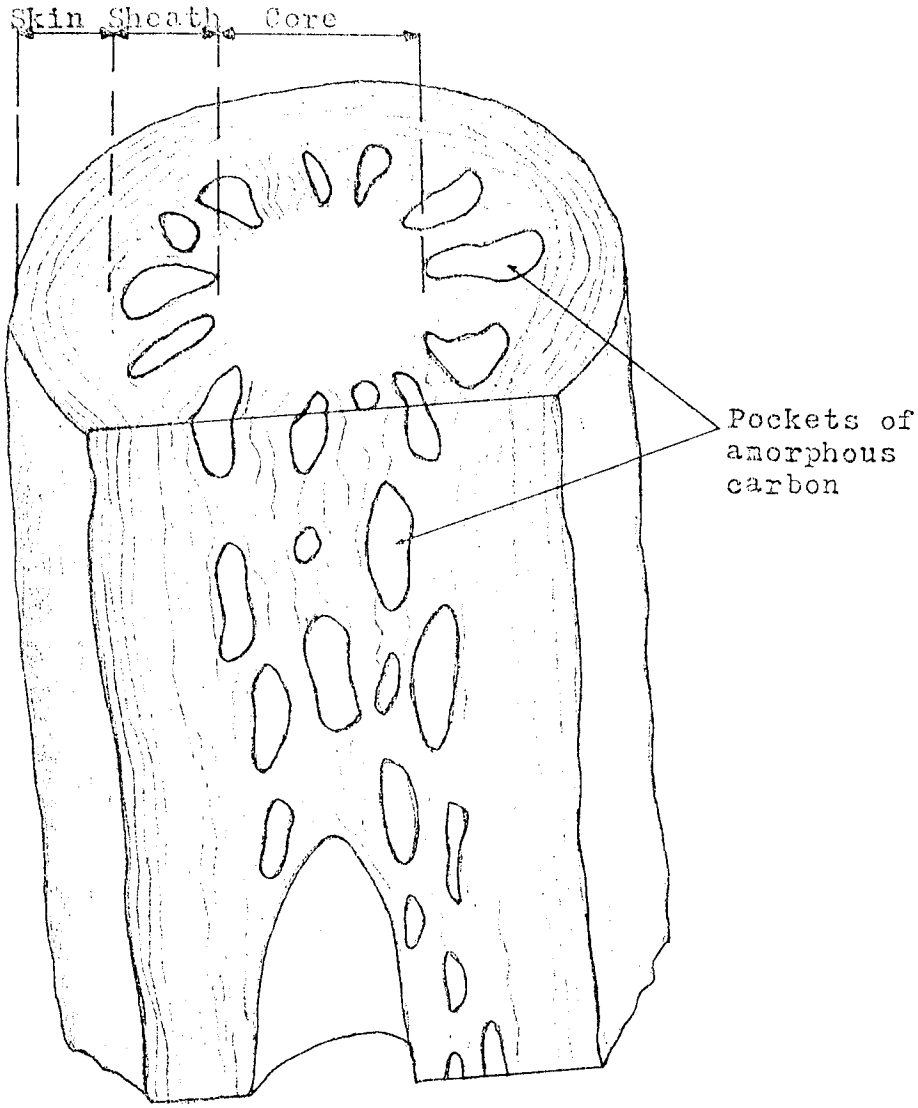

Fig. 3.4 Structural model for high modulus carbon fibre.

of the fibre and is honeycombed with numerous pockets of amorphous carbon, voids and cavities. The pockets of amorphous carbon vary randomly in size and shape but are aligned and elongated along the fibre axis. The pockets are surrounded by the crystalline radial webs. The amorphous areas, not including large flaws, constitute an average of 12% of the total fibre cross-sectional area with a spread of from 9 to 17%.[36]

3.1.5 Surface Studies

The presence of small quantities of chemical impurities in the surface of carbon fibre has been studied by high energy photoelectron spectroscopy[37,38] and by Auger electron spectroscopy.[39] The presence of oxygen, sulphur, chlorine and nitrogen was indicated. The concentration of oxygen is much larger at the surface than within the fibre; at a depth of 50nm no oxygen could be detected.[39] Silicon was also detected but only on the outermost layer of the surface and was thought to originate from surface treatment of the carbon fibres.

3.2 Previous Work on Field Emission from Carbon Fibres

The first recognition that carbon fibres could provide stable field emission in poor vacuum was due to Baker, et al.[6] in 1972. These workers were investigating

materials that would be suitable as field emitters in the pressure region 10^{-6} to 10^{-8} torr and after only limited success with silicon carbide whiskers turned to carbon fibres. The carbon fibres used were approximately seven micrometres in diameter and were mounted onto nickel tape with colloidal graphite (Aquadag). The fibres were then shaped into suitable emitter tips by controlled corona discharge in air and were subsequently found to emit in a vacuum of 10^{-3} torr, although at this pressure the emission was very noisy and the lifetime short. In the pressure range 10^{-7} to 10^{-8} torr, however, the lifetime of the emitters was found to exceed 2,400 hours for 10 μA emission current, which reduced to 500 hours at an emission current of 100 μA. Analysing the emission noise, they found it to be predominantly low frequency noise which diminished with increasing frequency and was negligible above 1000Hz. Baker, et al. also reported constructing a simple scanning electron microscope using a carbon fibre as the electron source. The microscope was operated with a pressure between 10^{-7} and 10^{-8} torr and had an initial resolution of better than 0.2 micrometres.

Following Baker's discovery of the potential advantages of using carbon fibre as a field emitter, Lea[40.] and later English, Lea and Liliburne[41.] made a prelimin-

ary assessment of the suitability of these fibres as an electron source. They used the high strength type of carbon fibre (Courtaulds HT - U), which was coated with tungsten (by the Fulmer Research Institute) and then electrolytically etched in a solution of IN potassium hydroxide. The tungsten coated carbon fibres were easier to handle and could be spot welded onto tungsten filaments, which enabled in situ heating of the tip. The emission pattern from such a fibre contained many small emission centres which were attributed to microspikes on the tip surface. The emission pattern, however, could be altered and by a combination of alternate heating in oxygen at 10^{-5} torr and in vacuum at 10^{-9} torr, a single emitting region was achieved. Emitters processed in this manner were reported to be fragile and consequently the emission current was limited to 5 μA which corresponded to an applied voltage of ∿2500 volts. The Fowler-Nordheim characteristics were investigated for the fibres and both the work function and the emitting area were found to be insensitive to the vacuum conditions. The fluctuations in emission current from a carbon fibre were compared with a tungsten emitter for a total current of about ½ μA. It was found that for an acceptably low level of noise from a tungsten emitter a vacuum of about 10^{-10} torr was required, whereas a carbon fibre emitter

possessed a similar noise level at 10^{-8} torr.

In 1974, Baker, et al.[42] reported further work on field emission from carbon fibres. They estimated that the conic half-angle of emission from their tips was between 30 and 45^{o} which may be compared with the value of 20^{o} for processed tips reported by Lea, et al.[41] Baker, et al. made the interesting observation that applying a voltage to a freshly prepared tip often resulted in a runaway phenomenon. Instead of the expected smooth increase in current with applied voltage, no current was obtained until a critical voltage was reached, at which point the current increased rapidly and uncontrollably, often resulting in the destruction of the tip. This difficulty was overcome by using a current limiting resistor of 100MΩ in series with the emitter and conditioning the tip by increasing the voltage until the emission current was in excess of the working current. They reported that the emission was noisy in the higher pressure region (above 5×10^{-7} torr) but could be slightly improved by heating the emitter or dramatically improved by the addition of a 100MΩ resistor in series with the emitter. Finally, they reported that carbon fibres had been mounted in three electron guns of conventional design which were then sealed into cathode ray tubes by a com-

mercial firm. All three tubes were reported to function, resulting in a spot diameter of 200 μm compared with 500 μm usually obtained from a conventional thermionic emitter. The displays, however, showed signs of flicker.

Further progress was made in 1975 by Braun, et al.[43] who measured the energy distribution of the electrons field emitted from a carbon fibre. The emitters were prepared by first electroplating one half of a short length of carbon fibre with copper and then electrolytically etching the other half in a solution of IN sodium hydroxide solution. The total emission current from these fibres was found to be reasonably stable for many days in a vacuum of 10^{-7} torr and short term fluctuations were of the order of ±3% of the current. The energy distribution of the emitted electrons was measured using a van Oostrom retarding potential analyser and the half width was found to be 210 ± 10 meV. In 1977, the energy distribution of electrons field emitted from carbon fibre was again reported by Heinrich, et al.[44] Four energy spectra of the emitted electrons after post-acceleration up to 30keV, in a vacuum of about 10^{-6} torr, were presented. In the case of very small emission currents (5×10^{-9}A) the half-width of the energy distribution was found to be 215meV. As the current was increased, however, the distributions

broadened and two or more maxima in the energy spectra were frequently observed in the current region between 10 and 100 nA. The presence of more than one peak was assumed to be caused by further emission sites being activated, by the increasing field strength, whose energy distributions are displaced against each other because of different surface potentials due to varied contamination. A further increase in the emission current to 10 μA resulted in half widths up to 1 eV. The broadening of the distribution was attributed to ion bombardment causing instabilities in the surface structure and to more than one emission centre contributing to the electron current.

Sangster,[45.] reporting on a field emission microwave amplifier, has briefly considered the possibility of using carbon fibre as the field emission cathode. This application requires a beam current of about 2mA which is not obtainable from the 7 μm diameter carbon fibres tested by Baker.[42.] Accordingly, Sangster et al.[46.] have investigated larger diameter fibres and multifibre arrays. It was found possible to extract a maximum emission current of 1mA from a single 11 μm diameter fibre and a maximum of 4.5mA from a 22 μm diameter fibre.

Faubel, et al.[47] have reported an electron bombardment ion source which uses carbon fibres as field emitters. Fibre bundles, approximately one millimetre in diameter, containing several thousand carbon fibres were used rather than a single fibre. The fibre bundles yielded currents of 1 - 5mA at an extraction voltage of 2 - 5 kV. At pressures below 10^{-6} torr the emission was stable within 1 - 3% and were found to be entirely insensitive to ion bombardment or spark discharges. It was also reported that a fibre bundle cathode had been in a vacuum region between 10^{-8} and 10^{-12} torr for more than 1000 hours without degradation.

CHAPTER 4

ELECTRON OPTICAL CONSIDERATIONS FOR THE APPLICATION OF A FIELD EMITTER TO A CATHODE RAY TUBE

4.1 Fundamental Limitations on Cathode Current Density

When high electron current densities are drawn from field emitters, various effects such as space charge, resistive heating and electron-electron interaction need to be considered. At high current densities, greater than about $6 \times 10^{10} Am^{-2}$, [48] the charge on the emitted electrons opposes the electric field and tends to reduce it. This space charge effect results in the current density increasing less rapidly than expected with applied voltage and can also increase the divergence of the electron beam. However, from the work of Swanson and Crouser[5] it seems that hundreds of microamperes may be drawn under constant current conditions before space charge effects become serious.

An upper limit on the current density which may be drawn from a given cathode is set by cathode resistive heating. Dyke and Trolan[49] found for tungsten emitters that at current densities higher than $10^{12} Am^{-2}$ the emitter temperature increases to a point at which surface material evaporates, is ionised rapidly in the electron beam and

becomes a plasma. This tends to neutralise the space charge and thereby to increase the electric field, the current density and the heating of the emitter. The end result of this cycle is a sudden surge of current (within 1 μs) which leads to a violent, low impedance vacuum arc which consumes emitter material and deforms the cathode. When extremely high current densities are required to be drawn from a field emitter, pulse techniques are used. Pulsing the emission current for times much less than the thermal time constant of the cathode tip permits a substantial increase in peak current.[48].

The effect of resistive heating can, however, be counteracted, under certain conditions, by the Nottingham effect.[50]. A stabilising cooling effect is provided by the energy exchange resulting from the difference between the average energy of the emitted electrons and that of the replacement electrons supplied from approximately the Fermi level of the bulk material. The average energy of the electrons emitted from the cathode apex is less than the Fermi energy if the cathode is cold, and greater than the Fermi energy at elevated cathode temperatures. The cathode temperature, therefore, tends to stabilise since the Nottingham effect is such that the cathode apex is heated if it is at a low temperature, and cooled if it is above an inversion temperature.

Boersch[51.] was the first to observe that in thermionic guns the Maxwellian energy distribution is broadened as the beam current is increased. This energy spread is generated by the Coulomb interaction between individual electrons in the electron beam, and has been analytically investigated by Loeffler.[52.] This investigation showed that high brightness electron guns will only have a low energy spread if their effective crossover is small. Fortunately, this is the case in a field emission gun and, therefore, an advantage of such a gun is the small energy spread of the beam.

It should further be noted that in electron optical instruments using continuous emission and having demountable ultra high vacuum systems, the emission is usually limited to about 10^9 Am^{-2} to ensure a reasonable cathode lifetime and stability under ion bombardment. Therefore, space charge effects and resistive heating are relatively unimportant during the majority of the cathode's lifetime. However, during operation of the cathode, the surface is roughened by sputtering and a vacuum arc may develop leading to the destruction of the emitter.

4.2 Conventional Design of a Cathode Ray Tube

The general form of a conventional cathode ray tube is illustrated in Fig. 4.1: but since, however, the design

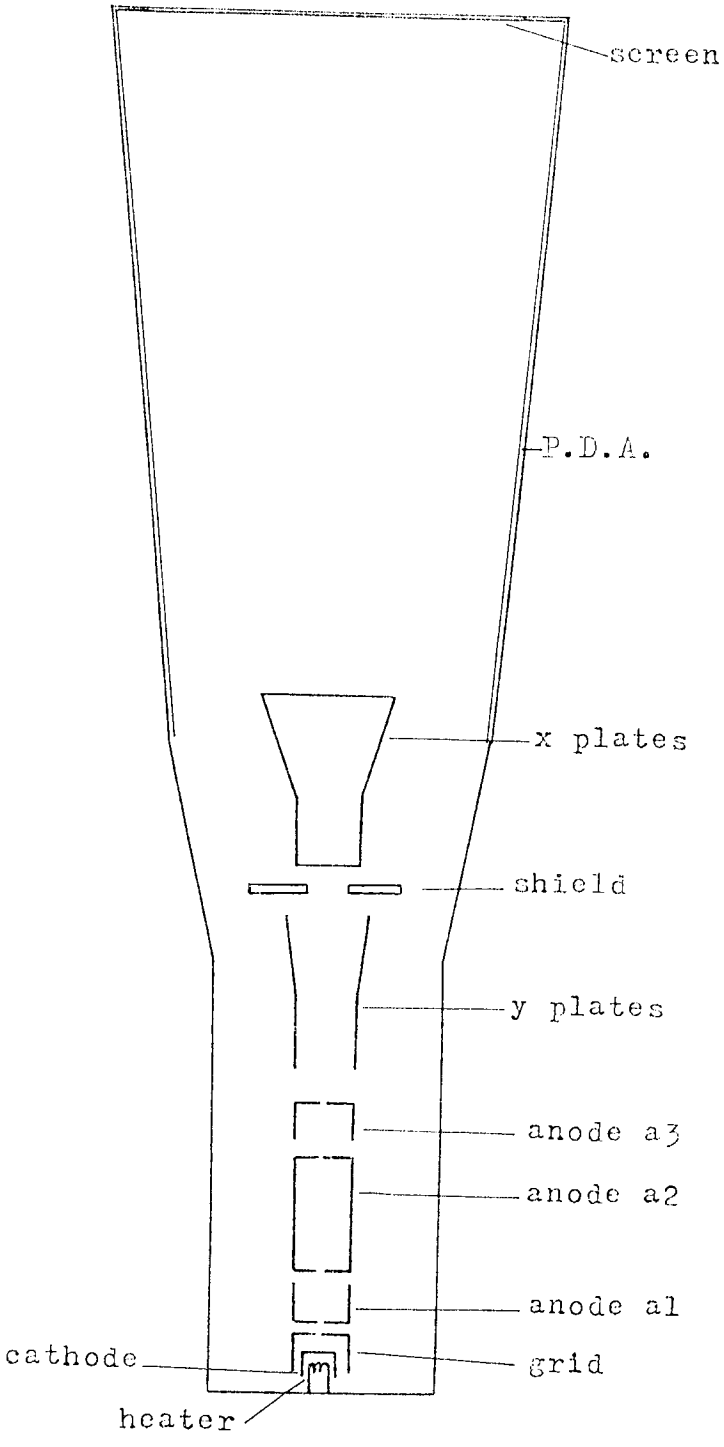

Fig. 4.1 Conventional cathode ray tube.

and construction are well documented[53-55] only a brief outline of the constituent parts will be presented here. The source of the electron beam is an indirectly heated oxide coated cathode, which consists of a nickel cap coated with barium and strontium oxides. Surrounding the cathode is another cylindrical electrode, concentric with it, and this is known as the grid. In front of the grid there is a series of three anodes. The grid is operated at a more negative potential than the cathode, while the first anode is operated several thousand volts more positive than the cathode. The electron trajectories cross at a section of the beam called the crossover which occurs between the grid and first anode. The final focussed spot on the tube screen is an image of the cross-over formed by the lens system of the second and third anode. Beyond the gun, the electron beam passes between two pairs of deflector plates arranged to deflect it independently along the vertical or horizontal axes of the face of the tube. In order to further accelerate the electron beam such that a brighter spot is produced on the phosphor screen, post-deflection acceleration is often used. This enables higher electron beam energies to be realised without drastically reducing the deflection sensitivity. In practice post-deflection accleration is usually achieved by coating the bulb with a graphite conducting band between

the plates and screen. This band is sometimes termed the post-deflection acceleration (P.D.A.) electrode or fourth anode.

4.3 Electron Optical Tube Distortions

Cathode ray tubes, in common with all other types of electron optical device, suffer from a number of aberrations. Chromatic aberration is present due to the differing energies of electrons emitted from the cathode. However, this type of aberration should be reduced when a field emitter is used as the cathode since the energy spread of the emitted electrons is relatively small (about 0.2 eV). A more important defect is due to spherical aberration of the focussing system, in which electrons at differing radial distances from the centre of the electron beam are brought to focus at different axial distances from the gun. A lack of symmetry in the focussing field through which the beam passes causes a distortion of of the spot known as astigmatism. Astigmatism can arise when the beam enters the field between the final anode and the deflector plates. The cathode ray tube should, therefore, be designed such that when the beam is undeflected all the deflector plates are at the same potential as the final anode. The interactions between the fields of the vertical and horizontal deflecting systems also gives rise to various distortions of the trace on the screen.

In cathode ray tubes there is an additional type of aberration, not found in light optics, which may occur through secondary electron emission.[56] This is due to the effect of secondary electrons being knocked out of the edges of apertures within the electron lens electrodes. The effect shows itself in a halo around an otherwise sharp image of the spot.

4.4 Review of Electron Guns Suitable for a Field Emission Cathode

The application of field emission cathodes as an electron source has centred on the electron microscope, and, in particular, on the scanning electron miscroscope. Although the requirements of such a device are not compatible with those of a cathode ray tube it is none the less instructive to examine the various designs of field emission electron gun that have previously been employed. The most significant example of this type of instrumental application of a field emission electron source has been developed by Crewe et al.[2,57,58] A simple scanning electron microscope was built [57] which used a field emission gun alone, without the aid of auxiliary lenses, and produced a focussed spot 10nm in diameter. A high resolution scanning transmission electron microscope was also built,[58] which used the same field emission gun in conjunction with a single demagnifying magnetic lens, and was capable of resolving 0.5 nm detail.

The field emission gun used by Crewe consisted of a (310) oriented tungsten cathode followed by a two electrode electrostatic lens. The first anode extracted the electrons from the tungsten tip while the second anode accelerated the electrons to the required beam energy; the position of the focus of the electron beam being determined by the voltage ratio on the two anodes. The shape of the anodes was chosen in order to minimise the spherical aberration of the electron gun and was based upon the computations of Butler.[59]. The lens used by Crewe is shown in Fig. 4.2 and consists of electrodes with complicated profiles which require a computer-controlled lathe for manufacture. This prompted Munro[60]. to perform a computer analysis of alternative electrode shapes, which led to a lens design (Fig. 4.3) with simpler electrodes than those of Crewe and, at the same time, improved optical properties.

The main disadvantage in the Crewe type of electron gun is the lack of flexibility inherent in the use of only two anodes. In electron microscopy it is desirable to maximise the electron current for any specified combination of electron beam voltage and probe diameter. In consequence the system magnification must be variable and the electron probe should have sufficient degrees of freedom to enable

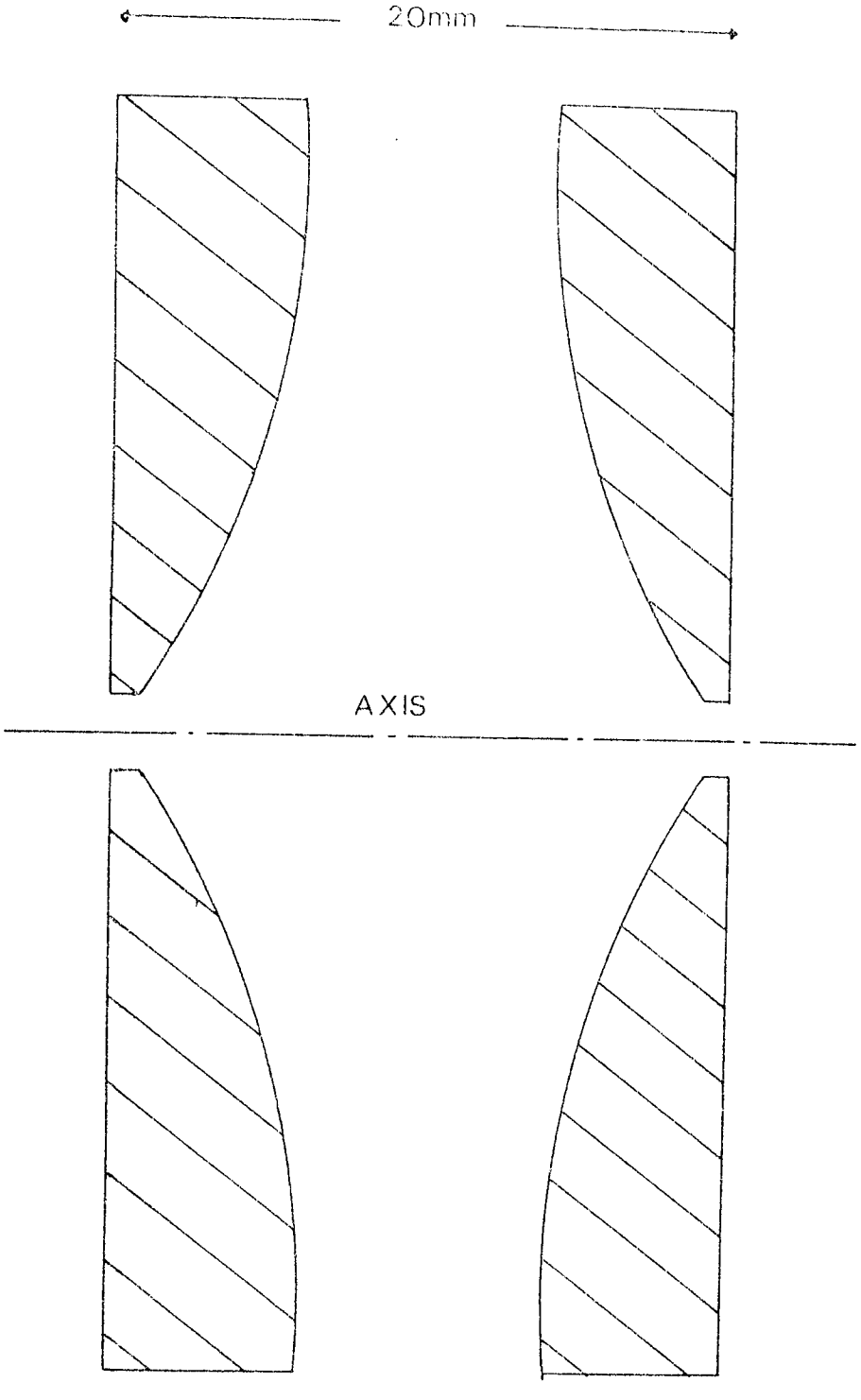

Fig. 4.2 Crewe lens.

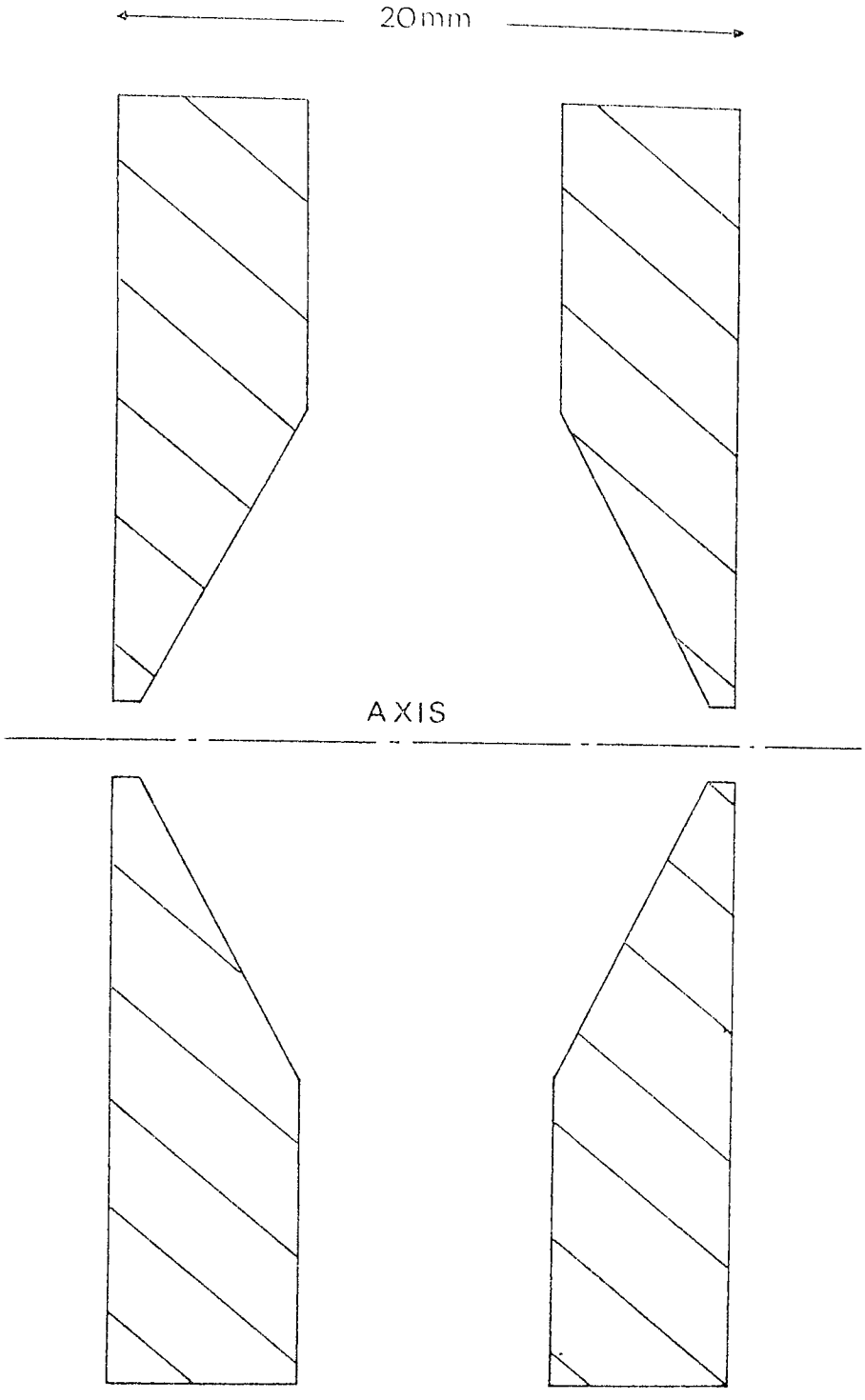

Fig. 4.3 Munro lens.

the cathode surface field, the electron beam current and the focus to be controlled independently. The Crewe type of gun can have an additional degree of freedom if the cathode tip dimensions are modified by surface diffusion at an elevated temperature,[61.] but this is undesirable since it is unnecessarily complicated and increases the likelihood of damage to the cathode surface. Alternative types of electron gun have, therefore, been designed and tested.

Kuroda et al.[62.] designed a three electrode electrostatic lens for use with a field emission scanning electron microscope. They found, as had Read[63.] earlier, that the focal length, and hence magnification, could be varied over a wide range without changing the distance between the tip and the first anode. They also found that low energy electron beams can be converged, whereas in the Crewe system they would be divergent.

Cleaver[64.] computed the properties of two types of field emission gun: the triode gun and the tetrode gun. The triode gun designed by Swann[65.] is shown in Fig. 4.4, and was used in conjunction with two magnetic lenses to form an electron beam which was suitable for use in a scanning electron microscope. A disadvantage of the triode gun is that because the acceleration of the electrons effectively occurs in one stage, electrons impinging on the anode surface liberate residual gas molecules, partially

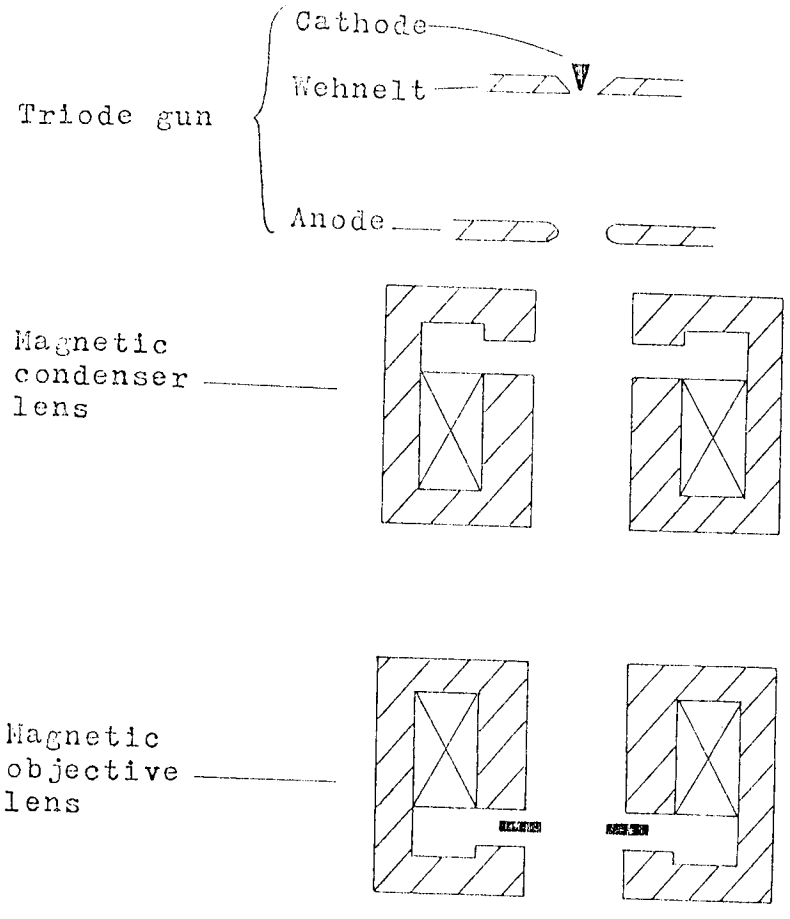

Fig. 4.4 Cleaver probe-forming system.

as ions, which leads tc the undesirable effects previously mentioned. In consequence Cleaver designed the tetrode gun, shown in Fig. 4.5, in which the acceleration of the electron beam occurs in two stages. It will be seen later, in Chapter 6, that the electron gun chosen for a field emission CRT was of this tetrode type. However, since there is no known previous work which considers the electron optics of using a field emitter in a CRT, as opposed to the different application of an electron microscope, it was decided to develop the tube in systematic stages and experimentally assess the performance at each stage. Therefore, before considering the design of such a tube in more detail, it is first necessary (in Chapter 5) to describe the experimental vacuum system which forms an electron optical testing facility.

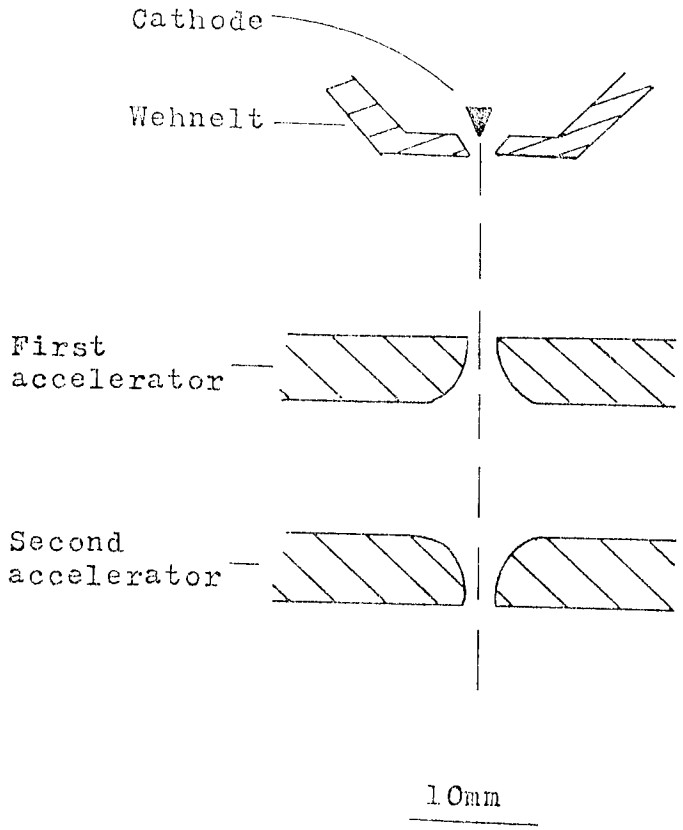

Fig. 4.5 Cleaver tetrode gun.

CHAPTER 5

DESIGN AND OPERATION OF AN ULTRA HIGH VACUUM SYSTEM AND SPECIMEN MANIPULATOR FOR THE DEVELOPMENT OF A PROTOTYPE CATHODE RAY TUBE

5.1 Introduction

A demountable ultra high vacuum system was designed and built that was suitable for the development and testing of a prototype cathode ray tube with a field emitter as the cathode. A general view of the experimental arrangement is shown in Fig. 5.1. The basic philosophy behind the design of the vacuum system was that it should be as simple as possible in order to arrive at a system which was reliable and easy to operate. The vacuum system was designed to be capable of achieving ultra high vacuum conditions (i.e. $\lesssim 10^{-9}$ torr), so that the pressure dependence of the known instabilities in emission from carbon fibres could be investigated, and also to provide sufficient flexibility for the potential investigation of other field emitter materials in the prototype cathode ray tube.

5.2 Vacuum Chamber

A photograph of the vacuum chamber and specimen manipulator is presented in Fig. 5.2. The vacuum system was designed to allow experimental investigations

rimental lay-ou

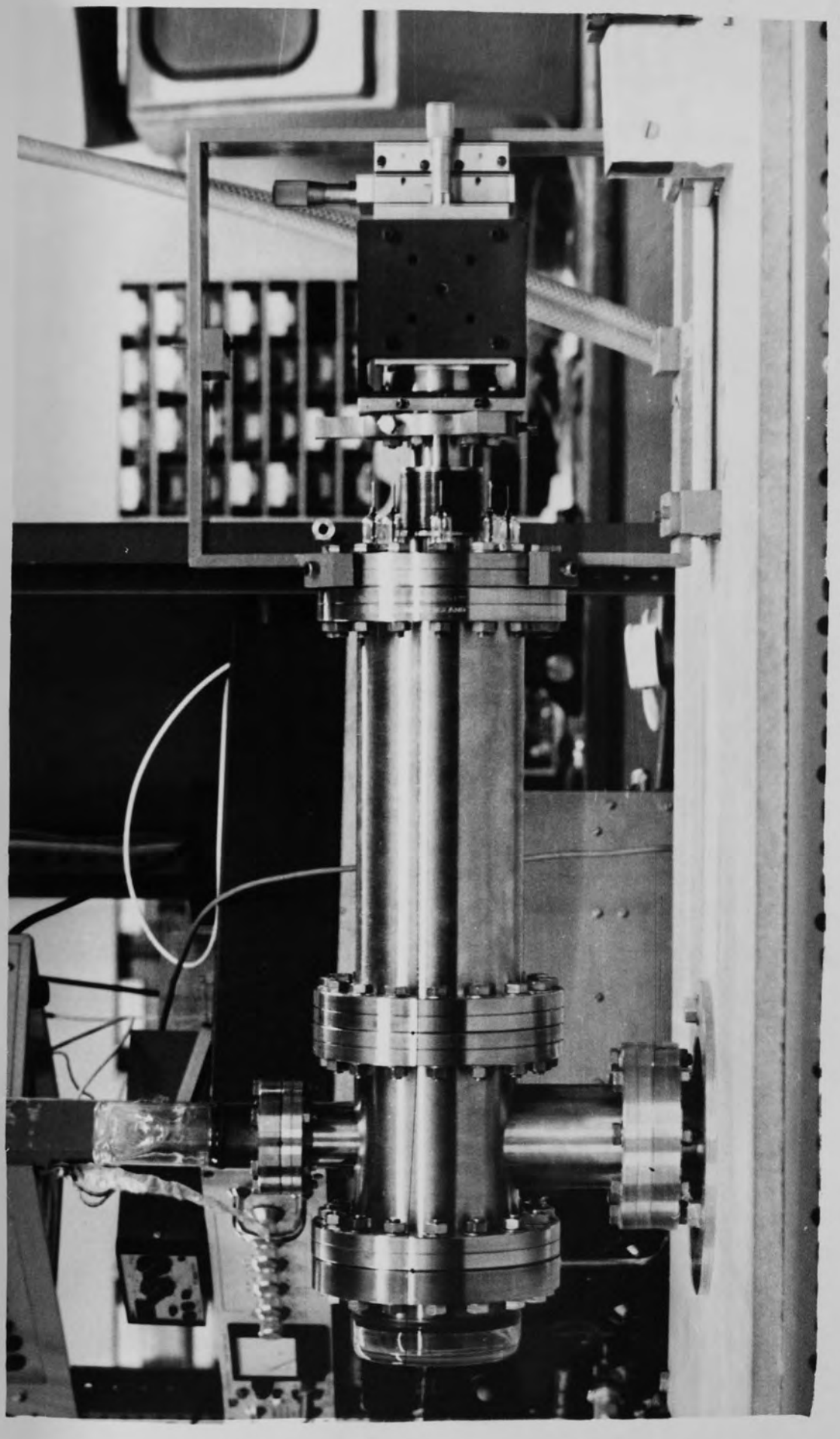

ıen manipulator.

at two separate stages in the development of the prototype cathode ray tube. The first stage was to examine the behaviour of a carbon fibre tip in a simple diode arrangement consisting of a field emitter and an extracting electrode. The configuration of vacuum components used at this stage is illustrated in Fig. 5.3(a) and comprised a four way manifold, a viewport and a specimen manipulator stage. The second stage in the development of the experimental instrument required an increase in the separation between the field emitter and phosphor screen, to allow the insertion of a complete electron gun and beam deflecting system, and was achieved by the addition of an extension tube to the existing vacuum components; as shown in Fig. 5.3(b).

The vacuum system is demountable with a vacuum seal being achieved by the use of copper gaskets. The four way manifold is constructed from stainless steel and its dimensions, which were determined by the factors listed below, are shown in Fig. 5.4 The 150mm outside diameter flanges were necessary for compatibility with the required dimensions of the viewport and specimen manipulator flange, the design of which will be considered later. The 114mm outside diameter rotatable flange was required to allow maximum conductance between the manifold and the diffusion pump. The 70mm outside

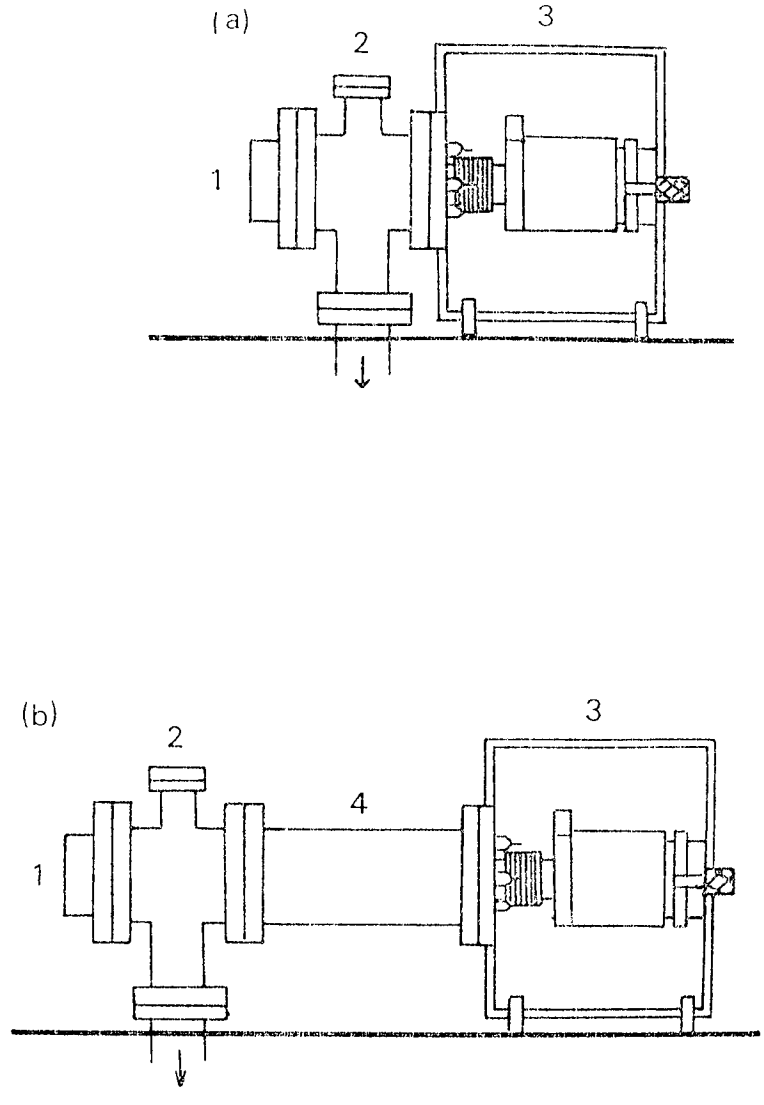

Fig. 5.3 Configuration of vacuum components.

(1) Viewport.

(2) Four way manifold.

(3) Specimen manipulator.

(4) Extension tube.

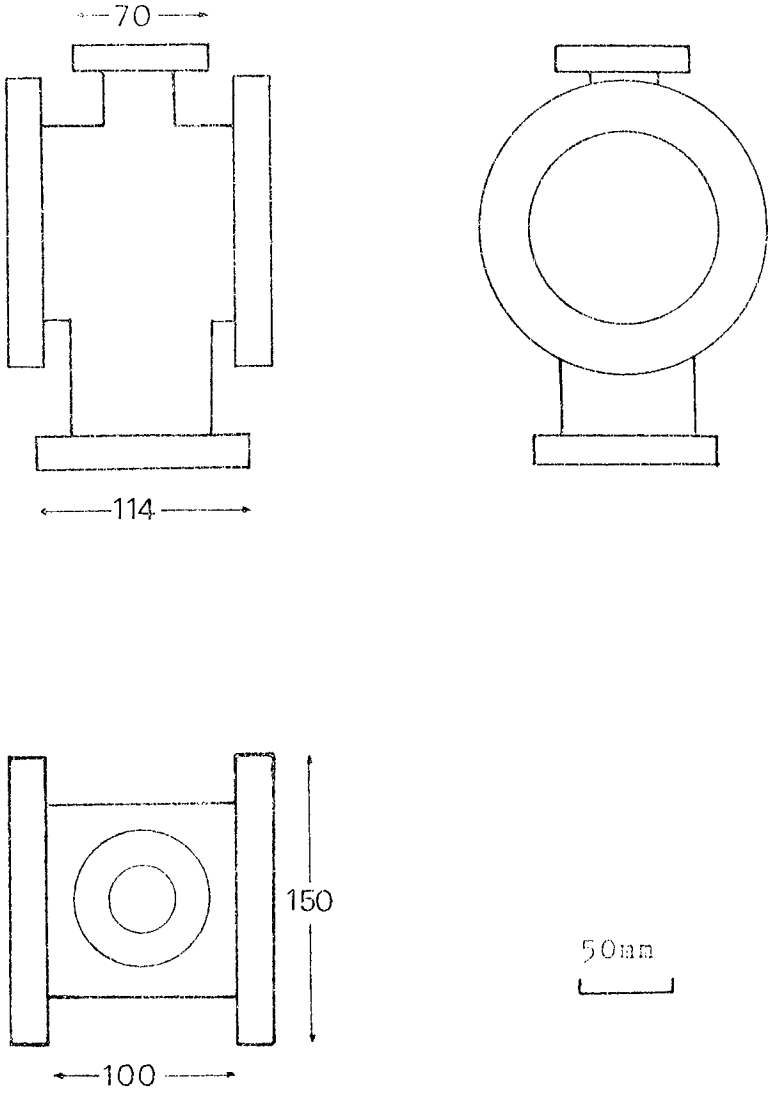

Fig. 5.4 Four way manifold.

Comprises four flanges, all with standard clearance holes and knife edge for mounting.

diameter flange was chosen as being the most suitable for adapting the experimental instrument to include additional components such as an ionisation gauge, a leak valve or a mass spectrometer head. The separation of the 150mm flanges was required to be as small as possible for the first stage of the experimental work and a distance of 100mm between flanges was chosen in order to retain easy access for a spanner to tighten the securing nuts and bolts.

The extension tube is a stainless steel tube with a fixed 150 mm outside diameter flange at one end and a rotatable 150mm flange at the other. The overall length of the extension tube is 260mm which was chosen such that when the complete electron gun (the development of which is described in the following chapter) is in position inside the vacuum chamber, there is a distance of 300mm from the second anode of the electrostatic lens to the phosphor screen: i.e. for compatibility with a conventional cathode ray tube.

5.3 Viewport and phosphor screen

An electrical connection to the phosphor screen was necessary in order to monitor the screen current, to dissipate the charge, and to apply a screen voltage. One method of achieving this electrical connection would be

to coat the face of a viewport with tin oxide and to insert an electrode through the glass. However, due to difficulties in ensuring a good electrical contact and because of the vulnerability of a glass viewport with a protruding pin, an alternative method was used. Referring to Fig. 5.5, this consisted of using a kodial viewport and mounting the screen internally. The screen comprised a pyrex disc, 80mm in diameter and 3mm thick, with an even coating of tin oxide to ensure good electrical conductivity and a relatively thin layer of type P31 phosphor. The screen was mounted in a specially shaped †Ceramtec holder and clamped in position by a small stainless steel plate, as shown in Fig. 5.5. The phosphor screen was, therefore, insulated from the earthed vacuum chamber by the Ceramtec seating allowing electrical connection to the screen via the stainless steel plate. The screen assembly was held in position inside the flange of the viewport by a sprung sheet of stainless steel.

5.4 Specimen Manipulator

A means of providing translation of a carbon fibre inside the vacuum system was required in order to allow accurate positioning of the fibre relative to the aperture in the extracting electrode of the electron gun.

†machinable ceramic

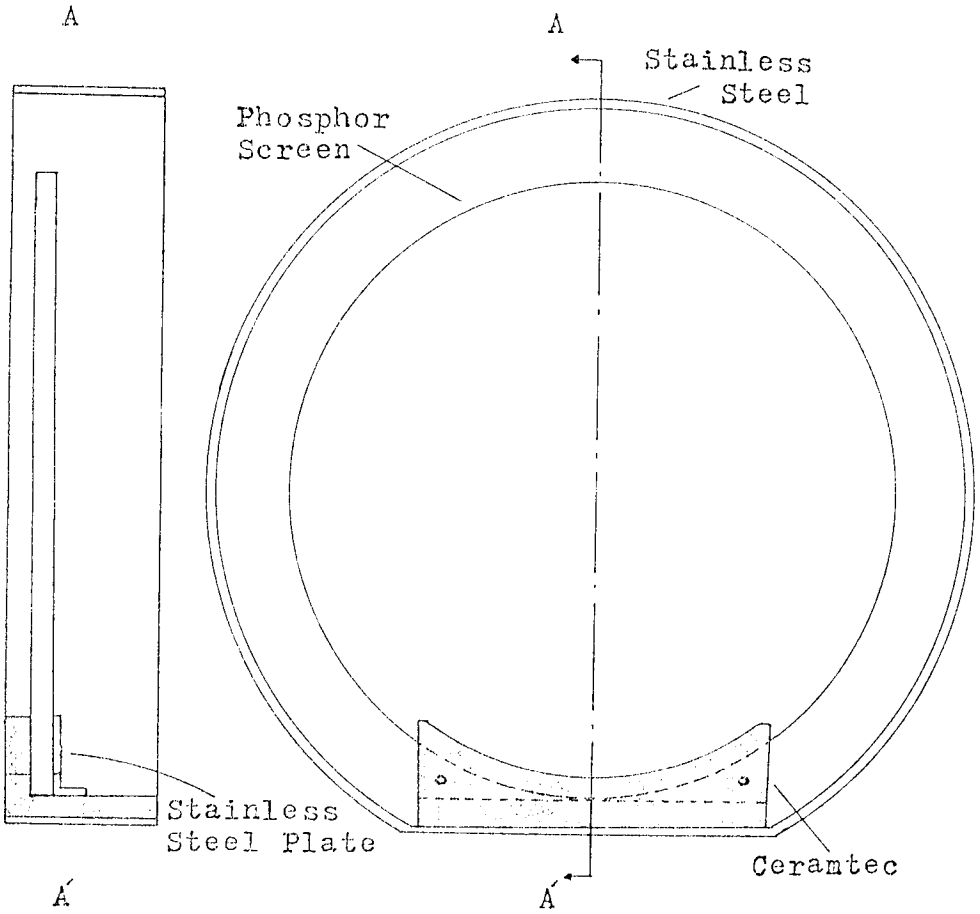

Fig. 5.5 Phosphor screen and holder.

The method chosen for achieving this manipulation, which had to fulfil the requirements of ultra high vacuum, was to utilise the flexibility of metal bellows. By restraining the movement of the bellows outside the vacuum to the three orthogonal directions, it was possible to transfer this motion to a fibre specimen holder inside the vacuum system. A photograph of the specimen manipulator is shown in Fig. 5.6. Precise translation of the metal bellows, and hence the carbon fibre, was provided by three micrometers which accurately positioned three carriages sliding within U-shaped frames mounted orthogonally to one another. The micrometer assembly was supported by a brass bridge which was connected to a 150mm flange.

The basis of the specimen manipulator stage is a two-flange bellows assembly, manufactured by Vacuum Generators to the author's specifications, which is shown in Fig. 5.7. The assembly uses a 150mm and 70mm outside diameter stainless steel flange interconnected with a stainless steel flexible metal bellows. The metal bellows has forty edge welded convolutions in order to provide sufficient manoeuvrability. The larger flange also contains eight electrical feedthoughs for connection with the various gun electrodes, deflector plates and phosphor screen. The electrical feed-

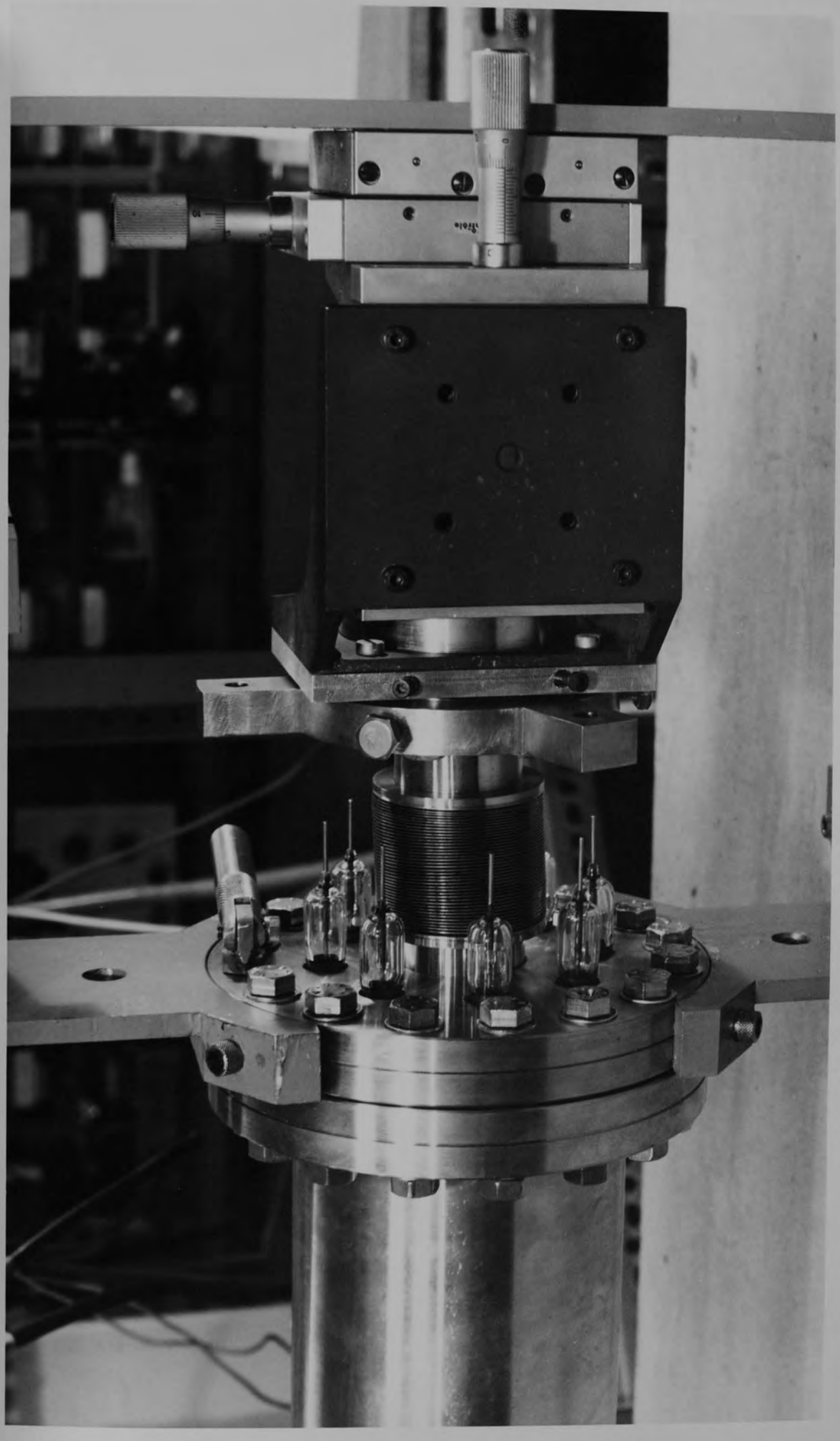

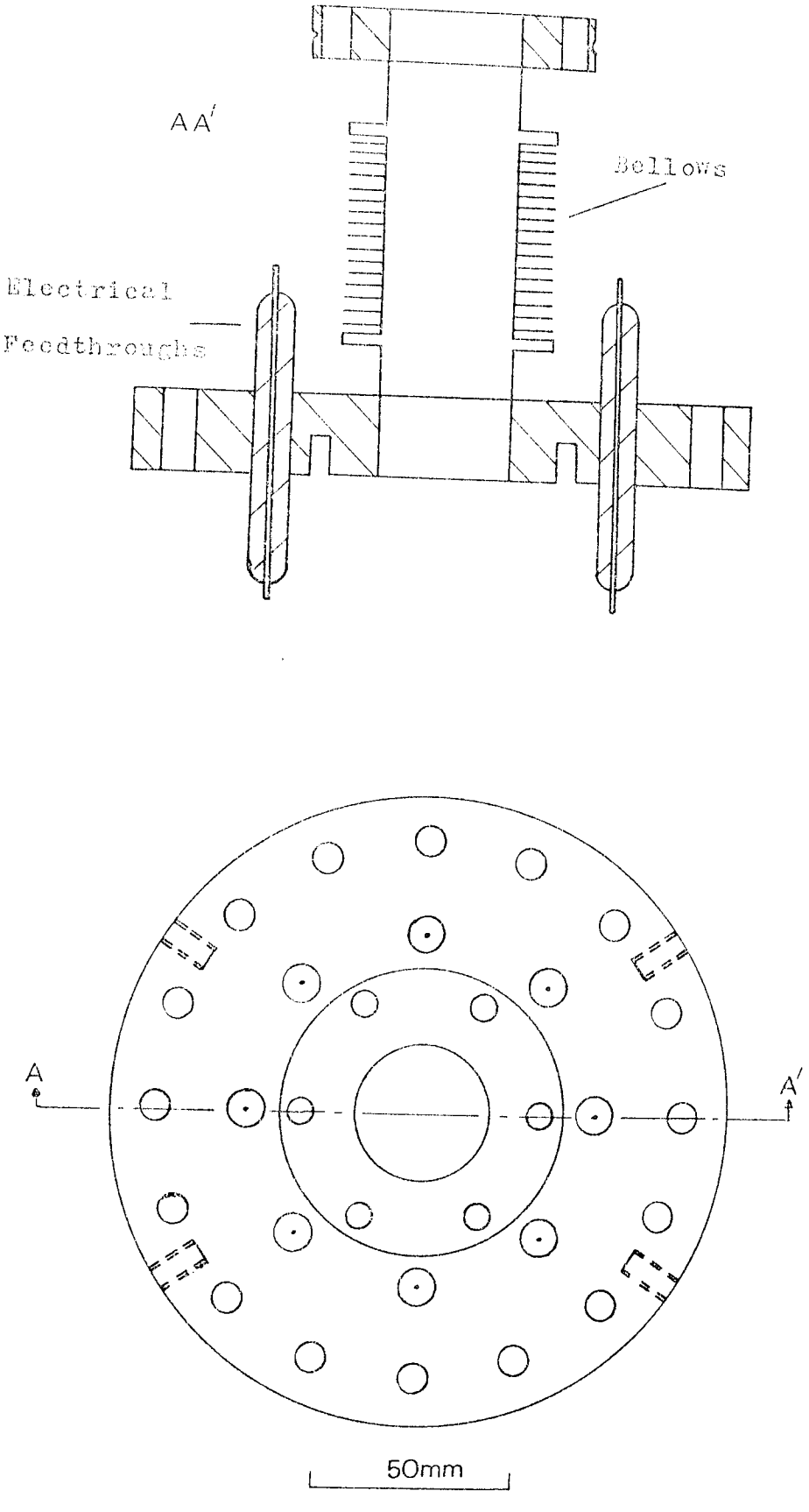

Fig. 5.7 Bellows assembly.

throughs are non-magnetic being constructed from pyrex with a molybdenum conductor and are rated as suitable up to a maximum of 15kV and 5A.

For a high temperature bake-out of the vacuum system, it is necessary to remove the micrometers (which are lubricated with oil) and the brass bridge (which has a different coefficient of thermal expansion to stainless steel) from the vacuum system. To facilitate this a V-shaped groove is provided in the smaller, 70mm, flange so that a tripod arrangement (Fig. 5.8) is able to clamp the two flanges together, thereby securing the bellows. The micrometer assembly and bridge may then be removed in unison, allowing the complete vacuum system to be baked to a high temperature (about 250^{o}C).

5.5 Specimen Holder

The specimen holder and the electrode assembly holder were both designed to be telescopic. The reasons for this were associated with the different experiments to be performed with the same holders. In the first few experiments a small tip-to-screen separation was required but in subsequent experiments, as more electrodes were added, the requirement was for a large separation. The specimen holder, shown in Fig. 5.9, consists of a small

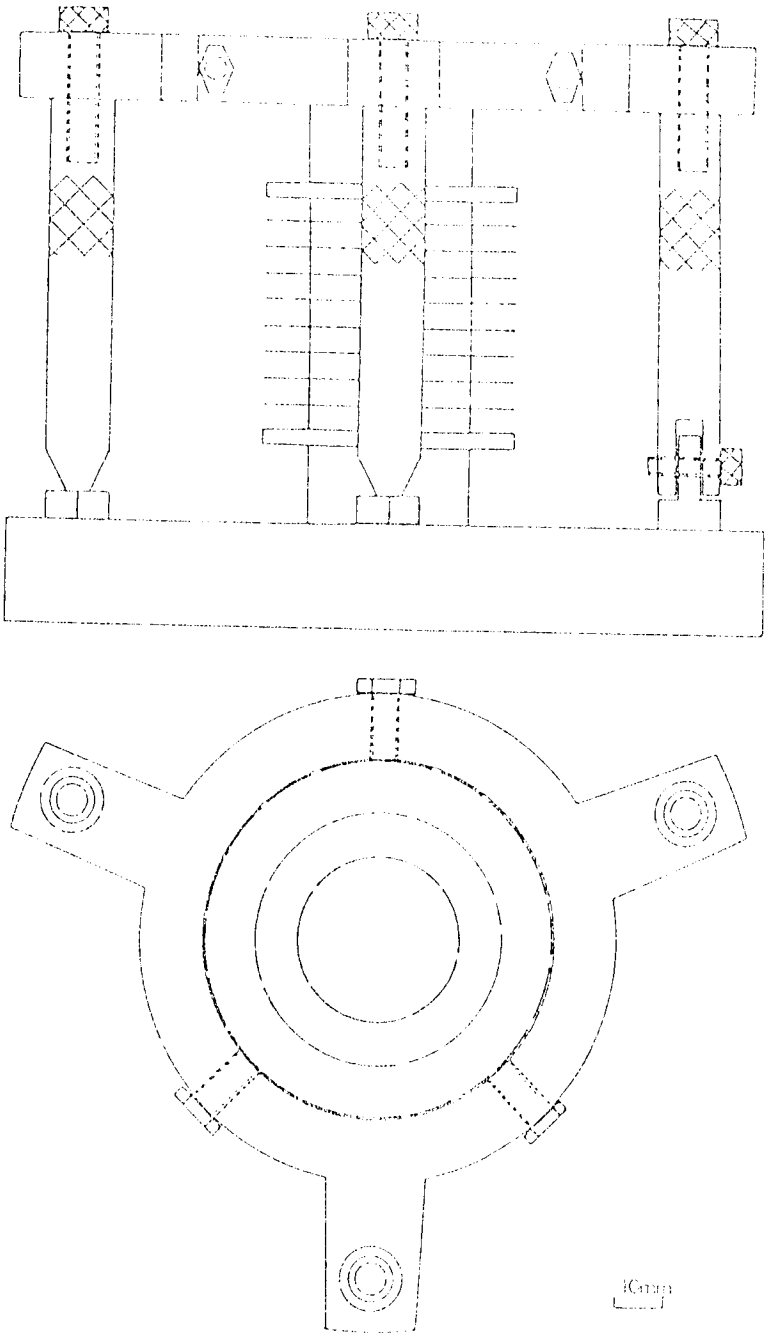

Fig. 5.8 Tripod clamp to enable bake-out.

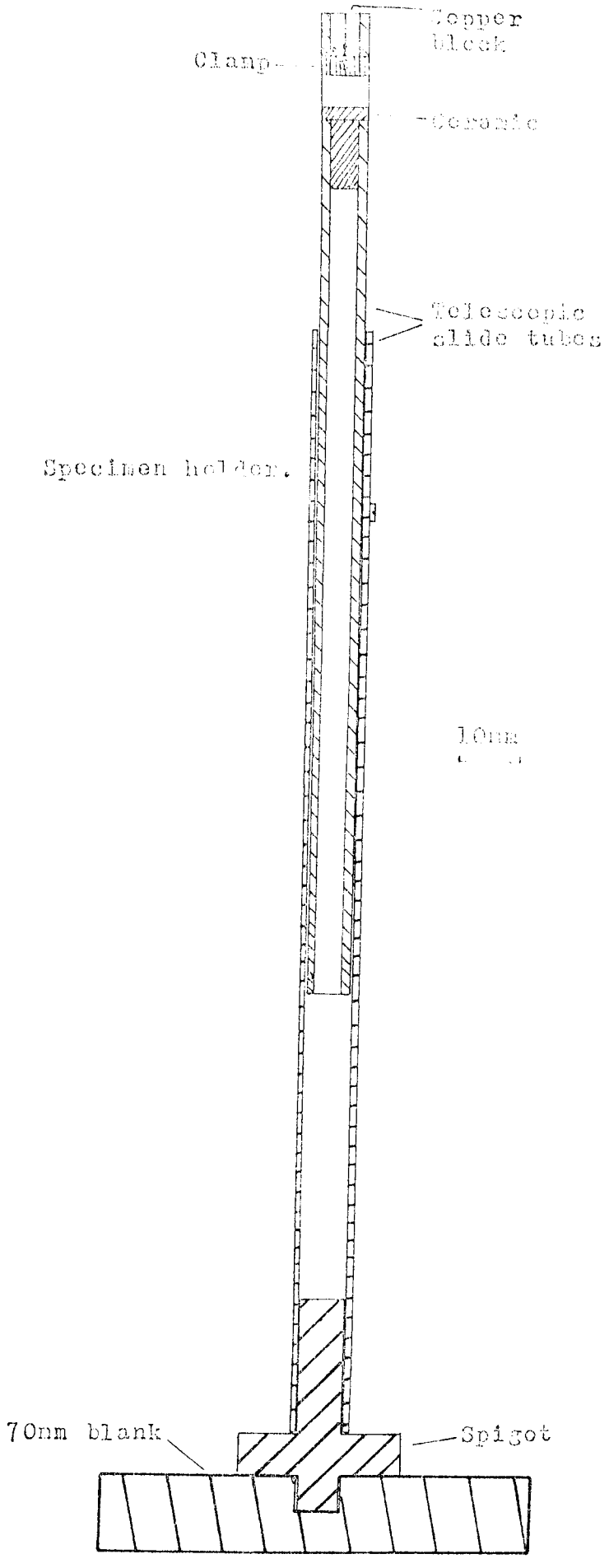

Fig. 2.9 Specimen holder.

copper block for holding the carbon fibre, and telescopic stainless steel slide tubes. The slide tubes are fixed onto a spigot which is screwed into a blind hole in a 70mm diameter stainless steel blank. The blank is bolted onto the small, 70mm diameter, flange of the two-flange bellows assembly, thus completing the vacuum seal. A carbon fibre mounted on the copper block, which is clamped at the other end of the telescopic tubes, may thus be translated inside the vacuum chamber by adjustment of the micrometer driven bellows.

The copper block, shown in Fig. 5.10, was designed to allow it to be interchangeable with a transmission electron microscope holder and the telescopic tubes used in the prototype cathode ray tube vacuum system. The copper block has a fine central slit into which a carbon fibre could be lowered. The fibre was securely mounted and a good electrical contact made by using a few drops of high conductivity silver paint. A small threaded hole was provided in the copper block so that a threaded rod could be inserted when handling of the fibre mount was necessary. The carbon fibre could thus be transferred between the various stages of electrolytic etching, electron microscopy of the tip profile and positioning in the vacuum chamber, without too high a risk of damage occurring to the fibre endform.

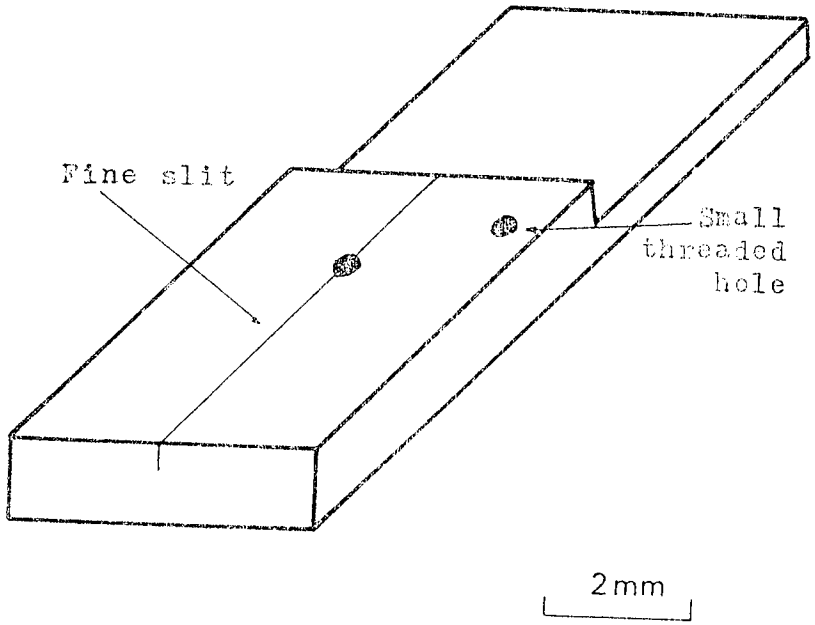

Fig. 5.10 Copper block.

5.6 Electrode Module

Before discussing the electrode assembly holder the method of mounting the electrodes will first be considered. The electrodes, which were made of an alloy of copper and nickel, were held at their required separation by four glass rods. The mounting of the electrodes into the glass rods was achieved by using the jigs and production techniques of the M-O Valve Company. When assembling the unit of electrodes, an additional dummy electrode was also provided. The dummy electrode, which was placed at the cathode end of the electrode assembly, contained a large aperture into which a hollow cylinder was spot-welded. The hollow cylinder provided a means of securing the electrode assembly inside the vacuum chamber.

The electrode assembly holder, shown in Fig. 5.11, whilst telescopic, is of relatively simple design. The holder consists of two concentric cylinders, with the outer cylinder welded to a small flange which may then be bolted to the large, 150mm diameter, flange of the two-flange bellows assembly. The hollow cylinder of the electrode assembly is then inserted into the holder enabling the electrodes to be secured inside the vacuum system and concentric with the chamber. The photograph

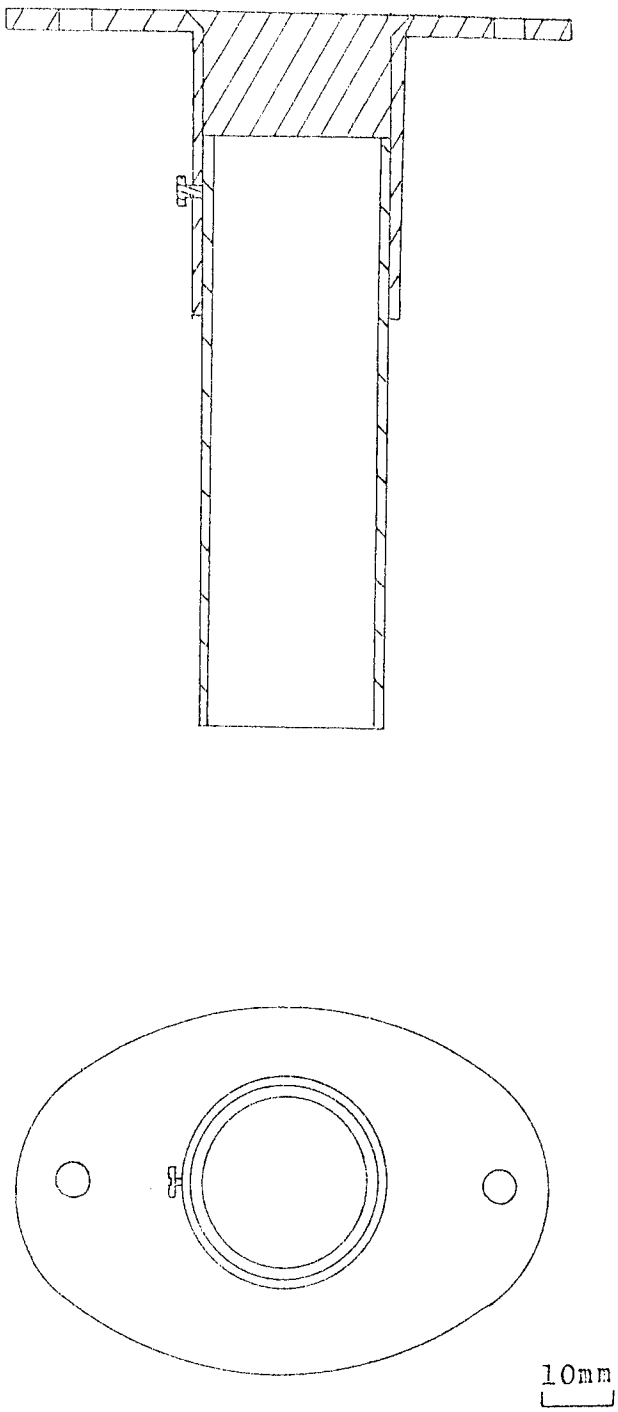

Fig. 5.11 Electrode assembly holder.

of Fig. 5.12 shows the specimen holder and the electrode assembly holder in use.

5.7 Pumping System

A schematic representation of the main pumping system is given in Fig. 5.13. The vacuum system is pumped by an Edwards water cooled, oil diffusion pump, type EO2. The oil used in the diffusion pump is Santovac 5 which has a critical backing pressure of ~ 0.3 torr which is provided by an Edwards two stage rotary pump, type ED50. A liquid nitrogen cooled trap and a water cooled baffle are situated between the diffusion pump and the vacuum chamber to reduce the backstreaming of oil vapour to negligible proportions. The water cooled baffle acts as a primary baffle, eliminating gross backstreaming of oil, so that there is no "line of sight" from the pump orifice to the main liquid nitrogen cooled baffle. The liquid nitrogen cooled trap also cryogenically pumps water vapour which is the main outgassing load from an unbaked system. The time taken for the two litre charge of liquid nitrogen to boil away from this trap is about sixteen hours. A sorption foreline trap is situated in the backing line to eliminate backstreaming of water vapour and oil vapour from the rotary pump. Provision is made for the regeneration of sorbent material by baking in situ.

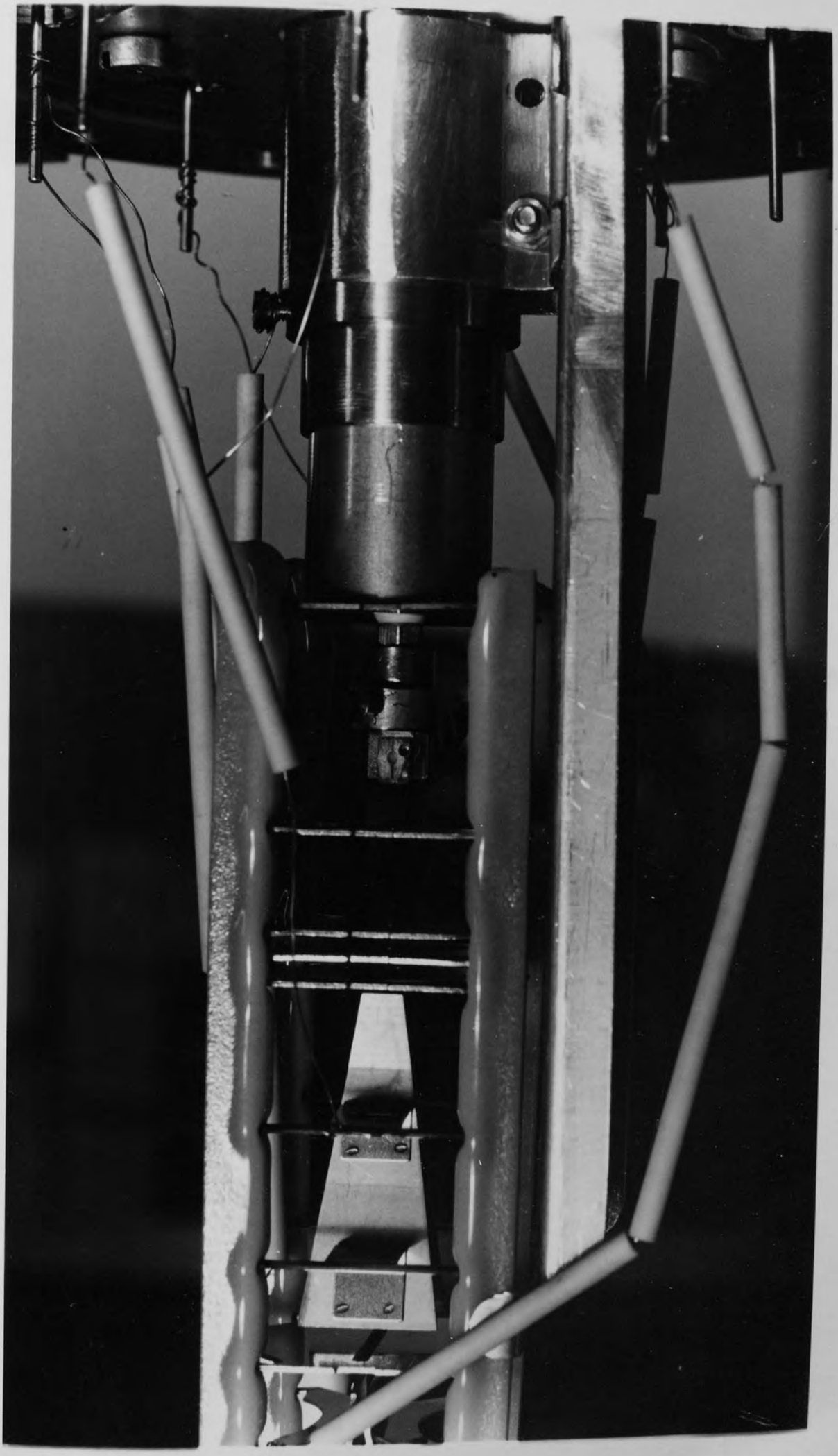

Fig. 5.13 Pumping system.

(1) Vacuum chamber.

(2) Liquid nitrogen trap.

(3) Water cooled baffle.

(4) Oil diffusion pump.

(5) Vacuum switch.

(6) Air admittance valve.

(7) Valve.

(8) Pirani gauge.

(9) Leak valve.

(10) Flexible bellows to reduce vibration.

(11) Sorption foreline trap.

(12) Isolation/air admittance valve.

(13) Rotary pump.

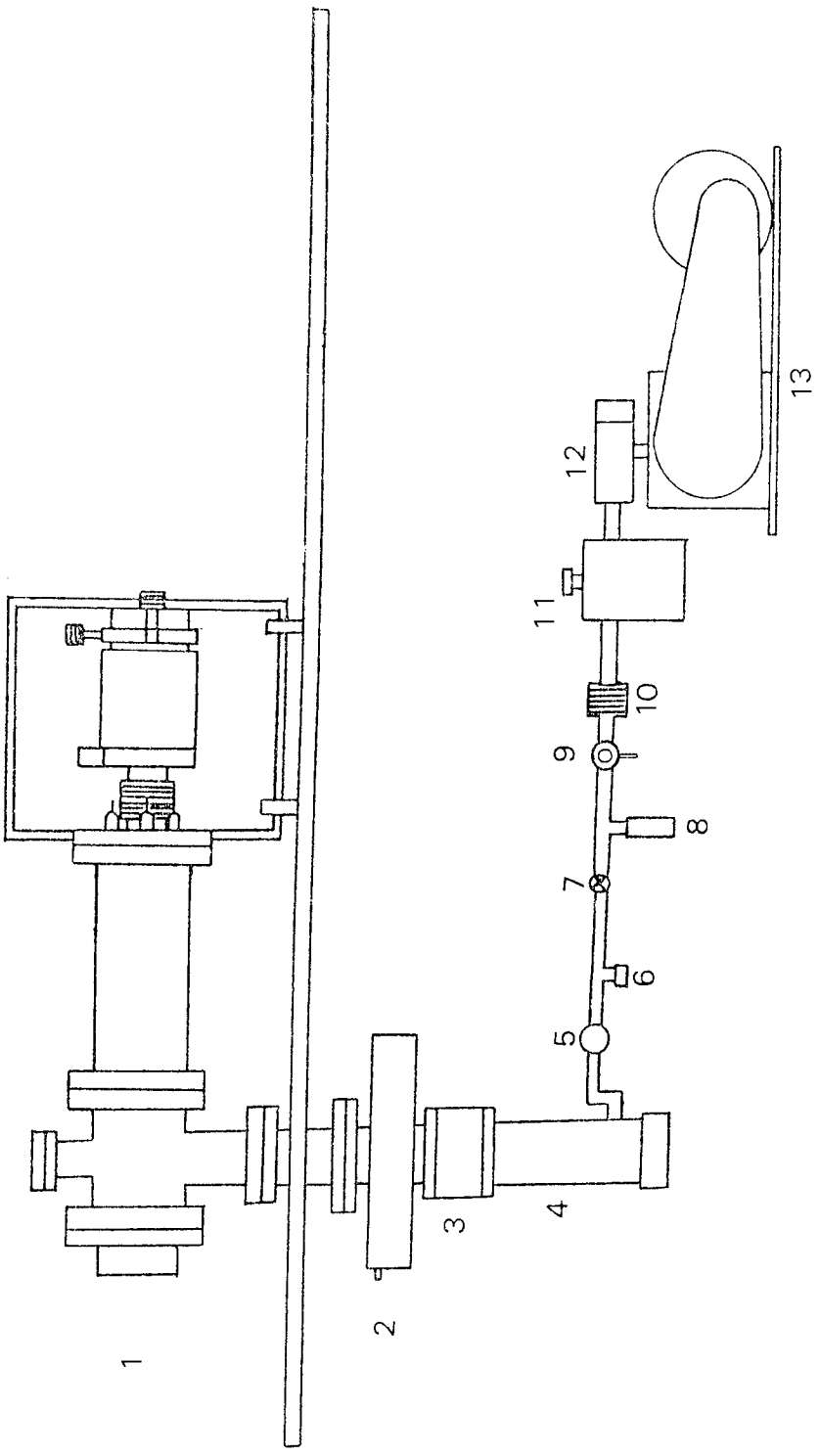
1
2
3
4
5
6
7
8
9
10
11
12
13

The vacuum system includes various safety features to protect it from failures in electricity or water, and also from operator error. A failsafe valve is used in conjunction with the rotary pump and combines isolation of the system with automatic air admission to the pump when switched off. The vacuum system is thus protected against oil suck-back when the rotary pump is switched off either deliberately or as the result of electricity failure. A built-in device delays air admittance to the pump until after the isolation has been completed, thus avoiding air entering the system. A vacuum switch, in the form of a capsule operated microswitch connected directly to the backing line of the vacuum system, provides control of electrical circuits at a pre-set pressure. The switch is connected such that the rotary pump will switch off above a pressure of about 25 torr thus protecting the rotary pump from a gross leak. The vacuum switch may be manually overriden in order to start evacuation of the system when at atmospheric pressure. The diffusion pump can only be switched on when both the rotary pump and the vacuum switch are operating. The diffusion pump is also protected against water failure by a switching device which monitors the water flow. If the diffusion pump is switched off for any reason it will remain off until manually restarted. The pressure in

the backing line is measured with a pirani gauge head and control unit, whilst the high vacuum in the chamber is measured with an ionisation gauge head and control unit.

An additional pumping system was used in the latter stages of experimental work to enable the analysis of the effect of residual gases on field emission from a carbon fibre. Gas from a cylinder was slowly and controllably leaked into the vacuum chamber via an all metal leak valve. The pipeline from the gas cylinder to the leak valve being first evacuated by a sorption pump, as shown in Fig. 5.14.

5.8 Performance of the Vacuum System

The vacuum system may be baked by enclosing the chamber in an aluminium oven. Two 850W heaters are automatically switched by a bake-out control unit enabling a predetermined bakeout temperature to be maintained; the temperature being monitored with a thermocouple. Alternatively, if a lower temperature bake is adequate the vacuum chamber may be heated by simply winding heater tapes around the flanges. After the system has been baked, the liquid nitrogen trap filled and the system allowed to cool, a vacuum pressure of $\lesssim 10^{-9}$ torr was routinely achieved.

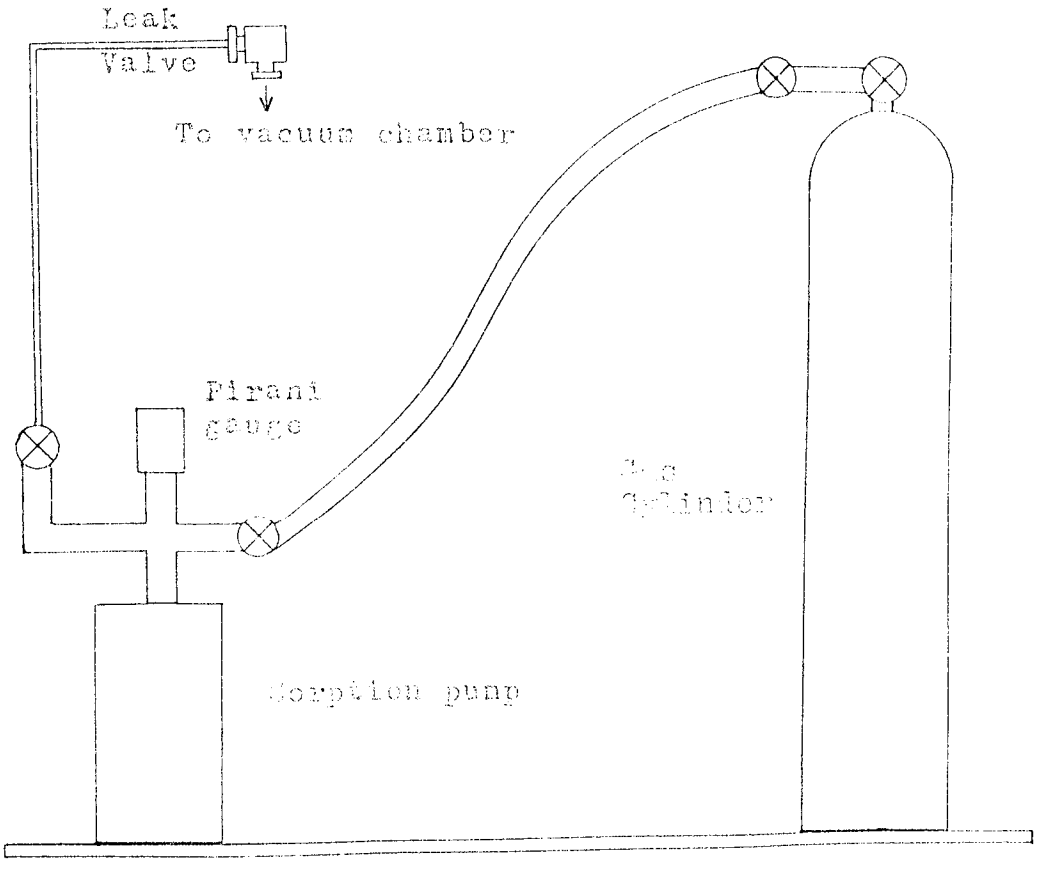

Fig. 5.14 Additional pumping system allowing use analysis.

CHAPTER 6

DEVELOPMENT AND PERFORMANCE OF A PROTOTYPE CATHODE RAY TUBE USING A CARBON FIBRE FIELD EMITTING CATHODE

6.1 Introduction

The systematic design, development and construction of a prototype cathode ray tube with a "cold" field emission electron source will be presented in this chapter. Such a tube offers the potential advantages of a small source size for high resolution applications, an instantaneous switch-on capability and eliminates heater power consumption. Individual carbon fibres manufactured and supplied by Courtaulds were used as the electron source. These fibres, whose fundamental field emitting properties were also investigated in this work (see Chapter 7), had a nominal diameter of 7 μm and were of the high modulus 'HM-U' type.

6.2 Mounting Techniques

The first stage in investigating the suitability of carbon fibre as a field emitting electron source was to find a reliable method for mounting the fibres and subsequently etching them to a sharp conical point of a few hundred of nm radius. The requirements for a satisfactory mount are good electrical conductivity between the fibre

and the fibre holder, high mechanical strength of the joint sufficient to withstand stresses imposed by the high electric field and also that the technique should be relatively quick and simple to perform. In this context, it must first be stated that the standard mounting techniques used for metal field emitters such as tungsten where the emitter is spot-welded to a heating loop is not possible with the present fibrous emitters.

The first method of mounting the carbon fibres that was examined was to electroplate them with copper in order to make the handling of the seven micron diameter fibres easier and also to provide a heat sink. This method had previously been used by Braun et al.[43] and consisted of attaching a fibre to a strip of copper with sellotape and lowering the suspended fibre into a bath of acidic copper sulphate solution where it was electrochemically plated. Unfortunately, it was found that during the plating process, the fibre tended to curl and kink which subsequently present serious alignment difficulties. In an attempt to prevent this distortion of the fibre, a small weight in the form of a strip of nickel tape was attached to the fibre. Although giving some improvement, this technique frequently caused the fibre to fracture when being moved into, or out of, the plating solution. This method of mounting a fibre was, therefore, discarded since it led to more rather than less handling problems,

and furthermore the weighting process itself involved first mounting the fibre onto nickel tape with silver paint as the adhesive.

An alternative approach to mounting the carbon fibres was to attach them to a strip of nickel tape which could then be spot-welded onto a suitable support. The fibres were fixed onto the tape with either a colloidal suspension of graphite in water (Aquadag) or silver paint. Although Aquadag was found to be a suitable adhesive it is also known to be a copious field emitter[42] and was, therefore, abandoned in favour of silver paint. This approach was found to be satisfactory and was used in the experimental work to be described in Chapter 7. Throughout the development of the prototype tube, however, the carbon fibre was inserted into a fine slot in a copper block (as described in 5.5) and secured with silver paint since the improved alignment of the emitter inherent in the use of this slotted holder was considered to be a more suitable mounting technique for this electron optical work. Once mounted, the fibre could be easily transferred between the etching process, microscopes for the examination of the tip profile, and the vacuum system.

6.3 Etching Procedure

After the fibre has been mounted in a suitable support it is desirable to shape the fibre into a conical endform. The apex of the shaped fibre should have as small a radius

of curvature as possible in order to minimise the applied voltage necessary to provide the high electric field required for the tunnelling of the electrons, and also to reduce the sputtering energy of positive ions formed by electron impact processes bombarding the tip. The method used to achieve a suitable emitting profile was to electrolytically etch the carbon fibres in a solution of sodium hydroxide. As will be discussed below, the effects of varying the strength of the electolyte and the initial etching current were examined. Conditions which consistently formed smooth, sharp, well-shaped tips used a 0.1N solution of sodium hydroxide and an initial etching current of 50μA.

Considering the etching procedure in more detail, a carbon fibre mounted on the copper block is lowered into a bath of sodium hydroxide until two or three millimetres are immersed in the solution. Referring to the experimental arrangement shown in Fig. 6.1(i), the bath containing the electrolyte consists of two pyrex beakers interconnected at their base by a pyrex tube and is shaped in this manner to prevent gas bubbles formed at the cathode disturbing the surface of the electrolyte in the region of the anodic fibre. A potential difference, derived from a stabilised power supply is applied between the fibre and a carbon rod cathode. The voltage is increased until

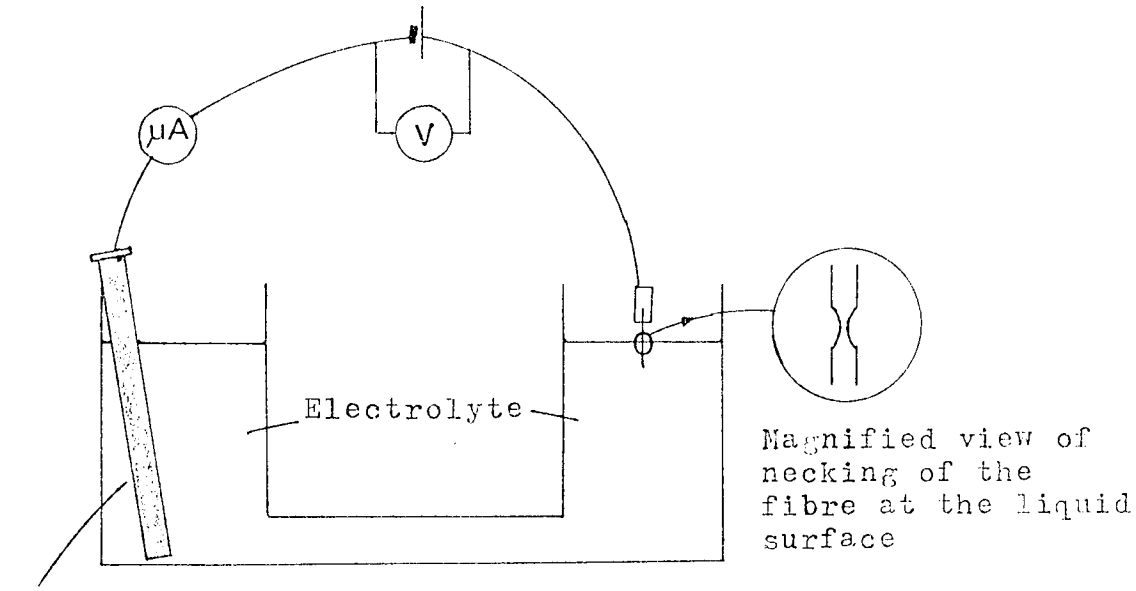

Fig. 6.1(i) Etching procedure.

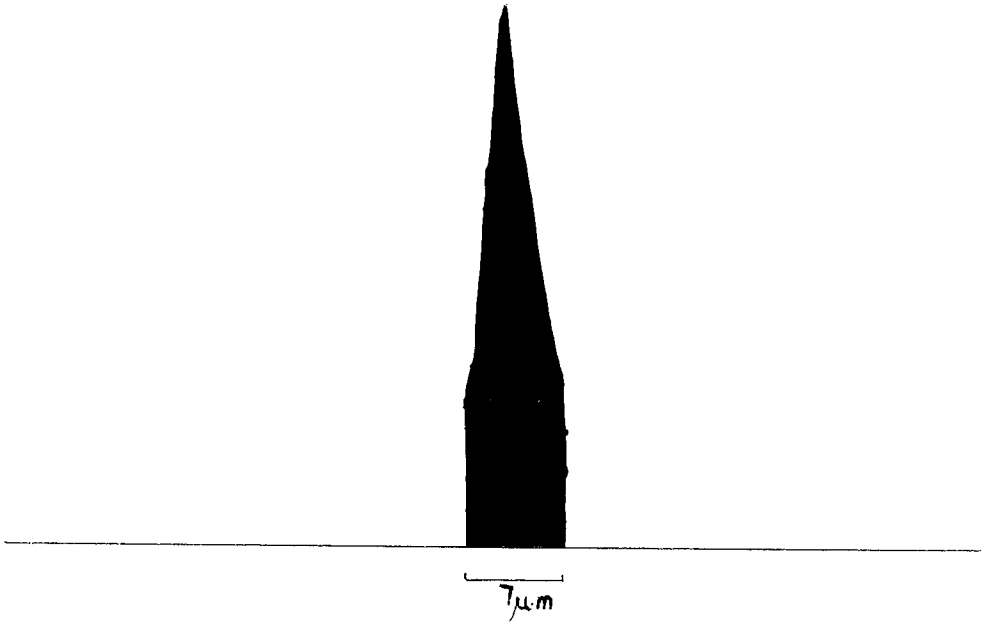

Fig. 6.1(ii) Electron micrograph of an etched carbon fibre tip.

the etching current is about 50μA, at which point the voltage is generally about two volts. As the process proceeds preferential etching occurs at the liquid-air interface which results in a gradual necking of the fibre. This necking continues until, as the etching current falls to zero, the bottom part of the fibre immersed in the liquid falls away leaving a conically shaped tip at the meniscus. The period of time for this process to take place is about two to three minutes. For a well formed field emitter the initial decrease in current with time is quite slow, but the rate of fall of current increases with time such that the reduction from about 10μA to zero occurs in a few seconds. If the fibre is etched in this manner a well shaped end-form is consistently and reproducibly achieved. The process is, however, dependent on the above conditions and in particular that the electrolyte should be freshly prepared and that the initial etching current should be carefully set. If the initial current or the concentration of the electrolyte is too high then the fibre is rapidly etched away resulting in a blunt and ragged end. Conversely, if the initial current or concentration of the electrolyte is too low then the fibre etches too slowly and a conical tip is not formed.

After the carbon fibre has been electrolytically etched, the resulting profile of the field emitter is examined microscopically before mounting and alignment of the fibre in the CRT module and subsequent evacuation in the experimental chamber. Initially, the tip profile was viewed with the aid of a transmission electron microscope and a typical micrograph is presented in Fig 6.1(*ii*). Field emitter tips were also viewed under an optical microscope and, although the apex of the emitter could not be resolved, with experience this method of examination was found adequate for determining the suitability of a given carbon fibre tip.

6.4 Background to the Design of a Prototype Tube

Conventional cathode ray tubes have been designed specifically for use with a thermionic cathode. In order to discover the difficulties involved in using a field emitter as the electron source in a cathode ray tube, an attempt was made at using the electron optical system of a conventional gun by simply replacing the thermionic cathode with a carbon fibre field emitter in a commercial tube manufactured by the M-O Valve Company. This was achieved by removing the heater and cathode coating, and then compressing the cathode cylinder into a flat stub to form a suitable mount for a carbon fibre.

A fibre was then fixed onto the cathode stub using silver paint as an adhesive and after etching, was inserted into a conventional grid cup and positioned about one millimetre behind the grid aperture by the use of spacers. The grid cup and field emitter were then mounted in a conventional electron gun and a cathode ray tube was produced using standard production processes at the M-O Valve Company.

The tube was tested using a standard industrial test bench and an additional high voltage power supply to enable the grid to be operated at a positive voltage. Although the carbon fibre emitted electrons copiously, allowing a current of thirty microamperes to be drawn, the proportion of the emission current reaching the screen was extremely small and erratic. The visual image of a spot formed on the phosphor screen suffered from aberrations and flickered severely. This distorted spot was only visible for a short time, which varied from a few seconds to a few minutes, before disappearing. Sometimes the spot would reappear of its own accord and it was often possible to coax the image back onto the screen by adjusting the voltages on the various anodes. However, even when a visual image was present the screen current was less than one microampere and the fluctuations in screen current were much greater than the fluctuations in total emission current.

The reasons for the unsatisfactory visual image obtained on the phosphor screen are attributable firstly to the nature of the new type of electron source and the unsuitability of the electron optics of a conventional cathode ray tube to image such a source. In addition, the aperture in a conventional grid cup is relatively small, about one millimetre in diameter, and since there is no provision for satisfactory prealignment of the fibre, nor any in situ adjustment of the tip, a high proportion of the total emission current is trimmed by the grid cup with only a small sample reaching the screen. The nature of the emission mechanism from carbon fibres is also of importance and will be discussed in Chapter 8. However, it can be stated briefly at this stage that the electrons are emitted from discrete and irregular regions on the surface of the emitter and these emission sites change with time. Therefore, if only a small sample of the electron emission is used to form the probe, the current in the probe will fluctuate with time; at times, there may, in fact, be no screen current present, thereby giving rise to the erratic visual display.

Following this preliminary investigation, it was concluded that the alignment of the carbon fibre and the aperture size in the grid cup were critical parameters. In addition, the electrostatic lens used in the conven-

tional tube had been designed to image a crossover formed between the grid and first anode, instead of the virtual source of a field emitter. It was, therefore, decided to develop an electron optical system specifically designed for use with a field emitter, rather than attempt to modify an existing electron gun. To facilitate the systematic testing of the electron gun during the various stages of this development, the demountable vacuum system described in the previous chapter was designed and constructed. The prototype cathode ray tube, which will be described in the following sections, although designed primarily for use with a carbon fibre field emitter, also provides an electron optical test facility for the future assessment of other field emitting materials.

6.5 Angular Confinement of Electrons Emitted from a Carbon Fibre

The first experiment performed in the demountable vacuum system was to examine the confinement of an electron beam emitted from a carbon fibre. For this, an etched tip was mounted in the vacuum chamber and positioned ∿40mm away from the phosphor screen. The screen was earthed via a picoammeter and a negative voltage of ∿1kV was applied to the carbon fibre such that a current of ∿10μA was emitted from the tip.

Figure 6.2 is a typical photograph of the field emission pattern obtained on the phosphor screen; as can be seen, this is irregular in shape and consists of several bright discrete regions. Although the pattern flickered with existing bright regions disappearing and new regions forming, the shape of the total pattern approximated to a circle and indicated a conic half-angle of $\sim 30^{o}$. This angle of emission was observed to be virtually independent of emission current above a value of one microampere which was the lowest current readily visible.

This experiment highlighted a very important point which had previously been reported by Cleaver[64.] working on tungsten field emitters for use in scanning electron microscopes; viz, that the inherent electron optical brightness (current density per solid angle) which makes field emitters so attractive in microscope applications is due to their small source size and is in spite of a relatively low angular current density. Therefore, when applying a field emitter to a device such as a cathode ray tube, which requires the beam to be focussed into a probe containing several microamperes of current in a spot several hundred microns in diameter, it is necessary to utilise fairly wide angles of emission if the total current drawn from the emitter is to be restricted to a reasonable level; i.e. that would ensure a long lifetime and stability.

Fig. 6.2 Field emission pattern from a carbon fibre.

The aim of the ensuing experiments was thus to maximise the current efficiency of an electron gun which was capable of focussing an electron beam into a probe with a spot size on the phosphor screen of about 0.5mm in diameter. All electron optical imaging devices introduce aberrations into the focussed spot but this problem is especially severe in electron microscopy where very small probe sizes are required, and therefore only narrow angle guns are used. In the application of this type of source to cathode ray tubes the situation is somewhat different. Thus, since the virtual source size of a field emitter is extremely small ($\sim$3nm), compared with the required probe size ($\sim$ 0.1mm), it is possible to tolerate relatively large aberrations caused by the imaging system. This property allows the acceptance of wide angles of emission and thereby increases the efficiency of the electron gun. There is, however, a limit to this procedure of increasing the acceptance angle since it is necessary to avoid excessive deflection defocussing and consequently the beam size must be restricted in the deflecting region.

6.6 Initial Diode Regime of the Prototype Electron Gun

The electron gun was chosen to be of the tetrode type, consisting of the micropoint field emitting source, an electrode for producing a high field for the emission of electrons, and a two-element electrostatic lens. The voltage on the extraction electrode controls the emitted

current but only has a limited effect on the focal properties of the lens; this property offers a potential approach for the stabilisation of the electron beam current by feedback techniques, such as those used by Cleaver[66] in a scanning electron microscope. As was previously seen (Chapter 4.4) in the design of field emission guns for electron microscopes, complex electrode shapes are often used so as to minimise aberrations.[57, 59] In designing the electron gun for the prototype cathode ray tube, however, it was decided to use flat electrodes with circular apertures in order to simplify their manufacture and to maintain a similarity between the electrodes used commercially in the guns of "production" CRT's. The parameters which, therefore, have to be chosen are the aperture sizes and the separation of the electrodes in order to arrive at an electron gun with a high current efficiency.

As a first step, an experiment was devised to investigate the properties of a simple diode regime consisting of the emitter and an apertured extraction electrode. This involved examining the proportion of the total emission current passing through the aperture in the extraction electrode and the subsequent angular spread of the electron beam. Three different aperture sizes were investigated for a range of field emitter

tip to extraction electrode separations of up to 10mm. The experimental arrangement for investigating different aperture sizes is illustrated in Fig 6.3 and utilises an electrode with a 10.5mm aperture which was aligned with the central axis of the vacuum chamber by using the glass rod electrode holder previously described in 5.6. Near the periphery of this electrode four small clearance holes had been accurately drilled which allowed other apertured electrodes to be bolted into position axially concentric with the former. To allow for a large divergence of the beam after passing through the apertured electrode, the distance between this electrode and the phosphor screen was set at twenty millimetres. Using an optical travelling microscope and the precise specimen manipulator, a carbon fibre field emitter was prealigned, outside the vacuum chamber with the centre of the aperture and the tip was then positioned in the plane of the electrode and the micrometer reading noted. After assembling the specimen stage and evacuating the vacuum chamber to a pressure of 10^{-9} torr, the field emitter tip to extraction electrode separation was adjusted between zero and ten millimetres in discrete steps and readings of the proportion of the total emission current reaching the screen were taken at each stage. The total emission current from the fibre was

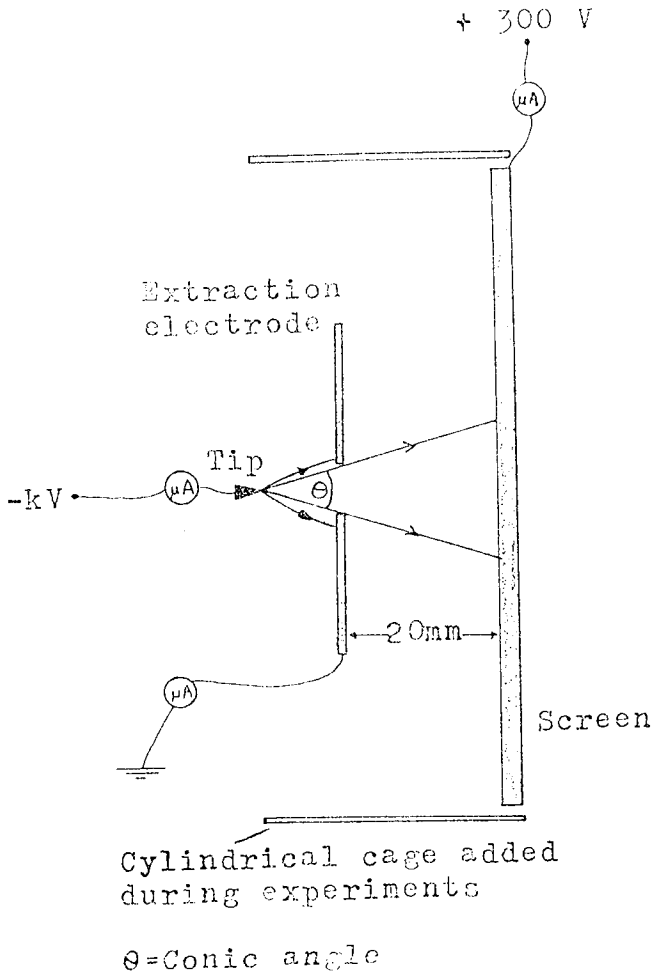

Fig. 6.3 Experimental arrangement for investigating different apertures in the extraction electrode.

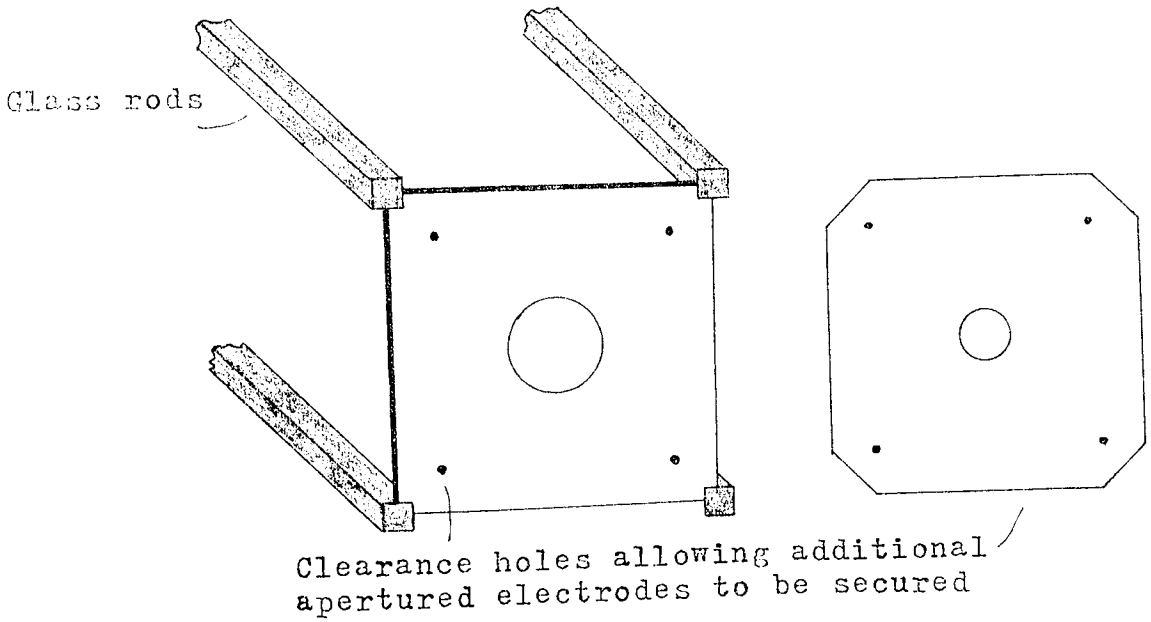

maintained at ten microamperes by adjusting the negative voltage applied to the tip for each emitter to extraction electrode separation. The extraction electrode and the phosphor screen were earthed via picoammeters which monitored the current trimmed by the former electrode and the current passing through the aperture and arriving at the screen. For each separation, finer lateral adjustments were made to the tip position which maintained the emission pattern central on the screen and thus ensured that the tip remained on the optical axis of the extraction electrode and screen.

The initial results from this experiment were apparently illogical, in so much as from ten microamperes emission from the carbon fibre tip only a small proportion was recorded on the anode and the remainder was undetected. The suggested explanation of this phenomenon is that electrons which bombard the screen produce secondary electrons with a yield of one and these secondaries then flow to earth via the vacuum chamber and the anode. To test this hypothesis, a stainless steel cylindrical cage was constructed which was held inside the vacuum chamber and insulated from it by glass rods. The experiment was repeated and the current hitting the cage was monitored with a picoammeter. The cage current was found to account for the formerly undetectable current and by applying a

positive voltage of about 300 volts to the screen it was found that the cage current dropped to zero and the currents on the screen and anode now added up to the ten microamperes emitted from the tip. With this modified arrangement the experiments were performed and the electrons passing through the aperture of the extraction electrode formed a circular image on the phosphor screen which was photographed using a 'Polaroid' camera. These photographs included the whole of the screen which is known to be eighty millimetres in diameter, allowing the image size to be measured and hence the divergence of the electron beam to be calculated.

The experiment was performed for three different aperture sizes of 10.5, 6.0 and 1.0 millimetres and the corresponding results are tabulated in Figs 6.4, 6.5 and 6.6: included are calculated values for the conic angle of the current passing through the aperture in the extraction electrode and reaching the screen. This conic angle was calculated as shown in Fig 6.7 and in every case was found to be slightly less than the angle that would be formed by a simple projection PP' of the aperture onto the screen. The results show that as the tip to extraction electrode separation is reduced, the larger the screen current becomes as more electrons are allowed to pass through the given aperture. Although

Fig. 6.4 Tabulated results for an extraction electrode with a 10.5mm diameter aperture.

Emitter to Extraction Electrode Separation (mm)	Tip Potential (kV)	Extraction Electrode Current (μA)	Screen Current (μA)	Image Diameter at Screen (mm)	Conic Angle (°)
10	-1.82	3.0	7.0	29	52
9	-1.77	3.0	7.0	31	56
8	-1.74	2.0	8.0	33	61
7	-1.70	1.5	8.5	35	66
6	-1.66	0.8	9.2	39	74
5	-1.64	0.2	9.8	44	82
4.5	-1.62	0.01	10	47	88
4	-1.60	0	10	50	92
3	-1.58	0	10	53	98
2	-1.53	0	10	55	102
1	-1.49	0	10	53	103
0	-1.46	0	10	50	102

Fig. 6.5 Tabulated results for an extraction electrode with a 6.0mm diameter aperture.

Emitter to Extraction Electrode Separation (mm)	Tip Potential (kV)	Extraction Electrode Current (μA)	Screen Current (μA)	Image Diameter at Screen (mm)	Conic Angle (°)
10	-1.95	6.0	4.0	17.5	32
9	-1.90	6.0	4.0	18	34
8	-1.85	6.0	4.0	20	39
7	-1.80	5.0	5.0	22	44
6	-1.75	4.5	5.5	25	51
5	-1.70	3.5	6.5	28	58
4	-1.65	2.3	7.7	32	67
3	-1.60	1.3	8.7	39	80
2.5	-1.57	0.5	9.5	45	90
2	-1.52	0.1	10	50	97
1.5	-1.46	0	10	50	99
1	-1.46	0	10	48	98
0.5	-1.45	0	10	47	99

Fig. 6.6 Tabulated results for an extraction electrode with a 1.0mm diameter aperture.

Emitter to Extraction Electrode Separation (mm)	Tip Potential (kV)	Extraction Electrode Current (μA)	Screen Current (μA)	Image Diameter at Screen (mm)	Conic Angle (°)
10	-1.80	9.5	0.5		
9	-1.80	9.5	0.5		
8	-1.75	9.5	0.5		
7	-1.75	9.5	0.5		
6	-1.70	9.0	1.0	4	9
5	-1.70	9.0	1.0	4.5	10
4	-1.65	9.0	1.0	5.5	13
3	-1.60	8.5	1.5	7	17
2	-1.55	7.5	2.5	10	26
1	-1.50	5.0	5.0	17	44
0.5	-1.45	2.0	8.0	25	63

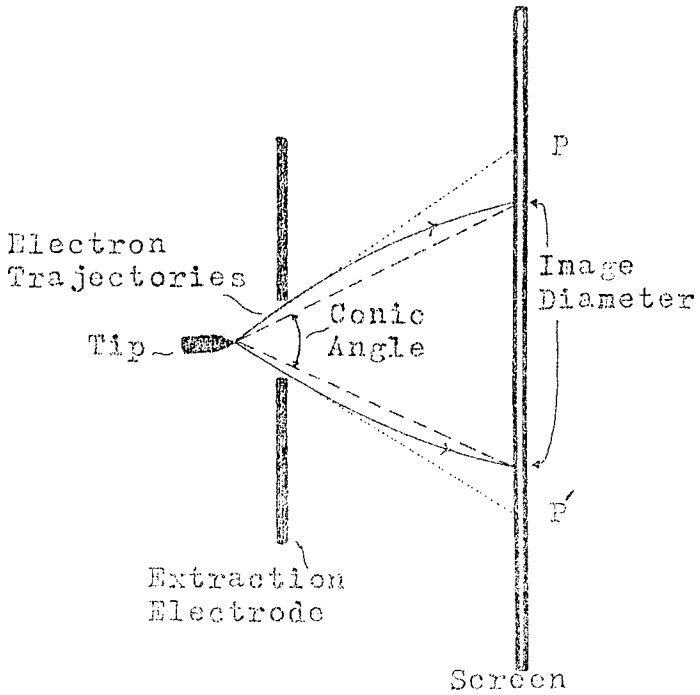

PP'=Projection of aperture

$$\text{Conic angle} = 2\tan^{-1}\left\{\frac{\text{Image Diameter(mm)}/2}{\text{Separation(mm)}+20\text{(mm)}}\right\}$$

Fig. 6.7 Diagram explaining nomenclature used in the analysis of the initial diode region.

the conic angle of emission is somewhat larger than in the case of an emitter to plane anode configuration, the angular current density (i.e. current per conic angle) is essentially the same for all three aperture sizes investigated. This experiment also indicated that there was no significant aperture lens effects over the range of apertures and separations investigated.

Since the main criteria for the design of the gun was to maximise the current efficiency it can be seen from the tabulated results that for negligible current to be trapped by the extraction electrode the separation from the tip of the emitter should be less than the radius of the electrode's aperture. There is no advantage to be gained by using excessively large apertures since the beam would in any case have to be limited at a subsequent electrode in order to reduce aberrations. The use of very small apertures create problems in alignment of the emitter and because of the consequent need for the emitter to be in the close proximity of the extraction electrode, the possibility of damage to the emitter is greatly increased. The conclusion drawn from this experiment was to use an extraction electrode with an aperture of diameter greater than one millimetre but less than six millimetres. The specific value for the aperture's diameter was chosen to be within the above range and compatible with the apertures in the elctrostatic lens now to be described.

6.7 Electron Optical Properties of the Electrostatic Lens

Following the investigation of the initial diode regime of the electron gun, the next stage in the development of a cathode ray tube using a field emission source was the design of a suitable electrostatic lens to form an image of the source on a screen. The form of an electrostatic lens for use with such a source will vary with the particular requirements of beam spot size and working distance. As was seen in section 4.4, various electrode shapes and configurations have been used by previous workers in order to achieve a lens performance which is suitable for its particular application.

The type of lens chosen for investigation was a two-anode electrostatic lens consisting of simple flat electrodes each with a circular aperture, square to the face of the electrode, where the electron optical properties were determined by the use of a digital computer. The two computer programmes used for this work were originally written by Munro[60] for use on an IBM computer and required modification in order to be suitable to be run on an ICL machine. After modification the programmes were tested with data previously used by Munro for computing the properties of one of his lens designs. Once the programmes were functioning correctly they could be used to calculate the properties of lens

designs which were of interest to this work. Copies of the two modified programmes are presented in Appendix I.

The first programme calculates the axial potential distribution in the lens using the finite element method with boundary conditions determined by the lens geometry. This is then used by the second computer programme to find the trajectories and the optical properties of the lens by solving the ray equation. The programme computes the image plane or object plane, the magnification, the spherical aberration coefficient and the chromatic aberration coefficient for a range of object-side and image-side voltage ratios.

The general form of the symmetrical lens geometry that was chosen for investigation is shown in Fig 6.8. It consists of two anodes, at potentials of V_O and V_I measured relative to the cathode. The distance of the cathode from the first anode is S_O, and the distance from the final anode to the focussed spot is S_I. The versions of the basic lens investigated have aperture diameters in the range 2 to 10mm. The thickness of the anodes is 0.6mm and in order to obtain a comparable set of results all the lenses have the same overall length of 10mm. The optical properties of each lens were computed at a constant image distance of S_I = 300mm, and

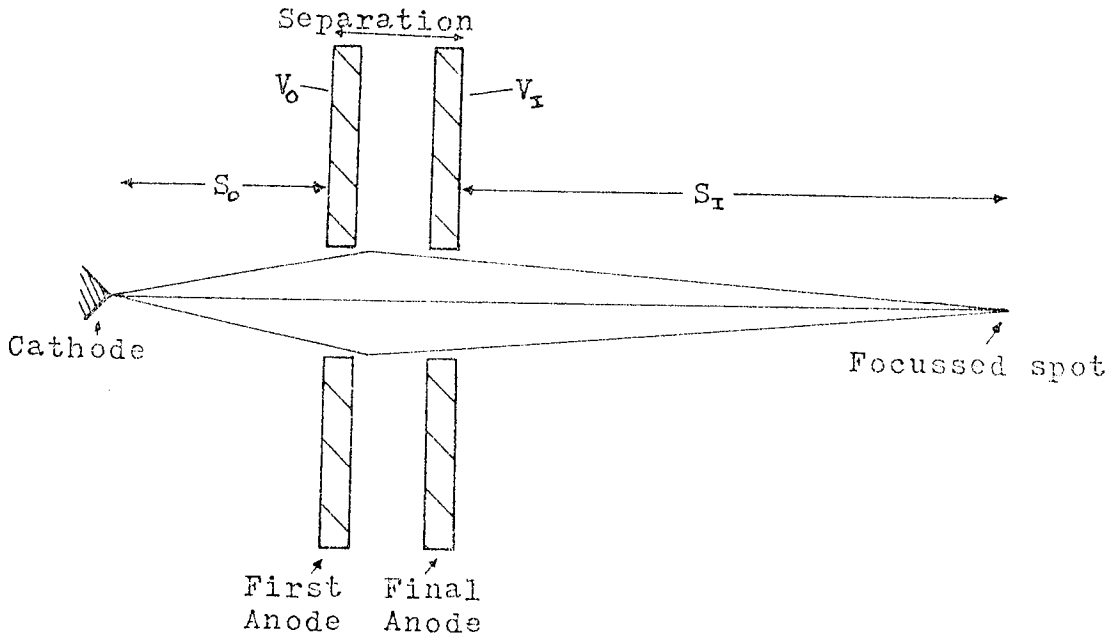

Fig. 6.8 General form of electrostatic lens investigated.

a constant first anode potential of V_O = 1kV. (The image distance of 300 mm was chosen to maintain comparability with conventional cathode ray tubes, so that standard deflector plates could later be used without a loss in sensitivity) Values of object distance S_O, magnification, and the coefficients of spherical and chromatic aberration (referred to the object side) were computed for voltage ratios of V_I/V_O = 2, 5, 10, 20 and 50. The results are summarised in Figs 6.9 - 6.12.

When analysing the properties of the lenses several points were considered. The ratio of the voltages applied to the anodes of the lens should be as low as possible in order to avoid providing excessively high power supplies, minimise the likelihood of voltage breakdown and to avoid problems in deflecting the beam. An optimum voltage ratio in the range V_I/V_O = 5 - 10 was therefore selected. The lens was required to conform with the general aim of designing an electron gun with a high current efficiency. The distance between the cathode and the first anode (the object distance) should therefore be relatively small and the aperture diameters of the lens should be as large as possible in order to accept a large proportion of the emitted electrons. However, the diameter of the electron beam emerging from the final anode has to be restricted to avoid excessive de-

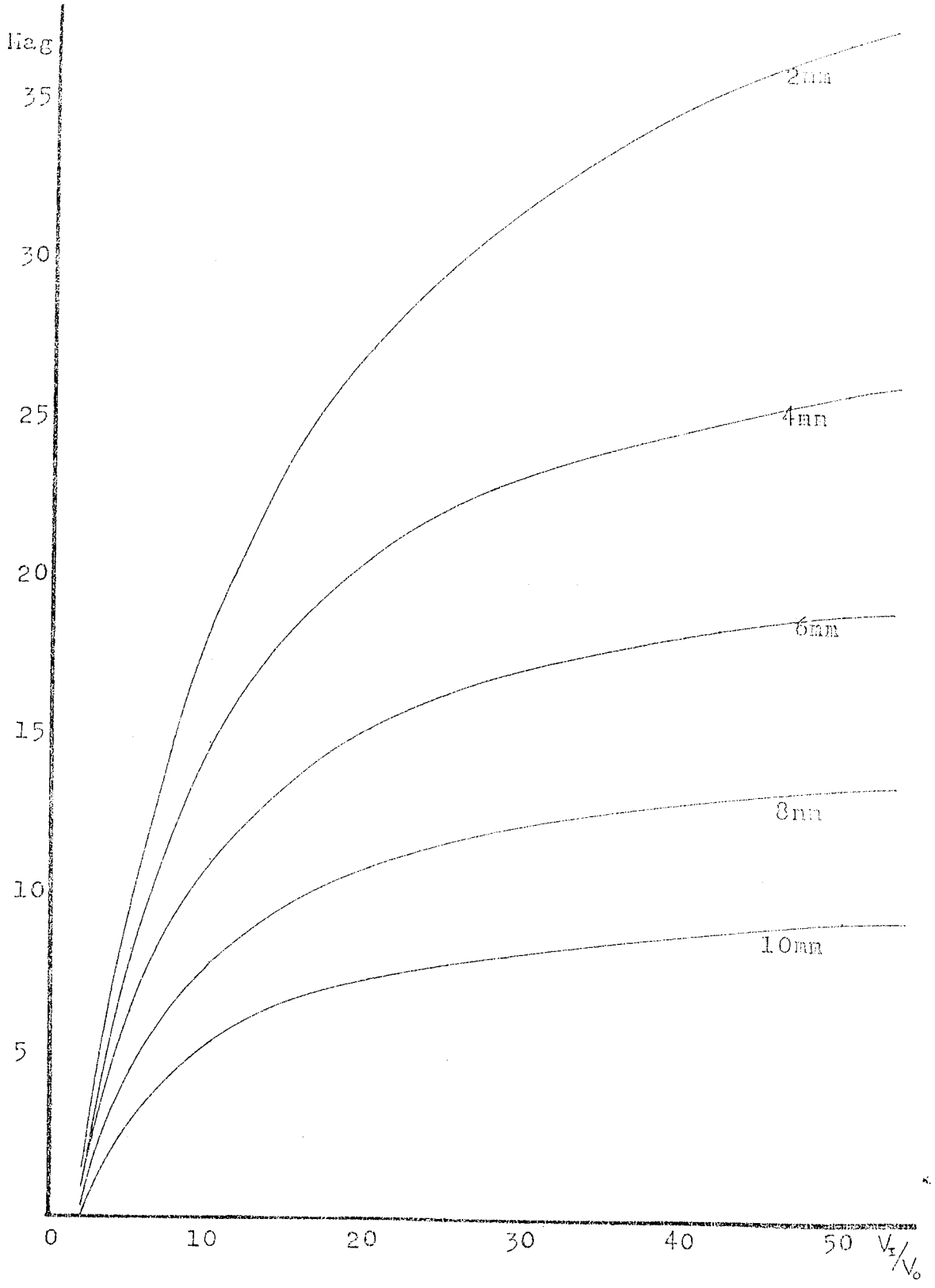

Fig. 6.9 Graph of magnification as a function of the voltage ratio V_I/V_o.

Electrostatic lenses, 10mm electrode separation and apertures of 2,4,6,8 and 10mm.

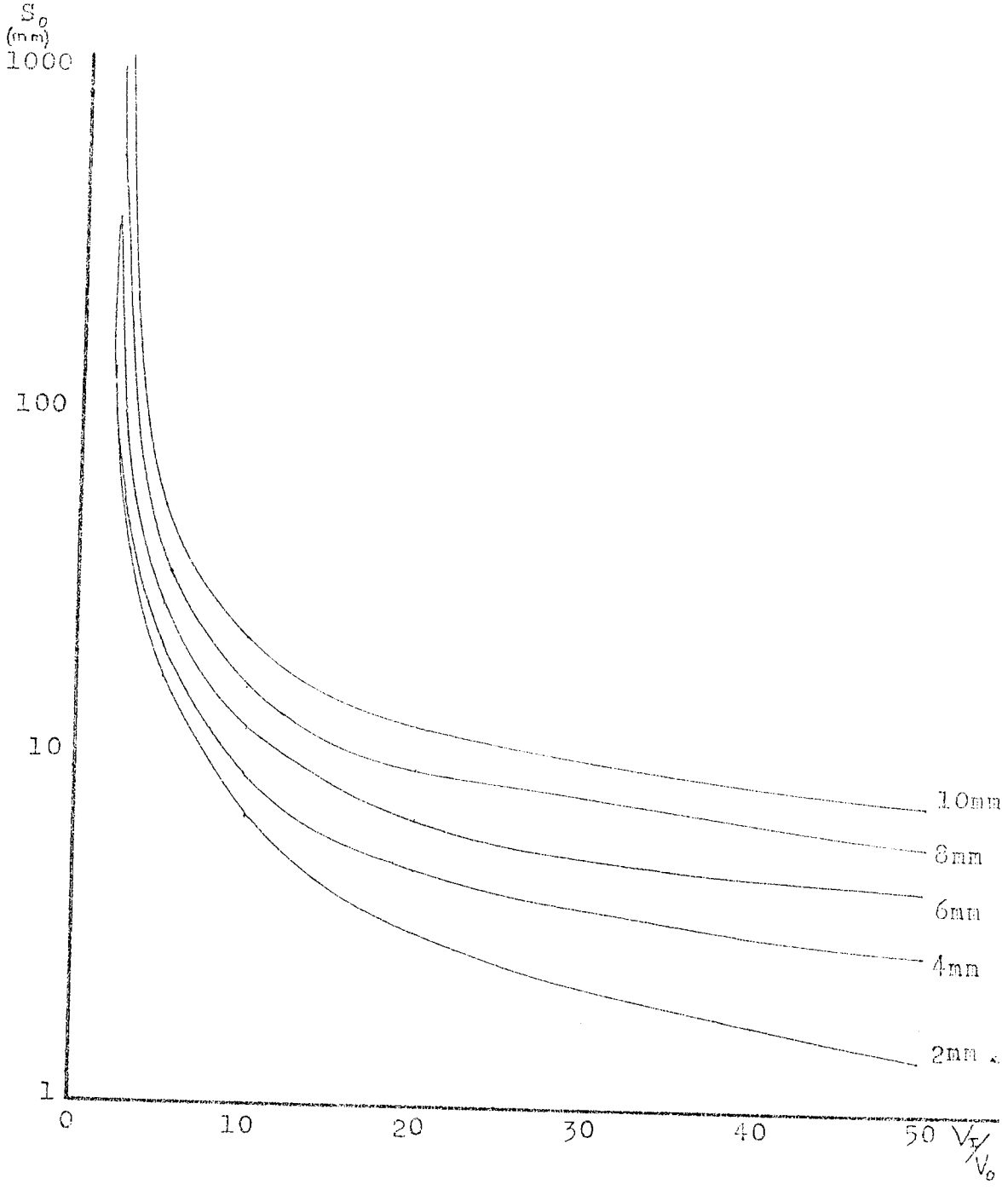

Fig. 6.10 Graph of object position S_o as a function of the voltage ratio V_r/V_o.

Fig. 6.11 Graph of spherical aberration as a function of the voltage ratio V_r / V_o.

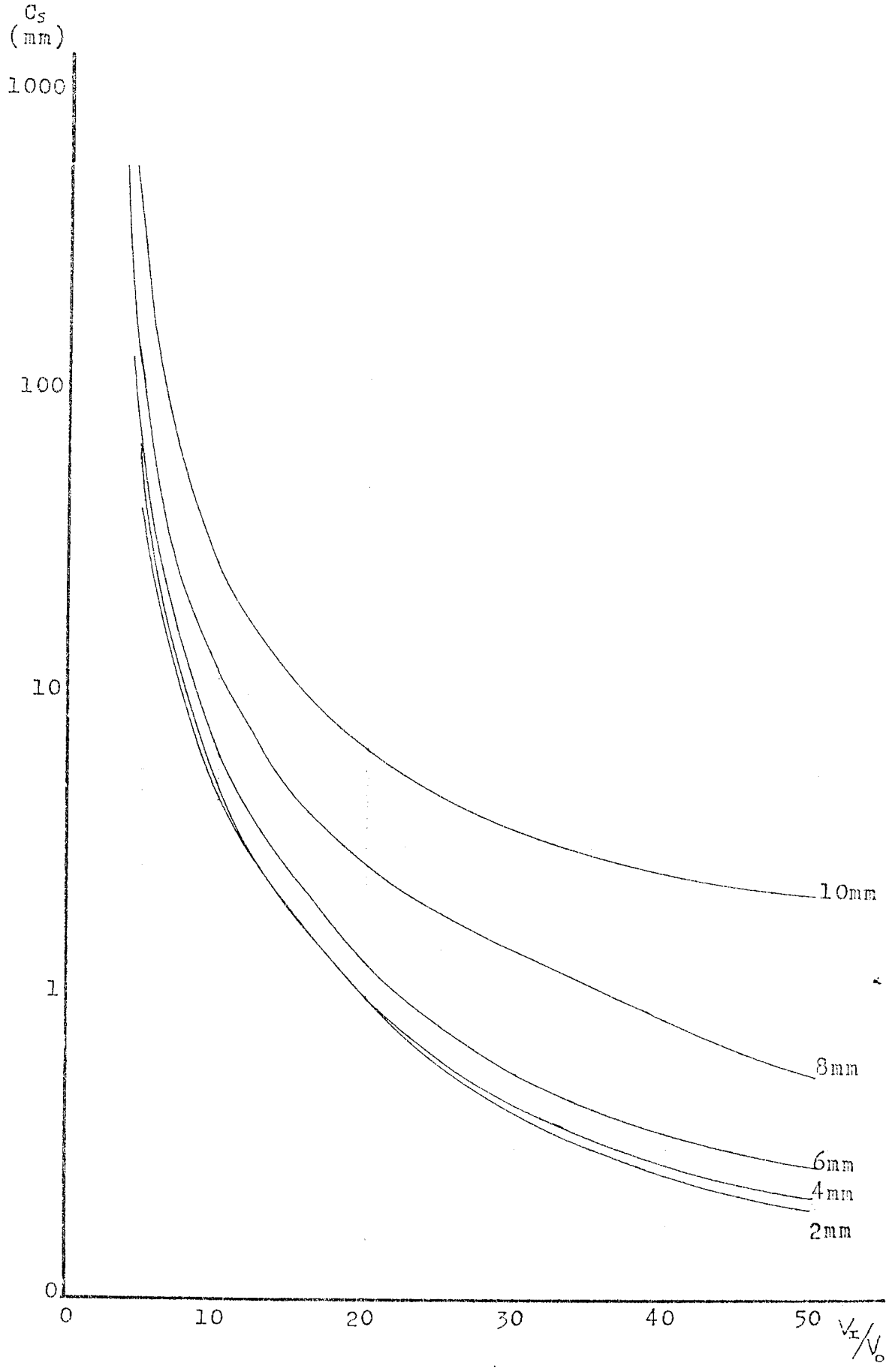

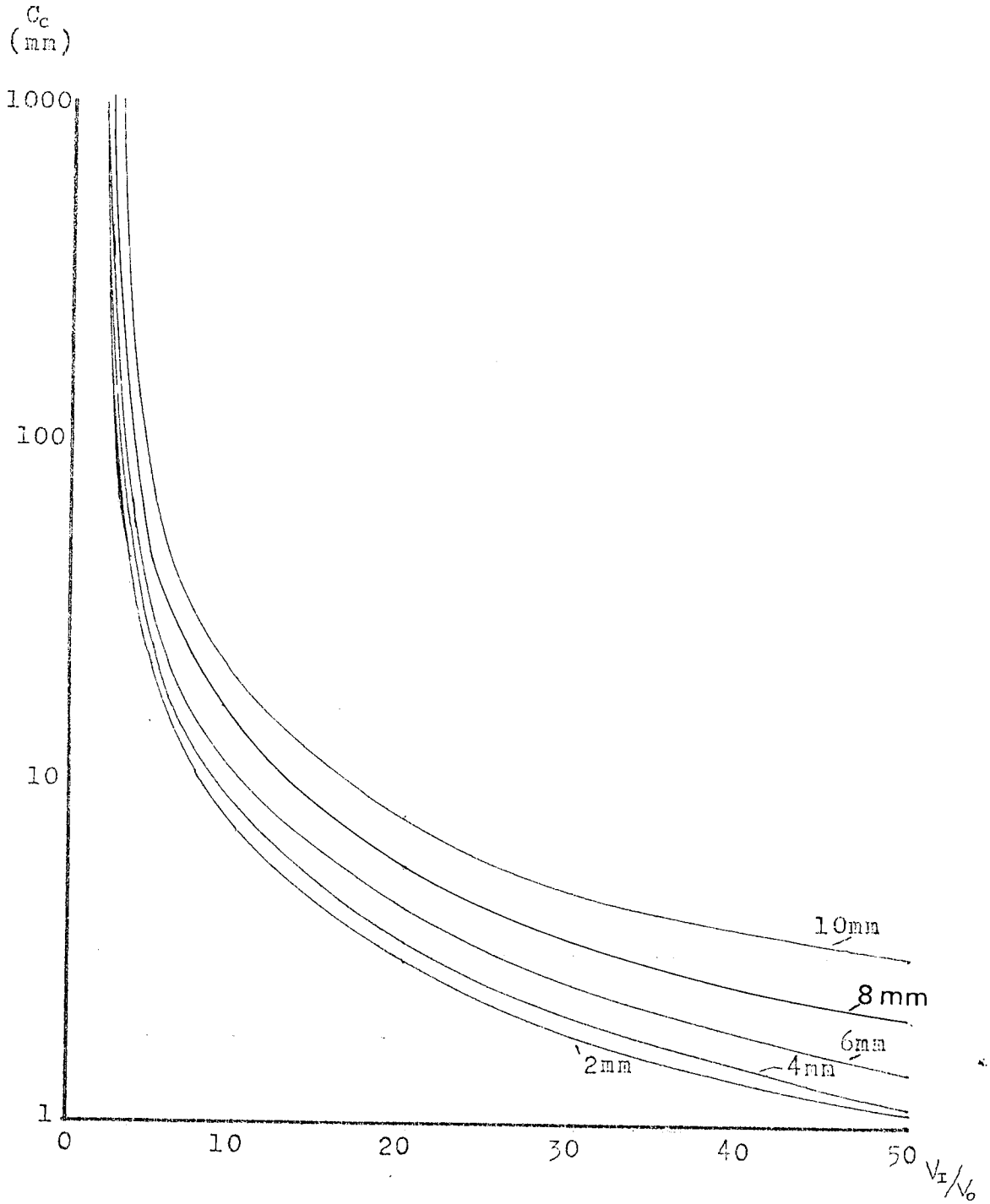

Fig. 6.12 Graph of chromatic aberration as a function of the ratio V_I/V_o .

flection defocussing and, to a lesser extent, reduce spherical aberrations.

Fig 6.10 shows that the required object distance between the electron source and lens increases with increasing aperture size. A lens consisting of two electrodes both with an aperture size of either two or four millimetres was, therefore, selected as being the most consistent with the previous points. In order to further optimise these lenses an overall electrode separation of 3mm was chosen as a constant parameter in each case. Scale drawings of the two lenses selected for detailed analysis are shown in Fig 6.13 and their computed properties are presented in Figs 6.14 - 6.19.

6.8 Testing of the Electrostatic Lenses

Based on the results obtained for the aperture sizes in the extraction electrode and the electrostatic lens, two electron guns were designed and tested. The first gun is shown in Fig 6.20 and uses the electrostatic lens with 2mm apertures and overall electrode separation of 3mm. The lens is required to produce a focussed spot when a voltage ratio $V_I/V_O \simeq 5$ is applied to the first and final anodes. Computations indicate that for this condition to be satisfied the cathode should be about 5mm from the first anode. The extraction electrode was,

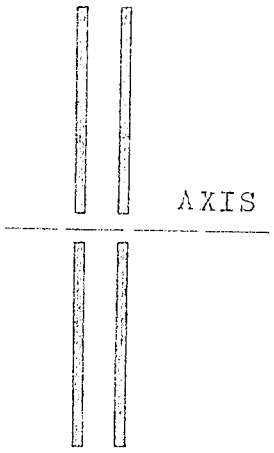

2mm apertures

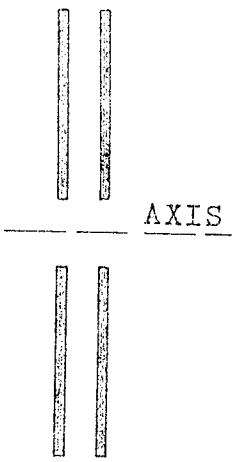

4mm apertures

Fig. 6.13 Scale drawing of lenses chosen for electron gun.

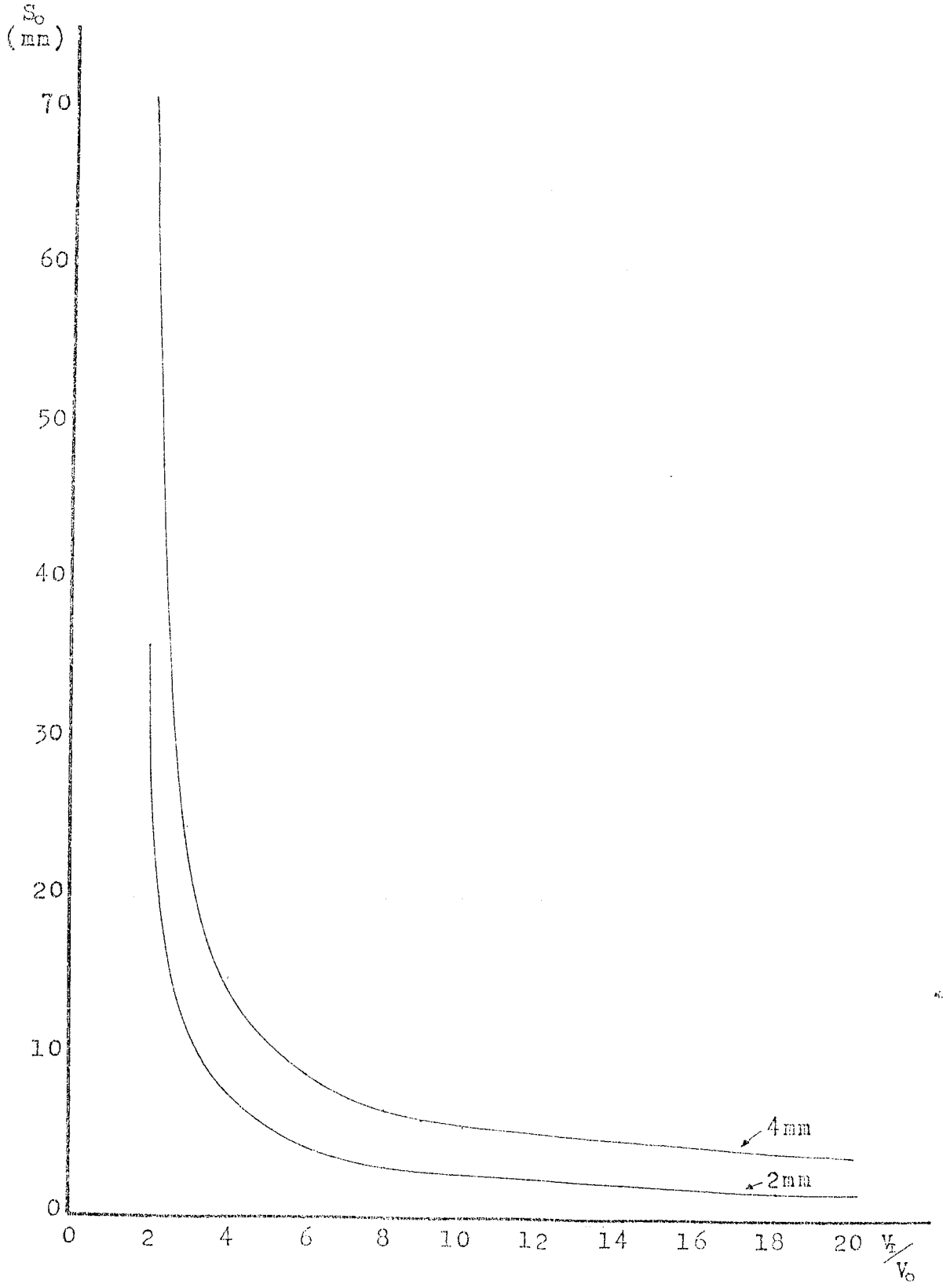

Fig. 6.14 Graph of object position as a function of the voltage ratio V_I/V_o. 3mm electrode separation and apertures of 2 and 4mm.

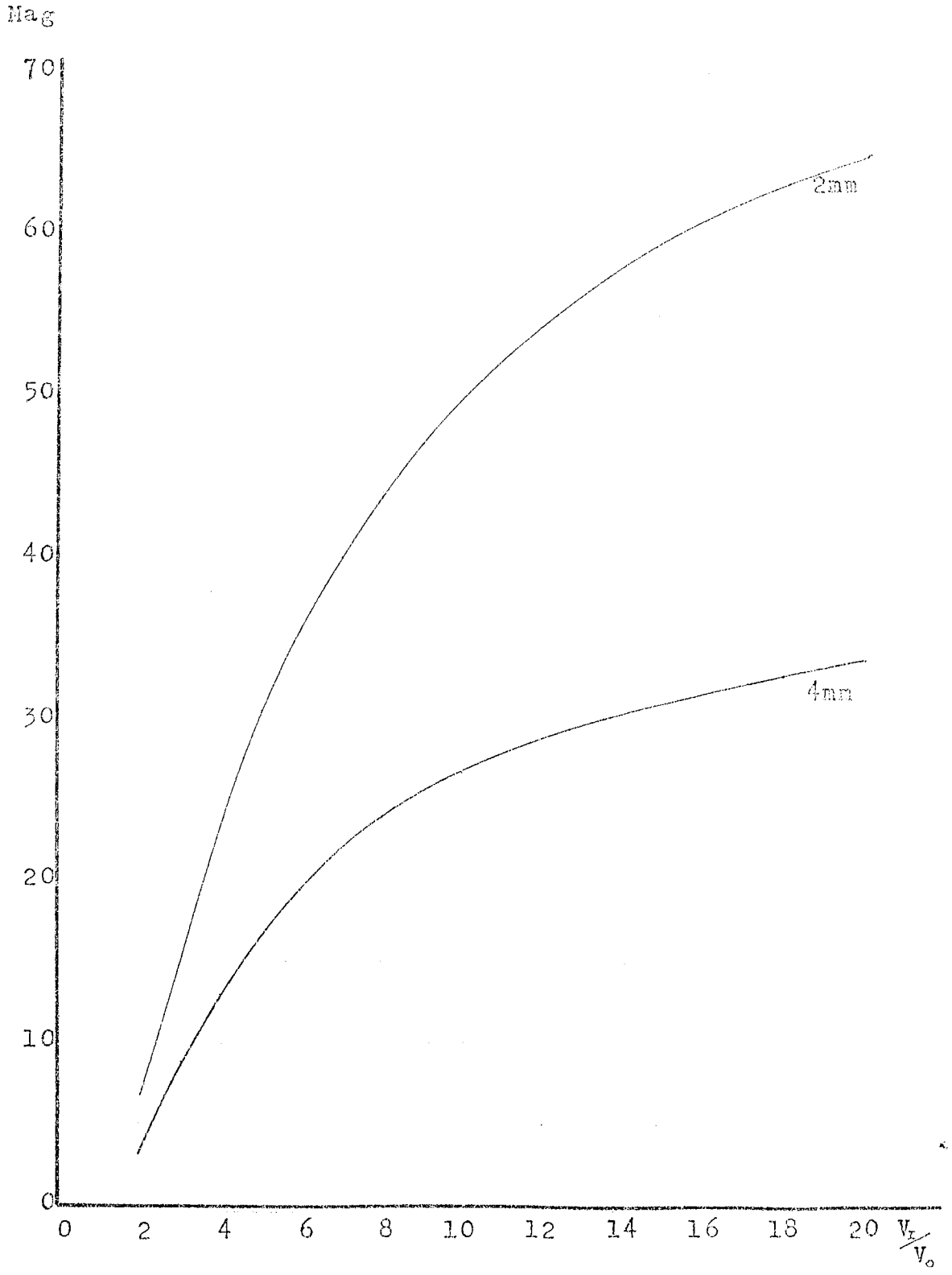

Fig. 6.15 Graph of magnification as a function of the voltage ratio V_I/V_o. 3mm electrode separation and apertures of 2 and 4mm.

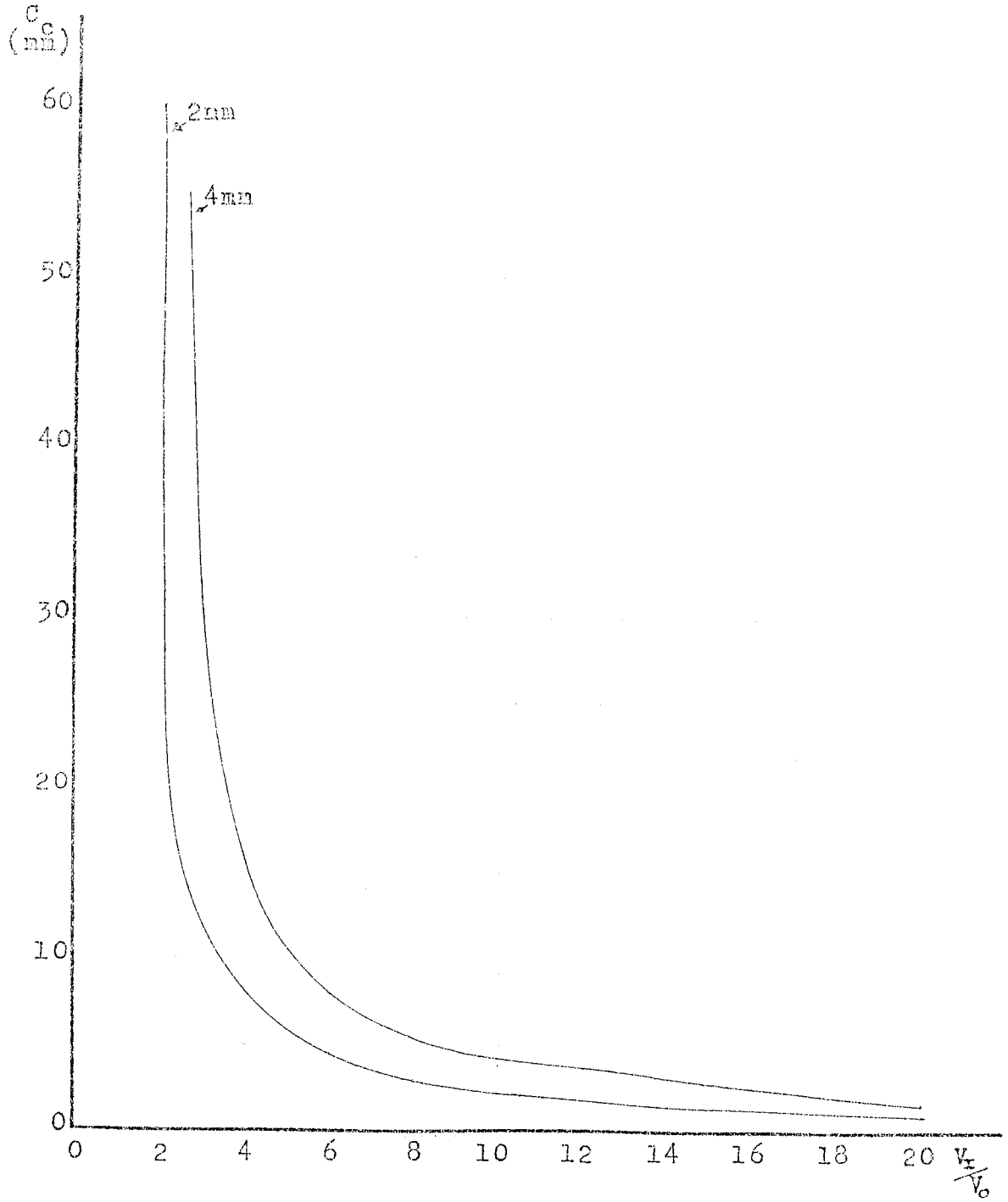

Fig. 6.16 Graph of chromatic aberration as a function of the voltage ratio V_I/V_o. 3mm electrode separation and apertures of 2 and 4mm.

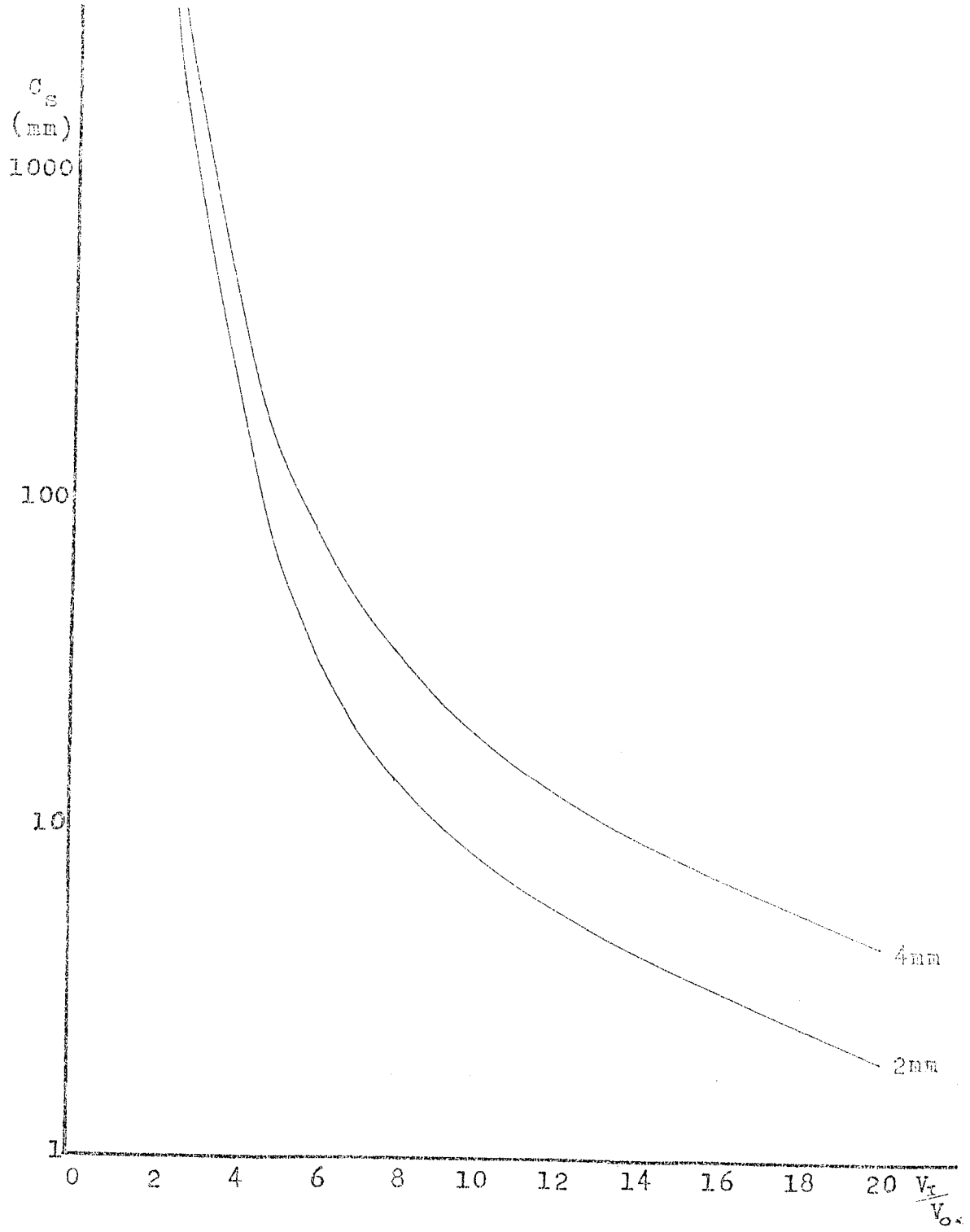

Fig. 6.17 Graph of spherical aberration as a function of the voltage ratio V_r/V_o. 3mm electrode separation and apertures of 2 and 4mm.

FIRST ANODE (kV)	FINAL ANODE (kV)	OBJECT DIST. (mm)	MAG	SPHER. AB. (mm)	CHROM. AB. (mm)
1.00	2.00	36.23	6.78	14542.03	60.03
1.00	5.00	5.58	30.53	65.22	6.15
1.00	6.00	4.40	35.79	34.52	4.55
1.00	7.00	3.66	40.18	21.34	3.60
1.00	8.00	3.15	43.91	14.58	2.96
1.00	9.00	2.79	47.10	10.67	2.52
1.00	10.00	2.51	49.87	8.20	2.18
1.00	20.00	1.41	65.20	2.01	0.95
1.00	50.00	0.82	75.29	0.70	0.40

Fig. 6.18 Properties of lens with 2mm apertures, a separation between anodes of 3mm and an image distance of 300mm.

FIRST ANODE (kV)	FINAL ANODE (kV)	OBJECT DIST. (mm)	MAG	SPHER. AB. (mm)	CHROM. AB. (mm)
1.00	2.00	70.46	3.50	51736.78	126.56
1.00	3.00	24.41	8.86	1878.26	32.13
1.00	4.00	14.90	13.19	416.53	16.73
1.00	5.00	10.99	16.64	164.86	10.96
1.00	6.00	8.89	19.42	86.18	8.04
1.00	7.00	7.59	21.70	52.86	6.30
1.00	8.00	6.71	23.59	35.90	5.16
1.00	9.00	6.08	25.19	26.15	4.35
1.00	10.00	5.60	26.56	20.04	3.76
1.00	20.00	3.77	33.75	4.69	1.50
1.00	50.00	2.95	38.33	1.10	0.39

Fig. 6.19 Properties of lens with 4mm apertures, a separation between anodes of 3mm and an image distance of 300mm.

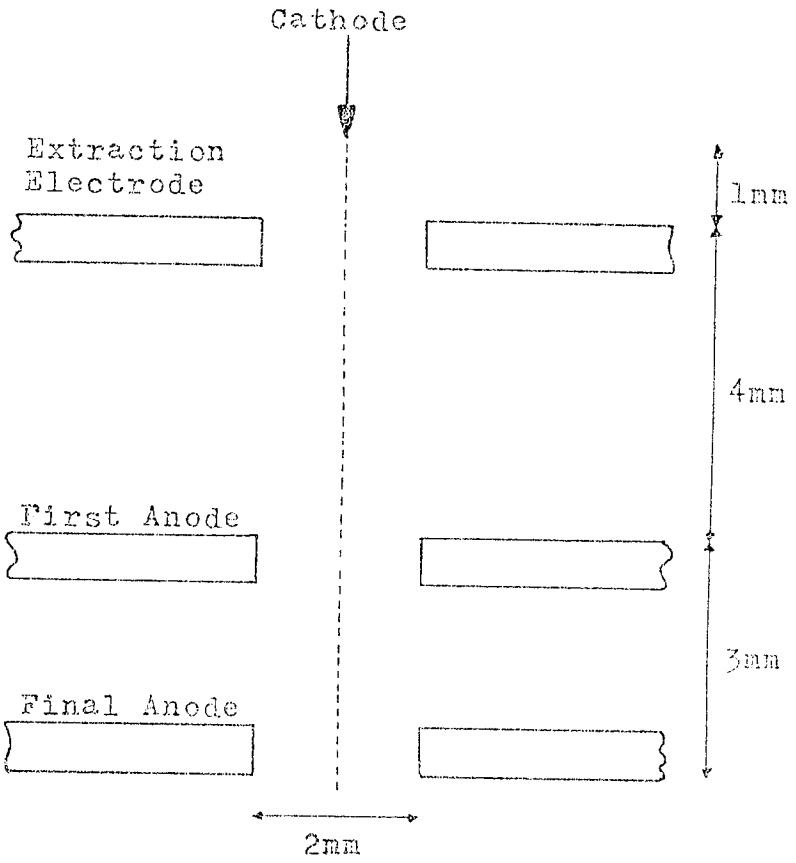

Fig. 6.20 First Electron Gun.

therefore, positioned 4mm from the first anode and the cathode positioned 1mm from the extraction electrode. The diameter of the aperture in the extraction electrode was also chosen to be 2mm. A larger diameter aperture would be of no advantage since the divergence of the electrons is restricted by the first anode. A smaller aperture diameter would unnecessarily limit the current passing this electrode and would also increase the probability of damage occurring to the cathode when aligning it in, or close to, the plane of the extraction electrode.

The second electron gun is shown in Fig 6.21 and uses the electrostatic lens with 4mm apertures and overall electrode separation of 3mm. Computations indicate that for a focus to be achieved with a lens voltage ratio $V_1/V_0 \simeq 5$, the cathode should be about 11mm from the first anode. The extraction electrode was, therefore, positioned 10mm from the first anode and the cathode positioned 1mm from the extraction electrode. The diameter of the aperture in the extraction electrode was chosen to be 3mm. The aperture size in the extraction electrode was chosen to be slightly smaller than the lens apertures to allow for divergence of the electron beam in the 10mm gap.

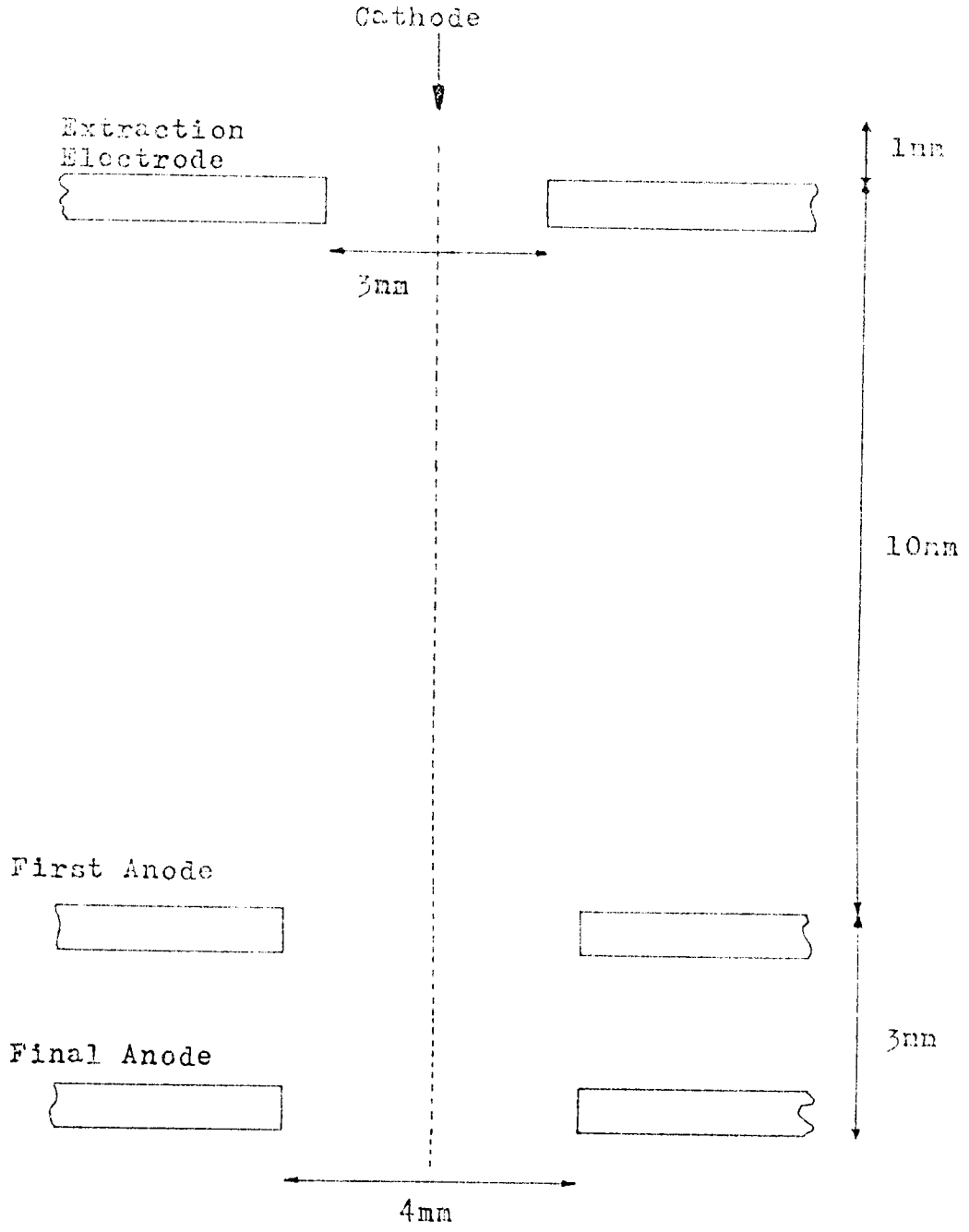

Fig. 6.21 Second Electron Gun.

The first electron gun was mounted in the vacuum chamber with a carbon fibre positioned at the required distance of 1mm from the extraction electrode. The vacuum system was evacuated to a pressure of 1×10^{-8} torr and the performance of the electron gun was examined. For this, the screen and the second anode were held at earth potential while negative voltages were applied to the cathode, extraction electrode and first anode. The second anode was chosen to be at earth potential to allow the beam to be deflected by low voltages when deflector plates were subsequently added. The extraction electrode and the first anode were held at the same voltage and initially were at earth potential. A negative voltage was applied to the cathode and was gradually increased until the carbon fibre emitted 10μA of current. The voltage difference between the cathode and extraction electrode necessary for 10μA emission varied between individual emitters but typically was in the range of 500 to 1000 volts. A negative voltage was then applied to the extraction electrode and first anode, while the negative voltage applied to the cathode was also increased in order to maintain 10μA emission. As the negative voltages were increased, the electron beam focussed on the phosphor screen 300mm from the second anode.

Fig 6.22 shows a sequence of images formed on the

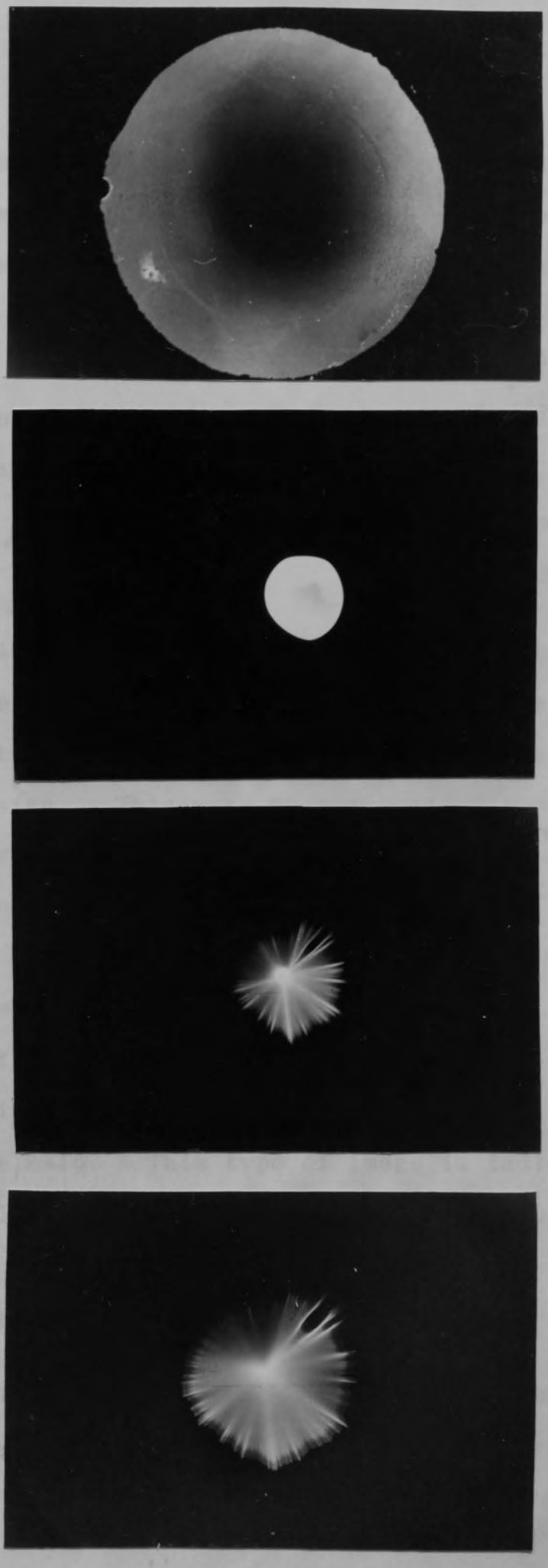

Fig. 6.22

Images formed on the phosphor screen as the first electron gun was focussed.

10mm

phosphor screen as the beam was focussed. The voltages applied to the electrodes for the focussed image were: cathode - 4.5kV, extraction electrode and first anode - 3.6kV, with the second anode and screen at earth potential. This corresponds to a voltage ratio V_1/V_0 = 5 as predicted by the computer programmes. The current reaching the screen in the focussed spot was, however, only 2μA compared with a total emission current of 10μA.

The second electron gun was tested using the same procedure as above and also produced a focussed image with a voltage ratio $V_1/V_0 \simeq 5$, in accordance with the computer aided design. This gun, however, had a much greater current efficiency with approximately 8μA reaching the screen from a total emission current of 10μA. The images formed on the phosphor screen as the beam was focussed were essentially the same as those shown in Fig 6.22 for the first gun. The focussed image consisted of the desired focussed spot with a dimmer but somewhat extensive halo. This type of image is indicative of a particular type of spot aberration caused by the liberation of secondary electrons from the edges of apertures within the electron lens electrodes.(56.)

The second electron gun was chosen for use in subsequent work since this had the more favourable current efficiency. Two approaches were followed in an attempt

to improve the aberrated image formed at the screen. Firstly, great care was taken in rounding the apertures in the electrodes so as to ensure that there were no jagged edges as this is known to partly eliminate secondary electron emission.(56.) Secondly, an additional electrode (see Fig 6.23) was positioned 10mm from the second anode in order to limit the electron beam and to hopefully eliminate the peripheral striations of light. The effect of this limiting electrode was investigated for two different aperture sizes of 2mm and 1mm. The images obtained on the phosphor screen using the electron gun with a 2mm aperture stop are shown in Fig 6.24. As the beam is focussed, radial striations of light appear surrounding the central circular image but separate from it by a dark zone. This outer ring of light diverges as the central image converges to a spot. The images obtained using the electron gun with a 1mm aperture stop are shown in Fig 6.25. These images are similar to those of Fig 6.24 but the intermediate dark zone is greater in extent and is, therefore, more promising for the present application.

The formation of an image consisting of a spot surrounded by a discrete halo ring may be explained by referring to Fig 6.26. In the presence of an optical defect, marginal rays are focussed first and the paraxial rays

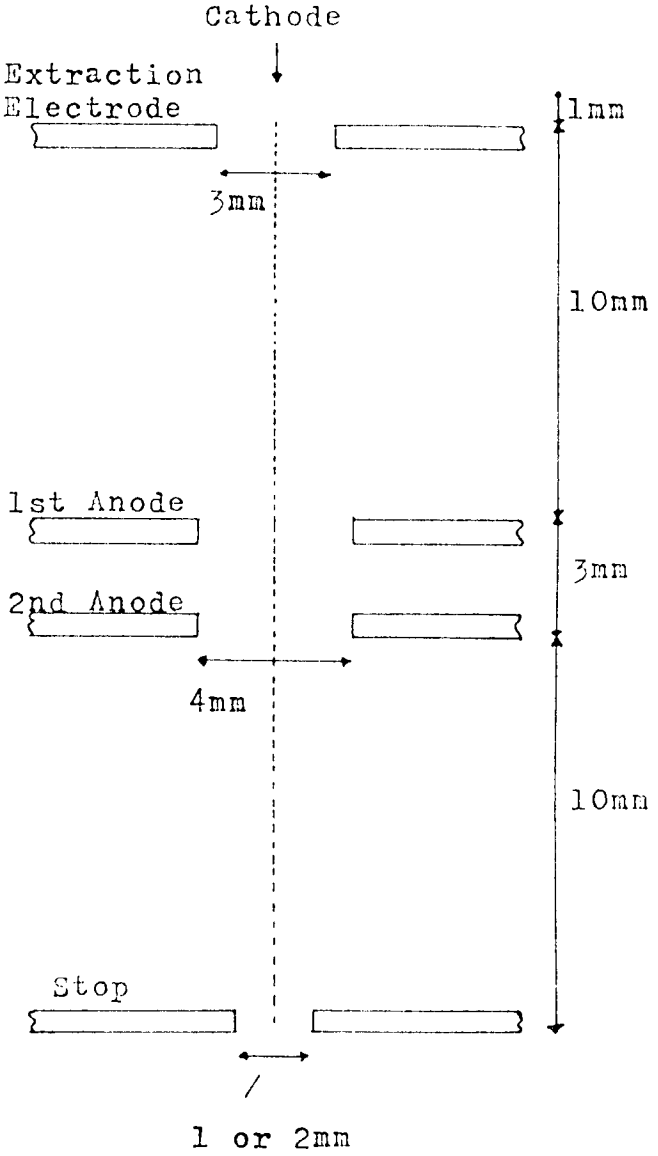

Fig. 6.23 Modified second electron gun: includes an aperture stop.

Fig. 6.24 Images formed on the phosphor screen as the second electron gun, with a 2mm aperture stop, was focussed.

10mm

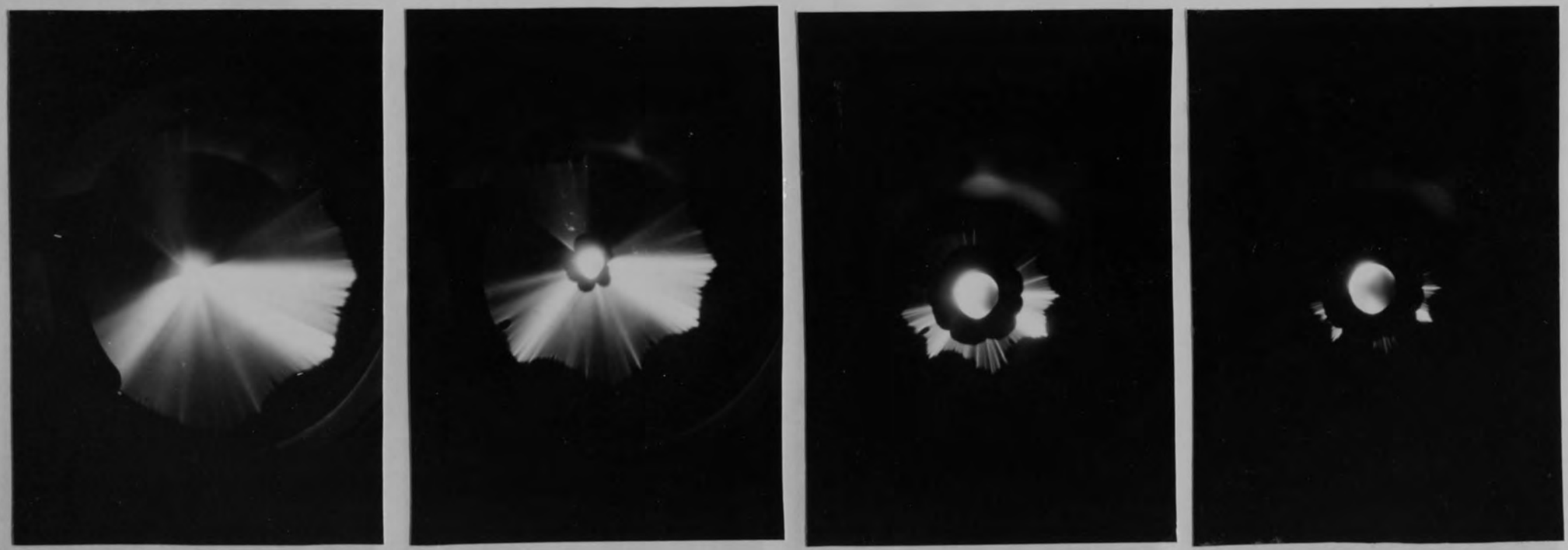

Fig. 6.25 Images formed on the phosphor screen as the second electron gun, with a 1mm aperture stop, was focussed.

10mm

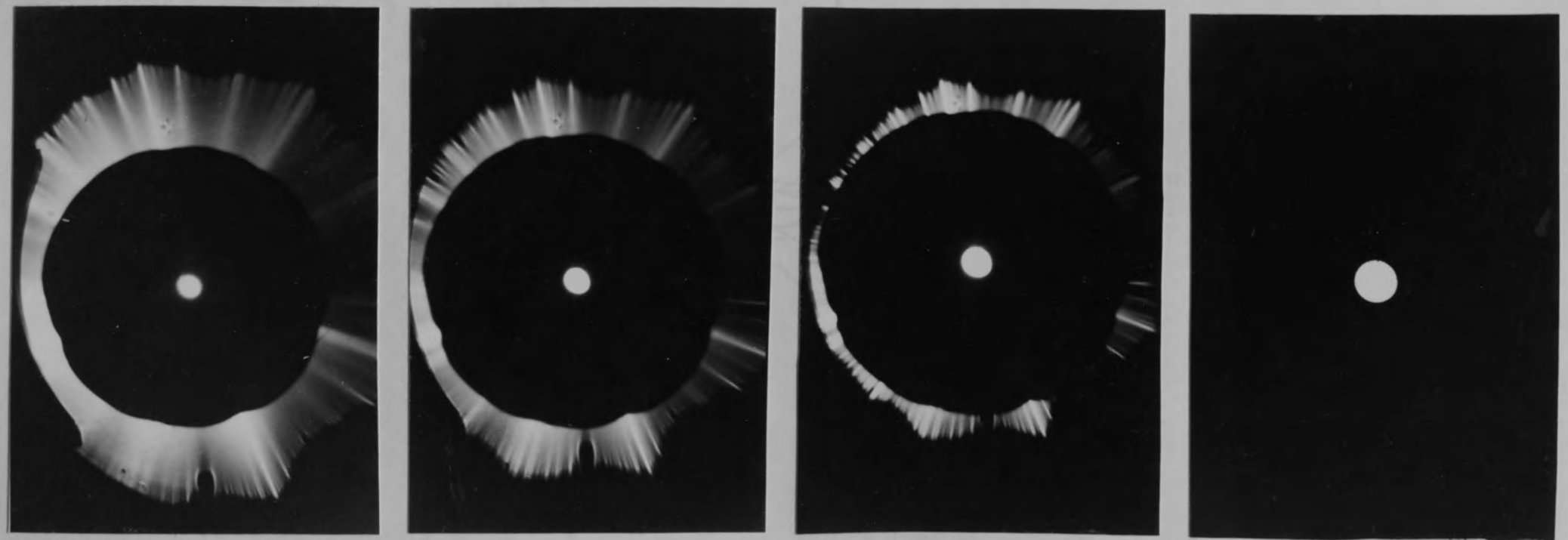

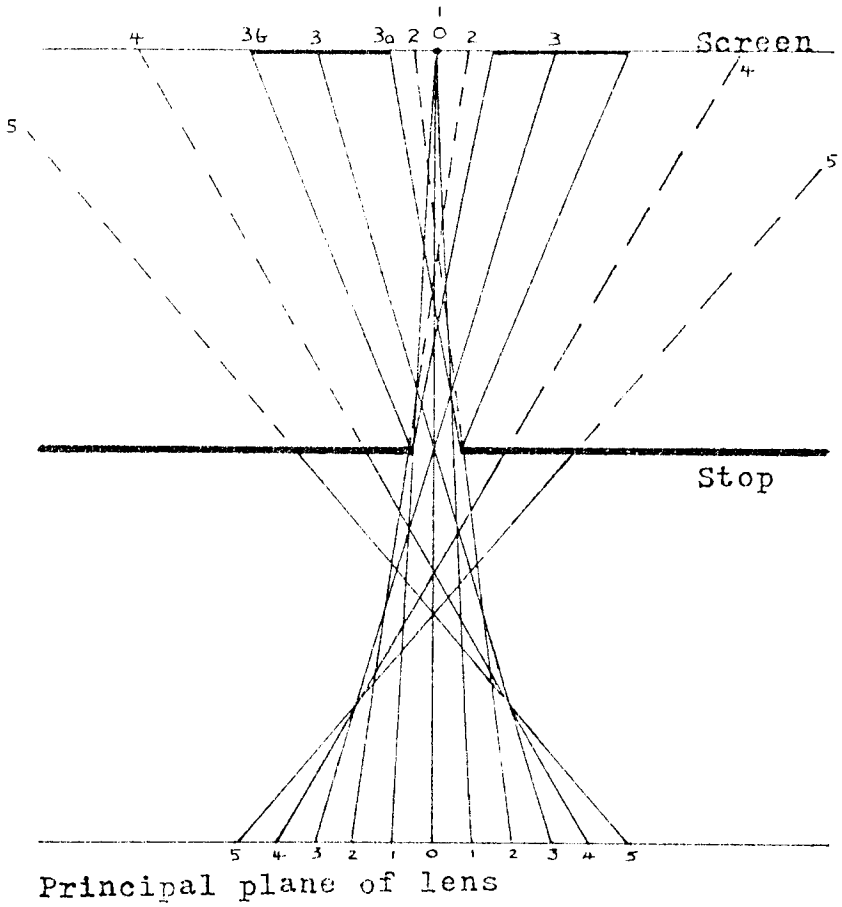

Fig. 6.26 Formation of a halo

are focussed last. The paraxial group of rays (0, 1) form a spot and a group surrounding ray(3) also pass through the aperture, producing the picture of an annular ring on the screen. The ray(2) is intercepted by the electrode so that a dark zone is left between the ring and the spot. Rays(5) and (6) are also intercepted so that the space outside the bright ring is dark again. In order to eliminate the unwanted outer ring of electron induced light, the electron gun was redesigned with the limiting aperture stop being positioned nearer to the principal plane of the lens, as is shown schematically in Fig 6.27. This design was successful with the resulting electron gun producing a well-focussed spot on the phosphor screen, as may be seen in Fig 6.28 which is a series of photographs taken of the images formed during focussing.

6.9 Performance of the Prototype Cathode Ray Tube

Having achieved a suitable electron gun which would form a well-focussed spot on the phosphor screen it was possible, with the addition of standard X and Y deflector plates and an inter-plate shield, to produce a complete prototype cathode ray tube which is suitable for assessing the performance and characteristics of the device with a field emission electron source. Fig 6.29 is a

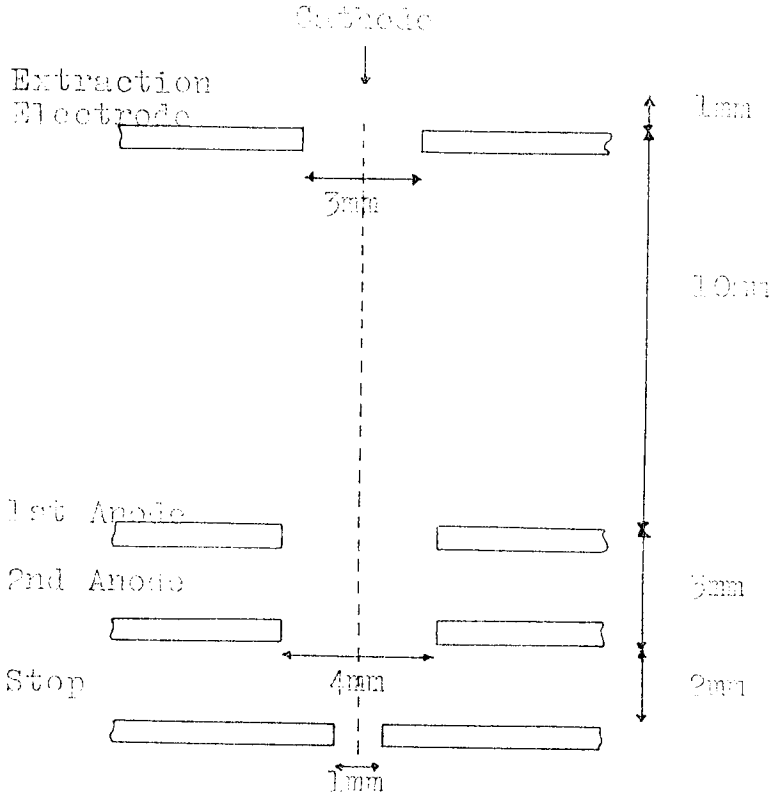

Fig. 6.27 Final design of electron gun.

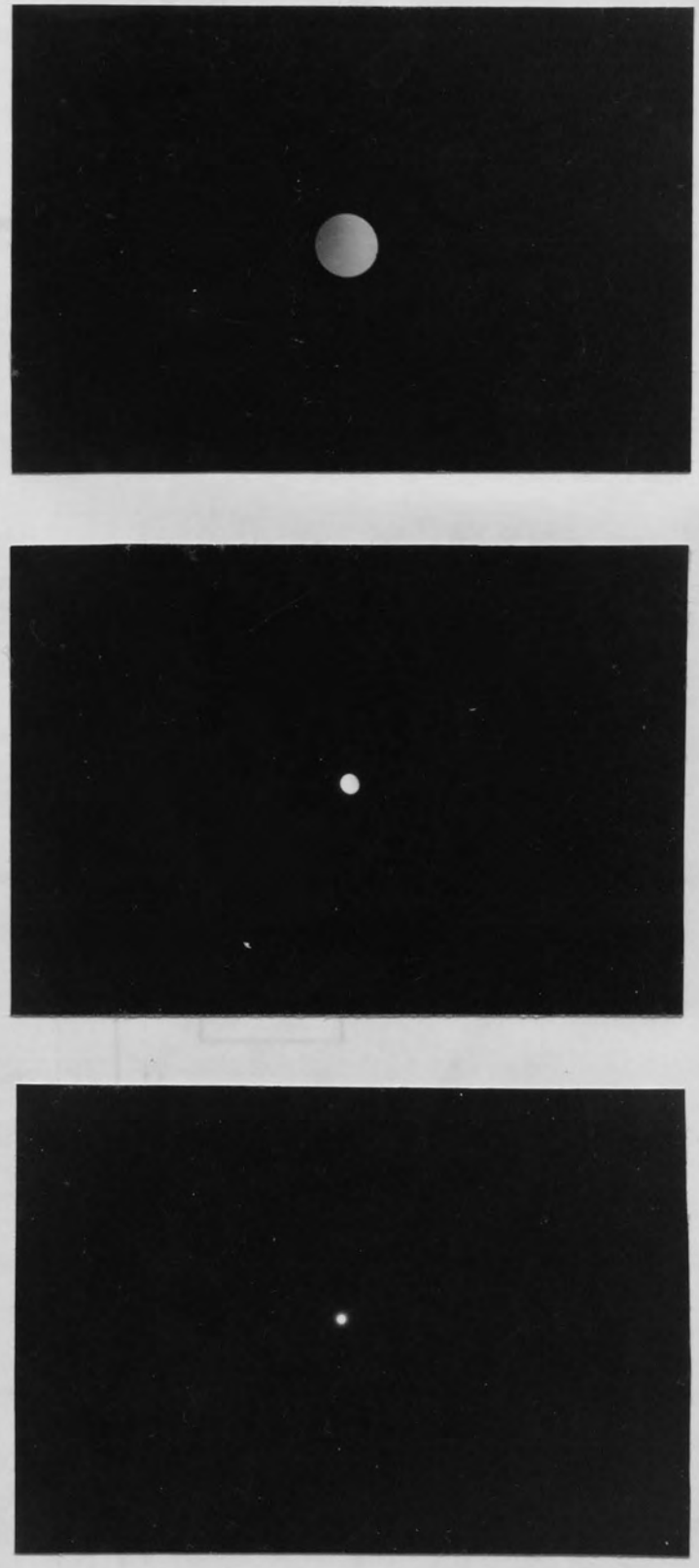

Fig. 6.28 Satisfactory images obtained on the phosphor screen as the electron gun was focussed.

Fig. 6.29 Drawing of the prototype cathode ray tube.

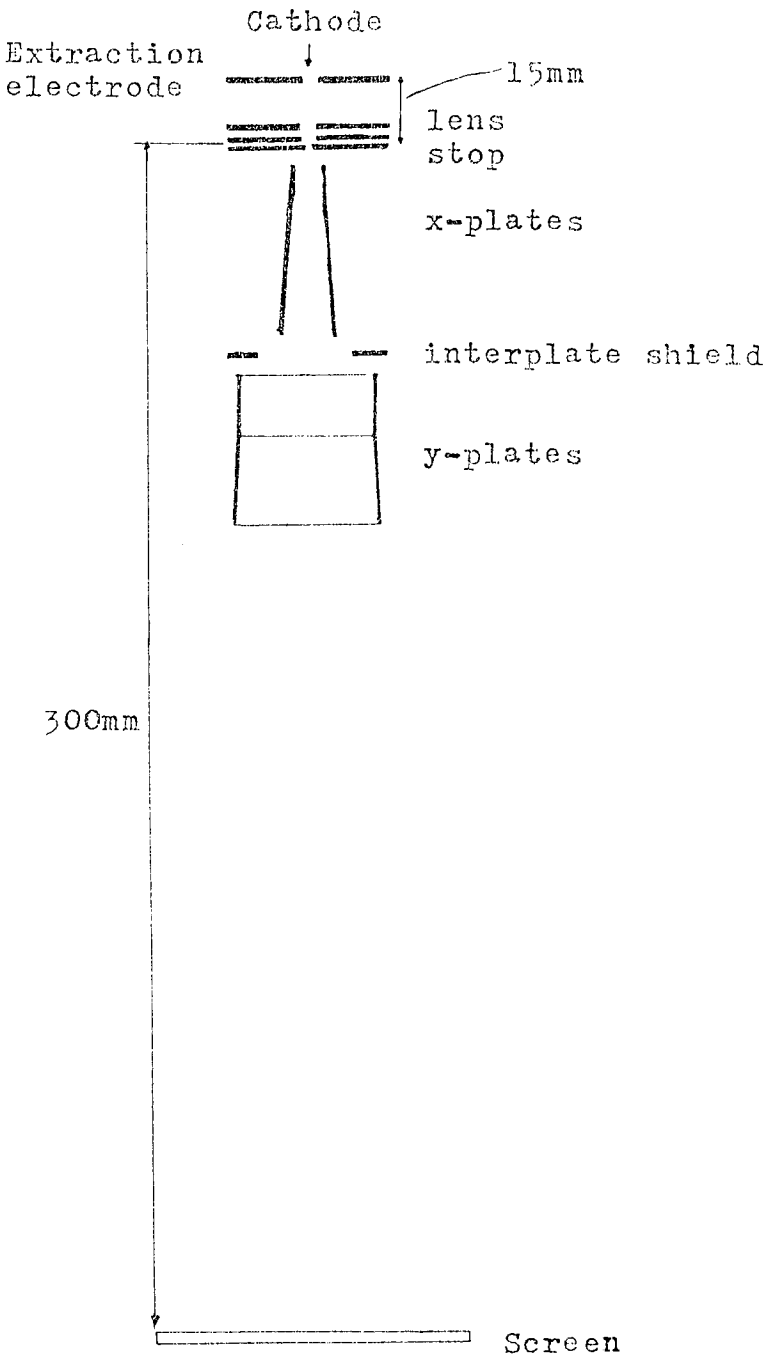

dimensioned drawing showing the overall layout of the tube, whilst Fig 6.30 is a photograph of the experimental electrode assembly which was positioned inside the ultra-high vacuum chamber relative to the field emitting tip and the phosphor display screen thus forming a demountable cathode ray tube.

To evaluate the performance of the tube, a carbon fibre emitter was electrolytically etched, in the manner previously described, and aligned with the extraction electrode before evacuating the chamber to a pressure of about 10^{-8}torr. After applying the necessary voltages to the tip, extraction electrode, electrostatic lens and aperture stop, and with the deflector plates and phosphor screen at earth potential, a good image was readily obtained on the screen. At first, however, the spot showed signs of 50Hz noise but this was easily eliminated simply by moving the high-voltage power supplies further away from the tube. To check that the deflector plates were functioning satisfactorily, two sinusoidal voltage signs, each of $\sim$50 volts amplitude, obtained from signal generators were applied simultaneously to the x- and y- plates. The electron beam was thus subjected to two mutually perpendicular simple harmonic motions so that the trace produced by the spot resulted in an ellipse when the potential differences were of the same

Fig. 6.30 Photograph of the experimental electrode module forming the basis of the prototype cathode ray tube.

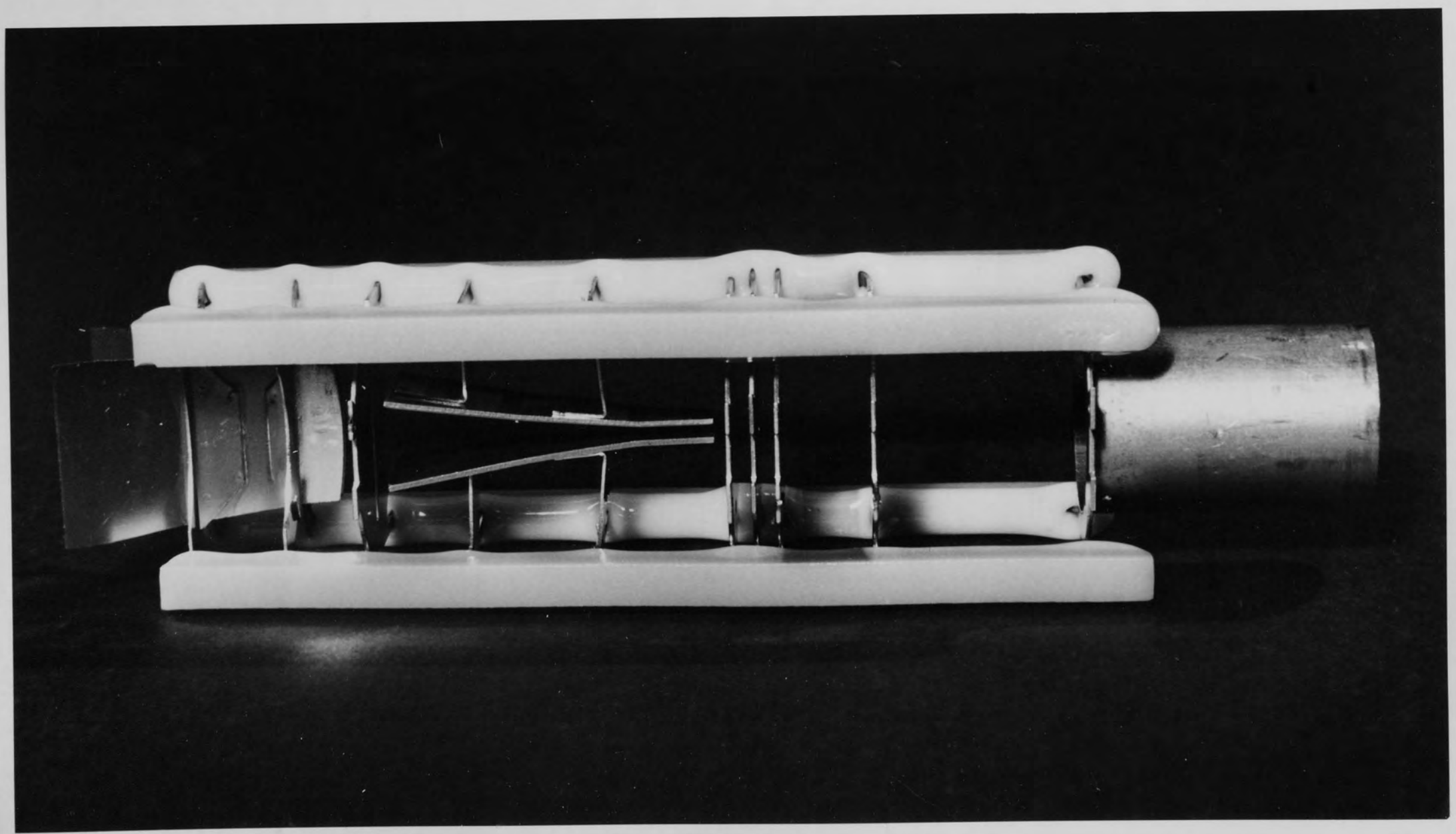

frequency and the more complex Lissajous figures when they were of different frequencies. Although the phases of the two generators were uncoupled which resulted in the pattern drifting with time, the photographs presented in Fig 6.31 show that the resulting traces are well defined and of adequate brightness.

To examine the performance of the tube in a more conventional mode of operation, i.e. for studying the variation of a voltage with time, an adjustable time base was applied to the x-plates; the latter being derived from the x-output of a conventional thermionic oscilloscope in the form of a sawtooth potential difference. When an alternating voltage from a signal generator was applied to the y-plates, the prototype tube functioned identically to a conventional tube, and by selecting a suitable time base a good visual display was achieved. A selection of sinusoidal waveforms within the frequency range of 10-50000Hz were displayed on the output screen and a sample of these standing waveforms is shown in Fig 6.32. A feature which is to some extent noticeable in all the photographs is that the trace appears dimmer in the centre of the image: this is unfortunately due to the phosphor screen being burnt during the course of the earlier experiments when the electron beam was stationary in the centre for long period of time.

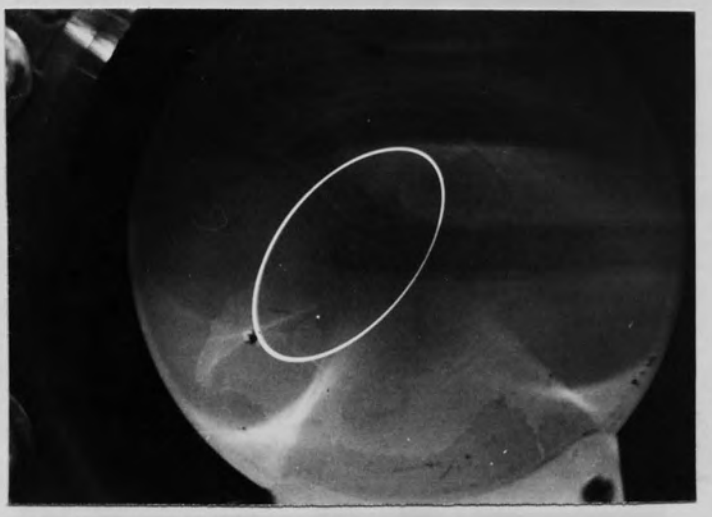

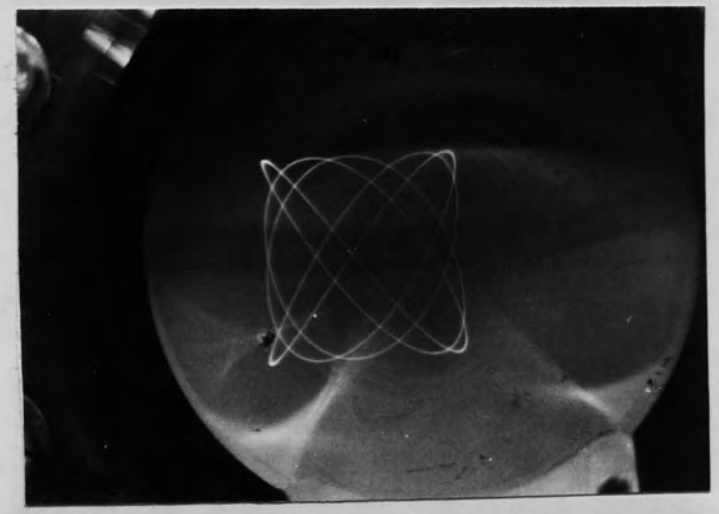

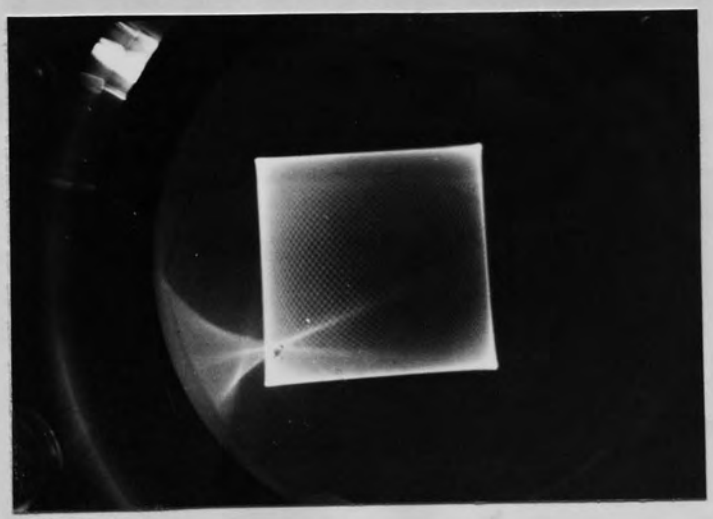

Fig. 6.31 Lissajous' figures displayed on the prototype cathode ray tube.

Note: Caustics are reflected room light.

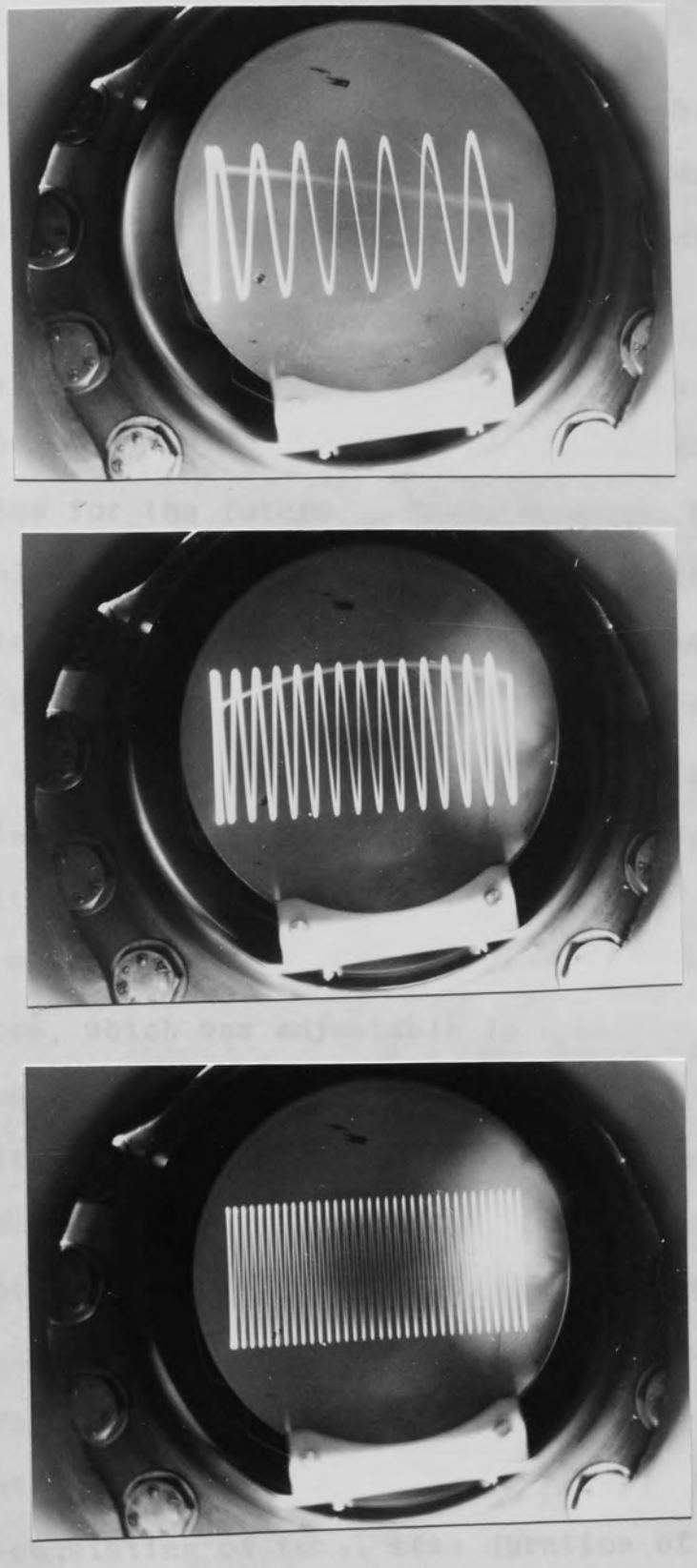

Fig. 6.32 Sinusoidal waveforms displayed on the prototype cathode ray tube.

Fig. 6.33 Single shot traces of varying duration as displayed on the prototype CRT.

Total
Scan
Duration

20 ms

1 s

5 s

50 s

trace was of constant light intensity and never showed any signs of fluctuating; scans of duration greater than about 2s however invariably fluctuated; whilst in the intermediate range, the traces on occasions were of variable light intensity.

6.10 Fluctuations of the Visual Display

To further investigate the temporal changes in light intensity of the visual display, a simple light detector was constructed. The photometer circuit is shown in Fig 6.34 and consists of a high-speed photodiode and a F.E.T. operational amplifier. To screen the light detector from unwanted electrical noise, the circuit was enclosed by a metal container with a fine metal mesh over the window of the photodiode. After the metal container was connected to the flange of the vacuum chamber's viewpoint as shown in Fig 6.34(b), the position of the electron beam in the form of a focussed spot was adjusted until the photodiode showed maximum response. The output from the detector was used to drive a chart recorder (J.J.Lloyd CR100). Although the response time of the light detector was limited by the writing speed of the recorder to about 1/5 second, this was satisfactory since it is known from the previous single shot work that the fluctuations in the light intensity occur within this detectable range.

A typical trace of the short-term light intensity variations using this light detector is presented in Fig 6.35 and shows that the intensity fluctuates considerably in any one second interval. Longer term variations are shown in Fig 6.36: here, a comparison is made with the light output from a conventional cathode ray tube and it can be seen that whilst the field emission tube fluctuates more severely in the short-term, the overall stability compares well with that of the conventional tube. It should, however, be noted that the thermionic tube was many years old and no doubt past its peak performance.

The reasons for the fluctuations in light intensity of the visual display are directly associated with instabilities of the current obtained from the field emitting tip. From observations of the image on the fluorescent screen of a field emission microscope, it is apparent that emission from several ($\sim$10 - 50) discrete, irregular regions on the cathode surface contribute to the total current emitted from a carbon fibre. By examining the intensity of light from these regions it is clear that the magnitude of the current emitted from individual emission sites changes with time (in fact at times there may be no current originating from a given site) and this results in variations in the total emission current.

Fig. 6.35 Light variations from the prototype CRT.

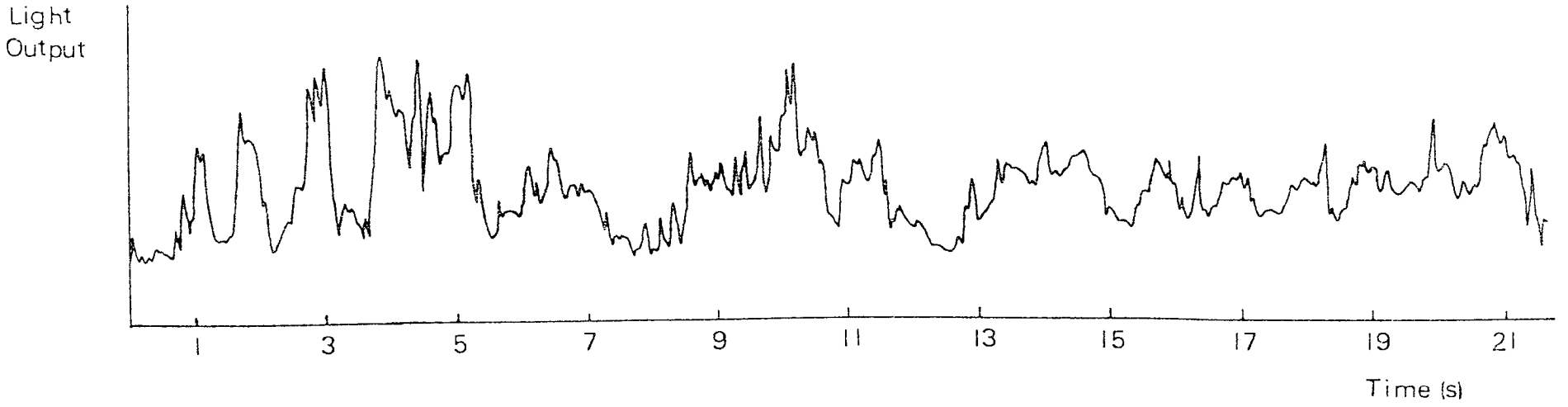

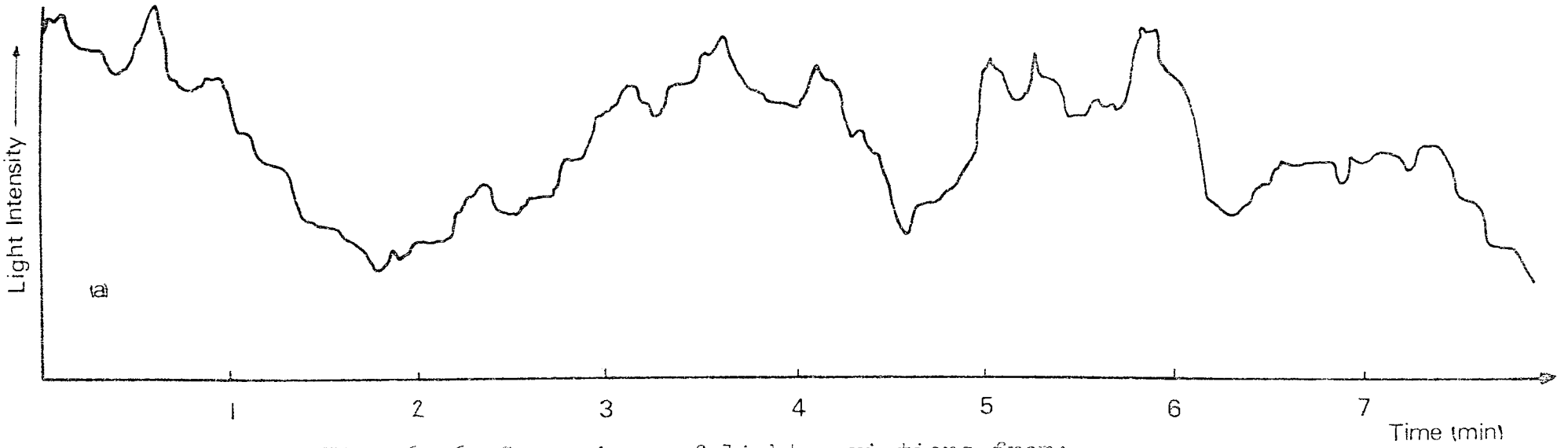

Fig. 6.36 Comparison of light variations from:
(a) a conventional CRT, and
(b) a field emission CRT.

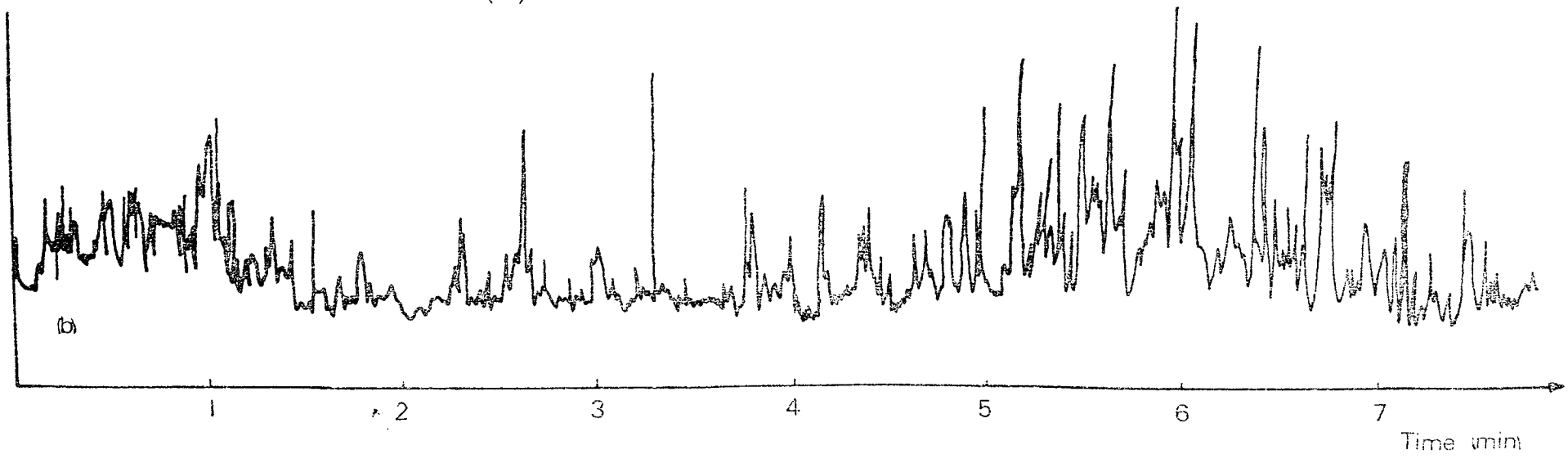

Since the prototype cathode ray tube was designed for high current efficiency, it is expected that the fluctuations in light intensity of the final image will be strongly correlated with the variations in the total current emitted from the tip as is confirmed by the recordings shown in Fig 6.37. In view of this correlation it is worthwhile examining methods of stabilising the total current emitted from the electron source with the view of subsequently stabilising the final visual display. The first method was to re-examine the effect of placing a high-valued resistor in series with the emitter, as previously employed by Baker et al.[43.] The reasoning behind this is that as the current flowing through the emitter and resistor varies this will alter the voltage dropped across the high-valued resistor resulting in the voltage applied to the tip being compensated. It was found that by adding a resistance of the order of $10^8\Omega$ the fluctuations in total emission current were dramatically reduced. Fig 6.38 allows a comparison to be made between typical total current-time traces obtained with (a) no stabilisation, (b) with a 100MΩ resistor in series and (c) with a 350MΩ resistor in series. As can be seen from these traces the addition of a high-valued series resistor provides a simple but effective method of stabilising the total current. An alternative method was also examined which involved the modification

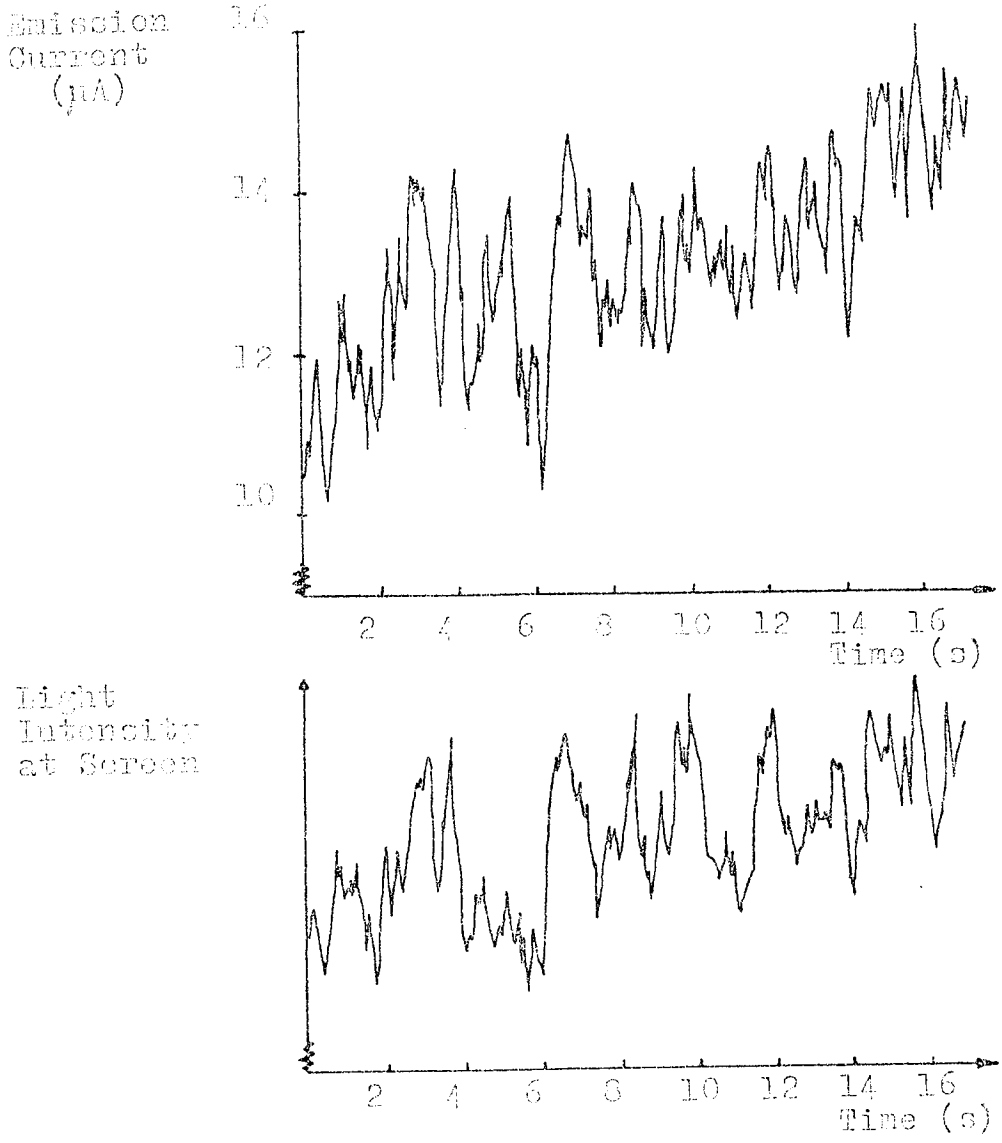

Fig. 6.37 Consecutive traces for the electron current from the emitter and the light intensity at the screen.

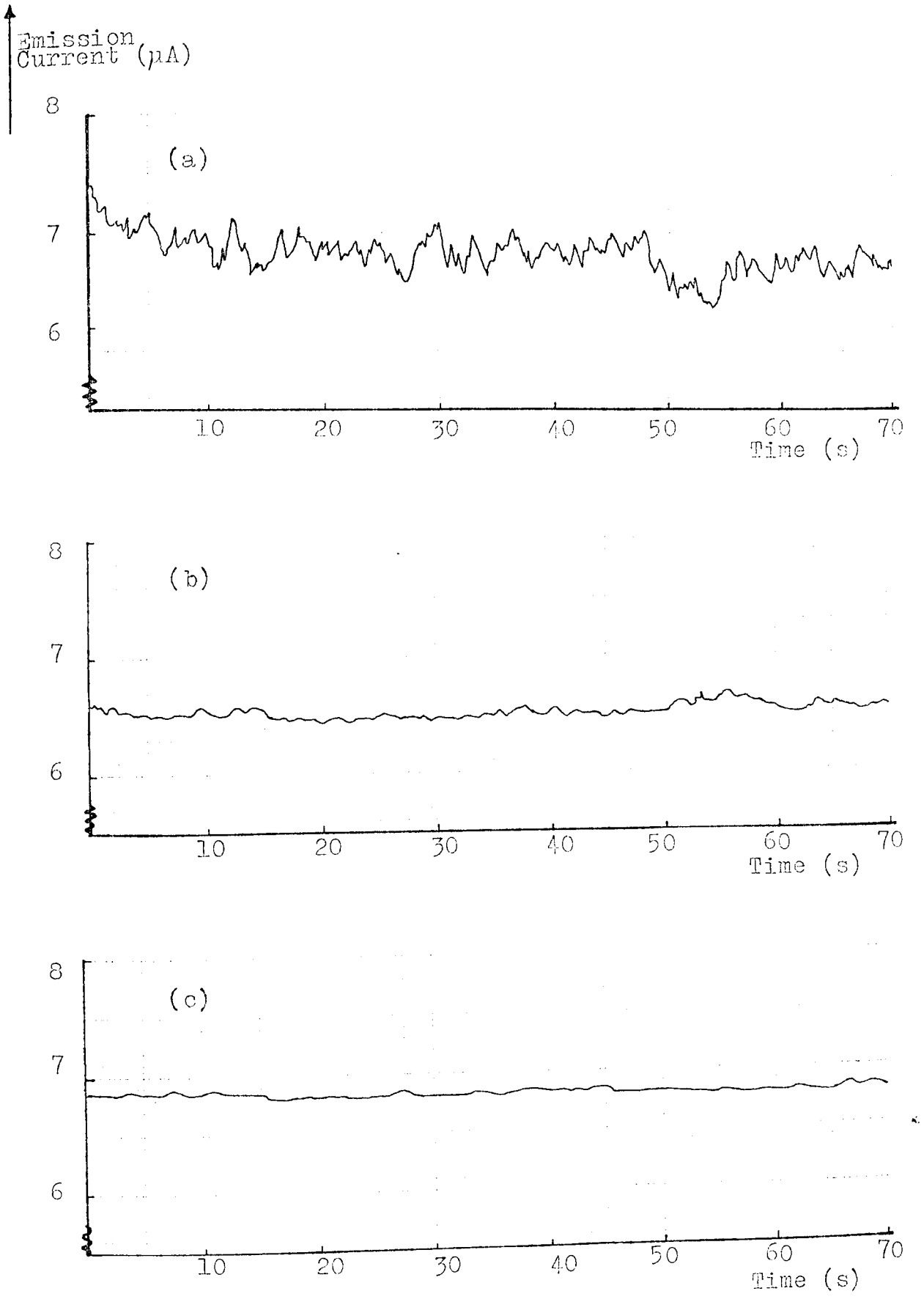

Fig. 6.38 Typical emission current fluctuations obtained (a) with no stabilisation; (b) with 100 MΩ in series; and (c) with 350 MΩ in series.

of a Brandenburg high voltage supply for constant current operation. This was tested using a simple diode arrangement consisting of the field emitter and fluorescent screen, and the essence of the modification to the power supply entailed removing the voltage stabilising feedback resistor chain and replacing it with the variable field emission load. The initial results were promising as shown in Fig 6.39 in which comparative total current-time traces show typical results for (a) no stabilisation, (b) with the 'constant current' power supply, and (c) with a 100MΩ resistor in series. As can be seen from these traces the use of the modified power supply produces a significant improvement in current stability and although in its present state it is inferior to the simpler addition of a series resistor, further modifications could be made to optimise the response of the supply to the frequency of fluctuation of the electron source.

There is, however, a serious drawback to both of these methods of stabilising the total emission current since they involve modulating the voltage applied to the emitter. Thus when these techniques are applied to the prototype cathode ray tube with fixed anode voltages, the varying emitter voltage (of ~100V) will lead to a change in the focal properties of the lens and the beam energy with the inevitable result of defocussing and varying

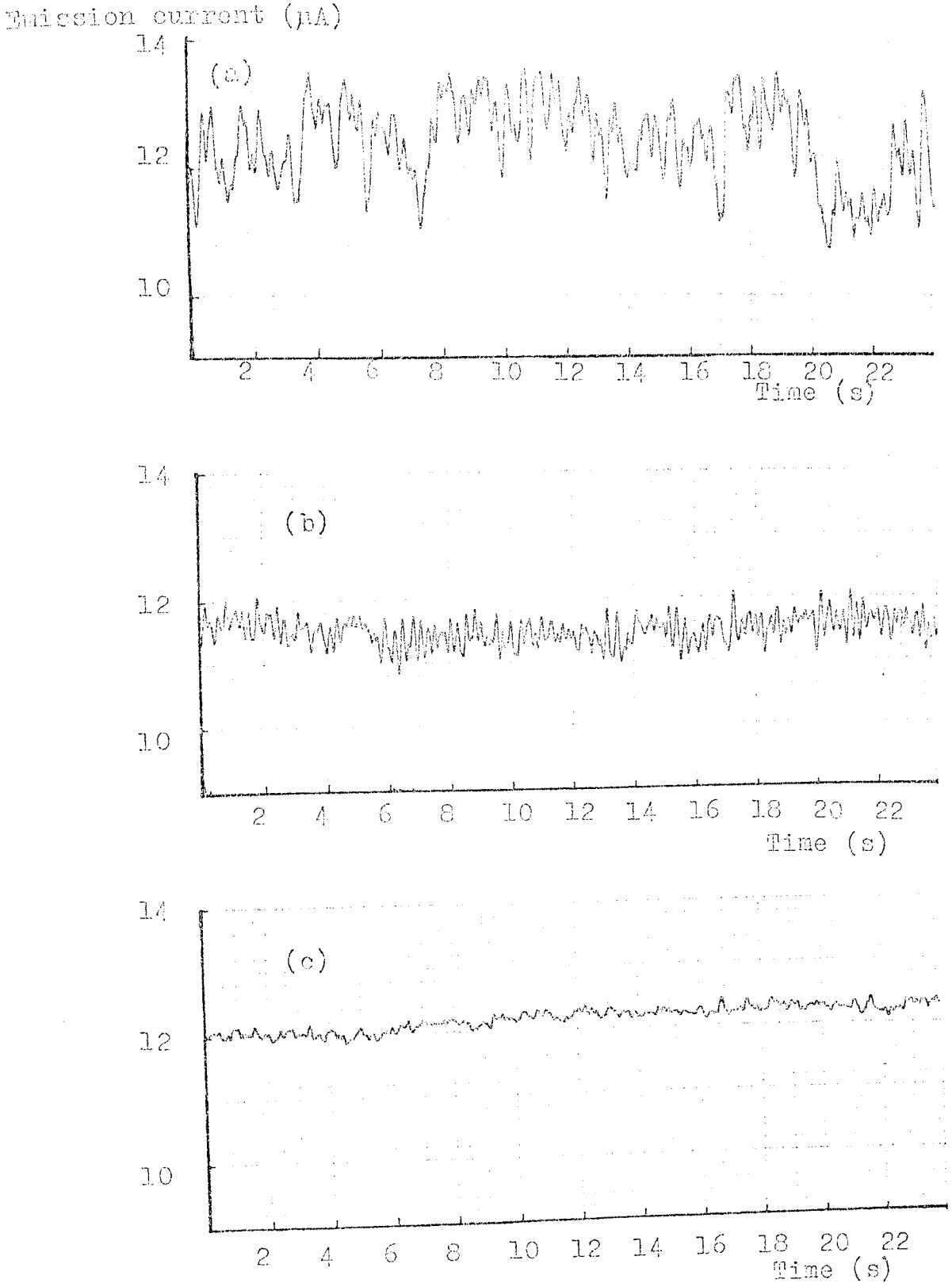

Fig. 6.39 Typical emission current fluctuations obtained (a) unstabilised; (b) with the 'constant-current' power supply; and (c) with 100MΩ in series.

the intensity of the final image. This effect was examined in the experimental system and found to result in an unacceptable variation of the image on the fluorescent screen with time. In fact, when measured with a travelling microscope, the 0.2mm focussed spot was found to be defocussed to about 1mm diameter by an emitter voltage change of 100V, which is typical of the magnitude of voltage change necessary to maintain a constant emission current of 10μA. Whilst it should be possible to eliminate the defocussing effect by arranging the voltages applied to the extraction electrode and first anode to vary in a similar manner to the voltage applied to the tip, there will remain fluctuations in light intensity due to the changing beam energy. It is suggested, however, that in future work the resulting magnitude of the light fluctuations should be investigated when the voltages are coupled in this manner.

The final method of stabilisation that will be considered uses a technique proposed by Cleaver[66.] for the stabilisation of the electron probe current in a scanning electron microscope with a tungsten field emission cathode. The essence of this technique involves collecting an annular sample of the near-axial beam current. This beam current monitor signal is then compared with a reference

level and an error signal derived which is used to determine the voltage applied to the extraction electrode. An advantage to this method is that although the voltage on the extraction electrode is varied there will be no change in the final beam energy. There is, however, the unavoidable consequence that varying this voltage will perturb the electric field in the electron gun and the repercussions of the defocussing of the beam must be examined. For this technique to be effective it is necessary to have a monitor signal which provides a good measure of the final beam current. Fortunately, the prototype cathode ray tube already has an electrode which is ideally suited for this purpose - viz, the electrode containing the limiting aperture stop. The outer part of the beam emerging from the second anode is incident upon this electrode and thus an annular sample of the near axial current is derived. Records of the photodiode screen current and the corresponding beam monitor signal are shown in Fig 6.40 indicating that both fluctuate essentially by discrete steps. Although a counterpart can be found in the monitor signal to nearly every step in the probe current, the amplitudes of the steps are not completely proportional. This lack of proportionality is consistent with the electron source containing several independently fluctuating emission sites

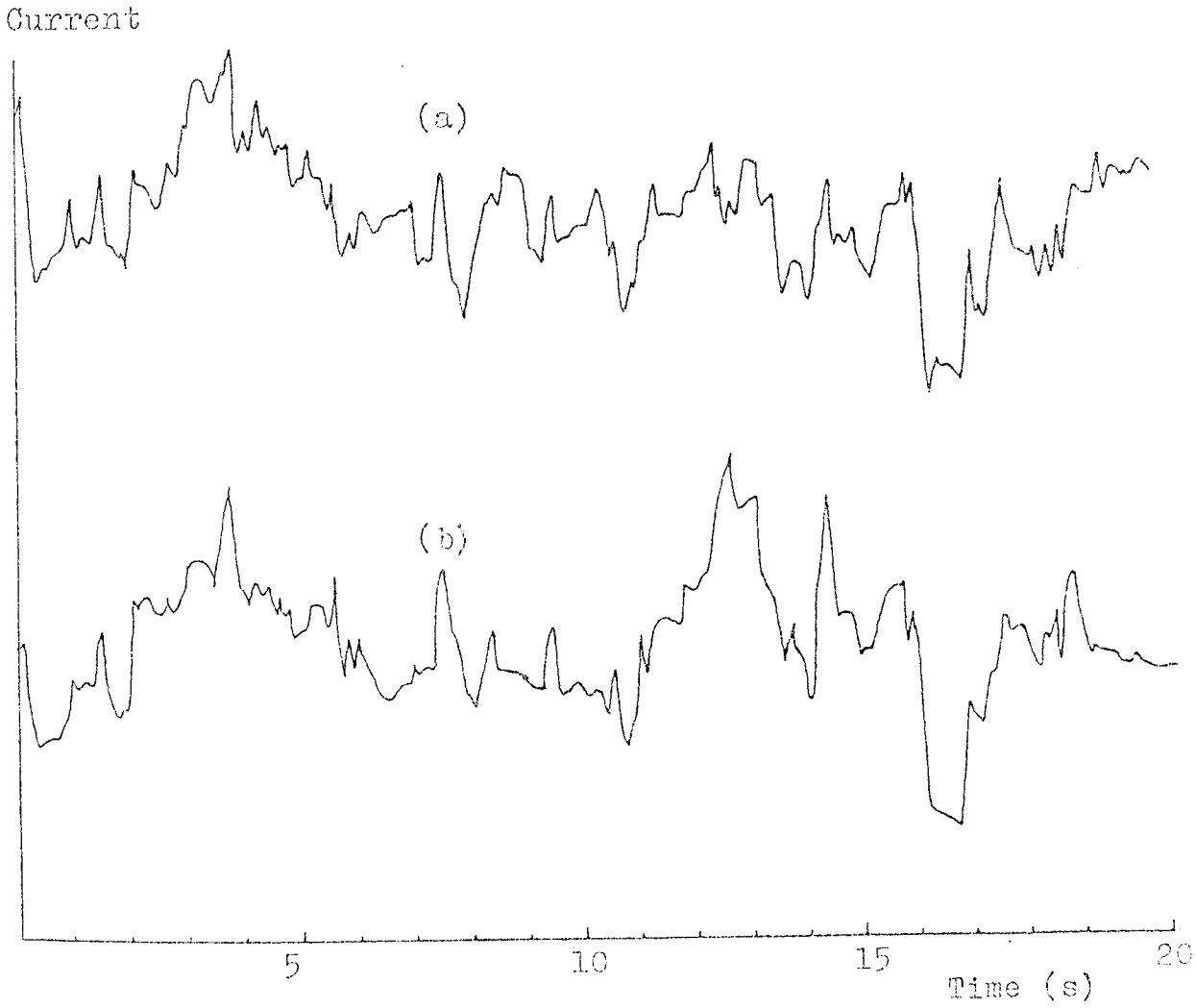

Fig. 6.40 Traces recorded simultaneously showing-
(a) the beam monitor signal, and
(b) the photodiode screen current.

which each make a contribution to the screen current and to the monitor signal. From direct visual observation of a field emission microscope image of the electron source it is found that the relative importance of each emission site varies with time. Therefore if the ratio of the contributions made to the two collected currents is different for each site then this will result in the relative amplitudes of the currents varying with time. The significance of this result is that maintaining the monitor signal constant will not necessarily ensure that the screen current is completely constant. There does, however, appear to be sufficient correlation between the two currents for this technique to be further evaluated in future work.

CHAPTER 7

STUDY OF THE PHYSICAL CHARACTERISTICS OF FIELD EMISSION FROM CARBON FIBRE

7.1 The Energy Distribution of Electrons Field Emitted from Carbon Fibre

Whilst the work reported in the previous chapter indicates that carbon fibre is a field emitting material potentially suitable for electron optical applications, there remain many questions to be posed about the physical mechanism by which the electrons are emitted. To obtain more fundamental evidence about this mechanism, several experimental investigations were performed and these are now presented. The first of these concerns the distribution of energies of electrons field emitted from a carbon fibre tip. The character of such energy spectra is determined partly by the nature of the electronic states from which the electrons are emitted, partly by the statistical distribution of the electrons among these states, and partly by the details of the tunnelling barrier through which emission occurs. Energy distribution measurements were originally used as a sensitive test of the validity of the theoretical model for field electron emission.(18.,67.) More recently, it has been realised that they contain detailed information about band structure effects, surface

states, and atoms chemisorbed on surfaces.[68.] In addition to being of intrinsic theoretical interest, the energy distribution should be narrow if the emitter is to be useful for high resolution guns.

Two groups of workers have previously reported energy distribution measurements for carbon fibre emitters. Firstly, Braun et al.,[43.] working at Aston's field emission laboratory used a van Oostrom type of retarding potential analyser. They reported a narrow half-width of 0.21 ± 0.1eV and concluded that it was comparable to the metallic type emission characteristics obtained from tungsten. The other group, Heinrick et al.[44.] also reported energy distributions obtained from carbon fibres but in their work the electrons had been previously accelerated to 30kV in a poorish vacuum pressure of about 10^{-6}torr. They found that in the case of small total electron current ($\approx 10^{-9}$A) the spectrum had a half width of 0.215eV and this increased with growing emission current up to 1eV for 10μA. The broadening of the spectrum was attributed to instabilities in the surface structure and to more than one emission site contributing to the electron current.

To obtain more detailed information, the electron energy spectrum of a carbon fibre field emitter was re-measured using an UHV advanced high resolution spectro-

meter facility[69], as shown in Fig 7.1 and Fig 7.2, which unlike the previous measurements enabled the emission spectrum to be related to the Fermi level of the substrate cathode; thus providing valuable information about the origin of the emitted electrons. With the application of a suitable field between the emitter and anode a spatial image of the electrons tunnelling from the emitter surface is projected onto a fluorescent anode screen. A sample of the nearly radially divergent electron beam (i.e. within a small solid angle) passes through a probe hole cut in the screen and is then subsequently energy analysed. The heart of the instrument is a differential type of spherical deflection analyser, which is based on a 180^{o} deflection analysing element formed from two concentric hemispheres of 50mm mean radius. The output of the analyser uses an electron multiplier to increase the sensitivity of collector current detection. The emission energy distribution is obtained directly from the analyser and has a nearly constant signal to noise ratio over the entire energy spectrum.

The mechanical layout of the spectrometer is shown in Fig 7.2. The analyser is housed in a stainless steel vacuum chamber which is pumped using an oil diffusion pump, liquid nitrogen cold trap and a titanium sublim-

Fig. 7.1 Field electron emission energy analyser.

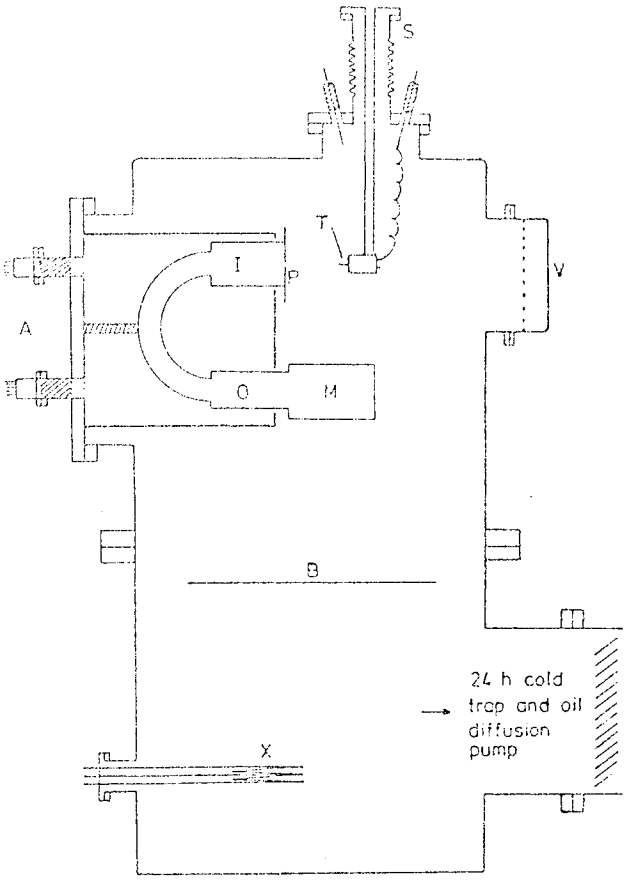

Fig. 7.2 Layout of analyser in vacuum chamber

A, analyser; O, output lenses; I, input lenses;
P, phosphor-coated anode; T, field emitter;
S, specimen manipulator; M, electron multiplier;
V, viewport; B, baffle plate;
X, sublimation pump filaments.

ation pump to an ultimate pressure in the 10^{-11} torr range. The mechanical design of the vacuum system makes use of demountable flanges from which the analyser and emitter assemblies are independently supported. The hemispherical analysing element with its associated input and output lenses, and electron multiplier is mounted horizontally, whilst the specimen stage and its electrical feedthroughs are mounted vertically from the top flange. A large viewing port assists in the specimen alignment procedure and enables the field emission pattern to be viewed on the anode screen. The emitter assembly is supported from a bellows-mounted manipulator stage which enables the tip to move in the planes parallel and normal to the screen, so that it can be aligned with the 1mm probe hole.

The essential features of the electron optical system are shown in Fig 7.3. The four element input lens was designed to decelerate the electrons to a low energy and form a real magnified image of the source at the entrance aperture of the hemispheres. For experimental flexibility the input lens system is capable of operating over a range of input energies (1-4keV) and a range of analysing energies (1-20eV). The deflecting element consists of two hemispheres of radii 40 and 60mm, which

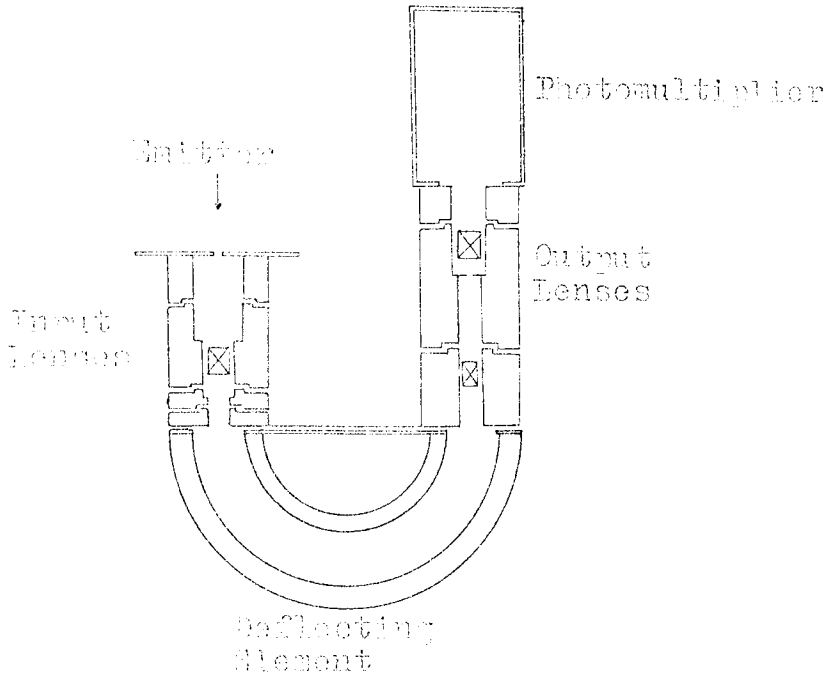

Fig. 7.3 Essential features of the electron optical system.

require a theoretical voltage difference of 1.67V to achieve the designed resolution of 20meV. The function of the output lens system is to reaccelerate the electron beam leaving the hemispheres and at the same time to collimate it into the electron multiplier. The performance of the spectrometer has previously been demonstrated[69] in terms of the energy spectra of a tungsten emitter at 300 and 80K, for which comparative theoretical data exist and was found to have a high sensitivity and a resolution of better than 30mV.

The energy spectra of three carbon fibre emitters were measured and were found to all have the same general features. The investigation of one of these emitters, from which was obtained the most comprehensive set of results, will now be presented. A carbon fibre emitter was prepared by electrolytic etching as previously described (Chapter 6) and after assembly in the spectrometer, the system was evacuated and baked for 18 hours at $\sim 230^{\circ}C$. Subsequent cooling and filling of the liquid nitrogen cold trap gave a chamber pressure of 1×10^{-10} torr. An increasing voltage was applied between the emitter and the anode screen until a total emission current of $1\mu A$ was drawn from the fibre. A number of interpolative adjustments were then made to the horizontal and vertical positions of the emitter, and the spectrometer input lens

voltages to obtain a maximum output signal which was displayed on an oscilloscope. Once the output signal had been optimised the energy spectra of the electrons field emitted from carbon fibre under various conditions could be examined. Spectra of interest were "frozen" on the storage oscilloscope, the previously calibrated[69.] position of the Fermi level on a metallic emitter was superimposed, and the results recorded using a Polaroid camera. (See also Fig. 7.5)

The distributions obtained were of two main types as can be seen from the typical examples presented in Fig 7.4, where the x-axis corresponds to electron energy in eV and ranges from high energy to low energy left to right, and the y-axis represents electron current per unit energy. The position of the Fermi level on a metallic emitter is shown in all cases as a superimposed white line. The first type of distribution has a single energy peak, whilst the other type contains an additional subsidary energy peak. Although both types frequently occur, the single peaked distribution is the more common. Fig 7.5 compares a typical single peaked energy distribution from a carbon fibre with that from a tungsten field emitter obtained previously with this spectrometer[69.] under identical temperature and pressure conditions. There are important differences between the features of the two

Fig. 7.4 Typical electron energy distributions from a carbon fibre field emitter.

The position of the Fermi level (FL) on a metallic emitter is also shown. The x-axis is electron energy in eV; (a): 0.1eV per division, (b): 0.2eV per division. The y-axis is electron current per unit energy.

A

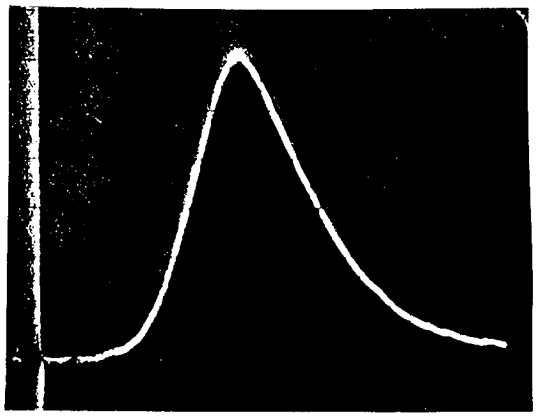

FL

B

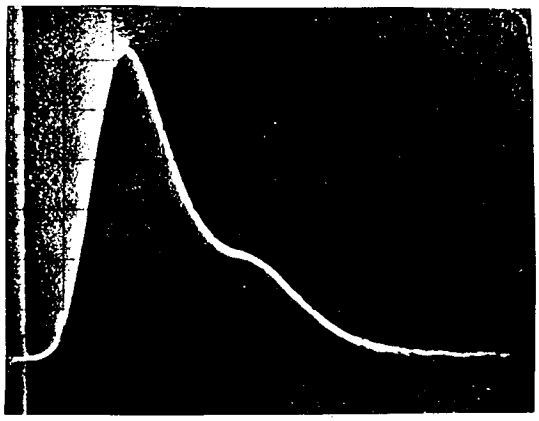

FL

distributions which are readily distinguished. The first and most important is the position of the Fermi level relative to the distributions which, in accordance with Young,[16] has been marked at a point 73% up the high energy slope of the tungsten reference emitter. It will be seen that the carbon fibre distribution exhibits a shift relative to the Fermi level of the metallic emitter. Other differences of interest are that the half-width of a carbon fibre distribution is generally broader than that of the tungsten emitter and that the shape of the carbon fibre spectrum is more symmetrical. To be specific, the carbon fibre spectrum presented in Fig 7.5 (which corresponds to an emission current of $\sim 1 \times 10^{-8}$A obtained at an emitter to screen potential difference of ~800V) is shifted ~0.45eV from the Fermi level of a metallic emitter; the half-width of the distribution is ~0.40eV compared to ~0.24eV for tungsten; and the high energy slope width (defined as the energy interval between the 90% and 10% peak height points) is ~0.24eV compared with the much sharper characteristic slope of width ~0.14eV for tungsten. More generally, the spectral shift was observed in all the distributions recorded and was found to increase from ~0.30eV to ~0.60eV with increasing emission current from $\sim 10^{-10}$A to $\sim 10^{-7}$A. The half-width of the distributions followed

Fig. 7.5 Electron energy spectra obtained from a carbon fibre emitter and a reference tungsten emitter[69].

The x-axis is electron energy in eV (0.2eV per division).
The y-axis is electron current per unit energy.

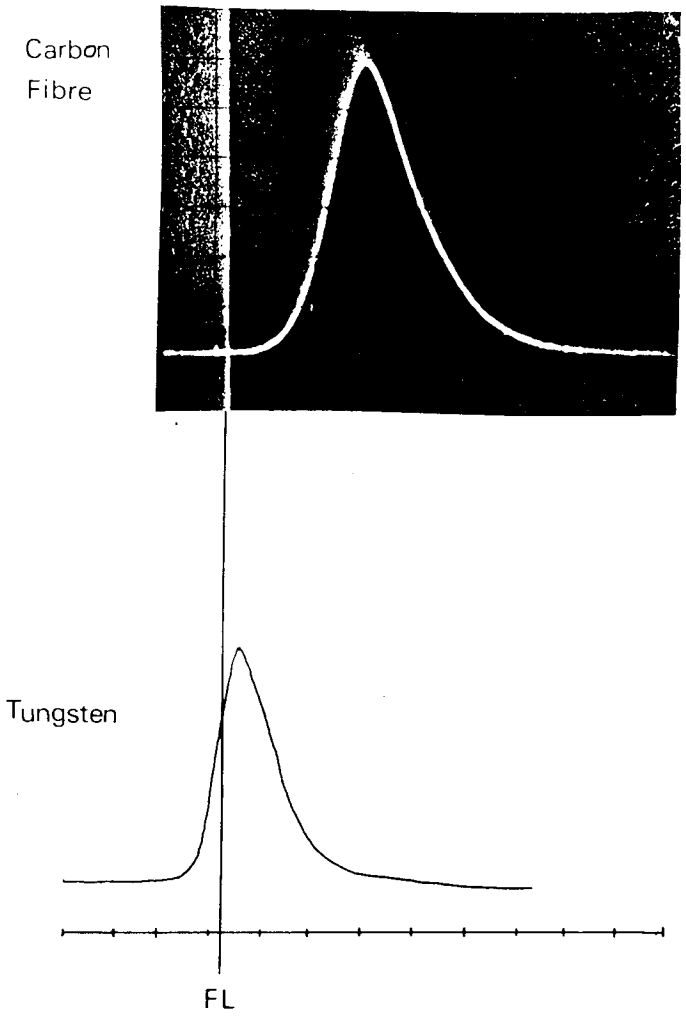
Carbon
Fibre
Tungsten
FL

this trend of increasing with growing emission current and the results were in the range of 0.24eV to 0.50eV for single energy peaks.

An interesting set of spectra was obtained during an experiment to investigate the effect of the applied field at the surface of the emitter. These spectra, presented in Fig 7.6 in the order in which they were recorded, were obtained for various emission currents of 5×10^{-9}A to 5×10^{-8}A with corresponding emitter to anode screen potential differences of 950V to 1110V. The spectrum shown in Fig 7.6(a) was obtained from an emission current of 1×10^{-8}A and comprises a single peak with a relatively narrow half-width of $\sim$0.25eV. The emission current was then increased to 5×10^{-8}A and the much broader double peaked spectrum shown in Fig 7.6(b) was recorded. At this stage the effect on the distribution of horizontal and vertical movement of the emitter was examined. It was found that moving the emitter, within the range $\pm$ 50μm, only changed the magnitude of the distribution peak and did not distort the shape or position of the peak in any way. To obtain more information on the origin of this additional peak the emission current was reduced to 3.5×10^{-8}A and the spectrum shown in Fig 7.6(c) was recorded. It will be noticed that in this case the high energy peak height is less than the low energy peak. The spectra

Fig. 7.6 Set of energy spectra obtained for different emission currents and fields.

The x-axis is electron energy in eV (0.2eV per division).
The y-axis is electron current per unit energy.

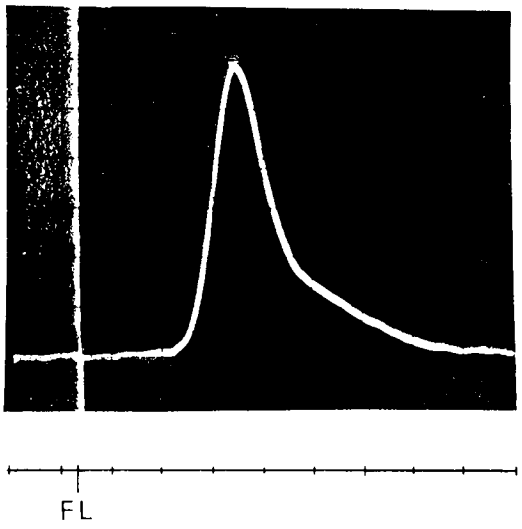

(a)

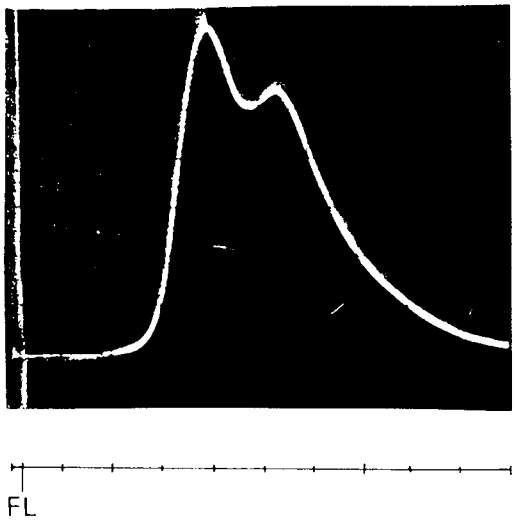

(b)

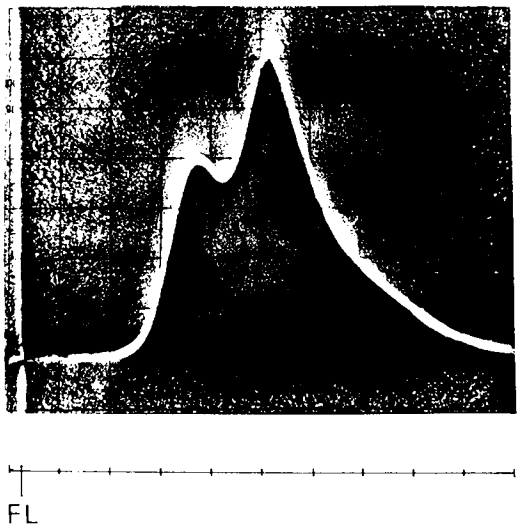

(c)

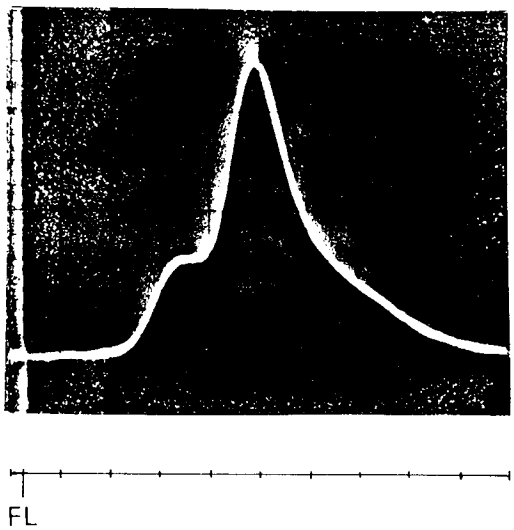

(d)

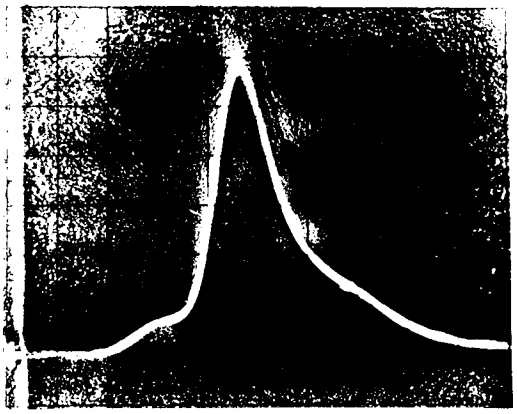

(e)

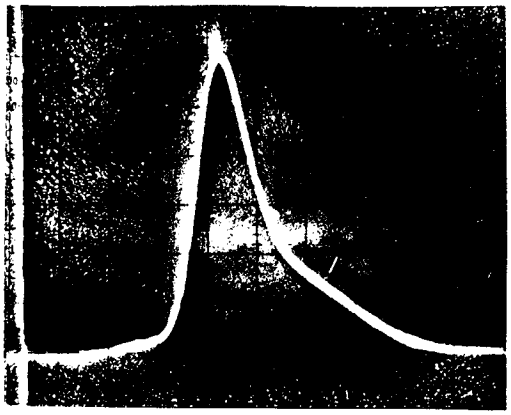

(f)

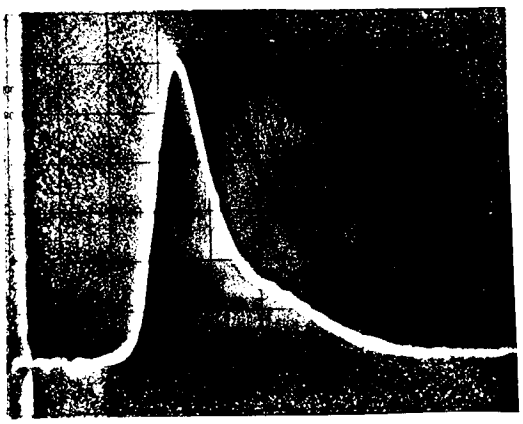

(g)

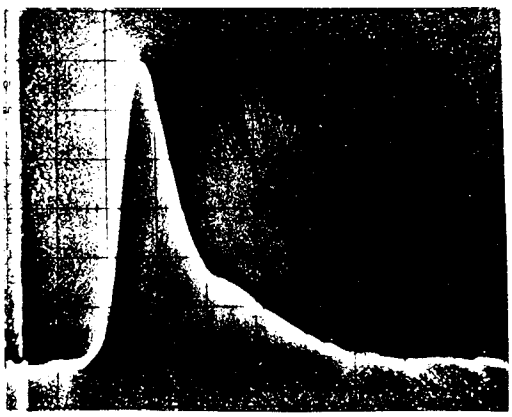

(h)

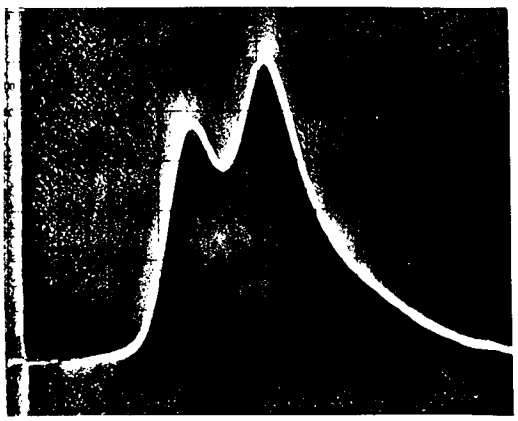

(i)

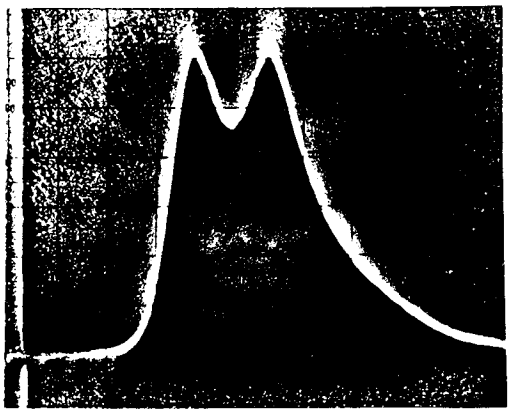

(j)

in Fig 7.6(d), Fig 7.6(e) and Fig 7.6(f) show the sequential reduction in the height of the subsidiary peak for emission currents of 3.5×10^{-8}A, 3×10^{-8}A and 2×10^{-8}A respectively. The original conditions corresponding to Fig 7.6(a) were reproduced (i.e. an emission current of 1×10^{-8}A) and the spectrum presented in Fig 7.6(g) was recorded which is seen to be identical to the former spectrum. Reducing the emission current further to 5×10^{-9}A has no significant effect on the shape of the spectrum which remains single peaked as shown in Fig 7.6(h). To check the reproducibility of the double peaked distributions the emission current was increased to 4.5×10^{-8}A and the spectrum of Fig 7.6(i) recorded. Increasing the emission current further led to an increase in the relative height of the high energy peak until at a current of 4.8×10^{-8}A the two peaks were of equal height as shown in Fig 7.6(j). Further increases in emission current led to the high energy peak being dominant as previously shown in Fig 7.6(b).

To recap, this set of results shows that as the emission current is increased the single peaked type of energy distribution is broadened and a subsidiary peak is formed. As the emission current is further increased the secondary peak increases in relative height and at large emission currents becomes dominant. The origin of the second peak is unlikely to be caused from another

macroscopic emission site as changes in the emitter position, over a range of ±50μm in the vertical and horizontal directions, had no effect on the shape of the distributions recorded. It is more likely that the observed change in the energy distributions is due either to the relative importance of two localised sites changing with applied field, or to the electron emission mechanism changing with applied field. These points will be considered further in the final chapter. For completeness, however, the current voltage characteristics that were recorded for this set of spectra are presented in Fig 7.7. The characteristics are plotted as the logarithm of the emission current versus $10^4/V$, where V is the voltage applied between the emitter and the anode: as can be seen the resulting graph is linear.

The final feature of this investigation is that the peak of the energy distribution was found to be photosensitive. This effect is illustrated in Fig 7.8 which shows two energy distributions recorded in succession with and without illumination. The procedure for obtaining this result involved repeatedly scanning the electron energy distribution in the dark to ensure that it was stable and reproducible. When this condition was satisfied the distribution was stored on the oscilloscope.

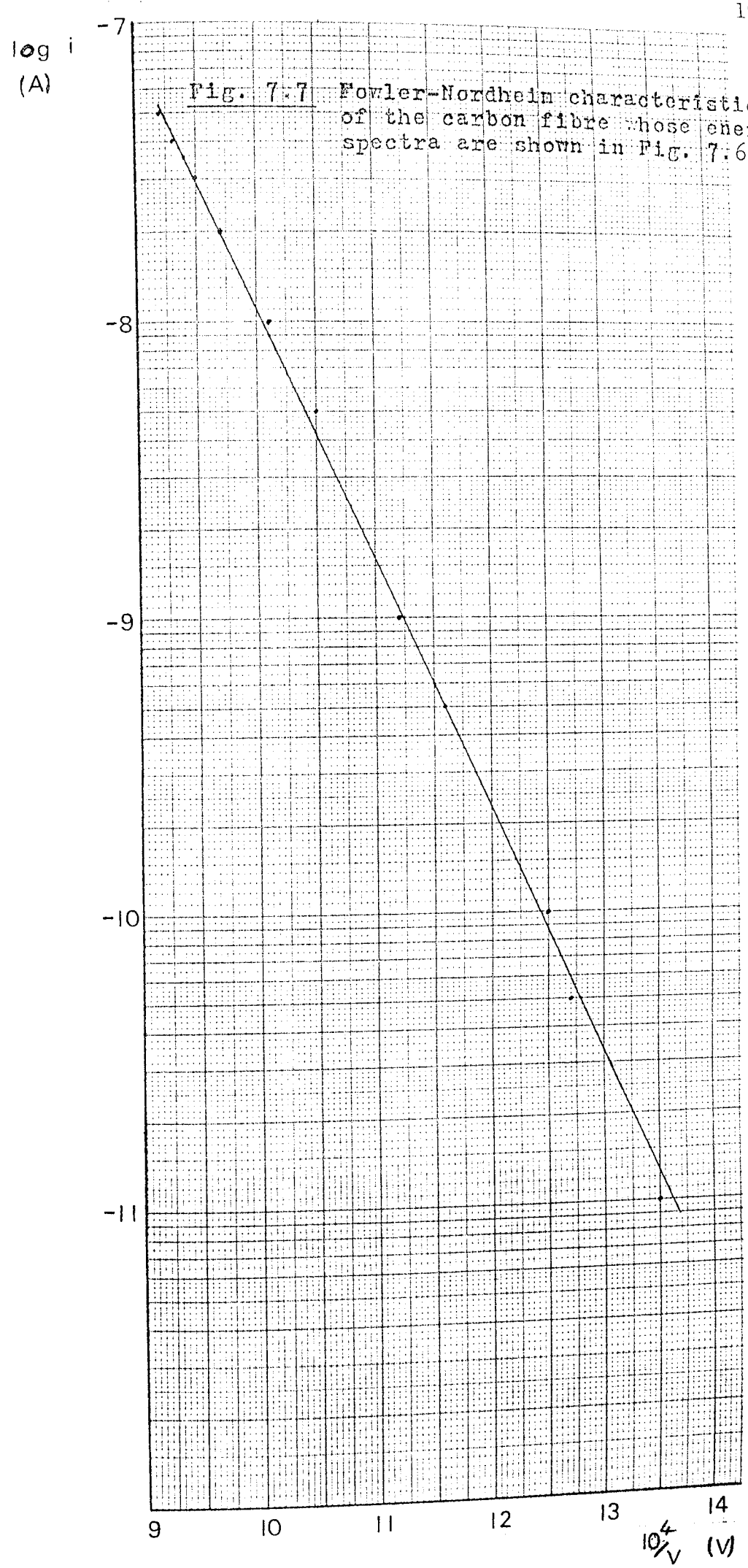

Fig. 7.7 Fowler-Nordheim characteristics of the carbon fibre whose energy spectra are shown in Fig. 7.6.

Fig. 7.8 Typical energy distributions showing the sensitivity of the emission to optical radiation.

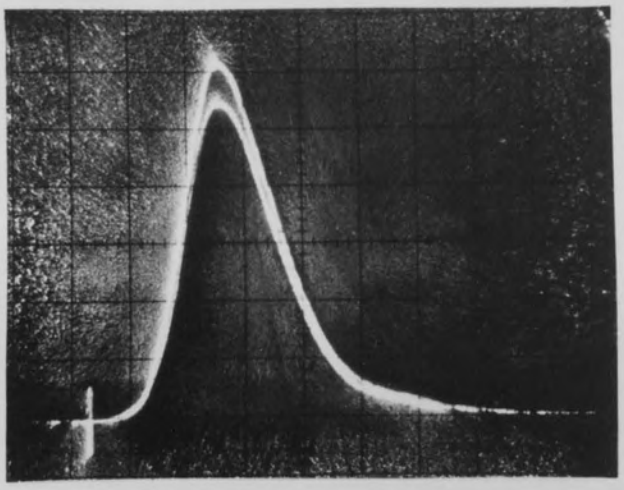

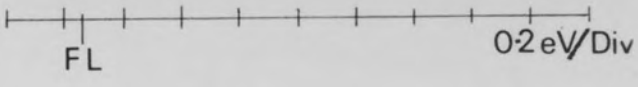
FL
0·2 eV/Div

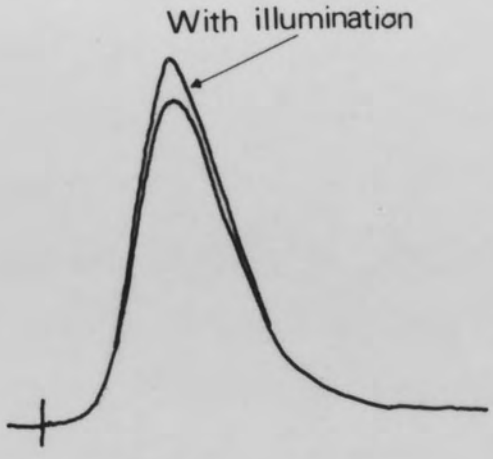
With illumination

It was found that when the emitter was illuminated the peak of the energy distribution increased in height indicating an increase in electron current. A typical record of this effect is shown in Fig 7.8 which was obtained for an emission current of $\sim 10^{-8}$A and an emitter to anode voltage of $\sim$1300V. If the emitter was kept in darkness after illumination and the energy distribution repeatedly scanned it was found that the height of the peak would gradually relax until after about 30s the original distribution, i.e. before illumination, was recovered. The photosensitivity of the energy distribution was reproducible and occurred with both of the two carbon fibre emitters used for this investigation. The dependence of this effect on the wavelength of the illumination was also examined by interposing filters between the lamp and the viewport. It was found that the emitters were insensitive to illumination with wavelengths longer than 470 nm.

7.2 The Observation of Electroluminescence from Carbon Fibre

During the course of the present work, it was noticed by direct visual observation that there is a faint pin-point of light associated with the stable field emission of electrons from a carbon fibre. It was also noted that this light spot was present over a wide range of emission current levels and this suggested that it was unlikely to be thermal in origin. In order to obtain

further information about the spectral nature of this emission, and thereby gain some insight into the physical mechanism responsible for this phenomenon, an image intensifier based optical spectrometer was used to measure the spectrum.

The experimental arrangement is shown in Fig 7.9 and is similar to that used by Hurley and Dooley[70] for studying the electroluminescence associated with point emission sites on high voltage electrodes. A carbon fibre was mounted with air-drying silver paint onto a bridge arrangement formed by spot welding a small section of nickel ribbon between the pillars of a standard scanning electron microscope filament, as shown in Fig 7.10. After the fibre had been electrolytically etched to form a suitable emitter, this subassembly was connected to electrically insulated high voltage feedthroughs and mounted inside the stainless steel vacuum chamber shown in Fig 7.11. The bakeable vacuum system was evacuated by an oil diffusion pump and was operated at a pressure of 10^{-7} torr. High voltages in the range of 1-3kV, from a stabilised power supply, were applied to the emitter via a 100MΩ current limiting resistor, whilst the earthed vacuum manifold acted as the anode. This voltage range resulted in emission currents of 10^{-7}-10^{-5}A. The emitted light could be observed through the axial view-

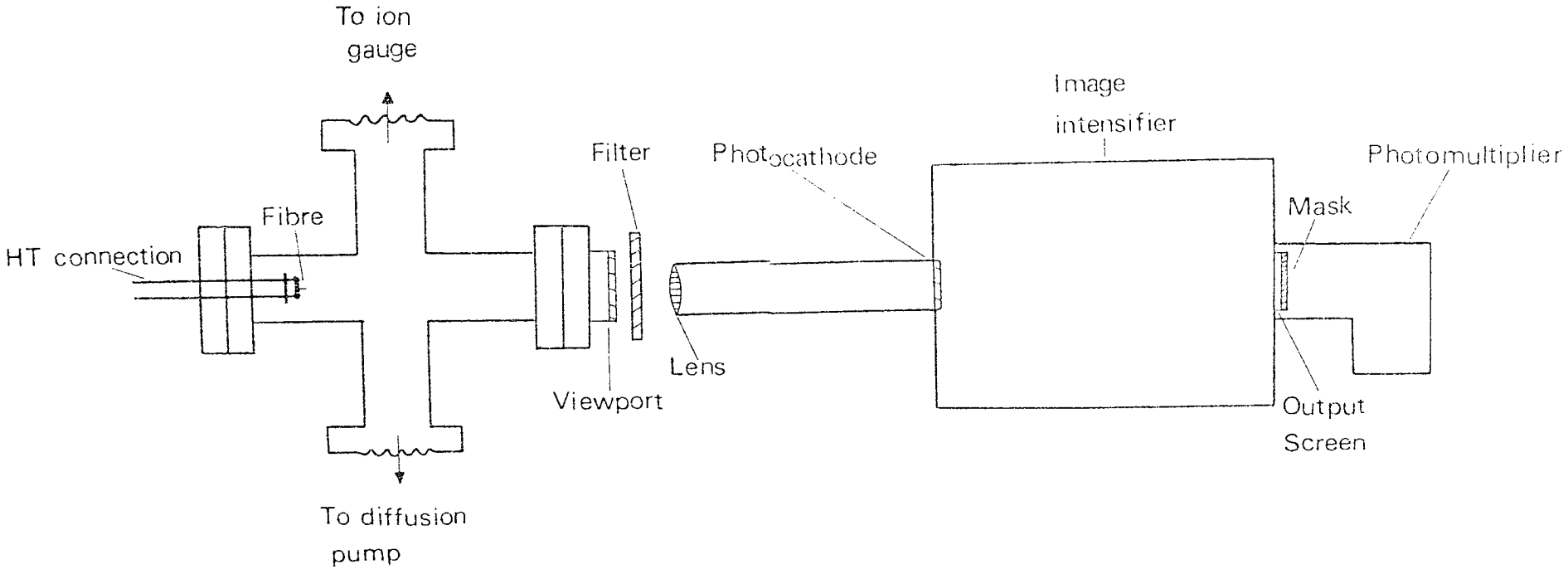

Fig. 7.9 Schematic representation of the experimental arrangement used to study electroluminescence from carbon fibre.

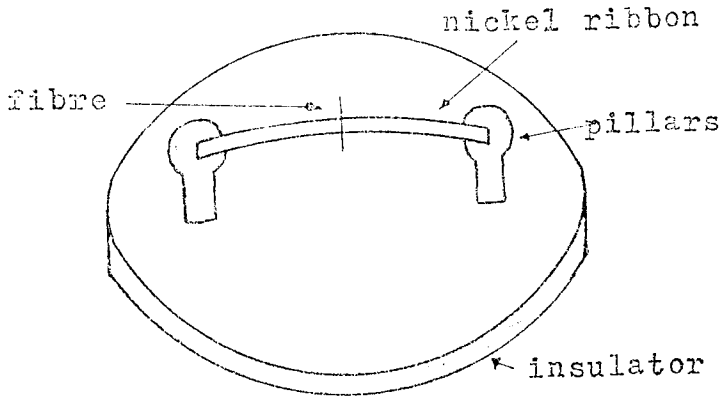

Fig. 7.10 Fibre mount.

Fig. 7.11 Photograph of the vacuum chamber and image intensifier.

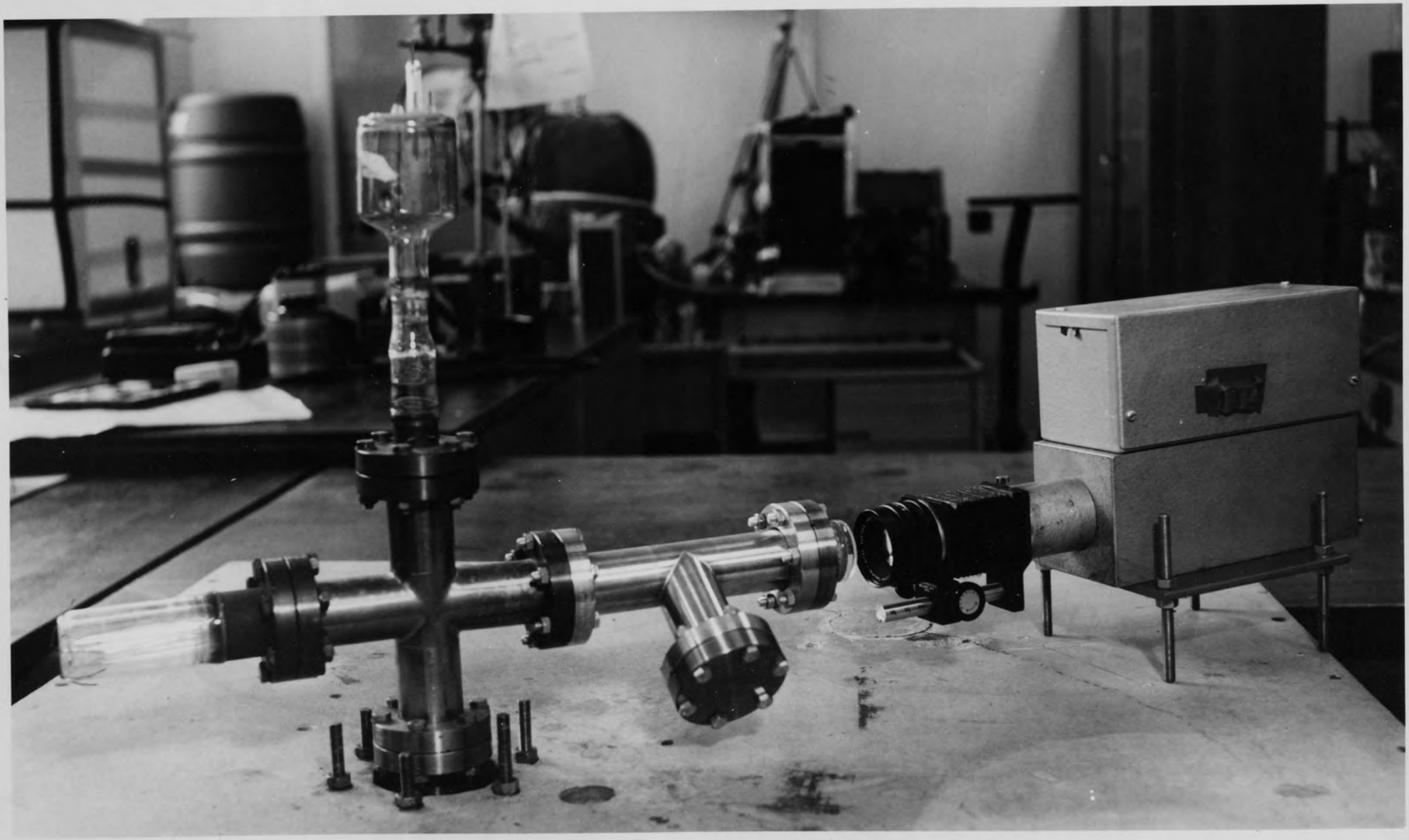

port with the image intensifier (Mullard CV6240) and a suitable lens system for focussing the image of the emitter onto the photocathode. The image intensifier could then be moved in the horizontal and vertical planes until the image of the emitted light associated with the field electron emission process was centred on the phosphor output screen, defined by crosswires. A mask with a central pin-hole could then be placed over the screen so that the systematic variation in the intensity of the optical emission with, say the applied electric field could be measured with a photomultiplier tube (EMI type 60948). By interposing a succession of sharp cut-off high-pass filters between the lens and the viewport, as indicated in Fig 7.9, it was also possible to measure the intensity of emitted radiation associated with incremental intervals of wavelength, and hence perform a spectral analysis of this source.

A photograph of the emitting carbon fibre and its bridge assembly as displayed on the output screen of the image intensifier, is presented in Fig 7.12. In this, the pin-point of light at the top of the fibre is clearly visible against the 12mm diameter ceramic disc, the conducting supports and the bridge wire to which the fibre is attached. The superimposed 90^{o} black lines are the crosswires in the eyepiece of the image intensifier. The

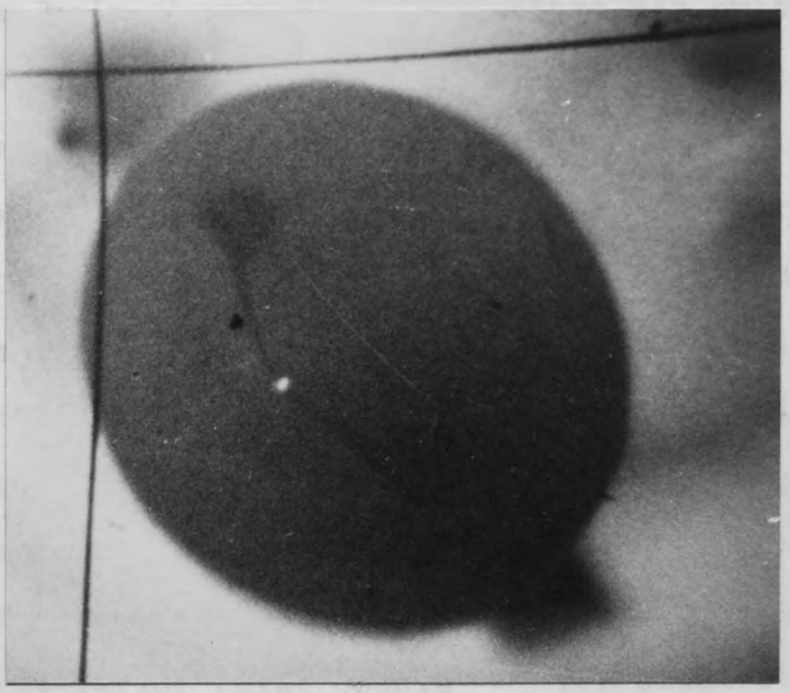

Fig. 7.12 Photograph showing the pin-point of light associated with field electron emission from a carbon fibre.

light spot was only observed when the fibre was emitting electrons and to investigate whether the optical emission is due to some form of electroluminescence process, measurements were made on how the total light intensity varied with the voltage applied across the field emitting diode. The data obtained is shown in Fig 7.13 which is a plot of the logarithm of the dark-corrected photomultiplier current against the inverse square root of the applied voltage. This graph is evidently linear within the limits of experimental accuracy and is in good agreement with the Alfrey-Taylor relationship[71.] for electroluminescence.

The spectrum of the observed radiation is shown in Fig 7.14 and is seen not to correspond to a black-body curve but resembles that obtained from electroluminescent materials such as those investigated by Hurley.[70.] It consists predominately of two peaks centred on 500 and 570nm and whilst having a fairly sharp short-wavelength cut-off, there is a long-wavelength tail extending into the infra-red. The origin of this electroluminescence process will be discussed in Chapter 8.

7.3 Changes in Emitter Profile Observed by Scanning Electron Miscroscopy

Earlier work on field emission from carbon fibres has provided little information about changes that occur

Fig. 7.13 Alfrey-Taylor plot for electroluminescence from a carbon fibre.

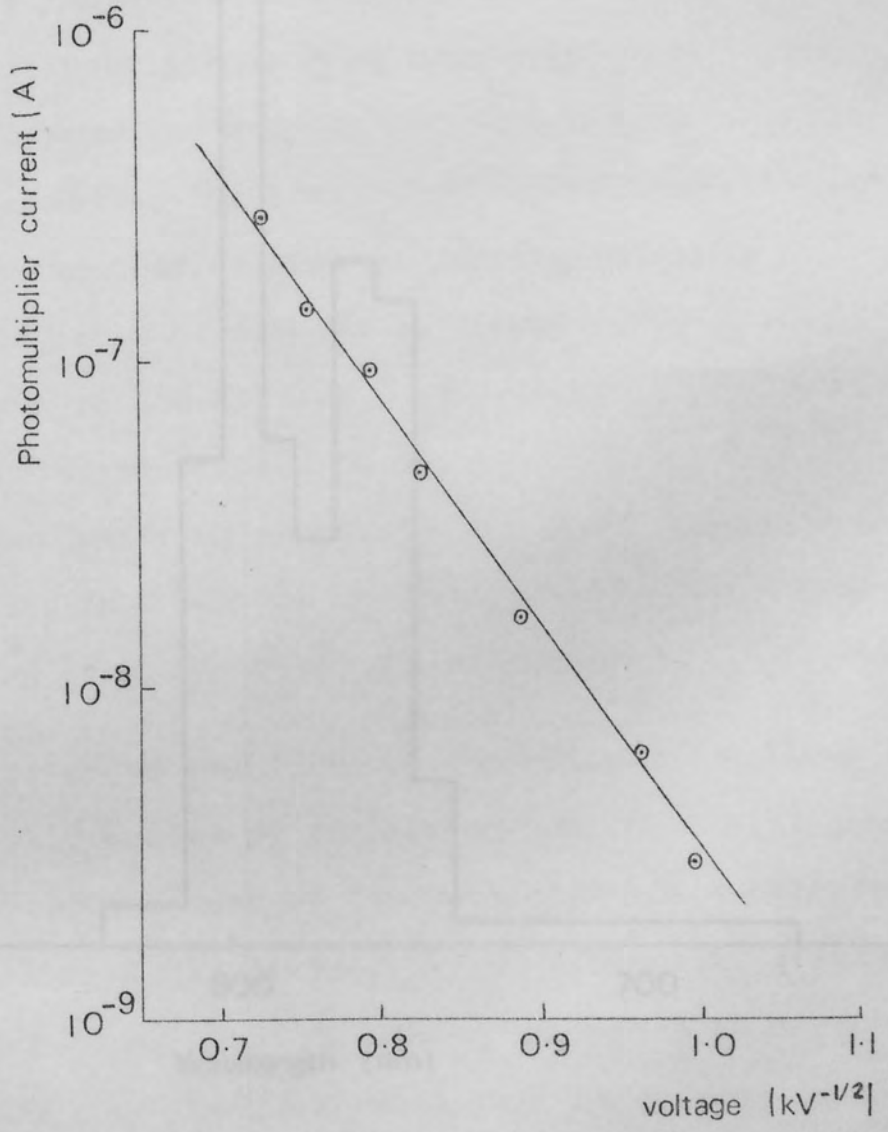

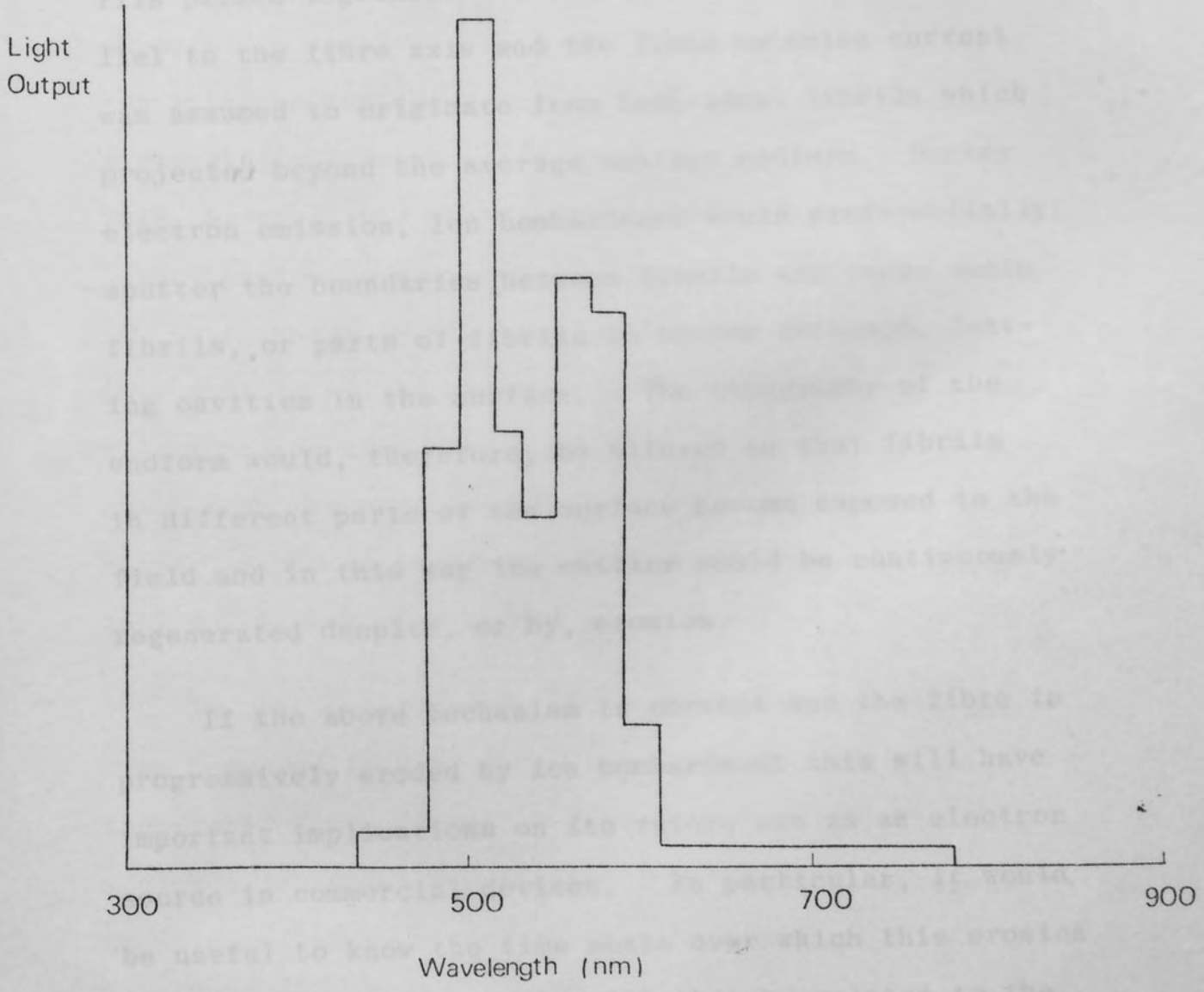

Fig. 7.14 Spectrum of radiation emitted from a carbon fibre during field electron emission.

in the emitter profile during electron emission. Braun et al.,[43] however, have suggested that the comparatively good emission current stability in poor vacuum is due to a mechanism of self-regeneration. According to their view, the fibre structure was considered to be composed of a large number of short fibrils packed together with their lengths roughly parallel to the fibre axis and the field emission current was assumed to originate from individual fibrils which projected beyond the average emitter endform. During electron emission, ion bombardment would preferentially sputter the boundaries between fibrils and cause whole fibrils, or parts of fibrils to become detached, leaving cavities in the surface. The topography of the endform would, therefore, be altered so that fibrils in different parts of the surface become exposed to the field and in this way the emitter would be continuously regenerated despite, or by, erosion.

If the above mechanism is correct and the fibre is progressively eroded by ion bombardment this will have important implications on its future use as an electron source in commercial devices. In particular, it would be useful to know the time scale over which this erosion takes place since not only will this be related to the lifetime of the emitter but also to the position of the electron optical source. It was, therefore, decided

to observe the emitter profile before and after fixed periods of electron emission. Since the etched carbon fibre emitters are extremely fragile there is always the danger in this type of study that the emitter end form may be damaged in transit between the vacuum system where emission takes place and the microscope used for viewing the specimen. To avoid this difficulty experiments involving relatively short periods of electron emission (up to one hour) were performed in situ in a scanning electron microscope (shown in Fig 7.15). This, however, had the limitation of restricting the investigation to emission in a vacuum pressure of about 10^{-5} torr, where as the pressure region of interest to this work is of the order of 10^{-8} - 10^{-7} torr, as typically found in commercial cathode ray tubes. To enable changes in the emitter profile to be examined at this higher vacuum an additional high vacuum system, shown in Fig 7.16, was also used.

In both experimental situations, whether the emission occurred in situ or in a separate vacuum chamber, the etched fibre was mounted with silver adhesive onto a nickel tab which had been spot-welded to a standard scanning electron microscope specimen holder. The emitter was earthed via a picoammeter and a high positive voltage was applied to the anode of the experimental

Fig. 7.15 Photograph of the scanning electron microscope used to examine the profile of the emitter.

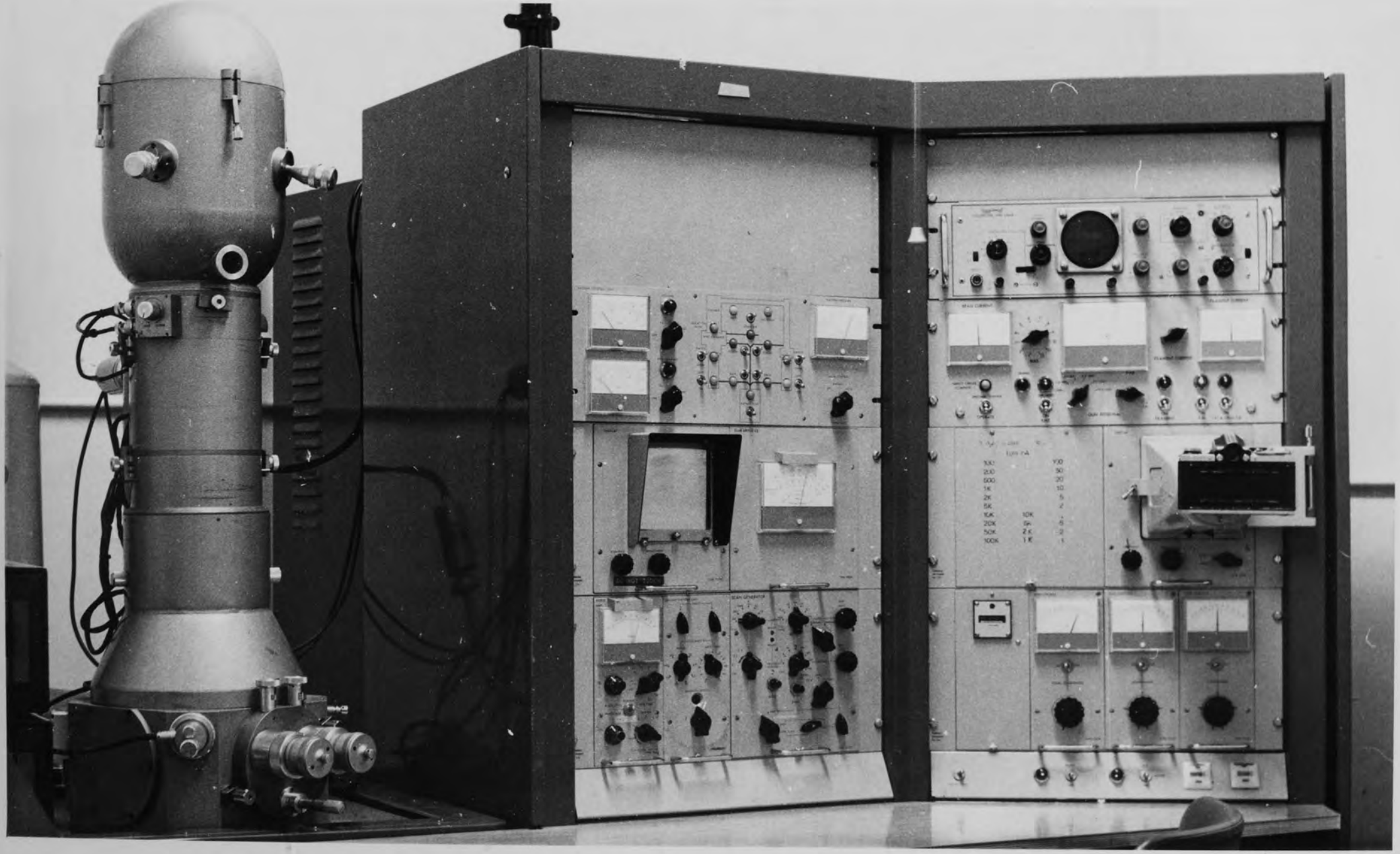

Fig.7.16 Photograph of the system used for obtaining emission under vacuum conditions of $\sim 10^{-7}$ torr.

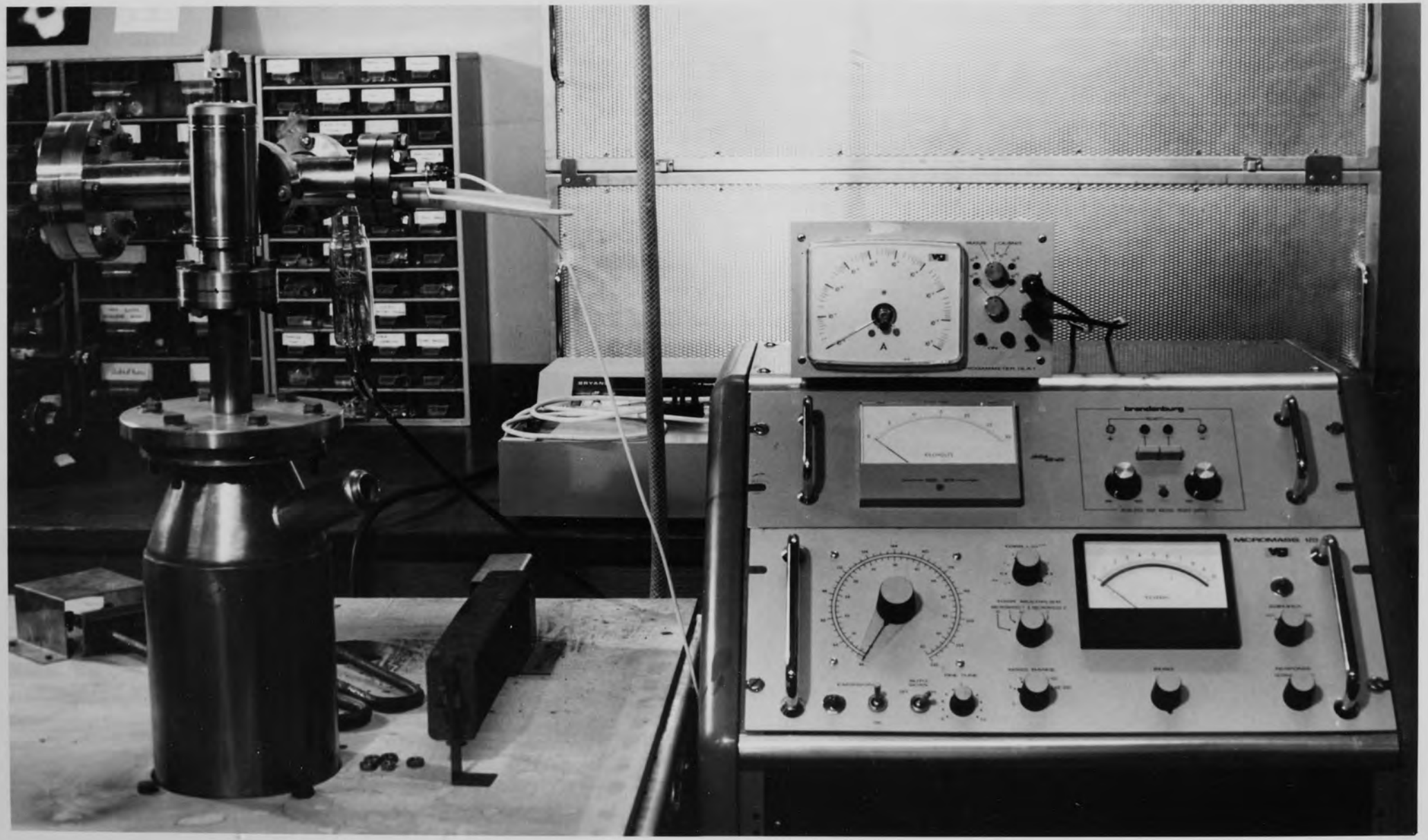
A
brandenburg

system via a high-valued (100MΩ) resistor in series with the power supply. When the experiment was performed in situ in the scanning electron microscope the anode consisted of a manoeuvrable electrical feed-through which was positioned above the fibre. The anode in the separate vacuum system was demountable, constructed from a copper-nickel electrode, and positioned about 1mm from the emitter so as to simulate the extraction electrode conditions in the prototype cathode ray tube. This anode, however, contained a 5mm diameter aperture to reduce the likelihood of accidental damage to the emitter during alignment.

The first experiment was performed in situ in the scanning electron microscope under a vacuum pressure of 2×10^{-5} torr. Photographs of the emitter were taken before emission and after a current of 10μA had been emitted for a total of two, four and ten minutes respectively. These photographs are presented in Fig 7.17 and as can be seen a remarkable change in the emitter profile has occurred after only two minutes of emission. Of interest also is the result that after a further eight minutes of emission the tip is substantially unchanged. This experiment was repeated to investigate whether this drastic change in emitter topo-

Fig. 7.17 Scanning electron micrographs of an emitter before and after in situ emission of 10μA in a vacuum of 2×10^{-5} torr.

Before emission

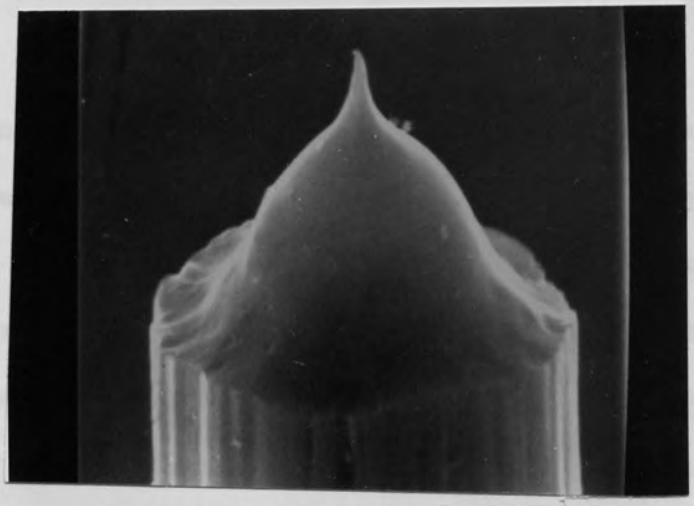

After two minutes emission

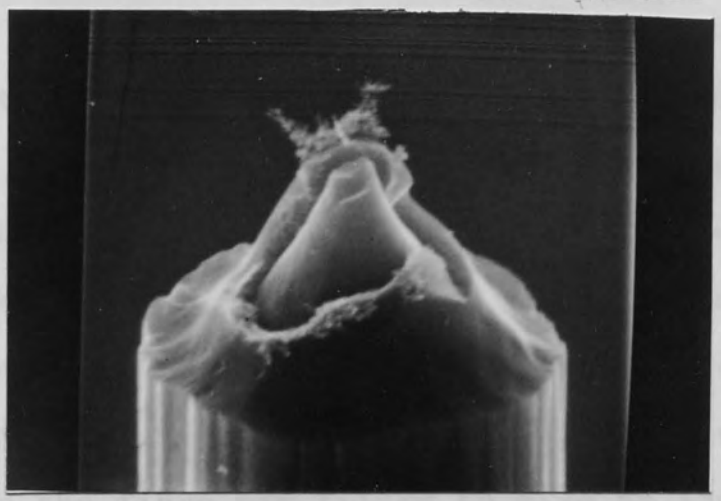

After four minutes emission

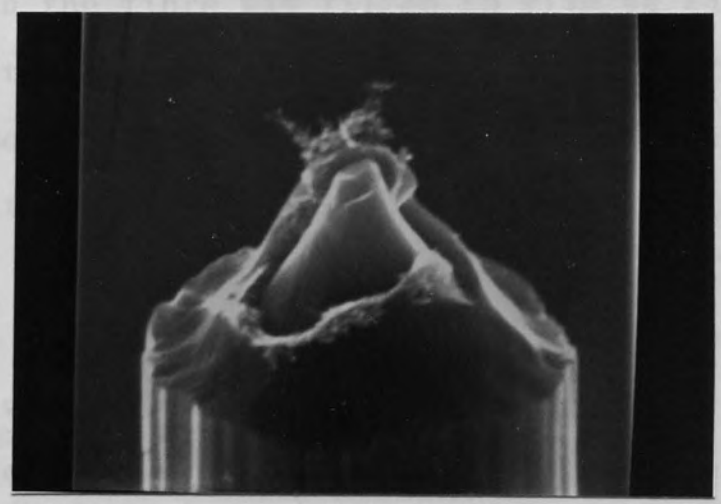

After ten minutes emission

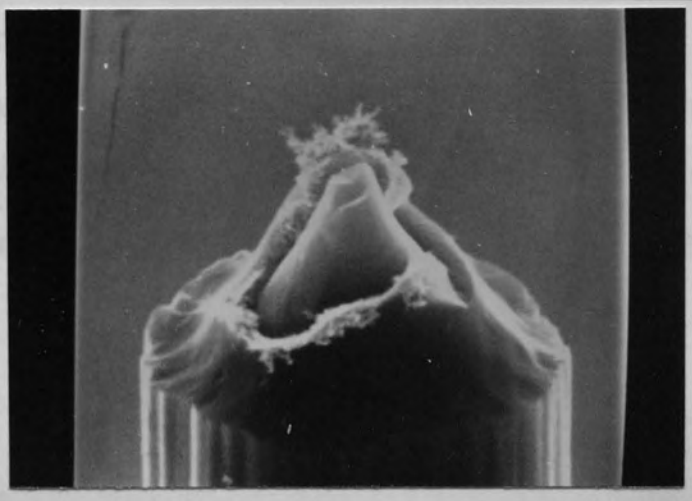

graphy was a normal event or sporadic. An etched carbon fibre was photographed before and after periods of one, five, fifteen and sixty minutes of emission at a reduced current level of 1μA. The experiment was again performed in situ with a vacuum pressure of 3×10^{-5}torr and the results are presented in Fig 7.18. The scale of these photographs may be judged by using the fact that the shank of the fibre is a nominal 7μm in diameter. As can be seen from Fig 7.18 the emitter profile has been drastically altered after only one minute of electron emission but remains unchanged in successive periods of emission up to a total of one hour. Fig 7.18(f) is a photograph taken at the end of the experiment when the fibre was tilted to give an additional perspective to the features of interest. The final experiment performed in situ in the scanning electron microscope at a pressure of 2×10^{-5}torr will now be described. A high positive voltage was gradually applied to the anode until at a voltage of ~3.2kV the first sign of emission was observed on the picoammeter corresponding to an emission current of $\sim 10^{-11}$A. The voltage was immediately turned off and the emitter examined. There was no indication of the tip profile having been changed so the high voltage was again applied to the anode. After a few seconds (less than ten) the current spontaneously

Fig. 7.18 Scanning electron micrographs of an emitter before and after in situ emission of 1μA in a vacuum of 3×10^{-7} torr.

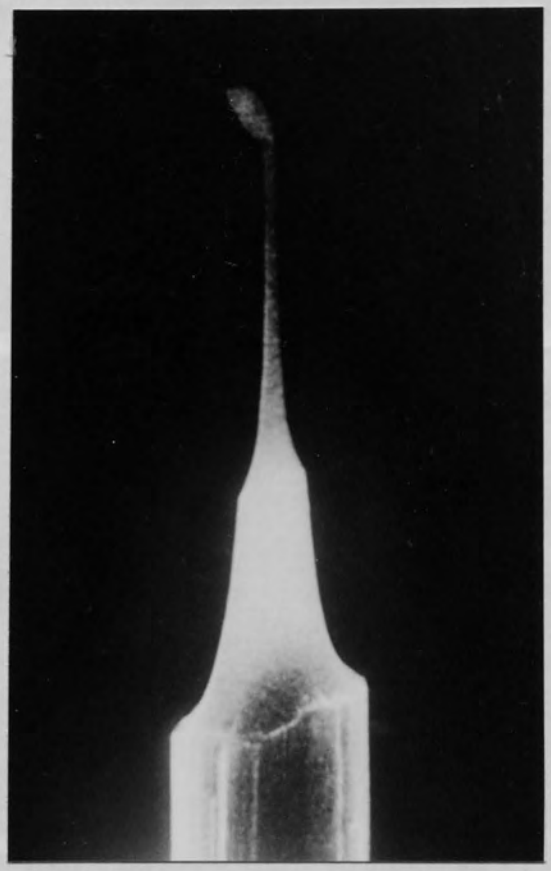

(a)

Before emission

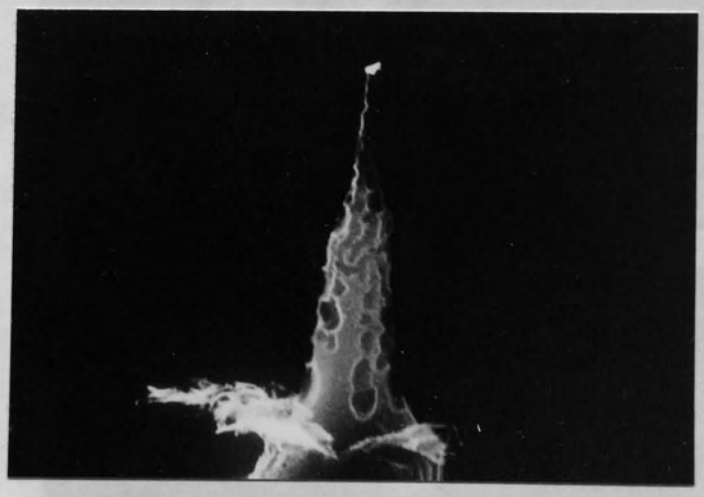

(b)

After one minute of emission

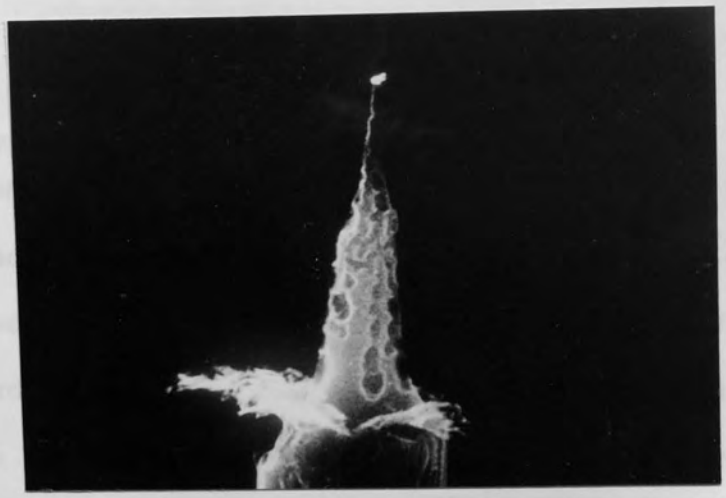

(c)

After five minutes emission

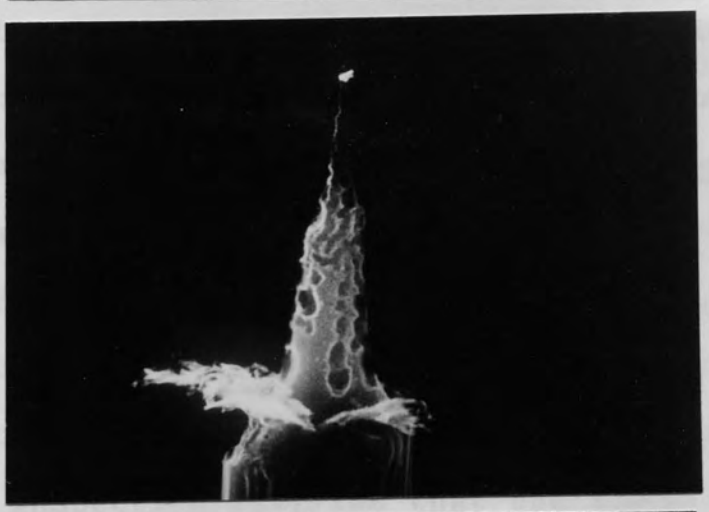

(d)

After fifteen minutes emission

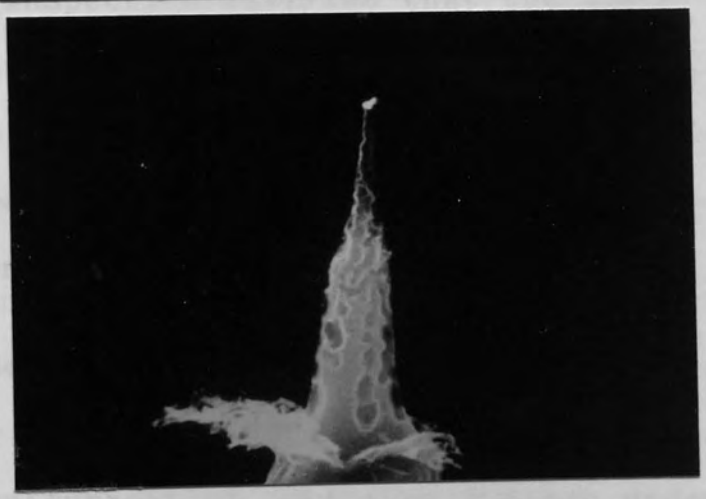

(e)

After one hour of emission

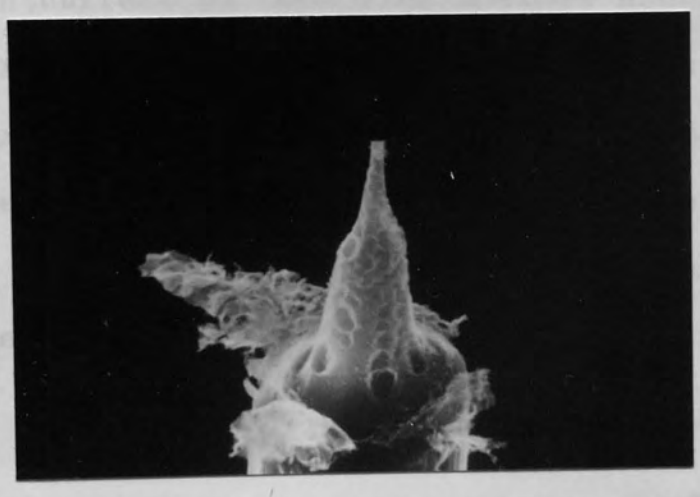

(f)

After one hour of emission

increased from $\sim 10^{-11}$A to $\sim 10^{-5}$A and was turned off after a period of about two seconds. The profile of the emitter was inspected using the scanning electron microscope and was found to have changed in a similar manner to the two previous emitters. The voltage was again applied to the anode and a current of 10μA was emitted for a total period of one and ten minutes before the fibre was re-inspected. The results were photographed at each stage of the experiment and are presented in Fig 7.19. Unfortunately these photographs are not quite as clear as the previous ones, due to an error incurred when having the film developed, but close inspection verifies that the fibre topography has changed after only two seconds of emission. It should also be noted that after the sudden surge in current an anode voltage of only $\sim$1.2kV was required for $\sim 10^{-11}$A emission current.

The influence of the vacuum pressure on the change in the emitter profile was next investigated by extracting an emission current of 10μA from a fibre under a pressure of 1×10^{-7}torr. The emitter was transferred between the auxilliary vacuum system and the microscope before and after emission for ten minutes and one hour duration. As can be seen from the photographs presented in Fig 7.20 the emitter profile has again been altered

Fig. 7.19 Scanning electron micrographs of an emitter which was observed to suddenly 'explode'.

Before emission

After two seconds emission

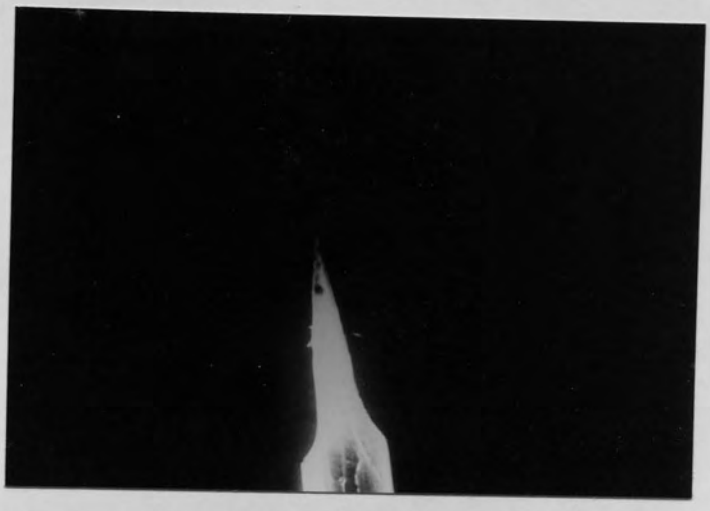

After one minute of emission

After ten minutes emission

Fig. 7.20 Scanning electron micrographs of an emitter before and after emission of 10μA in a vacuum of 1×10^{-7} torr.

Before emission

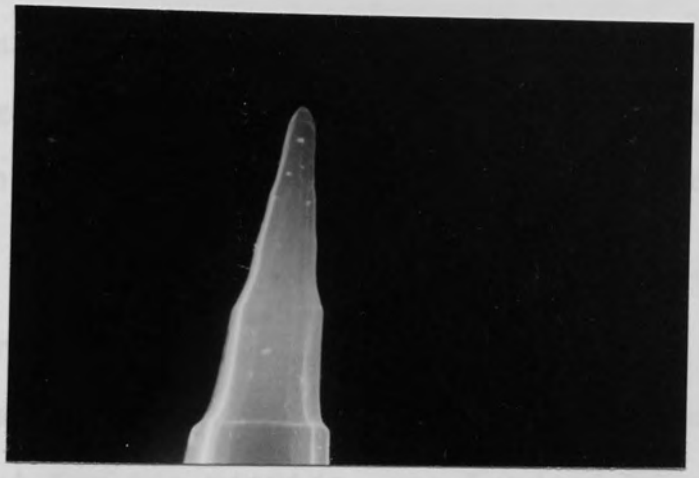

After ten minutes emission

After one hour of emission

in the same manner as before and therefore suggests that this change is characteristic of the mechanism by which carbon fibres start to emit electrons and is independent of vacuum conditions.

A long-term experiment was also performed in which the emitter was examined before and after period of emission of 10μA for ten minutes, one hundred hours and two hundred hours in a vacuum pressure of 1×10^{-7} torr. The corresponding photographs in Fig 7.21 were taken from different angles and directions which makes a direct comparison difficult. The indication is, however, that after the initial change in emitter geometry the fibre does not undergo any significant erosion, even after two hundred hours.

The drastic change in the emitter profile at the initiation of electron emission from a carbon fibre is reminiscent of a new type of electron emission process which has been demonstrated in recent years from metallic[72.] and semiconducting[73.] cathodes and involves a rapid change in the state of aggregation of the emitter. In this process, termed explosive electron emission, the application of a strong electric field to the cathode and the flow of a field emission current result in the explosive destruction of the end of the point of the emitter. The first stage in this process is the thermal vap-

Fig. 7.21 Scanning electron micrographs showing the long term effects of emission of 10μA in a vacuum pressure of 10^{-7} torr.

Before emission

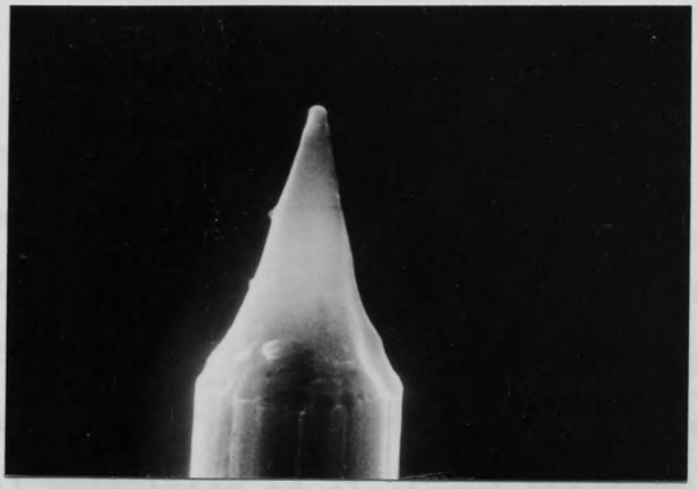

After five minutes emission

After 100 hours emission

After 200 hours emission

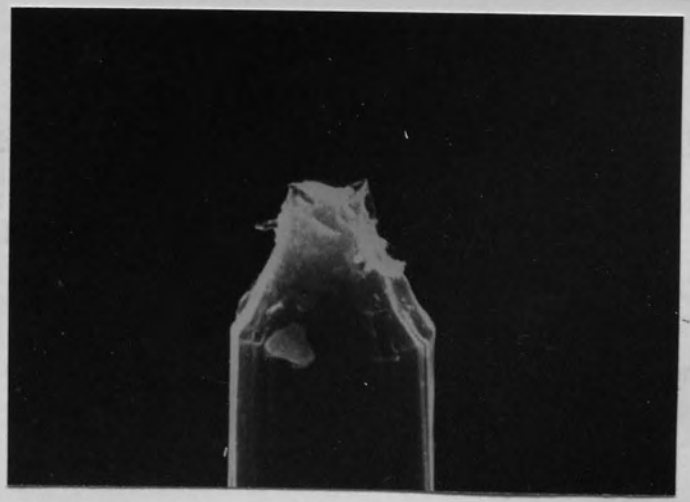

orisation of the end of the emitter as a result of a high electron emission density. This generates a localised, highly ionised plasma that initially surrounds the emitter. This plasma then undergoes spontaneous expansion and subsequent charge separation (due to vastly differing thermal velocities of electrons and positive ions) results in an increased field at the surface of the emitter. This has the effect of increasing both the emission current density and the rate of vaporisation of emitter material. A general feature of the explosive emission of point cathode is a stage of rapid current growth (typically of the order of 10^{-9}s) and a subsequent stage of current saturation. As mentioned in Chapter 3, this type of emission current behaviour was also observed by Baker et al.[42] Unless a current limiting resistor was placed in series with the emitter, a runaway phenomenon often resulted when a voltage was applied to a virgin tip. They found that no current was obtained until at a critical voltage it increased rapidly and uncontrollably, often resulting in the destruction of the tip.

7.4 Noise Characteristics of Carbon Fibre Field Emitters

7.4.1 Analysis of the Frequency Dependence of Emission Current Noise.

Extensive theoretical[74] and experimental[3] studies of the statistical fluctuation in the current from a tung-

sten field emitter have been previously carried out. The time fluctuations in the current were attributed to changes in two parameters: the emitter work function and the emitter surface geometry. Changes in the emitter work function are caused by a variation of the average coverage of absorbed residual gas atoms. Changes in the emitter surface geometry are due to bombardment by positive ions formed as a result of electron-atom interactions.

From the fluctuation of the visual display of the prototype cathode ray tube described in the previous chapter, it is apparent that there is a considerable amount of very low frequency noise associated with the emission of electrons from a carbon fibre. It was decided that the noise at higher frequencies should also be measured. The frequency dependent noise in the emission current in the range 20Hz to 40kHz was therefore examined using a Bruel and Kjaer logarithmic spectrum analyser. A typical spectrum obtained for an emission current of 10μA from a carbon fibre in a vacuum pressure of $\sim 10^{-8}$torr, is presented in Fig 7.22 in which the noise power in decibels is plotted as a function of frequency. Results were also obtained for various values of emission current in the range 1μA to 100μA and all the spectra were found to be of a similar shape. From the spectrum

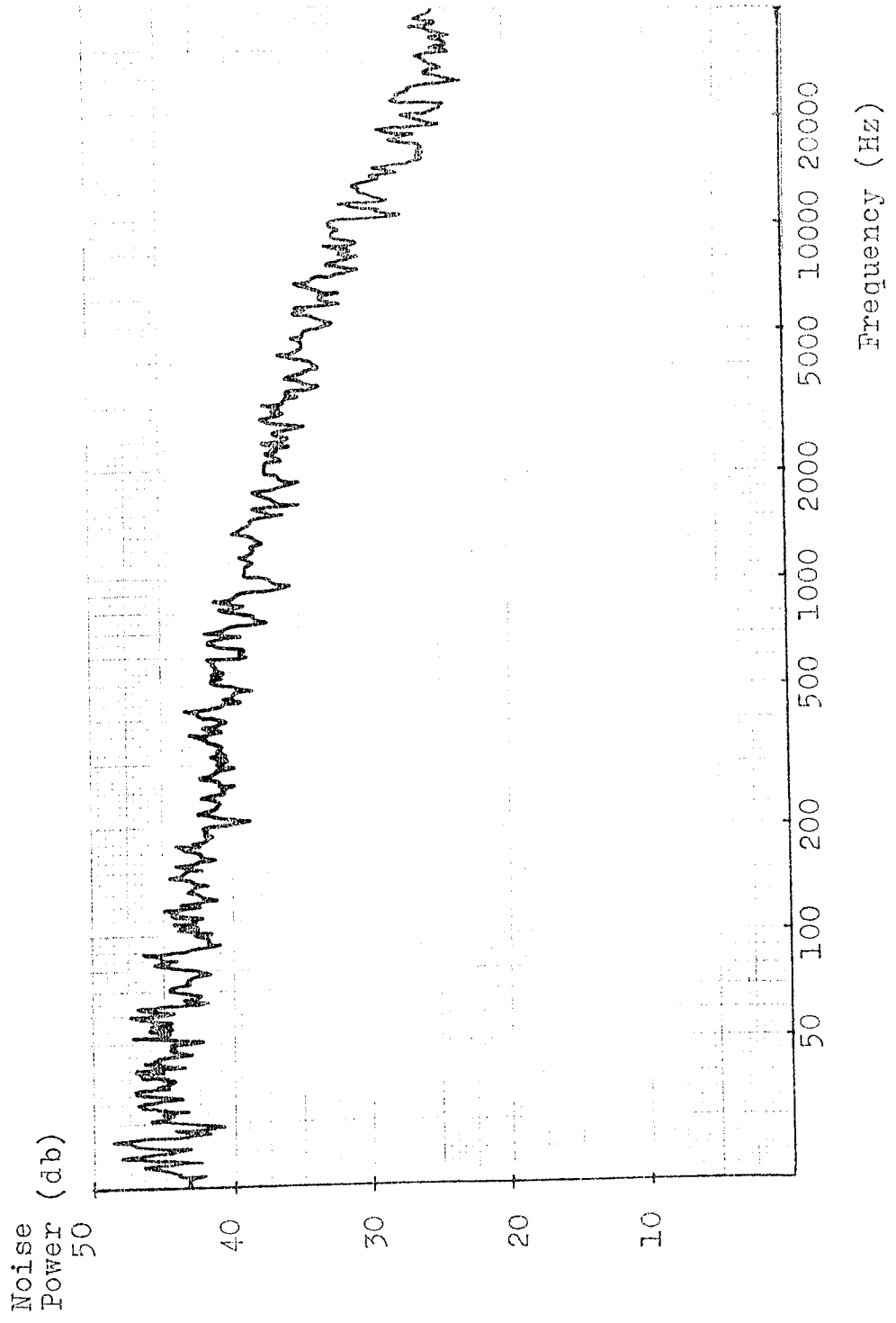

Fig. 7.22 Typical noise spectrum obtained from a carbon fibre.

in Fig 7.22 it can be seen that the noise power rapidly decreases with increasing frequency. Since the noise power contained in the upper frequency region is relatively small compared to the total noise power, it was considered sufficiently accurate in subsequent experiments to display the noise signal waveform on a chart recorder having a bandwidth of about 50Hz.

7.4.2 Influence of the Vacuum Environment on Emission Current Stability

The effect of the vacuum environment on the stability of the total current emitted from a carbon fibre emitter was examined and typical results are shown in Fig 7.23. As can be seen from these chart recordings, which show the variation in a nominal emission of about 20μA with time, the stability of the emitter significantly improves as the vacuum pressure is decreased from $\sim 10^{-5}$torr to $\sim 10^{-8}$torr. This is consistent with the general trend observed with other field emitting materials. It should however be noted that when a carbon fibre is operated under very high vacuum conditions ($\lesssim 10^{-10}$torr) the emission current still fluctuates and the field emission pattern still flickers. This is different from the case of a clean tungsten emitter under the same conditions which exhibits a stable field emission pattern. Conversely, whereas a carbon fibre may be satisfactorily operated under adverse vacuum conditions of $\sim 10^{-5}$torr, a tungsten

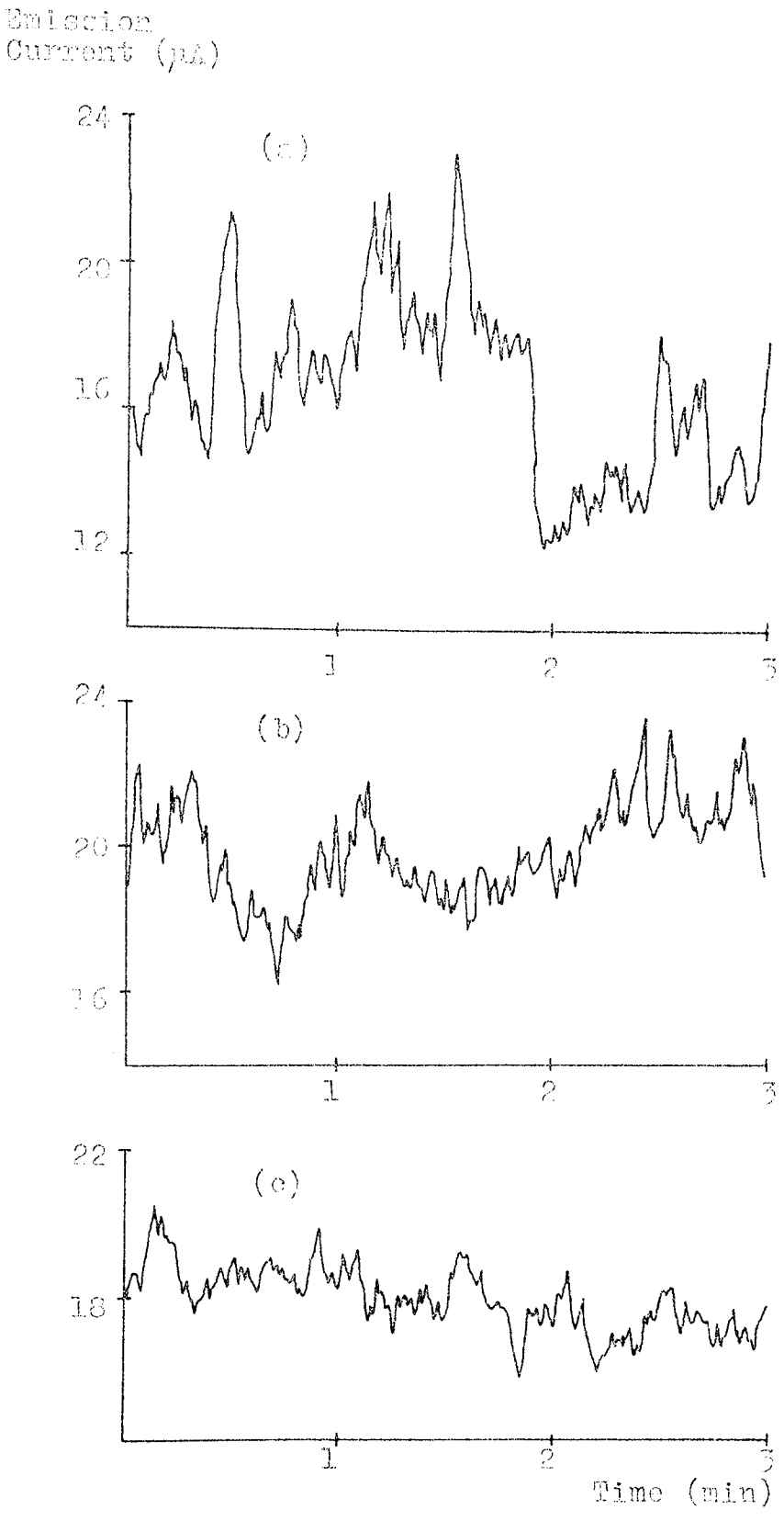

Fig. 7.23 Influence of the vacuum on the stability of the emitter.

(a) Pressure of 1×10^{-5} torr
(b) Pressure of 1×10^{-6} torr
(c) Pressure of 2×10^{-5} torr

emitter would be rapidly destroyed.

The effect of the level of the emission current on the stability of a carbon fibre emitter was also examined and typical results are shown in Fig 7.24. The chart recordings presented in this figure show the variation in emission current with time for four different nominal levels of 4, 10, 18, and 30μA all monitored under an identical vacuum pressure of $\sim 2 \times 10^{-8}$ torr. As can be seen from these recordings, the magnitude of the change in emission current, ΔI, from the average value, I, increases with increasing total current. If, however, these results are expressed as a fractional change in current, $\Delta I/I$; it is found that the emission noise decreases with increasing current. This result is contrary to that found for a tungsten emitter[76.] in which the emission noise $\Delta I/I$ increases with increasing emission current.

A preliminary investigation of the influence of residual gases present in the vacuum environment on the stability of the carbon fibre emitter was made. This experiment was performed with the prototype cathode ray tube using the additional pumping system which allows the admission of pure gases previously depicted in Fig 5.14. After evacuating the system in the normal manner, air was slowly and controllably admitted to the vacuum chamber

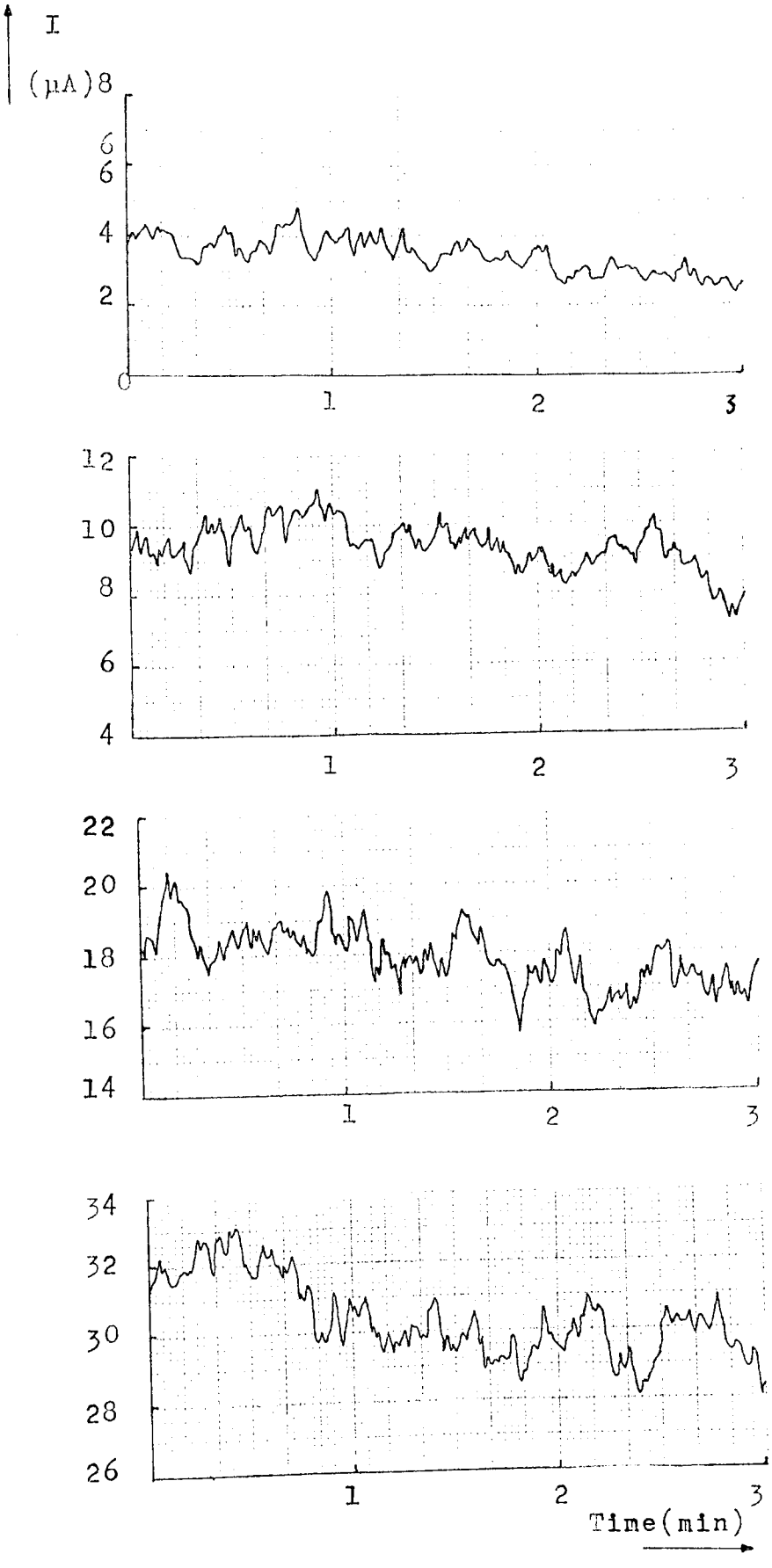

Fig. 7.24 Variation of current with time for different levels of emission current, obtained under an identical vacuum pressure of 2×10^{-8} torr.

until the pressure was $\sim 2 \times 10^{-6}$ torr and the fluctuation in total emission current was recorded on a chart recorder. The leak value was then closed and the chamber evacuated to a pressure of $\sim 5 \times 10^{-8}$ torr. The gas, whose effect was to be examined, was then admitted from a gas cylinder via the leak value until the chamber pressure was again $\sim 2 \times 10^{-6}$ torr, at which point the fluctuation of the emission current was re-measured. The effects of three gases - nitrogen, oxygen and helium - were recorded and typical examples of the total emission current stability before and after the admission of these gases are presented in Fig 7.25, Fig 7.26 and Fig 7.27. Referring to these recordings, and recalling the statistical nature of the fluctuations, it can be seen that when the predominant gas present is nitrogen or oxygen there is no significant difference from the stability of the emitter before their addition. Fig 7.27, however, shows that when helium is the prevalent gas there is a marked change in the electron emission from the carbon fibre. In all three cases the voltage applied for the extraction of the electrons from the emitter was constant before and after the respective gas was introduced. It can be seen that the introduction of helium into the vacuum chamber has had the effect of reducing the total emission current from an average value of $\sim 13\mu A$ to one

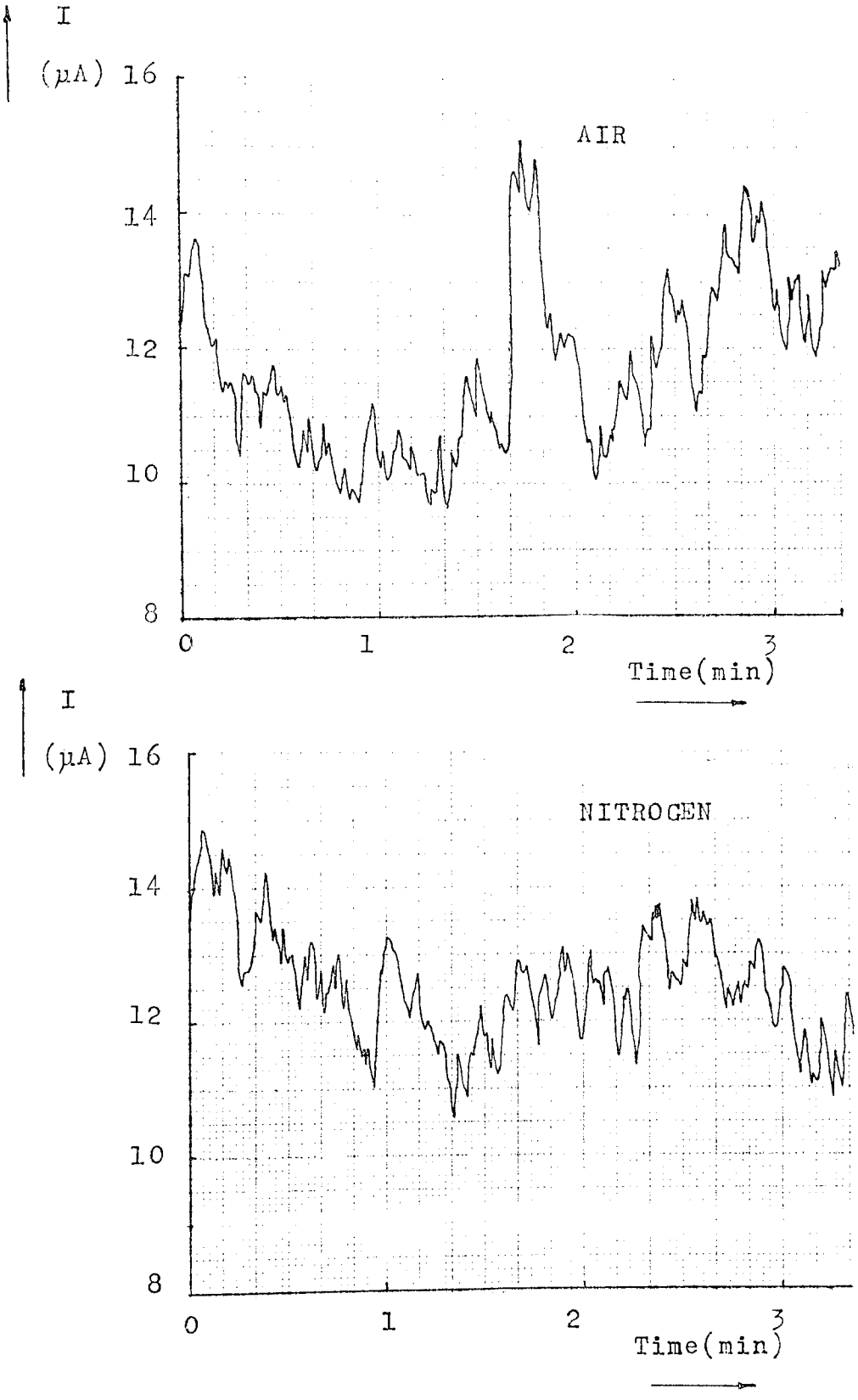

Fig. 7.25 Comparison of the stability of the emitter in air and in nitrogen.

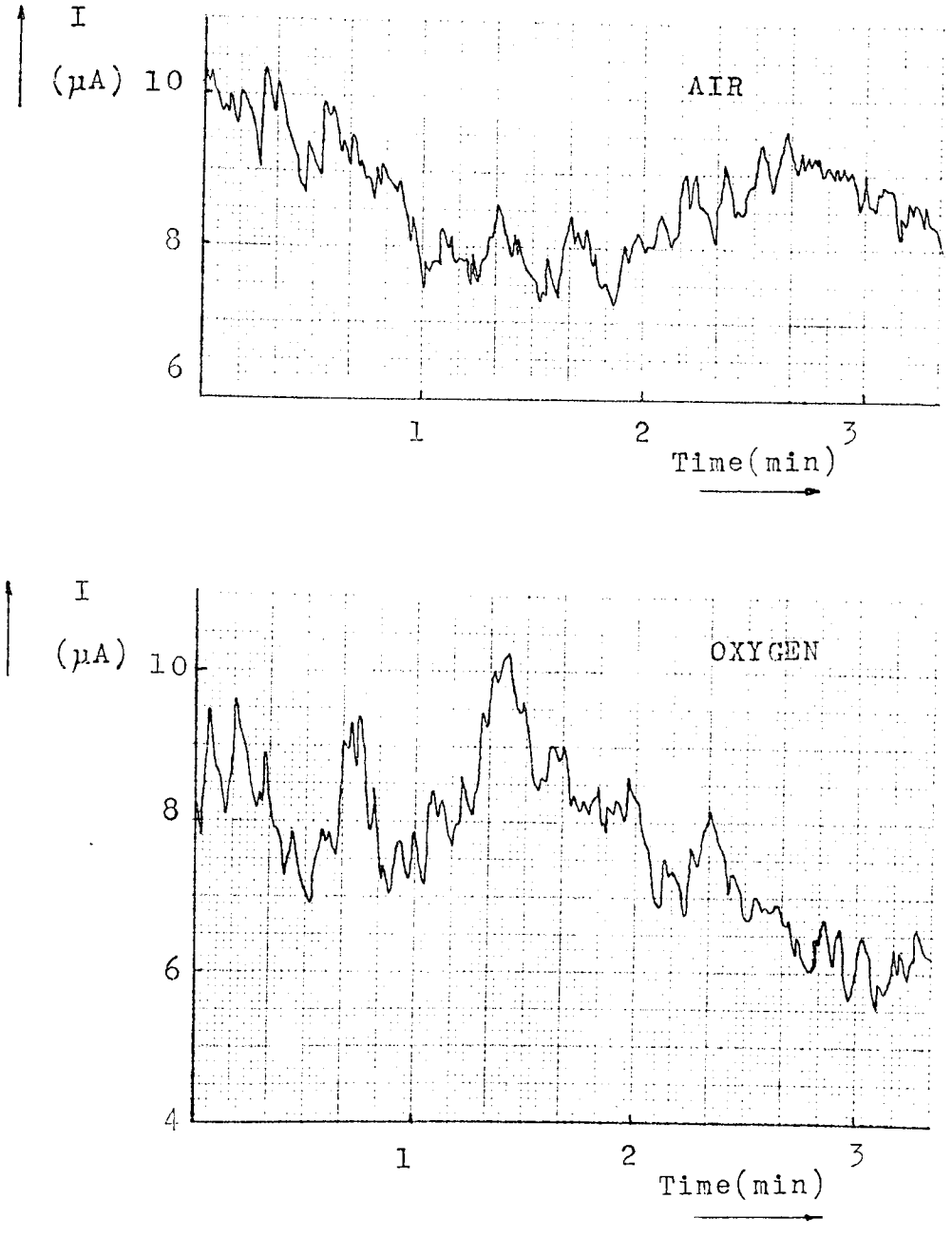

Fig. 7.26 Comparison of the stability of the emitter in air and in oxygen.

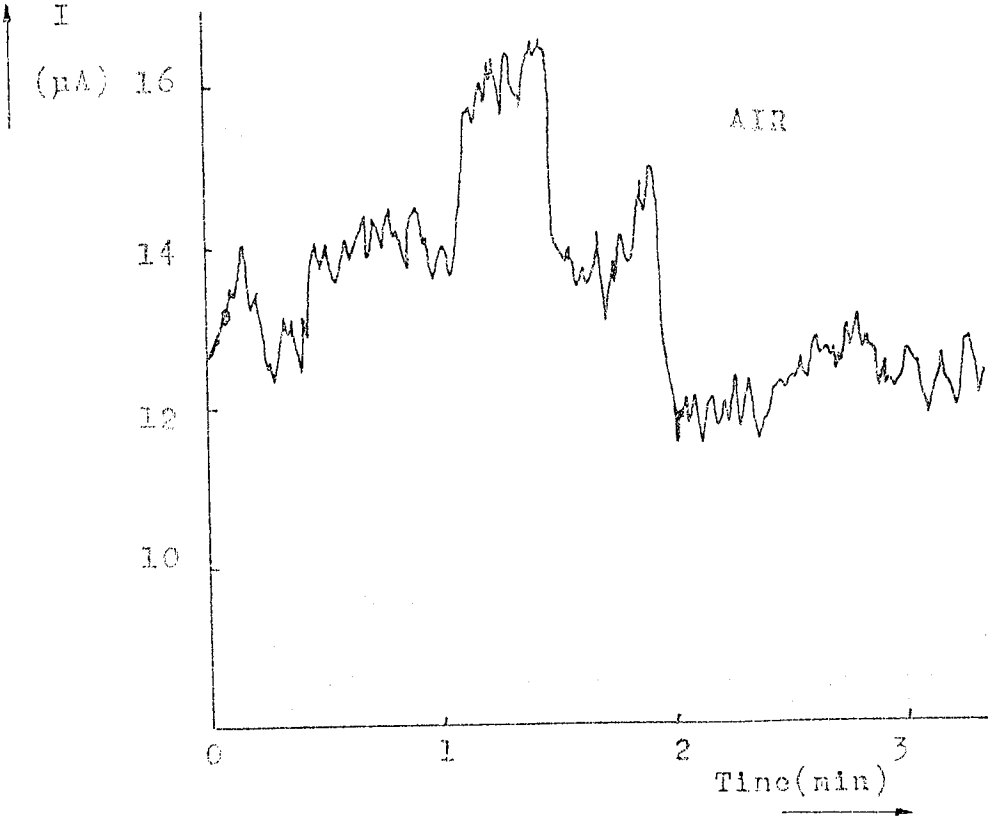

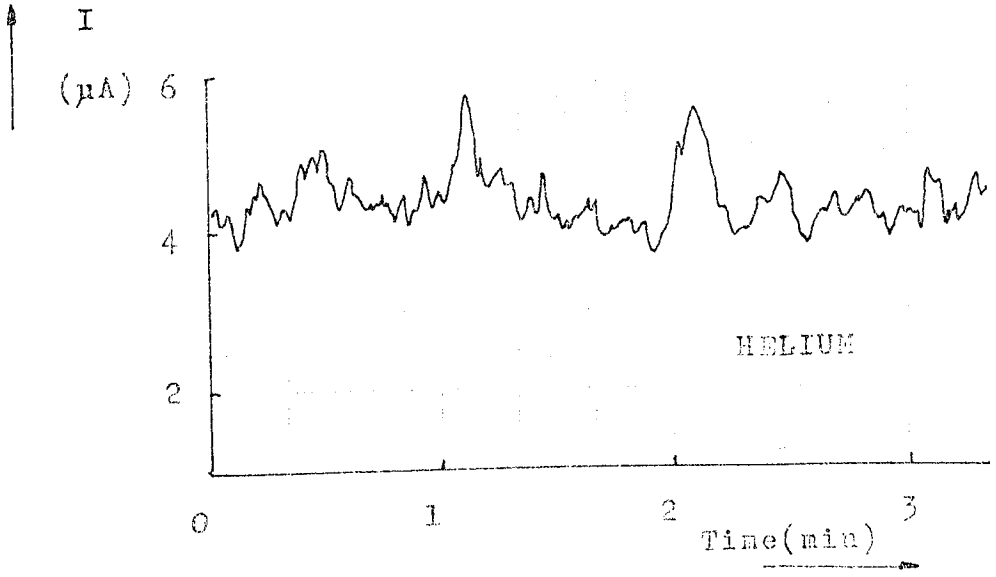

Fig. 7.27 Comparison of the stability of the emitter in air and in helium.

of $\sim 4\mu A$. The stability of the fibre in this environment is improved but this is probably due to the lowering of the total emission current rather than from the effect of the helium itself.

7.4.3 Investigation of the Spatial and Temporal Variations of the Field Emission Pattern.

To investigate the spatial and temporal fluctuations of the field emission pattern obtained from a carbon fibre a recording was made on cine-film. This was achieved using a relatively simple experimental arrangement consisting of an emitter placed opposite a phosphor screen with an extraction electrode interposed between the two. The emitter was earthed via a picoammeter and a high positive voltage was applied common to the extraction electrode and the screen until a total current of $10\mu A$ was emitted from the fibre. The resulting field emission pattern obtained on the phosphor screen was recorded with a cine-camera at a speed of twenty-four frames per second. The film was subsequently analysed using a projector which enabled successive frames to be individually stopped and viewed.

Analysis of the field emission pattern shows the emission to be composed of discrete irregular regions with the intensity of individual regions varying with

time. These regions are composed of spots of emission which flicker on and off. Viewing a typical length of film which recorded the pattern for twenty seconds and therefore contained 480 individual frames indicated that many of the emission spots lasted for at least twenty seconds whilst a few were only present for one frame. Since the duration of a single frames is 1/24th of a second this suggests that the "on-time" of an emission spot can be very small. Emission spots were often found to appear and disappear repeatedly in the same spatial position, and a table is presented in Fig 7.28 which illustrates the sequence in which two emission spots, designated A and B, were either on or off over a time period corresponding to 85 consecutive frames of film. A selection of these 85 frames has been made and photographs of the emission pattern in 7 frame groups are presented in Fig 7.29(a-g). Emission spot A is arrowed in Fig 7.29(a), whilst spot B is arrowed in Fig 7.29(f). As can be seen from these photographs even when only two emission spots are considered there are four different possible ways in which they can contribute to the total electron current. Three of these modes are illustrated in Fig 7.29(f); firstly in frames 57-59 where emission spot A is emitting electrons but B is not, secondly in frames 60-61 where both spots are contributing to the

Fig. 7.28 Table showing the sequence in which two emission spots were either on or off over a time period of 85 consecutive frames of 1/24th second duration.

FRAME NUMBER	SPOT A	FRAME NUMBER	SPOT A	FRAME NUMBER	SPOT A	SPOT B
1	OFF	29	ON	57	ON	OFF
2	OFF	30	ON	58	ON	OFF
3	OFF	31	ON	59	ON	OFF
4	OFF	32	ON	60	ON	ON
5	ON	33	ON	61	ON	ON
6	ON	34	ON	62	ON	OFF
7	ON	35	ON	63	OFF	OFF
8	ON	36	ON	64	OFF	OFF
9	ON	37	ON	65	OFF	OFF
10	ON	38	ON	66	OFF	OFF
11	ON	39	ON	67	OFF	OFF
12	OFF	40	ON	68	OFF	OFF
13	OFF	41	ON	69	OFF	OFF
14	ON	42	OFF	70	OFF	OFF
15	ON	43	ON	71	OFF	OFF
16	OFF	44	ON	72	OFF	OFF
17	ON	45	OFF	73	OFF	OFF
18	ON	46	OFF	74	OFF	OFF
19	ON	47	OFF	75	OFF	OFF
20	ON	48	OFF	76	OFF	OFF
21	ON	49	ON	77	OFF	OFF
22	ON	50	OFF	78	OFF	OFF
23	ON	51	OFF	79	OFF	OFF
24	ON	52	OFF	80	OFF	OFF
25	ON	53	ON	81	OFF	OFF
26	ON	54	ON	82	OFF	ON
27	ON	55	ON	83	OFF	OFF
28	ON	56	ON	84	OFF	OFF
				85	OFF	OFF

Fig. 7.29 A selection of frames showing the emission spots referred to in the previous figure.

Also note similarity of frame 21 to frame 85.

(a)

Frames 1,2,3,4,5,6,7.

(b)

Frames 11,12,13,14,
15,16,17.

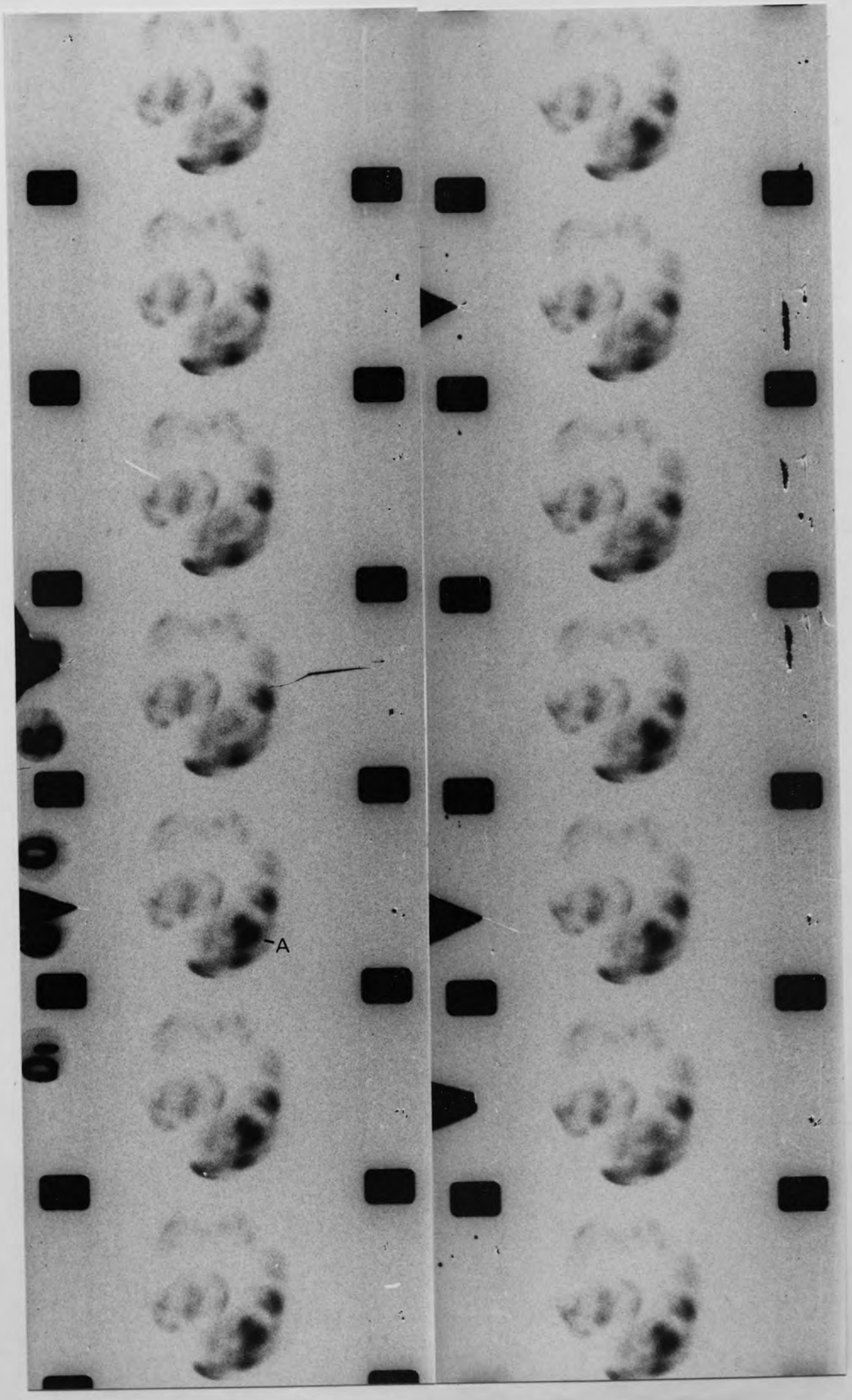
A

(c)

Frames 15,16,17,18,
19,20,21.

(d)

Frames 41,42,43,44
45,46,47.

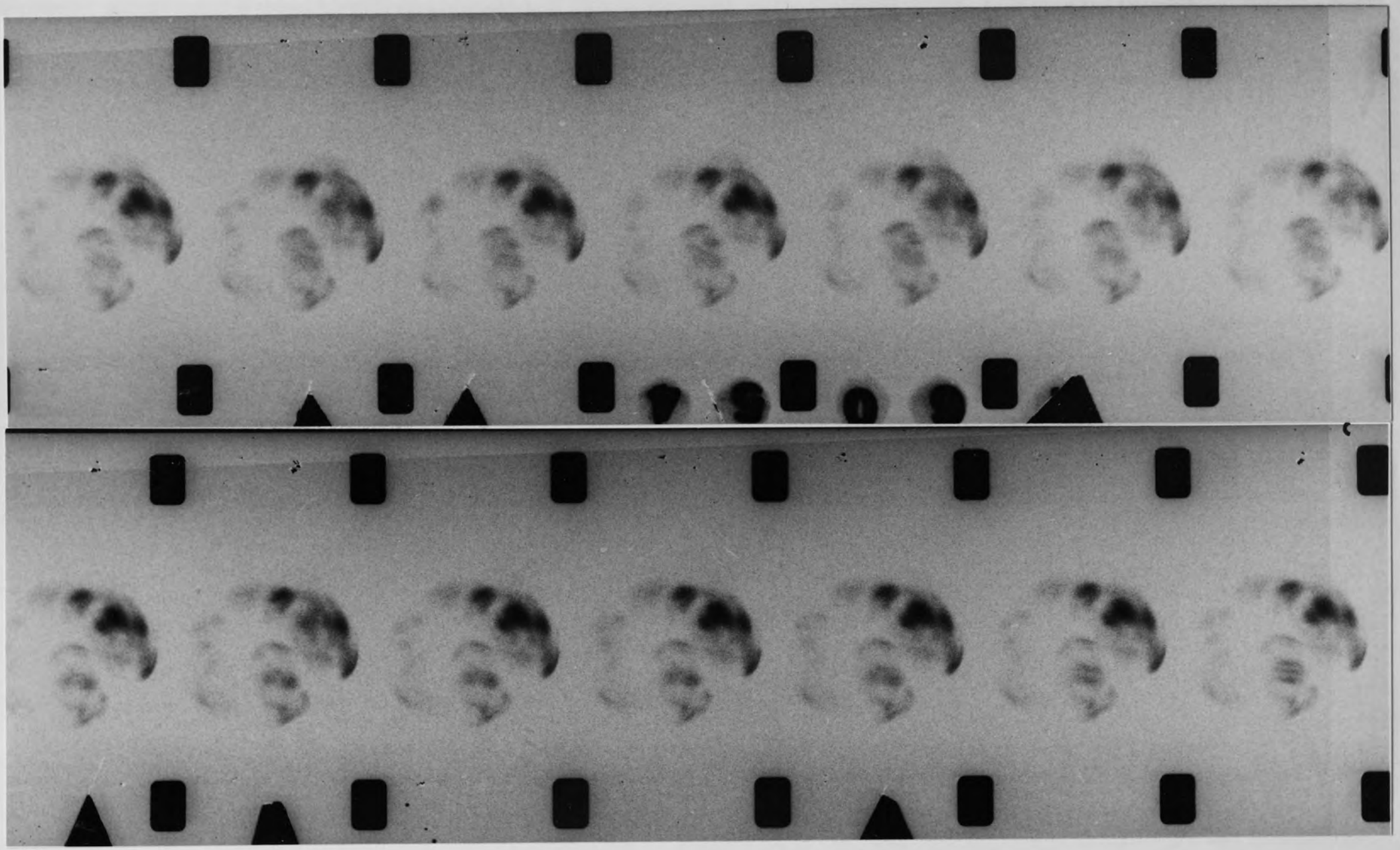

(e)

Frames 46,47,48,49,
50,51,52.

(f)

Frames 57,58,59,60
61,62,63.

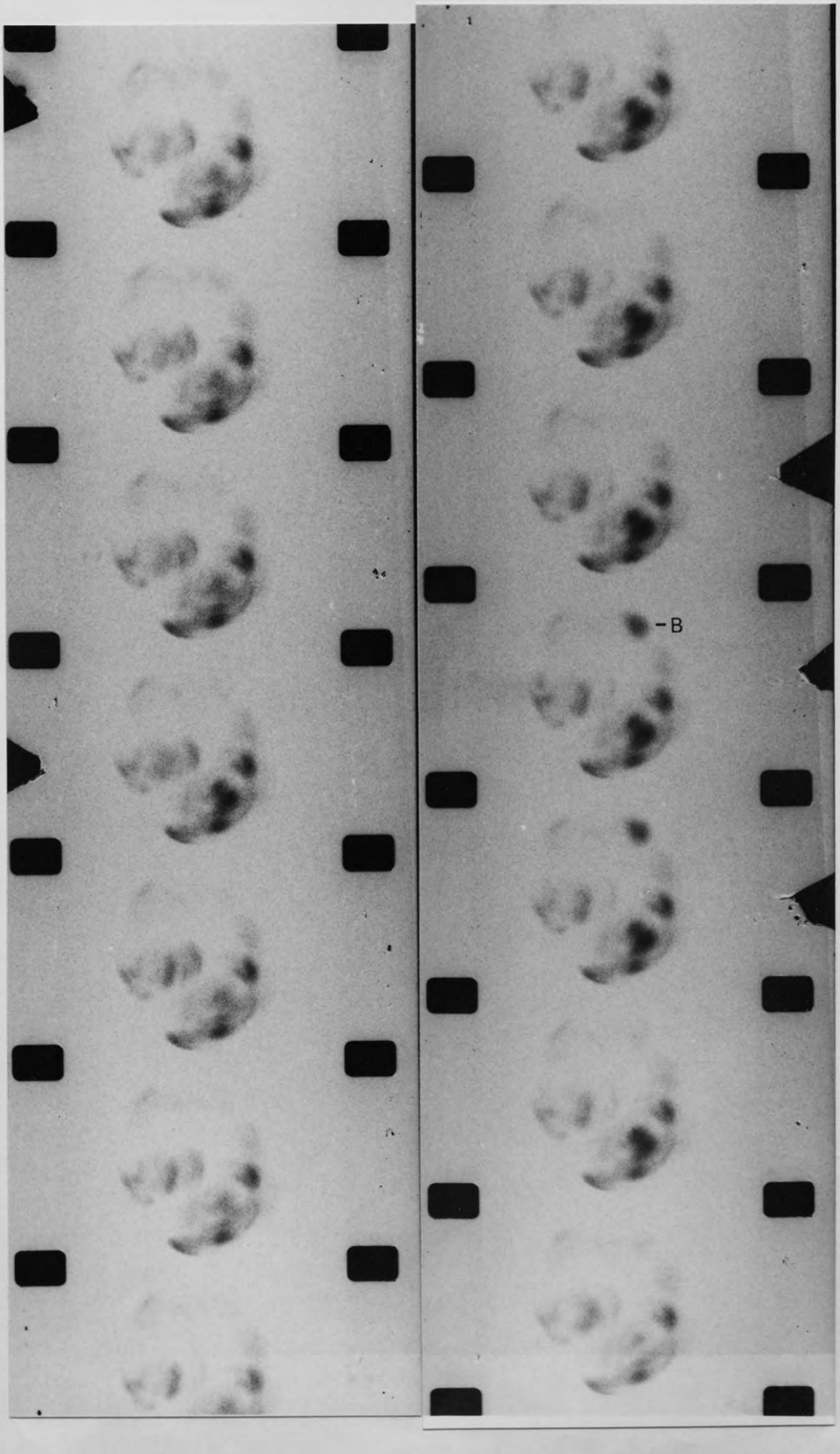
-B

(g)

Frames 79,80,81,82,
83,84,85.

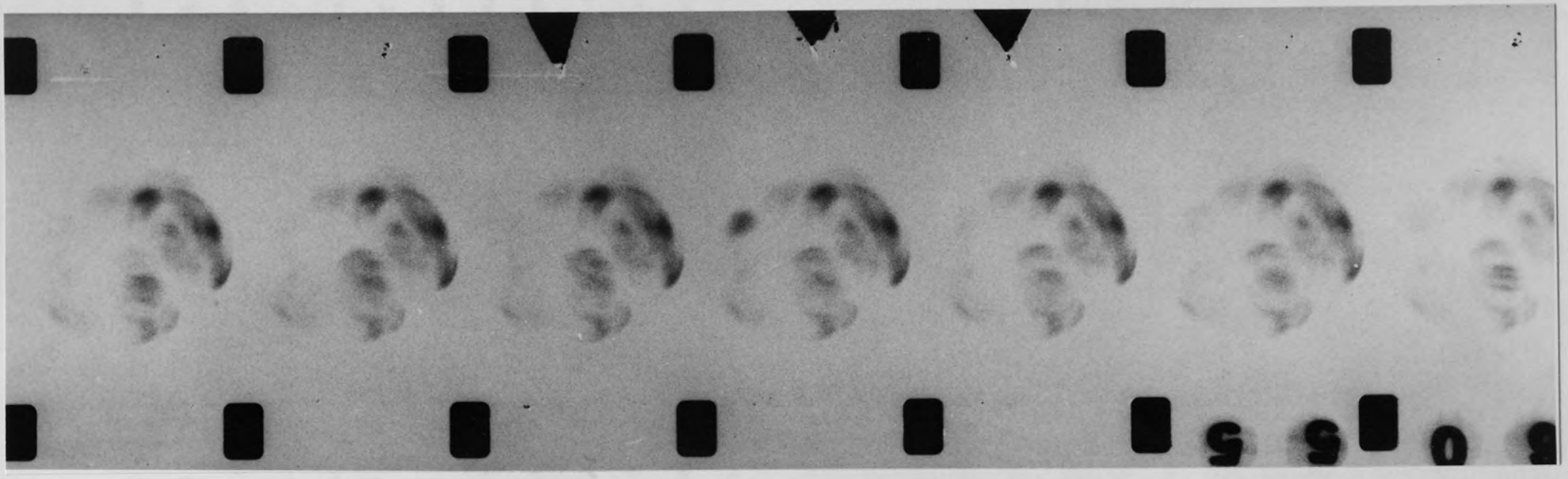

electron current, and thirdly in frame 63 where both spots are off. The fourth possibility is found in Fig 7.29(g) in frame 82 where emission spot B is emitting electrons when spot A is off. From these results it can be concluded that the emission current from a carbon fibre consists of contributions from several discrete points on the cathode surface which sporadically emit electrons independently of one another. The time for an individual emission spot to "switch-on" and "switch-off" is less than 1/24th of a second and it is suggested that future work should be done to investigate this area further with the ultimate aim of stabilising the emission process.

CHAPTER 8

DISCUSSION

Whilst it has been demonstrated that a carbon fibre field emitter has a satisfactory electron optical performance in a CRT and an adequate life-time, there is one important residual problem, viz the stability of the visual image, which manifests itself as a flickering of the final image. Since these fluctuations are almost certainly associated with this new type of electron source, it is therefore necessary to examine the physical processes by which electrons may be emitted from a carbon fibre. The initial work on field emission from carbon fibre by Baker [6., 42.] whilst indicating that this material was suitable for electron emission under poorish vacuum conditions gave no explanation for this phenomenon. The work by Lea [40.] indicated that the emission originated from asperities upon the tip surface and it was found that Fowler-Nordheim plots of the current and voltage characteristics were linear. Following this, other workers [43., 44.] measured the energy distribution of a carbon fibre emitter and interpreted their results in terms of a metallic type of emission originating from multiple centres which were formed where individual fibrils or microspikes, of about

5nm diameter, projected beyond the average emitter endform.

The theory of field emission from clean metal surfaces, as presented in Chapter 2, is in a satisfactory state and it is, therefore, understandable that it was found convenient to interpret the findings of previous work on emission from carbon fibres in terms of this theory. However, several of the effects described in the last chapter clearly indicate that the emission process is not metallic in nature: of particular significance in this connection are (a) the shift of the energy distribution with respect to the Fermi level of the substrate metal cathode, (b) the photosensitivity of the emission, and (c) the observation of an associated electroluminescence phenomenon. Accordingly, the previous model of a carbon fibre emitter consisting of emission sites emanating from the protrusion of fibrils at the surface from which 'metallic' emission occurs due to the graphitic nature of the fibre has to be discounted. Equally the theory of field emission from semiconductors is unlikely to be applicable, since electroluminescence has not been reported from a semiconducting field emitter. Referring back to Chapter 7.2, it will be recalled that the experimentally observed luminescent spectrum from a carbon fibre was broad in shape, such as would occur from photons

arising from inter-band electron relaxation processes. Whereas if electroluminescence were to be observed from a pure, crystalline, semiconducting emitter the corresponding spectrum would be expected to exhibit a sharp peak. This is because such a material contains few inter-band states and, therefore, the recombination process would have to involve a direct transition between the conduction and valence bands. It is, therefore, necessary to postulate an alternative model for the emission mechanism operating at a carbon fibre surface.

Re-examining the known structure of carbon fibre as discussed in Chapter 3.1.4, it will be recalled that, in addition to the graphitic layers present in the fibre, there are numerous pockets of amorphous carbon which are aligned along the fibre axis and constitute an average of 12% of the total cross-sectional area. (36.) These pockets of amorphous material are in intimate contact with the graphitic layers and so an alternative model for the emission mechanism is proposed based on composite emission sites, each comprising a semiconducting/insulating amorphous pocket and a metallic-like substrate provided by the graphitic layers of the carbon fibre. Such an emission regime has previously been proposed by Allen et al.(76) and Athwal and Latham (77) who have made studies

on broad-area high voltage electrodes. The similarities between their work and the present work, namely: the spectral shift in the field emission energy distributions and the electroluminescent spectra, support the applicability of this model to a carbon fibre.

The energy band representation of such a composite surface in the absence of an applied field is as shown in Fig. 8.1, where ϕ_1 and ϕ_2 are the work functions of the substrate metal and the semiconducting/insultating pocket respectively. The small band bending at the two interfaces is determined by the surface energy barriers which, in turn, are due to work function differences and the presence of surface states. When a high electric field is applied to this composite, the dielectric properties of the amorphous pocket will allow the field to penetrate into its surface modifying the band structure and potential barrier of Fig. 8.1. The resulting energy band diagram will depend on the properties of the amorphous material, i.e. whether it is semiconducting or insulating. In the case of a semiconductor the presence of charge in the conduction band and in surface states will screen the bulk from the applied field and limit its penetration to a thin surface region, as shown in Fig. 8.2(a). With a wide band-gap insulating material, however,

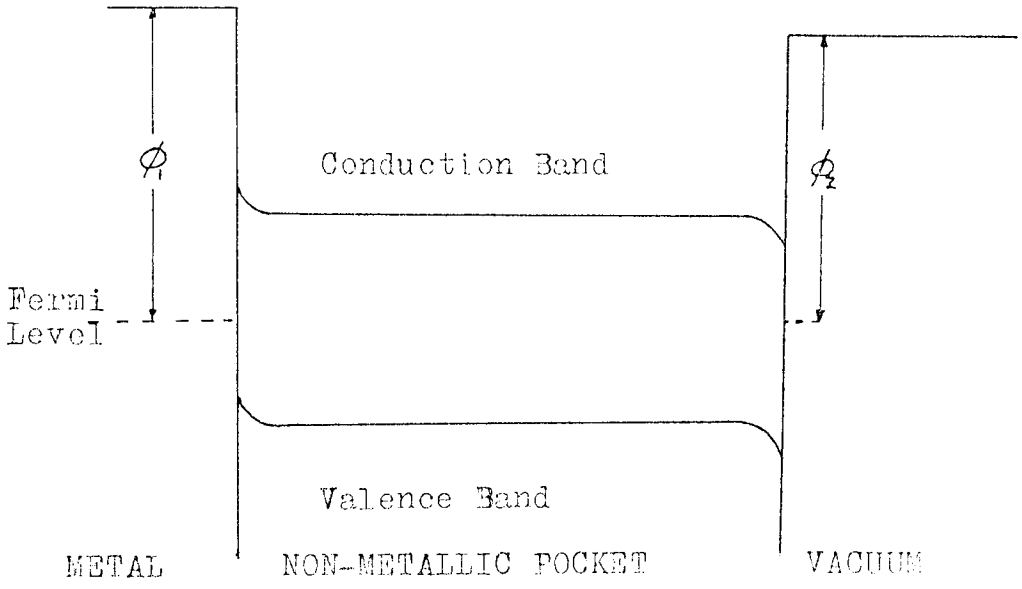

Fig. 8.1 Energy band and surface barrier configuration of the composite emission site in the absence of an applied field.

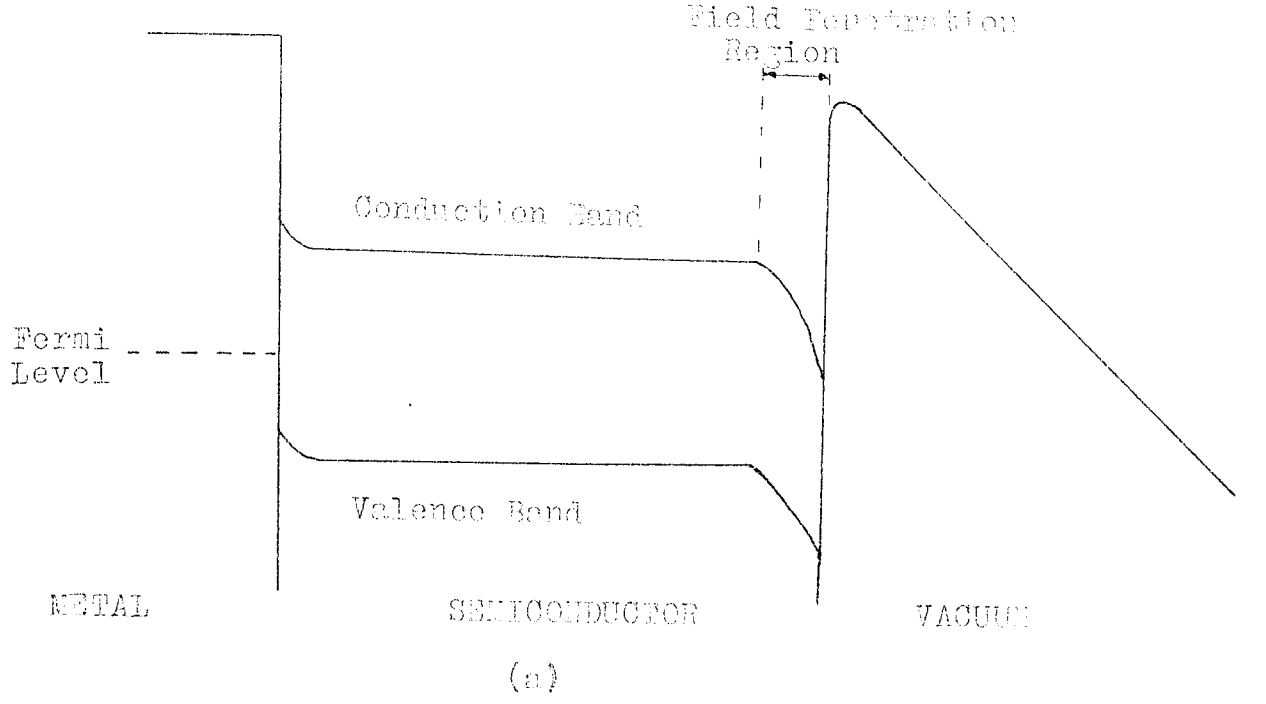

(a)

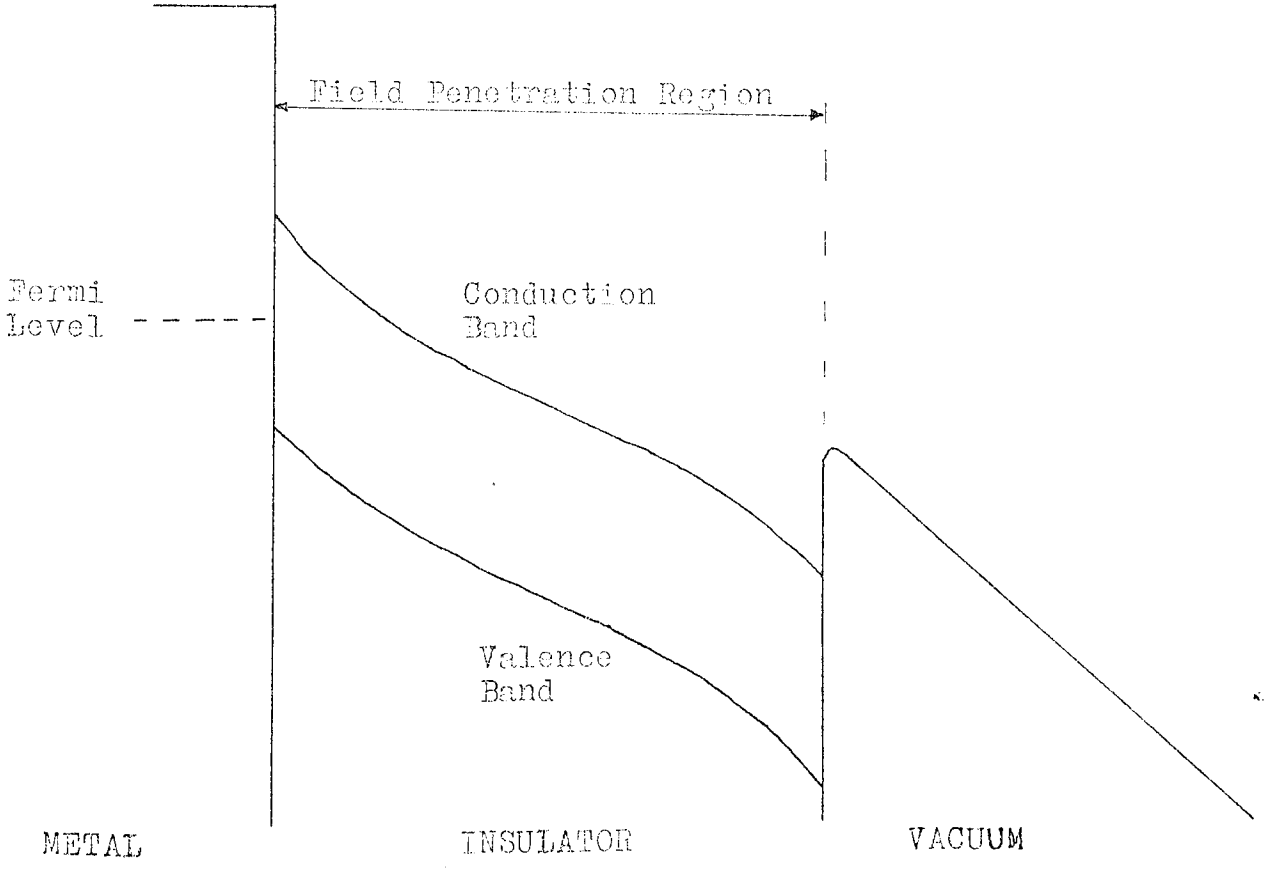

(b)

Fig. 8.2 Energy band and surface barrier configuration after the application of a high field.

the applied field will penetrate to the metal substrate and the resulting energy band diagram will be as shown in Fig. 8.2(b). From the electroluminescent spectra of visible photons recorded in 7.2 it follows that the band-gap of the amorphous material must be greater than $\sim$2.5eV which indicates an insulating rather than a semiconducting material. Referring to Fig. 8.2(b) there is a possibility that electrons can tunnel from the Fermi level in the metal into the conduction band of the insulator: such a process can either be a direct transition or via an impurity level in the band-gap. These electrons will then be accelerated or 'heated' by the penetrating field and some of them will acquire sufficient energy to be emitted over the surface potential barrier to give a spectrum that is shifted with respect to the Fermi level. Others will recombine across the band-gap near the insulator-vacuum interface to produce the observed luminescence. Such an emission model does, however, contain evident limitations. The first of these concerns the initial tunnelling of the electrons from the Fermi level of the metal substrate into the bottom of the conduction band of the insulator: in order for this to occur the barrier width must be $\lesssim$5nm which would require extreme band bending at the metal-insulator interface. Secondly, it does not readily explain how a

significant number of the hot electrons will be able to cross the insulator, which from structural and surface field considerations might have dimensions in the 0.1 - 1μm range, without losing most or all of their energy through electron-phonon scattering processes.

To overcome these difficulties it is proposed that at the initiation of electron emission from a virgin carbon fibre the etched emitter has a cone-like surface geometry which is favourable for providing the necessary field enhancement for the energy bands to be sufficiently distorted (Fig. 8.2(b)) to allow the tunnelling of electrons through the metal-insulator interface. This will result in a population of 'hot' electrons in the conduction band of the insulator which, although there will be inevitable losses due to electron-phonon scattering, will be able to create an avalanche of further charge carriers by the production of electron-hole pairs by impact ionisation. Following Athwal and Latham[77] it is then assumed that the latter respectively migrate to localised states at the insulator-vacuum and metal-insulator interfaces and create the necessary high field conditions for the insulating material to undergo a transition, in the form of an Ovshinsky type of switching process,[78] to a more stable high conductivity state. Support for the existence of this type of mechanism can be found in the

literature describing many insulators, such as: amorphous oxides, halides, sulphides and chalcogenide glasses.(79.) On switching, it is assumed that there is a rapid rearrangement of the energy band configuration shown in Fig. 8.2(b) to that illustrated in Fig. 8.3. The regime is now characterised by two very narrow high field regions at the metal-insulator and insulator-vacuum interfaces, with an extended intermediate low field region. Referring to Fig. 8.3, it is assumed that electrons tunnelling from the metal will be readily thermalised and hence be able to cross the extended low field region in the bottom of the conduction band before entering the second narrow high field region of ~10nm thick. In the latter region the electrons are heated through the 2-3eV necessary to escape over the depressed barrier, and for exciting the electron transitions required for producing the electroluminescent spectrum.

Such a model for the emission mechanism is attractive, since it provides a satisfactory interpretation of many of the experimental observations from carbon fibre emitters. It is reported in the literature that the transition to the high conductivity state on reaching a threshold voltage is extremely rapid, $\sim 10^{-10}$ seconds,(80.) and that after switching, the current at a given voltage

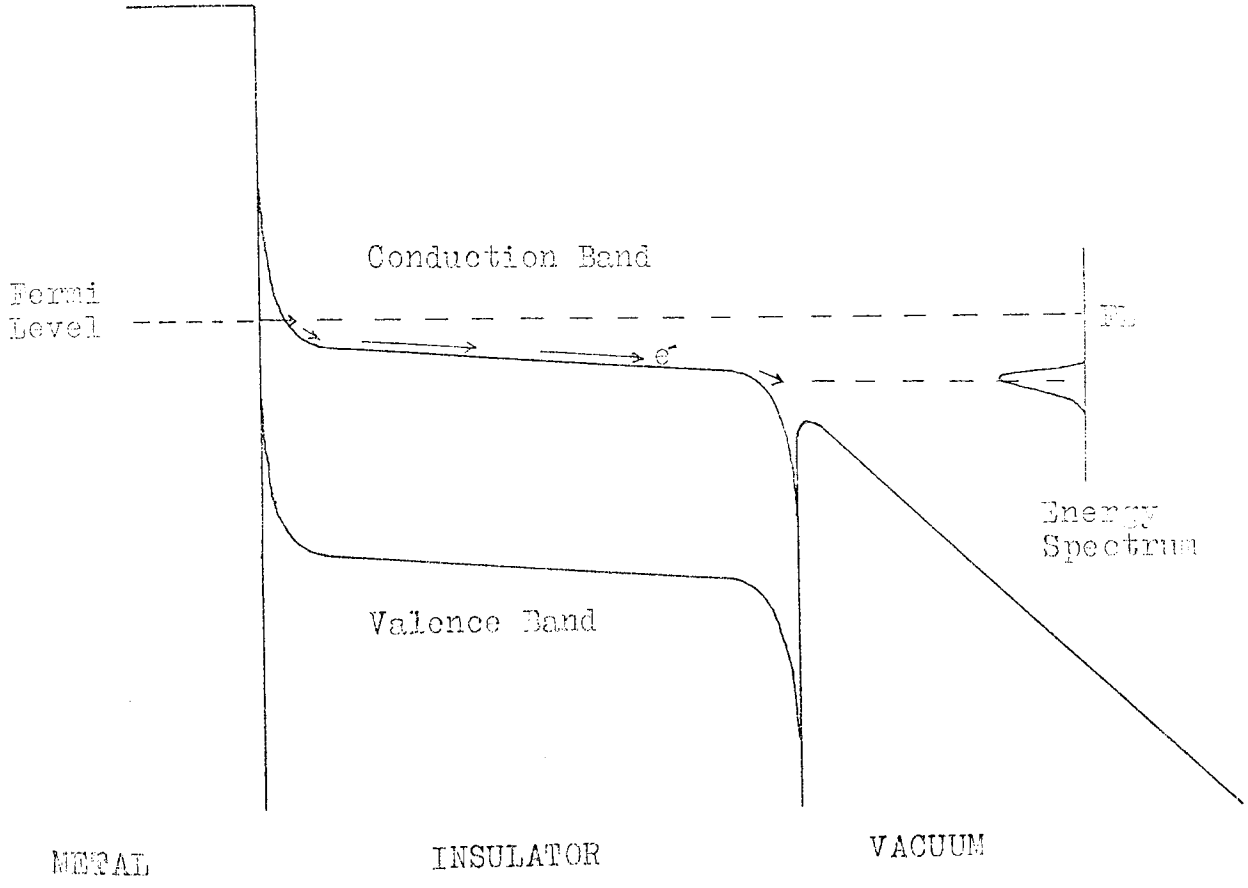

Fig. 8.3 Energy band and surface barrier configuration of the metal-insulator micro-emission site after switching.

is increased by a factor of up to 10^8. (79.) This is consistent with the starting procedure observed in 7.3 in which the current apparently instantaneously increased from 10^{-11}A to 10^{-5}A; it should, however, be noted that but for the 100MΩ current limiting resistor in series with the power supply, this latter value could be many orders higher. The reason for including the current limiting resistor stems from a confirmation of earlier work by Baker(42.) who found that applying a voltage to a freshly prepared emitter often resulted in a run-away phenomenon. Instead of the expected smooth increase in current with applied voltage, no current was obtained until a critical voltage was reached, at which point the current increased rapidly and uncontrollably often resulting in the destruction of the emitter. During this transition, in which the aggregation of emitter material is changed, it is proposed that a permanent electroforming of many of the emission sites, which each comprise of a microregime of an insulator overlaying a metal substrate, takes place such as is known to occur in metal-insulator-metal switching devices.(79.) These emission sites would then be permanently in the high conductivity state represented by the energy band diagram of Fig. 8.3 and this gives a plausible explanation of why the runaway phenomenon of emission current and the con-

sequent change in emitter profile only occur with a virgin emitter. Such a model is also consistent with the instability of the emitter being substantially unaffected by vacuum conditions in the range $\sim 10^{-5}$ to 10^{-10} torr, the residual gas species and the temperature in the range 90-300K. These instabilities of the carbon fibre emitter can be explained if it is assumed that a few of the emission sites are not irreversibly formed in the starting process. This is a likely possibility since the amorphous pockets present in these fibres are known to occur in differing sizes[36.] and with an increasing thickness of insulating material permanent forming becomes less likely.[79.] It is, therefore, envisaged that a few emission sites will reversibly switch between low and high conductivity states giving rise to the known fluctuations in the total emission current and the repetitive appearance and disappearance of emission pattern spots as observed with the cine-film results of Chapter 7.4.3.

Electroluminescent effects arise from the recombination of electrons and holes which may be created by two alternative mechanisms: either by field ionisation of a luminescent centre or by impact ionisation. Experimental observations, however, indicate that electro-

luminescence from carbon fibres only occurs in the presence of a finite emission current, rather than just the presence of an applied field. Thus, this may be explained on the basis of the proposed model by assuming that the luminescence is a consequence of electron excitation processes that occur due to the scattering of hot electrons, present during electron emission, in the surface of the emitter. The recombination of electrons and holes, which probably involve inter-band trapped states, will then give rise to the observed optical radiation.

The results obtained from measuring the energy spectra of the electrons emitted from carbon fibres may also be interpreted in terms of this model. Thus referring to Fig. 8.3, the observed shift in the energy distribution from the Fermi level of the metal substrate will arise from the combined effects of an initial energy loss in thermalising into the conduction band minimum, an ohmic energy loss in the low field region and finally, an energy loss due to phonon scattering in the high field region near to the insulator-vacuum interface. These losses may be expected to increase with increasing field and current, resulting in an increase in the shift of the distribution as is found experimentally. The shape

of the energy spectra which are found to be more symmetrical than those obtained from a metal (which have a characteristically steep high energy slope) is also consistent with the presence of hot electrons. The appearance of an additional peak in the energy distribution which frequently occurred should be studied in greater detail in future work. There is a possibility that this additional peak, whose dominance increases with applied field, is associated with a microscopic emission site, that was not permanently formed in the starting procedure, switching from a low conductivity state to a high conductivity state.

Assuming this model to be correct, it follows that there is a possibility of suppressing the switching phenomenon that gives rise to the flickering of the field emission pattern. Dearnaley et al.[79] have reported that the electrical characteristics of metal-insulator-metal devices (known to exhibit this switching mechanism) can be permanently 'formed' by the application of a voltage pulse of a few seconds' duration at room temperature in vacuum, providing the pulse height exceeds a certain critical voltage. This suggests the possibility of conditioning the carbon fibre emitters before their operation in a device. It is, therefore, suggested that future work

should investigate in more detail the starting procedure of applying a field to a virgin emitter. In particular once emission from the tip has commenced, the effect of applying pulses whose peak voltage is much greater than the steady d.c. value required for normal emission currents should be examined. It is hoped that in this manner it may be possible to permanently 'form' all of the emission sites. However, in order to prevent damage of the emitter being caused by excessive local heating, it is likely that the time duration of these pulses will have to be very short.

CONCLUSION

In order to investigate the suitability of using a carbon fibre field emitter as the electron source in a CRT, it was necessary to develop a demountable ultra high vacuum electron optical bench incorporating a high precision cathode manipulator. With this system it was possible to experimentally evaluate the performance of a range of field emission electron guns having various electrode geometries. As a result of this investigation, a 'tetrode' type of electron gun was adopted as the basis of a prototype field emitting cathode ray tube. The tetrode gun comprised a carbon fibre cathode, an 'extraction' electrode to provide the necessary high field for emission, and a two-anode electrostatic lens; the latter being designed with the aid of computer programmes. To eliminate an undesirable effect caused by secondary electrons appearing in the final image, it was also necessary to limit the beam emerging from the gun by including an additional aperture stop immediately following the lens apertures.

The electron optical performance of the prototype CRT was satisfactory, in that it produced a well focussed spot of $\sim$0.2mm which was suitable for forming a raster pattern of adequate intensity from a total emission current

of 10 μA. There remains, however, an undesirable aspect of using a carbon fibre electron source, namely the stability of the visual image. Various techniques have been examined for stabilising the emission from the cathode with the aim of suppressing the flickering of the final image. A simple, yet effective, method was found to be the insertion of a high-valued resistance ($\sim$ 100MΩ) in series with the cathode. This resulted in reducing the fluctuations from about $\pm$10% to less than $\pm$1%, for a total emission current of $\sim$10μA. A consequence of this method, however, was that a varying voltage was applied to the emitter and this resulted in an unacceptable change in the focus and energy of the electron beam. It is anticipated that future work will extend the examination of stabilisation techniques proposed in Chapter 6.10. For example, it would be interesting to know the result of feeding back a signal which is well correlated with the screen current, such as can be obtained from the electrode containing the limiting aperture stop, to the extraction electrode. An advantage of this method is that varying the voltage on the extraction electrode will control the emission current without affecting the final beam energy.

Since the problem of stability of the visual image is almost certainly related to the electron source, several experiments were performed to gain some insight into the

physical mechanism responsible for the electron emission. The first of these involved measuring the distribution of energies of electrons emitted from a carbon fibre tip, using an UHV advanced high resolution spectrometer. Two types of distribution were recorded having either a single peak or a double peak. For emission currents in the range 10^{-10}A to 10^{-7}A the half width and spectral shift of a single peaked spectrum were found to increase from 0.24eV to 0.50eV, and 0.30eV to 0.60eV respectively, with increasing field. More evidence for the emission mechanism was provided by the observation that there is optical radiation associated with electron emission. The variation in light intensity of this radiation with applied field was found to be in good agreement with the Alfrey-Taylor relationship for electroluminescence.

Examination of the noise characteristics of carbon fibre emitters showed that in a vacuum pressure of $\sim 10^{-8}$torr and for emission currents in the range 1μA to 10μA the noise was predominantly low frequency (< 500Hz). Reducing the vacuum pressure from $\sim 10^{-5}$torr to $\sim 10^{-8}$torr improved the stability of the emission, which was independent of whether the prevalent gas molecules were nitrogen, oxygen or helium. Analysis of a cine recording of the field emission pattern showed the emission to be composed of discrete irregular

regions with the intensity of individual regions varying with time. These regions consist of spots of emission which were found to "switch-on" and "switch off" in less than 1/24th of a second; i.e. the maximum frame speed of the camera. The experimental evidence obtained from these studies suggest that the emission mechanism is not analogous to either that associated with metallic or semiconducting emitters. Therefore an alternative emission regime has been proposed based on the concept of a composite emission site comprising an insulating amorphous pocket overlaying a metallic-like substrate: involving the important concept of "internal" electron heating. Such a model provides a plausible explanation of many of the experimentally observed properties of carbon fibre emitters.

Whilst the electron optical performance of the prototype CRT has been satisfactory, there remains one obvious residual problem which restricts its commercial development. This limitation is the instability of the emission current which manifests itself as a flickering of the visual image. It is therefore desirable that future work should investigate this aspect further. One suggested approach is to gain more quantitative data in order to test the proposed explanation for the physical mechanism responsible for the emission and

hence the instabilities. Such data can be obtained by extending the present results on field emission energy spectra, electroluminescence, scanning electron microscopy, and cine-photography of the field emission pattern. For example these would include

1) energy spectra: a quantitative analysis of the spectral shift with applied field, or the observation of the peak being photosensitive,
2) electroluminescence: determining the pressure dependence of the optical radiation,
3) scanning electron microscopy: examining the emitter profile before and after emission in a vacuum pressure $\lesssim 10^{-10}$torr,
4) cine-photography: refining the technique using high speed photography to determine the time the spot is in a given state (on or off).

Alternatively, another approach could be to accept that the instability is an inherent characteristic of the emission process and to re-examine techniques of stabilisation. An alternative technique to controlling the voltage of the extraction electrode by a feedback signal previously mentioned, is to maintain a constant emission current by varying the voltage applied to the emitter in a suitable manner. This may be achieved, for example, by the insertion of a high-

valued resistor in series with the emitter. Such a technique, however, has the undesirable consequence of varying the total beam energy and perhaps more seriously leads to the image defocussing, since the lens voltage ratio will also vary. With this point in mind, it is therefore, suggested that future work should re-examine the computer aided design of the lens with the aim of achieving a focussed beam that is less critically dependent on the anode voltages. Referring to Fig. 6.14, the present lens was designed to operate with a voltage ratio $V_I/V_O = 5$ and it is seen that a small change in this ratio will lead to an appreciable change in the required object position. If, however, a point on the curve of Fig. 6.14 is chosen where the gradient is shallower, then the lens is less sensitive to a changing voltage ratio and hence the focus is less critical. Such a modification to the electron gun could be achieved by choosing an operating ratio $V_I/V_O = 10$ which would necessitate reducing the extraction electrode to first anode separation to 5mm (allowing for an emitter to extraction electrode separation of 1mm as in the present design). This modification should result in the defocussing effect being tolerable. An alternative method for further work could be to investigate the elimination of this effect by arranging the voltage applied to the extraction electrode and first anode to vary

in a similar manner to the voltage applied to the emitter. However, due to the beam energy changing with the emitter voltage, there may still be some variation in the light intensity.

Finally, using a carbon fibre as an alternative electron source in cathode ray tubes has been demonstrated to be feasible providing fluctuations in light intensity of the visual display can be reduced.

APPENDIX

Programme 1

```
UAFORTRAN *LPO DATA6
      MASTER LENSPROG
      IMPLICIT REAL*8(A-H,O-Z)
      DIMENSION C(20,40),R(20,40),V(20,40),Z(20,40)
      DIMENSION F(10,20,40),P(20,40,5),A(20,40,20)
      DIMENSION V1(20),V2(40),V3(20),Z1(60)
      DIMENSION TITLE(20)
      EQUIVALENCE (A(1,1,1),P(1,1,1),V(1,1))
      EQUIVALENCE (A(1,1,6),F(1,1,1))
      IM=20
      JM=40
      READ(1,1) (TITLE(I),I=1,20),N,NSYM
 1    FORMAT(20A4/2I5)
      READ(1,2)
 2    FORMAT(1X)
      CALL MESH(Z,I1,J1,IM,JM)
      CALL MESH(R,I1,J1,IM,JM)
      I2=I1-1
      J2=J1-1
      IB=I1+1
      IS=(I1-1)*(J1-2)
      IF(NSYM.EQ.1) IS=(I1-1)*(J1-1)
      CALL SETFE(Z,R,F,I1,J1)
      CALL SETMET(F,I2,J2)
      READ(1,2)
      CALL SETCE(Z,R,Z1,V1,V2,V3,F,C,I1,J1,NSYM)
      CALL SETPE(F,P,I2,J2,NSYM)
      CALL PINTOA(A,IS,IB)
      CALL BANDSM(A,C,IS,IB)
      CALL CTOVE(C,V,V1,V2,V3,I1,J1,NSYM)
      WRITE(2,7) (TITLE(I),I=1,20)
 7    FORMAT(1X,20A4)
      CALL AXVE(Z,V,V2,I1,J1,NSYM)
      IF(N.EQ.0) STOP
      WRITE(6,7) (TITLE(I),I=1,20)
      WRITE(6,8)
 8    FORMAT(/1X,'COMPUTED POTENTIAL VALUES AT EACH MESH POINT'/)
      CALL WRITEV(V,I1,J1)
      STOP
      END
      SUBROUTINE MESH(Z,I1,J1,IM,JM)
      IMPLICIT REAL*8(A-H,O-Z)
      DIMENSION Z(1)
      DIMENSION N(15),XA(15),XB(15)
      READ(1,1) (N(L),L=1,15)
 1    FORMAT(5X,15I5)
      DO 2 L=1,15
      IF(N(L).EQ.0) GO TO 3
 2    CONTINUE
      JJ=15
```

```
      GO TO 4
    3 JJ=L-1
    4 J1=N(JJ)
      IF(J1.GT.JM) GO TO 11
      READ(1,5) IA,(XA(L),L=1,JJ)
    5 FORMAT(I5,3P15F5.0)
    6 READ(1,5) IB,(XB(L),L=1,JJ)
      IF(IB.EQ.0) GO TO 9
      IF(IB.GT.IM) GO TO 11
      F=FLOAT(IB-IA)
      DO 7 L=2,JJ
      JA=N(L-1)
      JB=N(L)
      C=FLOAT(JB-JA)
      Z1=XA(L-1)
      Z2=XA(L)
      Z3=XB(L-1)
      Z4=XB(L)
      DO 7 J=JA,JB
      KO=(J-1)*IM
      A=FLOAT(JB-J)
      B=FLOAT(J-JA)
      Z5=(A*Z1+B*Z2)/C
      Z6=(A*Z3+B*Z4)/C
      DO 7 I=IA,IB
      K=KO+I
      D=FLOAT(IB-I)
      E=FLOAT(I-IA)
    7 Z(K)=(D*Z5+E*Z6)/F
      IA=IB
      DO 8 L=1,JJ
    8 XA(L)=XB(L)
      GO TO 6
    9 I1=IA
      K=0
      DO 10 J=1,J1
      K1=(J-1)*IM
      DO 10 I=1,I1
      K=K+1
      K1=K1+1
   10 Z(K)=Z(K1)
      RETURN
   11 WRITE(6,12)
   12 FORMAT( 1X,'SPECIFIED MESH SIZE EXCEEDS',
     -  ' SPECIFIED ARRAY DIMENSIONS' )
      STOP
      END
      SUBROUTINE SETFE(Z,R,F,I1,J1)
      IMPLICIT REAL*8(A-H,O-Z)
      DIMENSION Z(1),R(1),F(1)
      DIMENSION ZA(6),RA(6),D(24)
      L=0
      KC=I1-1
      KD=(J1-1)*I1-1
      DO 2 KB=KC,KD,I1
      KA=KB-I1+2
      DO 2 K=KA,KB
      KP=K+I1
      ZA(1)=Z(K)
      ZA(2)=Z(K+1)
      ZA(3)=Z(KP+1)
      ZA(4)=Z(KP)
      ZA(5)=Z(K)
      ZA(6)=Z(K+1)
      RA(1)=R(K)
      RA(2)=R(K+1)
```

```
      RA(3)=R(KP+1)
      RA(4)=R(KP)
      RA(5)=R(K)
      RA(6)=R(K+1)
      M=0
      DO 1 N=1,4
      Z1=ZA(N)
      Z2=ZA(N+1)
      Z3=ZA(N+2)
      R1=RA(N)
      R2=RA(N+1)
      R3=RA(N+2)
      B1=R2-R3
      B2=R3-R1
      B3=R1-R2
      C1=Z3-Z2
      C2=Z1-Z3
      C3=Z2-Z1
      DET=B1*C2-B2*C1
      R0=(R1+R2+R3)/3.
      X=R0/DET
      D(M+1)=(B1*B1+C1*C1)*X
      D(M+2)=(B1*B2+C1*C2)*X
      D(M+3)=(B1*B3+C1*C3)*X
      D(M+4)=(B2*B2+C2*C2)*X
      D(M+5)=(B2*B3+C2*C3)*X
      D(M+6)=(B3*B3+C3*C3)*X
1     M=M+6
      F(L+1)=D(1)+D(18)+D(22)
      F(L+2)=D(2)+D(23)
      F(L+3)=D(3)+D(15)
      F(L+4)=D(17)+D(20)
      F(L+5)=D(4)+D(7)+D(24)
      F(L+6)=D(5)+D(8)
      F(L+7)=D(9)+D(21)
      F(L+8)=D(6)+D(10)+D(13)
      F(L+9)=D(11)+D(14)
      F(L+10)=D(12)+D(16)+D(19)
2     L=L+10
      RETURN
      END
      SUBROUTINE SETMET(F,I2,J2)
      IMPLICIT REAL*8(A-H,O-Z)
      DIMENSION F(1)
      X=1.E10
2     READ(1,3) JA,JB,IA,IB
3     FORMAT(4I5)
      IF(JA.EQ.0) RETURN
      KC=((JA-1)*I2+IB-1)*10
      KD=((JB-2)*I2+IB-1)*10
      KE=I2*10
      DO 5 KB=KC,KD,KE
      KA=KB-(IB-IA)*10+1
      DO 5 K=KA,KB
5     F(K)=F(K)*X
      GO TO 2
      END
      SUBROUTINE SETCE(Z,R,Z1,V1,V2,V3,F,C,I1,J1,NSYM)
      IMPLICIT REAL*8(A-H,O-Z)
      DIMENSION Z(1),R(1),Z1(1),V1(1),V2(1),V3(1),F(1),C(1)
      I2=I1-1
      I3=I1-2
      IR=(J1-3)*I2+1
      IS=(J1-2)*I2
      IF(NSYM.EQ.1) IS=(J1-1)*I2
      DO 1 I=1,I1
```

```
 1      Z1(I)=R(I)
        CALL READV1(Z1,V1,I1)
        K=1
        DO 2 J=1,J1
        Z1(J)=Z(K)
 2      K=K+I1
        CALL READV1(Z1,V2,J1)
        IF(NSYM.EQ.1) GO TO 11
        K=I1*J1-I2
        DO 3 I=1,I1
        Z1(I)=R(K)
 3      K=K+1
        CALL READV1(Z1,V3,I1)
11      DO 4 I=1,IS
 4      C(I)=0
        K=0
        I=2
        DO 5 L=1,I3
        C(L)=-F(K+3)*V1(I-1)-(F(K+6)+F(K+14))*V1(I)-F(K+17)*V1(I+1)
        K=K+10
 5      I=I+1
        C(I2)=-F(K+3)*V1(I-1)-F(K+6)*V1(I)
        K=0
        J=2
        DO 6 L=1,IR,I2
        M=K+10*I2
        C(L)=C(L)-F(K+3)*V2(J-1)-(F(K+9)+F(M+2))*V2(J)-F(M+7)*V2(J+1)
        K=M
 6      J=J+1
        IF3=3
        C(1)=C(1)+F(IF3)*V1(1)
        IF(NSYM.EQ.1) GO TO 14
        IS1=IS-1
        I=2
        DO 13 L=IR,IS1
        C(L)=C(L)-F(M+7)*V3(I-1)-(F(M+6)+F(M+14))*V3(I)-F(M+13)*V3(I+1)
        M=M+10
13      I=I+1
        C(IS)=C(IS)-F(M+7)*V3(I-1)-F(M+6)*V3(I)
        C(IR)=C(IR)+F(K+7)*V3(1)
        RETURN
14      L=12*(J1-2)+1
        C(L)=C(L)-F(K+3)*V2(J-1)-F(K+9)*V2(J)
        RETURN
        END
        SUBROUTINE READV1(Z1,V1,I1)
        IMPLICIT REAL*8(A-H,O-Z)
        DIMENSION Z1(1),V1(1)
        READ(1,1) IB,VB
 1      FORMAT(I5,F10.0)
        IF(IB-1) 2,4,2
 2      WRITE(6,3)
 3      FORMAT(1X,'ERROR IN BOUNDARY POTENTIAL DATA')
        STOP
 4      IA=IB
        VA=VB
        READ(1,1) IB,VB
        X=(VB-VA)/(Z1(IB)-Z1(IA))
        DO 5 I=IA,IB
 5      V1(I)=VA+(Z1(I)-Z1(IA))*X
        IF(IB-I1) 4,6,2
 6      RETURN
        END
        SUBROUTINE SETPE(F,P,I2,J2,NSYM)
        IMPLICIT REAL*8(A-H,O-Z)
        DIMENSION F(1),P(1)
```

```
      IS=I2*(J2-1)
      IF(NSYM.EQ.1) IS=I2*J2
      IT=10*I2
      K=0
      IX=I2*(J2-1)
      DO 2 LC=I2,IX,I2
      LA=LC-I2+1
      LB=LC-1
      DO 1 L=LA,LB
      L1=L+IS
      L2=L1+IS
      L3=L2+IS
      L4=L3+IS
      M=K+IT
      P(L)=F(K+8)+F(K+20)+F(M+5)+F(M+11)
      P(L1)=F(K+19)+F(M+12)
      P(L2)=F(M+7)
      P(L3)=F(M+6)+F(M+14)
      P(L4)=F(M+13)
    1 K=K+10
      LC1=LC+IS
      LC2=LC1+IS
      LC3=LC2+IS
      LC4=LC3+IS
      M=K+IT
      P(LC)=F(K+8)+F(M+5)
      P(LC1)=0.
      P(LC2)=F(M+7)
      P(LC3)=F(M+6)
      P(LC4)=0.
    2 K=K+10
      IR=IS-I2+1
      DO 3 L=1,IR,I2
      L2=L+2*IS
    3 P(L2)=0.
      IF(NSYM.EQ.0) RETURN
      LA=IX+1
      LB=IS-1
      DO 8 L=LA,LB
      L1=L+IS
      L2=L1+IS
      L3=L2+IS
      L4=L3+IS
      P(L)=F(K+8)+F(K+20)
      P(L1)=F(K+19)
      P(L2)=0.
      P(L3)=0.
      P(L4)=0.
    8 K=K+10
      IS1=IS+IS
      IS2=IS1+IS
      IS3=IS2+IS
      IS4=IS3+IS
      P(IS)=F(K+8)
      P(IS1)=0.
      P(IS2)=0.
      P(IS3)=0.
      P(IS4)=0.
      RETURN
      END
      SUBROUTINE PINTOA(A,IS,IB)
      IMPLICIT REAL*8(A-H,O-Z)
      DIMENSION A(1)
      KADD=(IB-5)*IS
      KA=2*IS+1
      KB=5*IS
```

```
      DO 1 K=KA,KB
      J=K+KADD
1     A(J)=A(K)
      KB=(IB-3)*IS
      DO 2 K=KA,KB
2     A(K)=0.
      RETURN
      END
      SUBROUTINE BANDSM(A,B,IS,IW)
      IMPLICIT REAL*8(A-H,O-Z)
      DIMENSION A(1),B(1)
      IE=IS-IW+1
      IR=IS-1
      LB=(IW-1)*IS
      DO 1 LA=1,IR
      LB=LB+1
      IF(LA.GT.IE) LB=LB-IS
      KA=LA
      KB=LB
      KP=0
      LX=LA+IS
      DO 1 L=LX,LB,IS
      X=A(L)/A(LA)
      KA=KA+1
      KB=KB-IR
      KP=KP+IR
      B(KA)=B(KA)-X*B(LA)
      DO 1 K=KA,KB,IS
      N=K+KP
1     A(K)=A(K)-X*A(N)
      B(IS)=B(IS)/A(IS)
      LA=IS
      LB=IS
      DO 3 J=1,IR
      LA=LA-1
      LB=LB-1
      IF(LA.GE.IE) LB=LB+IS
      X=B(LA)
      LX=LA+IS
      K=LA
      DO 2 L=LX,LB,IS
      K=K+1
2     X=X-A(L)*B(K)
3     B(LA)=X/A(LA)
      RETURN
      END
      SUBROUTINE CTOVE(C,V,V1,V2,V3,I1,J1,NSYM)
      IMPLICIT REAL*8(A-H,O-Z)
      DIMENSION C(1),V(1),V1(1),V2(1),V3(1)
      KC=2*I1
      KD=(J1-1)*I1
      IF(NSYM.EQ.1) KD=I1*J1
      L=0
      DO 1 KB=KC,KD,I1
      KA=KB-I1+2
      DO 1 K=KA,KB
      L=L+1
1     V(K)=C(L)
      DO 2 I=1,I1
      V(I)=V1(I)
      IF(NSYM.EQ.1) GO TO 2
      K=I+KD
      V(K)=V3(I)
2     CONTINUE
      K=1
      DO 3 J=2,J1
```

```
      K=K+I1
    3 V(K)=V2(J)
      RETURN
      END
      SUBROUTINE AXVE(Z,V,V2,I1,J1,NSYM)
      IMPLICIT REAL*8(A-H,O-Z)
      DIMENSION Z(1),V(1),V2(1)
      WRITE(2,5)
      IT=I1*J1
      DO 1 I=I1,IT,I1
      ZMM=Z(I)*1000.
    1 WRITE(2,6) ZMM,V(I)
      IF(NSYM.EQ.0) GO TO 4
      IR=IT-I1
      DO 3 J=I1,IR,I1
      I=IT-J
      ZMM=Z(I)*1000.
    3 WRITE(2,6) ZMM,V(I)
    4 WRITE(2,7)
      WRITE(2,2) NSYM
    2 FORMAT(1X,'NSYM=',I1)
      IF(NSYM.EQ.1) GO TO 9
      WRITE(2,7)
      RETURN
    9 WRITE(2,10) V2(J1)
      RETURN
    5 FORMAT(//1X,'AXIAL POTENTIAL DISTRIBUTION'///
     - 1X,' Z(MILLIMETRES)        V(VOLTS)'/)
    6 FORMAT(1X,F15.4,F15.6)
    7 FORMAT(1X,30X)
   10 FORMAT(1X,F15.6,'  = CENTRAL ELECTRODE POTENTIAL')
      END
      SUBROUTINE WRITEV(V,I1,J1)
      IMPLICIT REAL*8(A-H,O-Z)
      DIMENSION V(I1,J1)
      JMAX=((J1+4)/5)*5
      DO 4 JC=5,JMAX,5
      JA=JC-4
      JB=JC
      IF(JB.GT.J1) JB=J1
      WRITE(6,1) (J,J=JA,JB)
    1 FORMAT(1X,4X,5I15)
      DO 2 I=1,I1
    2 WRITE(6,3) I,(V(I,J),J=JA,JB)
    3 FORMAT(1X,I4,5G15.5)
    4 WRITE(6,5)
    5 FORMAT(1X,79X)
      WRITE(6,5)
      RETURN
      END
      FINISH
```

Typical data for programme 1.

```
      FLAT PLATE LENS WITH A 6MM HOLE AND SEPARATION OF 3 MM
0     0

         1     5     7    33    35    39
   1  -7.  -3.  -2.4 -0.6   0.    4.
  15  -7.  -3.  -2.4 -0.6   0.    4.
  17  -7.  -3.  -2.4 -0.6   0.    4.

         1     5     7    33    35    39
   1  20.   20.   20.   20.   20.   20.
  15   3.    3.    3.    3.    3.    3.
  19   0.    0.    0.    0.    0.    0.

   5    7     1    15
  33   35     1    15


   1    0.
  19    0.
   1    0.
   7    0.
  33 1000.
  39 1000.
   1 1000.
  19 1000.
****
```

Programme 2

```
UAFORTRAN *CR1 DATA6
      MASTER LENSTWO
      IMPLICIT REAL*8(A-H,O-Z)
      COMMON ZA(201),VNA(201),SVNA(201),SSVNA(201),
     -  Z(201),VN(201),SVN(201),SSVN(201),
     -  V(201),T(201),TM(201),U(201),UM(201),VH(201),
     -  R(201),S(201),SPARE(201),
     -  TITLE(20),VOA(100),VIA(100),ZOA(100),ZIA(100),
     -  H,VC,NI,NSYM,NVOA,NVIA
      READ(5,10) (TITLE(I),I=1,20)
10    FORMAT(20A4)
      NI=201
      READ(1,1)MAG
 1    FORMAT(I1)
      IF(MAG.LT.0.OR.MAG.GT.3) GO TO 20
      DO 3 I=1,100
      READ(1,2) VOA(I)
 2    FORMAT(F10.0)
      IF(VOA(I).EQ.0.) GO TO 4
 3    CONTINUE
      I=101
 4    NVOA=I-1
      DO 5 I=1,100
      READ(1,2) VIA(I)
      IF(VIA(I).EQ.0.) GO TO 6
 5    CONTINUE
      I=101
 6    NVIA=I-1
      CALL READVE(ZA,VNA,N,NSYM,VC)
      CALL DERIV1(ZA,VNA,SVNA,N)
      CALL DERIV1(ZA,SVNA,SSVNA,N)
      NI1=NI-1
      H=(ZA(N)-ZA(1))/FLOAT(NI1)
      Z(1)=ZA(1)
      DO 7 I=2,NI1
 7    Z(I)=Z(I-1)+H
      Z(NI)=ZA(N)
      CALL INTP3(ZA,VNA,N,Z,VN,NI)
      CALL INTP3(ZA,SVNA,N,Z,SVN,NI)
      CALL INTP3(ZA,SSVNA,N,Z,SSVN,NI)
      IF(MAG.EQ.0) CALL E210
      IF(MAG.EQ.1) CALL E211
      IF(MAG.EQ.2) CALL E212
      IF(MAG.EQ.3) CALL E213
      STOP
20    WRITE(6,21)
21    FORMAT(1X,'AN ILLEGAL VALUE HAS BEEN SPECIFIED FOR MAG')
      STOP
      END
      SUBROUTINE E210
```

```
      IMPLICIT REAL*8(A-H,O-Z)
      COMMON ZA(201),VNA(201),SVNA(201),SSVNA(201),
     -  Z(201),VN(201),SVN(201),SSVN(201),
     -  V(201),T(201),TM(201),U(201),UM(201),VH(201),
     -  R(201),S(201),SPARE(201),
     -  TITLE(20),VOA(100),VIA(100),ZOA(100),ZIA(100),
     -  H,VC,NI,NSYM,NVOA,NVIA
      WRITE(2,101) (TITLE(I),I=1,20)
101   FORMAT(1X,'OPTICAL PROPERTIES OF'//1X,20A4//)
      WRITE(2,102)
      WRITE(2,106)
      IF(NSYM.EQ.0) WRITE(2,111)
      IF(NSYM.EQ.1) WRITE(2,121)
      DO 12 NVO=1,NVOA
      VO=VOA(NVO)
      WRITE(2,14)
14    FORMAT(1X)
      DO 12 NVI=1,NVIA
      VI=VIA(NVI)
      VMULT=(VI-VO)/(VC-VN(1))
      VADD=VO-VN(1)*VMULT
      DO 5 I=1,NI
      V(I)=VN(I)*VMULT+VADD
      T(I)=SVN(I)*VMULT/V(I)
      U(I)=SSVN(I)*VMULT/V(I)
5     VH(I)=DSQRT(V(I))
      CALL SUBINT(T,TM,NI)
      CALL SUBINT(U,UM,NI)
      R(1)=1.
      S(1)=0.
      CALL RAYFE(H,T,TM,U,UM,R,S,NI)
      ZI=Z(NI)-R(NI)/S(NI)
      P1=5./24.
      P2=14./3.
      DO 6 I=1,NI
      A1=(1.25*U(I)*U(I)+P1*T(I)*T(I)*T(I)*T(I))*R(I)*R(I)
      A2=(P2*T(I)*R(I)-1.5*S(I))*T(I)*T(I)*S(I)
6     SPARE(I)=(A1+A2)*R(I)*R(I)*VH(I)
      CS=AREA(SPARE,1,NI,H)/(S(NI)**4*16.*VH(NI))
      DO 7 I=1,NI
7     SPARE(I)=(0.5*T(I)*S(I)+0.25*U(I)*R(I))*R(I)/VH(I)
      CC=AREA(SPARE,1,NI,H)*VH(NI)/(S(NI)*S(NI))
      FP=-1./S(NI)
      ZP=ZI-FP
      ZQI=ZI*1000.
      ZQP=ZP*1000.
      FQP=FP*1000.
      CQS=CS*1000.
      CQC=CC*1000.
12    WRITE(2,115) VO,VI,ZQI,ZQP,FQP,CQS,CQC
      STOP
102   FORMAT(1X,'FOR ZERO MAGNIFICATION CONDITIONS')
106   FORMAT(/1X,'(THE ABBERRATION COEFFICIENTS ARE ',
     -  'REFERRED TO THE IMAGE SIDE)')
111   FORMAT(///1X,'OBJ. SIDE  IM.  SIDE      IMAGE      PRINC',
     -  '      FOCAL     SPHER.    CHROM.'/
     -  1X,'   VOLTAGE   VOLTAGE      PLANE      PLANE      LENGTH',
     -  '      AB.       AB.'//
     -  1X,' VO(VOLTS) VI(VOLTS)    ZI(MM)     ZP(MM)      F(MM)',
     -  '   CSI(MM)    CCI(MM)'///)
121   FORMAT(///1X,'       OUTER    CENTRAL      IMAGE     PRINC',
     -  '      FOCAL     SPHER.    CHROM.'/
     -  1X,'   VOLTAGE   VOLTAGE      PLANE      PLANE      LENGTH',
     -  '      AB.       AB.'//
     -  1X,' VO(VOLTS) VI(VOLTS)    ZI(MM)     ZP(MM)      F(MM)',
     -  '   CSI(MM)    CCI(MM)'///)
```

```
115   FORMAT(1X,2F10.0,5F10.2)
      END
      SUBROUTINE E211
      IMPLICIT REAL*8(A-H,O-Z)
      COMMON ZA(201),VNA(201),SVNA(201),SSVNA(201),
     -  Z(201),VN(201),SVN(201),SSVN(201),
     -  V(201),T(201),TM(201),U(201),UM(201),VH(201),
     -  R(201),S(201),SPARE(201),
     -  TITLE(20),VOA(100),VIA(100),ZOA(100),ZIA(100),
     -  H,VC,NI,NSYM,NVOA,NVIA
      WRITE(2,101) (TITLE(I),I=1,20)
101   FORMAT(1X,'OPTICAL PROPERTIES OF'//1X,20A4//)
      WRITE(2,102)
      WRITE(2,106)
      IF(NSYM.EQ.0) WRITE(2,111)
      IF(NSYM.EQ.1) WRITE(2,121)
      DO 3 I=1,100
      READ(1,2) ZOA(I)
2     FORMAT(3PF10.0)
      IF(ZOA(I).EQ.0.) GO TO 4
3     CONTINUE
      I=101
4     NZOA=I-1
      DO 12 NVO=1,NVOA
      VO=VOA(NVO)
      WRITE(2,14)
14    FORMAT(1X)
      DO 12 NVI=1,NVIA
      VI=VIA(NVI)
      VMULT=(VI-VO)/(VC-VN(1))
      VADD=VO-VN(1)*VMULT
      DO 5 I=1,NI
      V(I)=VN(I)*VMULT+VADD
      T(I)=SVN(I)*VMULT/V(I)
      U(I)=SSVN(I)*VMULT/V(I)
5     VH(I)=DSQRT(V(I))
      CALL SUBINT(T,TM,NI)
      CALL SUBINT(U,UM,NI)
      WRITE(2,14)
      DO 12 NZO=1,NZOA
      ZO=ZOA(NZO)
      R(1)=Z(1)-ZO
      S(1)=1.
      CALL RAYFE(H,T,TM,U,UM,R,S,NI)
      ZI=Z(NI)-R(NI)/S(NI)
      P1=5./24.
      P2=14./3.
      DO 6 I=1,NI
      A1=(1.25*U(I)*U(I)+P1*T(I)*T(I)*T(I)*T(I))*R(I)*R(I)
      A2=(P2*T(I)*R(I)-1.5*S(I))*T(I)*T(I)*S(I)
6     SPARE(I)=(A1+A2)*R(I)*R(I)*VH(I)
      CS=AREA(SPARE,1,NI,H)/(S(NI)**4*16.*VH(NI))
      DO 7 I=1,NI
7     SPARE(I)=(0.5*T(I)*S(I)+0.25*U(I)*R(I))*R(I)/VH(I)
      CC=AREA(SPARE,1,NI,H)*VH(NI)/(S(NI)*S(NI))
      AM=-VH(1)/(VH(NI)*S(NI))
      ZQO=ZO*1000.
      ZQI=ZI*1000.
      CQS=CS*1000.
      CQC=CC*1000.
12    WRITE(2,115) VO,VI,ZQO,ZQI,AM,CQS,CQC
      STOP
102   FORMAT(1X,'FOR LOW MAGNIFICATION CONDITIONS')
106   FORMAT(/1X,'(THE ABBERRATION COEFFICIENTS ARE ',
     -  'REFERRED TO THE IMAGE SIDE)')
111   FORMAT(///1X,'OBJ. SIDE  IM.  SIDE     OBJECT     IMAGE',
```

```
     -  '        MAG     SPHER.     CHROM.'/
     -  1X,'   VOLTAGE    VOLTAGE      PLANE      PLANE',
     -  15X,' AB.        AB.'//
     -  1X,' VO(VOLTS) VI(VOLTS)    ZO(MM)     ZI(MM)        M',
     -  '    CSI(MM)    CCI(MM)'//)
 121  FORMAT(///1X,'       OUTER    CENTRAL       OBJECT      IMAGE',
     -  '        MAG     SPHER.     CHROM.'/
     -  1X,'   VOLTAGE    VOLTAGE      PLANE      PLANE',
     -  15X,' AB.        AB.'//
     -  1X,' VO(VOLTS) VC(VOLTS)    ZO(MM)     ZI(MM)        M',
     -  '    CSI(MM)    CCI(MM)'//)
 115  FORMAT(1X,2F10.0,2F10.2,F10.5,2F10.2)
      END
      SUBROUTINE E212
      IMPLICIT REAL*8(A-H,O-Z)
      COMMON ZA(201),VNA(201),SVNA(201),SSVNA(201),
     -  Z(201),VN(201),SVN(201),SSVN(201),
     -  V(201),T(201),TM(201),U(201),UM(201),VH(201),
     -  R(201),S(201),SPARE(201),
     -  TITLE(20),VOA(100),VIA(100),ZOA(100),ZIA(100),
     -  H,VC,NI,NSYM,NVOA,NVIA
      WRITE(2,101) (TITLE(I),I=1,20)
 101  FORMAT(1X,'OPTICAL PROPERTIES OF'//1X,20A4//)
      WRITE(2,102)
      WRITE(2,106)
      IF(NSYM.EQ.0) WRITE(2,111)
      IF(NSYM.EQ.1) WRITE(2,121)
      DO 3 I=1,100
      READ(1,2) ZIA(I)
  2   FORMAT(3PF10.0)
      IF(ZIA(I).EQ.0.) GO TO 4
  3   CONTINUE
      I=101
  4   NZIA=I-1
      DO 12 NVO=1,NVOA
      VO=VOA(NVO)
      WRITE(2,14)
 14   FORMAT(1X)
      DO 12 NVI=1,NVIA
      VI=VIA(NVI)
      VMULT=(VI-VO)/(VC-VN(1))
      VADD=VO-VN(1)*VMULT
      DO 5 I=1,NI
      V(I)=VN(I)*VMULT+VADD
      T(I)=SVN(I)*VMULT/V(I)
      U(I)=SSVN(I)*VMULT/V(I)
  5   VH(I)=DSQRT(V(I))
      CALL SUBINT(T,TM,NI)
      CALL SUBINT(U,UM,NI)
      WRITE(2,14)
      DO 12 NZI=1,NZIA
      ZI=ZIA(NZI)
      R(NI)=ZI-Z(NI)
      S(NI)=-1.
      CALL RAYBE(H,T,TM,U,UM,R,S,NI)
      ZO=Z(1)-R(1)/S(1)
      P1=5./24.
      P2=14./3.
      DO 6 I=1,NI
      A1=(1.25*U(I)*U(I)+P1*T(I)*T(I)*T(I)*T(I))*R(I)*R(I)
      A2=(P2*T(I)*R(I)-1.5*S(I))*T(I)*T(I)*S(I)
  6   SPARE(I)=(A1+A2)*R(I)*R(I)*VH(I)
      CS=AREA(SPARE,1,NI,H)/(S(1)**4*16.*VH(1))
      DO 7 I=1,NI
  7   SPARE(I)=(0.5*T(I)*S(I)+0.25*U(I)*R(I))*R(I)/VH(I)
      CC=AREA(SPARE,1,NI,H)*VH(1)/(S(1)*S(1))
```

```
      AM=(VH(1)*S(1))/VH(NI)
      ZQO=-(ZO*1000.)-3.
      ZQI=ZI*1000.
      CQS=CS*1000.
      CQC=CC*1000.
12    WRITE(2,115) VO,VI,ZQO,ZQI,AM,CQS,CQC
      STOP
102   FORMAT(1X,'FOR HIGH MAGNIFICATION CONDITIONS')
106   FORMAT(/1X,'(THE ABBERRATION COEFFICIENTS ARE ',
     -  'REFERRED TO THE OBJECT SIDE)')
111   FORMAT(///1X,'OBJ. SIDE  IM.  SIDE     OBJECT      IMAGE',
     -  '       MAG     SPHER.    CHROM.'/
     -  1X,'   VOLTAGE   VOLTAGE      PLANE      PLANE',
     -  15X,' AB.        AB.'//
     -  1X,' VO(VOLTS) VI(VOLTS)   ZO(MM)     ZI(MM)        M',
     -  '   CSO(MM)   CCO(MM)'//)
121   FORMAT(///1X,'       OUTER   CENTRAL       OBJECT      IMAGE',
     -  '       MAG     SPHER.    CHROM.'/
     -  1X,'   VOLTAGE   VOLTAGE      PLANE      PLANE',
     -  15X,' AB.        AB.'//
     -  1X,' VO(VOLTS) VC(VOLTS)   ZO(MM)     ZI(MM)        M',
     -  '   CSO(MM)   CCO(MM)'//)
115   FORMAT(1X,2F10.0,2F10.2,F10.3,2F10.2)
      END
      SUBROUTINE E213
      IMPLICIT REAL*8(A-H,O-Z)
      COMMON ZA(201),VNA(201),SVNA(201),SSVNA(201),
     -  Z(201),VN(201),SVN(201),SSVN(201),
     -  V(201),T(201),TM(201),U(201),UM(201),VH(201),
     -  R(201),S(201),SPARE(201),
     -  TITLE(20),VOA(100),VIA(100),ZOA(100),ZIA(100),
     -  H,VC,NI,NSYM,NVOA,NVIA
      WRITE(2,101) (TITLE(I),I=1,20)
101   FORMAT(1X,'OPTICAL PROPERTIES OF'//1X,20A4//)
      WRITE(2,102)
      WRITE(2,106)
      IF(NSYM.EQ.0) WRITE(2,111)
      IF(NSYM.EQ.1) WRITE(2,121)
      DO 12 NVO=1,NVOA
      VO=VOA(NVO)
      WRITE(2,14)
14    FORMAT(1X)
      DO 12 NVI=1,NVIA
      VI=VIA(NVI)
      VMULT=(VI-VO)/(VC-VN(1))
      VADD=VO-VN(1)*VMULT
      DO 5 I=1,NI
      V(I)=VN(I)*VMULT+VADD
      T(I)=SVN(I)*VMULT/V(I)
      U(I)=SSVN(I)*VMULT/V(I)
5     VH(I)=DSQRT(V(I))
      CALL SUBINT(T,TM,NI)
      CALL SUBINT(U,UM,NI)
      R(NI)=1.
      S(NI)=0.
      CALL RAYBE(H,T,TM,U,UM,R,S,NI)
      ZO=Z(1)-R(1)/S(1)
      P1=5./24.
      P2=14./3.
      DO 6 I=1,NI
      A1=(1.25*U(I)*U(I)+P1*T(I)*T(I)*T(I)*T(I))*R(I)*R(I)
      A2=(P2*T(I)*R(I)-1.5*S(I))*T(I)*T(I)*S(I)
6     SPARE(I)=(A1+A2)*R(I)*R(I)*VH(I)
      CS=AREA(SPARE,1,NI,H)/(S(1)**4*16.*VH(1))
      DO 7 I=1,NI
7     SPARE(I)=(0.5*T(I)*S(I)+0.25*U(I)*R(I))*R(I)/VH(I)
```

```
      CC=AREA(SPARE,1,N1,H)*VH(1)/(S(1)*S(1))
      FP=1./S(1)
      ZP=ZO+FP
      ZQO=ZO*1000.
      ZQP=ZP*1000.
      FQP=FP*1000.
      CQS=CS*1000.
      CQC=CC*1000.
12    WRITE(2,115) VO,VI,ZQO,ZQP,FQP,CQS,CQC
      STOP
102   FORMAT(1X,'FOR INFINITE MAGNIFICATION CONDITIONS')
106   FORMAT(/1X,'(THE ABBERRATION COEFFICIENTS ARE ',
     -  'REFERRED TO THE OBJECT SIDE)')
111   FORMAT(///1X,'OBJ. SIDE  IM.  SIDE     OBJECT      PRINC',
     -  '      FOCAL     SPHER.     CHROM.'/
     -  1X,'   VOLTAGE    VOLTAGE      PLANE      PLANE      LENGTH',
     -  '      AB.        AB.'//
     -  1X,' VO(VOLTS) VI(VOLTS)   ZO(MM)     ZP(MM)      F(MM)',
     -  '    CSO(MM)    CCO(MM)'//)

121   FORMAT(///1X,'       OUTER    CENTRAL      IMAGE     PRINC',
     -  '      FOCAL     SPHER.     CHROM.'/
     -  1X,'   VOLTAGE    VOLTAGE      PLANE      PLANE      LENGTH',
     -  '      AB.        AB.'//
     -  1X,' VO(VOLTS) VC(VOLTS)   ZI(MM)     ZP(MM)      F(MM)',
     -  '    CSO(MM)    CCO(MM)'//)
115   FORMAT(1X,2F10.0,5F10.2)
      END
      SUBROUTINE READVE(Z,V,N,NSYM,VC)
      IMPLICIT REAL*8(A-H,O-Z)
      DIMENSION Z(1),V(1)
      READ(5,5)
 5    FORMAT(///////)
      N=0
 1    N=N+1
      READ(5,21) Z(N),V(N)
21    FORMAT(1X,F15.4,F15.6)
      Z(N)=Z(N)*0.001
      IF(Z(N).EQ.0..AND.V(N).EQ.0.) GO TO 7
      IF(N.GT.200) GO TO 2
      GO TO 1
 7    N=N-1
      READ(5,8) NSYM
 8    FORMAT(1X,5X,I1)
      IF(NSYM.EQ.0) VC=V(N)
      IF(NSYM.EQ.1) READ(5,9) VC
 9    FORMAT(1X,F15.6)
      RETURN
 2    WRITE(6,3)
 3    FORMAT(1X,'ERROR IN AXIAL POTENTIAL DISTRIBUTION')
      STOP
      END
      SUBROUTINE DERIV1(X,Y,Y1,N)
      IMPLICIT REAL*8(A-H,O-Z)
      DIMENSION X(1),Y(1),Y1(1)
      DIMENSION S(100),A(100),D(100)
      IF(N-100) 13,13,11
11    WRITE(6,12)
12    FORMAT(1X,'INCREASE DIMENSIONS OF S,A,D')
      STOP
13    CALL SPL3(X,Y,S,N,A,D)
      N1=N-1
      DO 1 I=1,N1
1     Y1(I)=(Y(I+1)-Y(I))/D(I)-(S(I)+S(I)+S(I+1))*D(I)/6.
      Y1(N)=(Y(N)-Y(N1))/D(N1)+S(N1)*D(N1)/6.
      RETURN
```

```
      END
      SUBROUTINE SPL3(X,Y,B,N,A,D)
      IMPLICIT REAL*8(A-H,O-Z)
      DIMENSION X(1),Y(1),B(1),A(1),D(1)
      N1=N-1
      DO 1 I=1,N1
1     D(I)=X(I+1)-X(I)
      DO 2 I=2,N1
      B(I)=6.*((Y(I+1)-Y(I))/D(I)-(Y(I)-Y(I-1))/D(I-1))
2     A(I)=2.*(D(I-1)+D(I))
      DO 3 I=3,N1
      IO=I-1
      P=D(IO)/A(IO)
      B(I)=B(I)-P*B(IO)
3     A(I)=A(I)-P*D(IO)
      B(N1)=B(N1)/A(N1)
      N2=N-2
      DO 4 J=2,N2
      I=N-J
4     B(I)=(B(I)-D(I)*B(I+1))/A(I)
      B(1)=0.
      B(N)=0.
      RETURN
      END
      SUBROUTINE INTP3(X,Y,N,XI,YI,NI)
      IMPLICIT REAL*8(A-H,O-Z)
      DIMENSION S(100),T(100),U(100)
      DIMENSION X(1),Y(1),XI(1),YI(1)
      IF(N-100) 13,13,11
11    WRITE(6,12)
12    FORMAT(1X,'INCREASE DIMENSIONS OF S,T,U')
      STOP
13    CALL SPL3(X,Y,S,N,T,U)
      I=1
      J=0
1     J=J+1
      H=X(J+1)-X(J)
      A=S(J)/(6.*H)
      B=S(J+1)/(6.*H)
      C=Y(J)/H-S(J)*H/6.
      D=Y(J+1)/H-S(J+1)*H/6.
      JP=J+1
2     IF(XI(I)-X(1)) 3,3,4
3     YI(I)=Y(1)
      GO TO 8
4     IF(XI(I)-X(N)) 6,5,5
5     YI(I)=Y(N)
      GO TO 8
6     IF(XI(I)-X(JP)) 7,7,1
7     D1=X(JP)-XI(I)
      D2=XI(I)-X(J)
      YI(I)=A*D1*D1*D1+B*D2*D2*D2+C*D1+D*D2
8     I=I+1
      IF(I-NI) 2,2,9
9     RETURN
      END
      SUBROUTINE SUBINT(B,BM,N)
      IMPLICIT REAL*8(A-H,O-Z)
      DIMENSION B(1),BM(1)
      N1=N-1
      N2=N-2
      IF2=2
      BM(1)=0.5*(B(1)+B(IF2))
      BM(N1)=0.5*(B(N1)+B(N))
      DO 1 I=2,N2
1     BM(I)=0.0625*(9.*(B(I)+B(I+1))-B(I-1)-B(I+2))
```

```
      RETURN
      END
      SUBROUTINE RAYFE(H,T,TM,U,UM,R,S,NI)
      IMPLICIT REAL*8(A-H,O-Z)
      DIMENSION T(1),TM(1),U(1),UM(1),R(1),S(1)
      G=0.5*H
      N1=NI-1
      DO 1 I=1,N1
      V1=G*S(I)
      W1=G*(-0.5*T(I)*S(I)-0.25*U(I)*R(I))
      V2=G*(S(I)+W1)
      W2=G*(-0.5*TM(I)*(S(I)+W1)-0.25*UM(I)*(R(I)+V1))
      V3=H*(S(I)+W2)
      W3=H*(-0.5*TM(I)*(S(I)+W2)-0.25*UM(I)*(R(I)+V2))

      V4=H*(S(I)+W3)
       W4=H*(-0.5*T(I+1)*(S(I)+W3)-0.25*U(I+1)*(R(I)+V3))
      R(I+1)=R(I)+(2.*V1+4.*V2+2.*V3+V4)/6.
    1 S(I+1)=S(I)+(2.*W1+4.*W2+2.*W3+W4)/6.
      RETURN
      END
      SUBROUTINE RAYBE(H,T,TM,U,UM,R,S,NI)
      IMPLICIT REAL*8(A-H,O-Z)
      DIMENSION T(1),TM(1),U(1),UM(1),R(1),S(1)
      G=0.5*H
      N1=NI-1
      DO 1 J=1,N1
      K=NI-J
      I=K+1
      V1=-G*S(I)
      W1=-G*(-0.5*T(I)*S(I)-0.25*U(I)*R(I))
      V2=-G*(S(I)+W1)
      W2=-G*(-0.5*TM(K)*(S(I)+W1)-0.25*UM(K)*(R(I)+V1))
      V3=-H*(S(I)+W2)
      W3=-H*(-0.5*TM(K)*(S(I)+W2)-0.25*UM(K)*(R(I)+V2))
      V4=-H*(S(I)+W3)
      W4=-H*(-0.5*T(K)*(S(I)+W3)-0.25*U(K)*(R(I)+V3))
      R(K)=R(I)+(2.*V1+4.*V2+2.*V3+V4)/6.
    1 S(K)=S(I)+(2.*W1+4.*W2+2.*W3+W4)/6.
      RETURN
      END
      FUNCTION AREA(Y,IA,IB,H)
      IMPLICIT REAL*8(A-H,O-Z)
      DIMENSION Y(1)
      AREA=0.
      I=IA+1
    1 IF(I-IB) 2,3,4
    2 AREA=AREA+Y(I-1)+4.*Y(I)+Y(I+1)
      I=I+2
      GO TO 1
    3 AREA=AREA+1.5*(Y(I-1)+Y(I))
    4 AREA=AREA*H/3.
      RETURN
      END
      FINISH
```

Typical data for programme 2

```
z
100.

500.
600.
700.
800.
900.
1000.
2000.

100.
150.
200.
250.
300.

****
```

References

1. W.P.Dyke, "Field Emission, A Newly Practical Electron Source." I R E Trans. Mil. Electron. MIL-4, 38-45, (1960).

2. A.V.Crewe, M.Isaacson and D.Johnson, "A Simple Scanning Electron Microscope." Rev. Sci. Instrum., 40, 241-246, (1969).

3. L.W.Swanson and N.A.Martin, "Field Electron Cathode Stability Studies: Zirconium/Tungsten Thermal-Field Cathode." J. Appl. Phys., 46, 2029-2050, (1975).

4. A.vanOostrom, "Field Emission Cathodes." J.Appl. Phys., 33, 2917-2922, (1962).

5. L.W.Swanson and L.C.Crouser, "Angular Confinement of Field Electron and Ion Emission." J.Appl. Phys., 40, 4741-4749, (1969).

6. F.S.Baker, A.R.Osborn and J.Williams, "Field Emission from Carbon Fibres: A New Electron Source." Nature, 239, 96-97, (1972).

7. R.H.Fowler and L.Nordheim, "Electron Emission in Intense Electric Field." Proc. Roy. Soc. London., A119, 173-181, (1928).

8. L.Nordheim, "The Effect of the Image Force on the Emission and Reflexion of Electrons by Metals." Proc. Roy. Soc. London., A121, 626-639, (1928).

9. R.H.Good and E.W.Muller, "Field Emission." Handbuch der Physik, 21, 176-231, Springer-Verlag, Berlin, (1956).

10. D.Park, Introduction to the Quantum Theory, p.104, McGraw-Hill Book Company, (1964).

11. R.E.Burgess, H.Kroemer and J.M.Houston, "Corrected Values of Fowler-Nordheim Field Emission Functions v (y) and s(y)." Phys. Rev., 90, p. 515, (1953).

12. I.Tamm: See for example - D.Frankl, Electrical Properties of Semiconductor Surfaces, p. 192, Pergamon Press, (1967); where reference is made to I.Tamm, Physik Z. Sowj., 1, p. 733, (1932).

13. W.Shockley, "On the Surface States Associated with a Periodic Potential." Phys. Rev., 56, 317-323, (1939).

14. R.Stratton, "Field Emission from Semiconductors." Proc. Roy. Soc. London., B68, 746-757, (1955).

15. R.Stratton, "Theory of Field Emission from Semiconductors." Phys. Rev., 125, 67-82, (1962).

16. J.R.Arthur, "Energy Distribution of Field Emission from Germanium." Surface Sci., 2, 389-395, (1964).

17. R.Stratton, "Energy Distribution of Field Emitted Electrons." Phys. Rev., 135, 794-805, (1964).

18. R.D.Young, "Theoretical Total-Energy Distribution of Field-Emitted Electrons." Phys. Rev., 113, 110-114, (1959).

19. A.Modinos, "Field Emission from Surface States in Semiconductors." Surface Sci., 42, 205-207, (1974).

20. P.Handler, "Energy Level Diagrams for Germanium and Silicon Surfaces." J. Phys. Chem. Solids, 14, 1-8, (1960).

21. W.B.Shepherd and W.T.Peria, "Observation of Surface State Emission in the Energy Distribution of Electrons Field-Emitted from (100) Oriented Ge." Surface Sci., 38, 461-498, (1973).

22. T.A.Edison. U.S.Pat. 223898, (1880).

23. R.Bacon, A.A.Polozzi and S.E.Slosarik, Society of the Plastics Industry 21st Technical and Management Conference, Section 8E, Feb., (1966).

24. W.Watt, L.N.Phillips and W.Johnson, "High-Strength High-Modulus Carbon Fibres." The Engineer, 221, 815-816, (1966).

25. A.E.Standage and R.Prescott, "High Elastic Modulus Carbon Fibre." Nature, 211, p. 169, (1966).

26. J.D.Bernal, "The Structure of Graphite." Proc. Royl. Soc. Lond., A106, 749-773, (1924).

27. W.N.Reynolds. The Physical Properties of Graphite. Elsevier (1968).

28. G.E.Bacon, "A note on the rhombohedral modification of graphite." Acta. Cryst., 3, p. 320, (1950).

29. D.J.Johnson and C.N.Tyson, "The fine structure of graphite fibres." Brit. J. Appl. Phys. (J. Phys. D), 2, 787-795, (1969).

30. W.Ruland, "X-ray diffraction studies of carbon and graphite." Chemistry and Physics of Carbon, 4, 1-84, (1969).

31. A.Fourdeaux, R.Perret and W.Ruland, International Conference on Carbon Fibres their Composites and Applications, The Plastics Institute, London, Paper 9, (1971).

32. R.Perret and J.Ruland, "Single and Multiple x-ray Small Angle Scattering of C Fibres." J. Appl. Cryst., 2, 209-218, (1969).

33. B.J.Wicks and R.A.Coyle, "Microstructural inhomogeneity in carbon fibres." J.Mat. Sci., 11, 376-383, (1976).

34. W.Watt and W.Johnson, "Mechanism of Oxidation of Polyacrylonitrile Fibres." Nature, 257, 210-212, (1975).

35. P.W.Manders, "Carbon Fibre Structure by Electrolytic Etching." Nature, 271, 142-143, (1978).

36. F.R.Barnet and M.K.Norr, "A Three-Dimensional Structural Model for a High Modulus Pan-Based Carbon Fibre." Composites, 7, 93-99, (1976).

37. M.Barber, P.Swift, E.L.Evans and J.M.Thomas, "High Energy Photo electron Spectroscopic Study of Carbon Fibre Surfaces." Nature, 227, 1131-1132, (1970).

38. F.Hopfgarten, "Esca studies of carbon and oxygen in carbon fibres." Fibre Sci. and Techn., 12, 283-294, (1979).

39. F.Hopfgarten, "Surface study of Carbon Fibres with ESCA and AUGER Electron Spectroscopy." Fibre Sci. and Tech., 11, 67-79, (1978).

40. C.Lea, "Field Emission from Carbon Fibres." J. Phys. D: Appl. Phys., 6, 1105-1114, (1973).

41. T.H.English, C.Lea and M.T.Lilburne, "The Carbon Fibre Field Emitter as an Electron Gun Source." Scanning Electron Microscopy, Systems and Applications, Newcastle (London: Inst. of Phys.), 12-14, (1973).

42. F.S.Baker, A.R.Osborn and J. Williams, "The Carbon-fibre Field Emitter." J.Phys. D: Appl. Phys., 7, 2105-2115, (1974).

43. E.Braun, J.F.Smith and D.E.Sykes, "Carbon Fibres as Field Emitters." Vacuum, 25, 425-426, (1975).

44. H.Heinrich, M.Essig and J.Geiger, "Energy Distribution of Post-Accelerated Electrons Field-Emitted from Carbon Fibres." Appl. Phys., 12, 197-202, (1977).

45. A.J.Sangster, "Field-Emission Microwave Amplifiers: a reappraisal." Solid State and Electron Devices, 1, 151-157, (1977).

46. A.Knox, J.Moss and A.J.Sangster, IEE Colloquim on Electron Emission, Feb. 1977, Digest 1977/5.

47. M.Faubel, W.M.Holber and J.P.Toennies, "A Low Background Cold Cathode Ion Source for Molecular Beam Detection." Rev. Sci. Instr., 49, 449-451, (1978).

48. W.P.Dyke and W.W.Dolan, "Field Emission." Adv. Electronics and Electron Phys., 8, 89-183, (1956).

49. W.P.Dyke and J.K.Trolan, "Field Emission: Large Current Densities, Space Charge, and the Vacuum Arc." Phys. Rev., 89, 799-808, (1953).

50. F.M.Charbonnier, R.W.Strayer, L.W.Swanson, and E.E.Martin, "Nottingham Effect in Field and T.F. Emission: Heating and Cooling Domains and Inversion Temp." Phys. Rev. Lett., 13, 397-401, (1964).

51. H.Boersch, "Experimentelle Bestimmung der Energieverteilung in thermisch ausgelösten Elektronenstrahlen." Z. Physik, 139, 115-146, (1954).

52. K.H.Loeffler, "Energy-Spread Generation in Electron-Opitcal Instruments." Z. Agnew. Phys., 27, 145-149, (1969).

53. H.Moss, Narrow Angle Electron Guns and Cathode Ray Tubes, Adv. Electronics and Electron Phys. Supplement 3.

54. C.DeVere, Cathode Ray Tubes, Tektronix (1967).

55. G.Parr and O.H.Davie, The Cathode Ray Tube and its Applications, London: Chapman and Hall Ltd. (1959).

56. L.M.Myers, Electron Optics : Theoretical and Practical, Chapman and Hall, (1939).

57. A.W.Crewe, D.N.Eggenberger, J.Wall and L.M.Welter, "Electron Gun Using a Field Emission Source." Rev. Sci. Instrum., 39, 576-583, (1968).

58. A.V.Crewe, J.Wall and L.M.Welter, "A High-Resolution Scanning Transmission Electron Microscope." J. Appl. Phys., 39, 5861-5868, (1968).

59. J.W.Butler, Proc. Sixth Int. Congr. for Electron Microscopy, Kyoto 1, p.191, (1966).

60. E.Munro, Ph.D. Dissertation, Cambridge University, (1972).

61. J.L.Boling and W.W.Dolan, "Blunting of Tungsten Needles by Surface Diffusion." J.Appl. Phys., 29, 556-559, (1958).

62. K.Kuroda and T.Suzuki, "Analysis of accelerating lens system in field-emission scanning electron microscope." J. Appl. Phys., 45, 1436-1441, (1974).

63. R.H.Read, "Asymmetric electrostatic lens of three apertures." J. Sci. Instrum., 3, 127-131, (1970).

64. J.R.A.Cleaver, "Field Emission Guns for Electron Probe Instruments." Int. J. Electronics, 38, 513-529, (1975).

65. D.J.Swann, Ph.D. Dissertation, Cambridge University (1971).

66. J.R.A.Cleaver, "Stablization of the Electron Probe Current in the Scanning Electron Microscope with a Field Emission Cathode." Int. J. Electronics, 38, 531-540, (1975).

67. R.D.Young and E.W.Muller, "Experimental Measurement of the Total-Energy Distribution of Field-Emitted Electrons." Phys. Rev., 113, 115-120, (1959).

68. J.W.Gadzuk and E.W.Plummer, "Field Emission Energy Distribution (FEED)." Rev. Mod. Phys., 45, 487-548, (1973).

69. E.Braun, R.G.Forbes, J.Pearson, J.M.Pelmore and R.V.Latham, "An Advanced Field Electron Emission Spectrometer." J.Phys. E: Sci. Instrum., 11, 222-228, (1978).

70. R.E.Hurley and P.J.Dooley, "Electroluminescence Produced by High Electric Field at the Surface of Copper Cathodes." J.Phys. D: Appl. Phys., 10, L195-L201, (1977).

71. G.F.Alfrey and J.B.Taylor, "Discussion on the Mechanism of Electroluminescence of Zinc Sulphide." Br. J. Appl. Phys., 6, Suppl. 4, S44-S49, (1955).

72. V.M.Zhukov and G.N.Fursei, "Explosive Electron Emission from Copper Points." Sov. Phys. Tech. Phys., 21, 1112-1117, (1976).

73. V.M.Zhukov, G.N.Fursei, E.I.Givargizov, I.D.Ventova and N.V.Egorov, "Explosive Emission of Semiconducting Point Cathodes." Sov. Phys. Tech. Phys., 21, 1110-1112, (1976).

74. C.Kleint, "Surface Diffusion Model of Adsorption-Induced Field Emission Flicker Noise." Surface Sci., 25, 394-410, (1971).

75. D.J.Swann and K.C.A.Smith, "Lifetime and Noise Characteristics of Tungsten Field Emitters." Scanning Electron Microscopy, Proceedings of the Sixth Annual Scanning Electron Microscope Symposium, IIT Research Institute, Chicago, 41-48, (1973).

76. N.K.Allen, B.M.Cox and R.V.Latham, "The source of high β electron emission sites on broad-area high-voltage alloy electrodes." J. Phys. D: Appl. Phys., 12, 969-978, (1979).

77. C.S.Athwal and R.V.Latham. Proc. IX Int. Sym on Discharges and Electrical Insulation in Vacuum (Eindhoven) - to be published in Physica C (1981).

78. K.W.Boer and S.R.Ovshinsky, "Electrothermal Initiation of an Electronic Switching Mechanism in Semiconducting Glasses." J. Appl. Phys. 41, 2675-2681, (1970).

79. G.Dearnaley, A.M.Stoneham and D.V.Morgan, "Electrical Phenomena in Amorphous Oxide Films." Rep. Prog. Phys., 33, 1129-1191, (1970).

80. D.Adler, H.K.Henisch and N. Mott, "The Mechanism of Threshold Switching in Amorphous Alloys." Rev. Mod. Phys., 50, 209-220, (1978).